UNIVERSIDADE FEDERAL DE MINAS GERAIS

Instituto de Geociências

Programa de Pós-Graduação em Geologia

Raíssa Santiago Mendes

EVOLUÇÃO CRUSTAL, GEOCRONOLOGIA E GEOLOGIA ISOTÓPICA DO ORÓGENO ARAÇUAÍ-RIBEIRA (AROS) NO SUL DO ESPÍRITO SANTO

Nº 57

Belo Horizonte

DATA (16/02/2022)

Raíssa Santiago Mendes

EVOLUÇÃO CRUSTAL, GEOCRONOLOGIA E GEOLOGIA ISOTÓPICA DO ORÓGENO ARAÇUAÍ-RIBEIRA (AROS) NO SUL DO ESPÍRITO SANTO

Versão Final

Tese apresentada ao programa de Pós-graduação em Geologia do Instituto de Geociências da Universidade Federal de Minas Gerais como requisito parcial para obtenção do título de Doutora em Geologia.

Área de concentração: Geologia Regional.

Orientador: Prof. Dr. Fabrício de Andrade Caxito

Coorientador: Prof. Dr. Antonio Carlos Pedrosa Soares

Belo Horizonte
2022

S235e
2022

Santiago, Raíssa.

Evolução crustal, geocronologia e geologia isotópica do Orógeno Araçuaí-Ribeira (AROS) no sul do Espírito Santo [manuscrito] / Raíssa Santiago Mendes. – 2022.

196 f., enc. il. (principalmente color.)

Orientador: Fabrício de Andrade Caxito.

Coorientador: Antônio Carlos Pedrosa Soares.

Tese (doutorado) – Universidade Federal de Minas Gerais, Instituto de Geociências, 2022.

Área de concentração: Geologia Regional.

Bibliografia: f. 143-158.

Inclui apêndice.

1. Tempo geológico – Teses. 2. Geoquímica – Espírito Santo – Teses. 3. Orogenia – Espírito Santo – Teses. 4. Geologia isotópica – Espírito Santo – Teses. I. Caxito, Fabrício de Andrade. II. Pedrosa-Soares, Antônio Carlos. III. Universidade Federal de Minas Gerais. Instituto de Geociências. IV. Título.

CDU: 550.93(815.2)

Ficha catalográfica elaborada por Elisabete Quatrini Vieira – CRB6 2210

Biblioteca “Vitória Pedersoli”, Instituto de Geociências da UFMG

UNIVERSIDADE FEDERAL DE MINAS GERAIS

PROGRAMA DE PÓS-GRADUAÇÃO EM GEOLOGIA DO IGC-UFMG

FOLHA DE APROVAÇÃO

EVOLUÇÃO CRUSTAL, GEOCRONOLOGIA E GEOLOGIA ISOTÓPICA DO ORÓGENO ARAÇUAÍ-RIBEIRA (AROS) NO SUL DO ESPÍRITO SANTO

RAÍSSA SANTIAGO MENDES

Tese submetida à Banca Examinadora designada pelo Colegiado, como requisito para obtenção do grau de Doutora em GEOLOGIA, área de concentração GEOLOGIA REGIONAL, pelo Programa de Pós-graduação em Geologia do Instituto de Geociências da Universidade Federal de Minas Gerais.

Aprovada em 16 de fevereiro de 2022, pela banca constituída pelos membros:

Prof. Fabrício de Andrade Caxito - Orientador
UFMG

Profa. Monica da Costa Pereira Lavalle Heilbron
UERJ

Prof. Fernando Flecha de Alkmim
UFOP

Prof. Lauro Cézar Montefalco de Lira Santos
UFPE

Prof. Alexandre Uhlein
UFMG

Prof. Jorge Geraldo Roncato Júnior
UFMG

Belo Horizonte, 16 de fevereiro de 2022.

À minha família,
em especial aos meus pais,
Fátima e José, e ao meu irmão, Rafael.
Aos meus queridos sobrinhos Mel e José.

AGRADECIMENTOS

Agradeço o apoio e incentivo de pessoas e instituições sem as quais a concretização dessa tese não teria acontecido.

Ao orientador, professor Dr. Fabrício Caxito pela amizade, confiança e apoio em mais um projeto de pesquisa. Pelo entusiasmo e encanto pela geologia, acompanhado sempre de discussões prazerosas e enriquecedoras. Agradeço por me encorajar e me mostrar que seria possível.

Ao coorientador, professor Dr. Antonio Carlos Pedrosa Soares pela oportunidade, dedicação, por compartilhar comigo todo seu conhecimento geológico com discussões e sugestões engrandecedoras e pelo apoio imensurável.

À professora Drª. Mirna Neves, pela amizade e parceria de longa data. Por todo incentivo, suporte, sugestões para o trabalho e, principalmente, pelo acolhimento em Alegre – os campos não poderiam ter sido melhores!

Ao professor Dr. Elton Dantas pelo suporte e significativa contribuição para o trabalho.

À Universidade Federal de Minas Gerais - UFMG e ao Instituto de Geociências - ICG pela oportunidade de ampliar meus estudos. E aos professores do Programa de Pós-Graduação em Geologia, em especial Mahyra, Tiago e Rosaline.

Ao William Campos por sua paciência, solicitude e eficiência. Aos funcionários do CPMTC/IGC/UFMG, em especial, à Denise, Carlos, Stênio, Jhonny e Hélvio por toda ajuda e disposição, vocês foram essenciais.

Ao Laboratório de Geocronologia da Universidade de Brasília (UnB) e ao Laboratório de Geoquímica Isotópica da Universidade Federal de Ouro Preto pelas análises isotópicas.

Ao Laboratório de Geotectônica, Geodiversidade e Mapeamento Geológico (Geo3) do CPMTC-IGC-UFMG e ao Projeto MOBILE (geolifemobile.com), Instituto Serrapilheira (Serra-1912-31510), por financiarem essa pesquisa.

À Coordenação de Aperfeiçoamento de Pessoal de Nível Superior (CAPES) pela bolsa de estudos durante dois anos do doutorado.

Aos amigos de graduação e pós-graduação desse Brasil que juntos traçamos bons caminhos e construímos laços através de incentivos, amparo e discussões sobre geologia e a vida, em especial, ao Salomão Calegari, Márcio Dantas, Rhander Taufner, Filipe Temporim, Sofia Marques, Ângelo Geovani e às meninas cravejadas

de turmalina paraíba da geotectônica: Carol Deluca, Cris Araújo e Paula Serrano. Obrigada por me ajudarem e escutarem nos meus momentos de dúvida.

Às minhas companheiras de vida: Fefê, Iza, Gabi, Nanik, Ly, Magrela, Ka, Mila e as julias: Ju Mello, Ju Almeida, Ju Peixoto e Ju França – amor incondicional.

E finalmente, meus maiores agradecimentos são para aqueles que faltam palavras para expressar tamanha gratidão: à minha família, em especial aos principais responsáveis para a realização deste trabalho, meu pais, Fátima e José. Por estarem sempre presentes, com todo amor, carinho e dedicação. Por tudo que me ensinam e proporcionam, apoiando minhas decisões e me motivando a continuar. E pela maneira que veem o próximo e a vida. Meus exemplos de generosidade, caráter e determinação! E ao meu melhor parceiro de campo de todos os tempos: José Mendes!

RESUMO

O sistema orogênico Araçuaí-Ribeira (AROS) constitui uma parte da Província Mantiqueira desenvolvida durante a formação do Gondwana Ocidental no Neoproterozoico superior. Assim como diversos cinturões orogênicos formados durante o evento Pan-Africano/Brasiliano, o AROS é caracterizado por arcos magmáticos neoproterozoicos intra-oceânicos e continentais. O orógeno Ribeira compreende os arcos magmáticos intra-oceânicos a transicionais tonianos-criogenianos Serra da Prata e Rio Negro, e ambos os orógenos apresentam rochas correlacionáveis ao arco continental ediacarano Rio Doce, sugerindo uma evolução geodinâmica complexa. O batólito Caxixe, definido neste trabalho, é um batólito composto, multi-intrusão, amplamente distribuído no sul do Espírito Santo, com cerca de 110 Km de extensão e largura entre 12 e 21 Km. É composto principalmente por biotita-ortognaisses granodioríticos a graníticos, com afinidade geoquímica cálcio-alcalina, metaluminosa a ligeiramente peraluminosa, magnesiana, de assinatura tipo I, com ligeiro enriquecimento em elementos terras raras leves (ETRL) em relação aos pesados (ETRP), anomalias positivas a levemente negativas de Eu e anomalias negativas de Nb-Ta. A maior parte do batólito Caxixe e dos plútons adjacentes apresenta idades entre 580 e 608 Ma, com parâmetros $\varepsilon Hf_{(t)}$, $\varepsilon Nd_{(t)}$ e $^{87}Sr/^{86}Sr$ diferenciados indicando importante contaminação crustal. Estas características são típicas de rochas do arco Rio Doce. Porém, rochas tonianas (840-860 Ma) ocorrem localmente neste batólito como *roof pendants* e megaxenólitos. Estas apresentam $\varepsilon Hf_{(t)}$, $\varepsilon Nd_{(t)}$ e $^{87}Sr/^{86}Sr$ tipicamente juvenis, plotando na curva do manto empobrecido. Estas rochas representam fragmentos de arcos de ilha, provavelmente a terminação norte do arco magmático Serra da Prata. Completando o edifício magmático do batólito Caxixe e adjacências, ocorrem também intrusões sin-colisionais de granada-leucogranitos a 575 Ma, intrusões máficas sin- a tardi-colisionais a 560 Ma e leucogranitos pós-colisionais a 503 Ma. Os paragnaisses aluminosos e os hornblenda-biotita gnaisses que ocorrem como encaixantes destes plútons apresentam geoquímica semelhante a bacias relacionadas a arco magmático e espectro de idades U-Pb em zircão detrítico com picos principais entre 600 a 800 Ma, representando rochas sedimentares e volcaniclásticas provenientes do sistema de arcos magmáticos do AROS. Assim, os 360 Ma de atividade magmática e sedimentar registrados no batólito Caxixe e adjacências no sul do Espírito Santo são de enorme relevância para

o entendimento da evolução tectônica do Gondwana Ocidental, registrando as etapas pré-, sin- e pós-colisionais do AROS. O modelo de evolução tectônica proposto envolve a docagem das rochas do arco magmático toniano na margem continental do paleocontinente Angola, seguida pela inversão da polaridade de subducção e desenvolvimento do arco continental Ediacarano Rio Doce por fusão da margem continental e dos terrenos acoplados. O processo evoluiu para a colisão entre os paleocontinentes São Francisco e Angola e o colapso orogênico no Cambriano.

Palavras-chave: Geocronologia LA-ICPMS e SHRIMP U-Pb; Geoquímica Isotópica Hf-Nd-Sr; Arco Magmático; *Roof-pendants*; Orogenia Brasiliana

ABSTRACT

The Araçuaí-Ribeira orogenic system (AROS) constitutes a part of the Mantiqueira Province developed during the formation of Western Gondwana in the Late Neoproterozoic. Similar to several orogenic belts formed during the Pan-African/Brazilian event, the AROS is characterized by intra-oceanic and continental Neoproterozoic magmatic arcs. The Ribeira orogen comprises the Serra da Prata and Rio Negro intra-oceanic Tonian-Cryogenian transitional arcs and both the Ribeira and Araçuaí orogens are characterized by the Ediacaran Rio Doce continental arc, suggesting a complex geodynamic evolution. The Caxixe batholith, defined in this work, is a multi-intrusion composite batholith widely distributed in the southern Espírito Santo state, with approximately 110 km in length and width ranging between 12 and 21 km. It is composed mainly of granodioritic to granitic biotite-orthogneisses, with calc-alkaline geochemical affinity, metaluminous to slightly peraluminous, magnesian, type I, with slight enrichment in light rare earth elements (LREE) in relation to heavy ones (HREE), positive to slightly negative anomalies of Eu and negative anomalies of Nb-Ta. Most of the Caxixe batholith and adjacent plutons have ages between 580 and 608 Ma, with differentiated $\varepsilon Hf_{(t)}$, $\varepsilon Nd_{(t)}$ and $^{87}Sr/^{86}Sr$ indicating important crustal contamination. These characteristics are typical of rocks of the Ediacaran Rio Doce arc. However, Tonian rocks (840-860 Ma) occur locally in this batholith as roof pendants and megaxenoliths. These present typically juvenile $\varepsilon Hf_{(t)}$, $\varepsilon Nd_{(t)}$ and $^{87}Sr/^{86}Sr$ ratios, plotting on the depleted mantle curve. These rocks represent fragments of juvenile island arcs, probably the northern end of the Serra da Prata magmatic arc. Completing the magmatic edifice of the Caxixe batholith and vicinities, there are also syn-collisional garnet-bearing leucogranites at ca. 575 Ma, syn- to tardi-collisional mafic intrusions at ca. 560 Ma and post-collisional leucogranite intrusions of about 503 Ma. The peraluminous paragneisses and hornblende-biotite gneisses that occur as country rocks to these plutons present geochemistry similar to magmatic arc basins and U-Pb age spectra of detrital zircon with main peaks between 600 and 800 Ma, indicating derivation from sedimentary and volcaniclastic rocks related to the magmatic arc systems. Thus, the 360 Ma of magmatic and sedimentary activity recorded in the Caxixe batholith and its surroundings in the southern Espírito Santo state are of enormous relevance for the understanding of the tectonic evolution of Western Gondwana, recording the pre-, syn- and post-collisional stages of the

orogenic building of the AROS. We propose a model of tectonic evolution with the docking of the Tonian magmatic arc rocks in the passive continental margin of the Angola paleocontinent, followed by the subduction polarity inversion and development of the Rio Doce continental arc in the Ediacaran by melting of the continental margin and docked terranes. This was followed by collision between the São Francisco and Angola paleocontinents and orogenic collapse in the Cambrian.

Keywords: Geochronology LA-ICPMS and SHRIMP U-Pb; Hf-Nd-Sr isotope geochemistry; Magmatic Arc; Roof-pendants; Brasilian Orogeny

LISTA DE ILUSTRAÇÕES

Capítulo I

Capítulo II

Capítulo III

Capítulo IV

Capítulo V

SUMÁRIO

CAPíTULO I

INTRODUÇÃO

I.1 Caracterização do problema e motivação da pesquisa

Orógenos neoproterozoicos do Gondwana Ocidental formaram-se durante a convergência dos blocos paleocontinentais Amazônia, São Francisco-Congo, Paranapanema (Rio de La Plata), Angola e Kalahari, além de blocos alóctones menores. A amalgamação dos paleocontinentes resultou no consumo de oceanos neoproterozoicos como Goiás-Pharusiano e Adamastor. Como consequência houve a instalação de arcos magmáticos (oceânicos e continentais) em limites de placas convergentes, seu amadurecimento, o fim de sua atividade culminando no fechamento das bacias oceanicas até a colisão continental, concomitantemente à formação de bacias sedimentares (e.g., Pimentel & Fuck 1992; Pedrosa-Soares et al., 1998, 2001; Heilbron et al., 2004, 2021; Tupinambá et al., 2012; Caxito et al., 2014, 2021; Brito-Neves et al. 2014; Basei et al., 2018; Tedeschi et al., 2016; Peixoto et al., 2017; Hartmann et al., 2019; Amaral et al., 2020; Brown et al., 2020; Decol et al., 2021).

Considerando que o processo evolutivo tectônico de formação de orógenos baseia-se largamente na abertura e fechamento de bacias oceânicas, os estudos de arcos magmáticos e suas bacias sedimentares são essenciais para contribuir na compreensão da história evolutiva do Gondwana Ocidental. No contexto deste trabalho, estes estudos visam contribuir especificamente à compreensão da evolução geodinâmica da Província Mantiqueira (Almeida et al., 1981), um sistema orogênico com mais de 3.000 km de comprimento e 100-500 km de largura na costa leste da América do Sul (Fig. I.1). Os orógenos Araçuaí e Ribeira são segmentos desse complexo sistema orogênico desenvolvido durante a formação do Gondwana ocidental no Neoproterozoico Superior.

Estudos recentes (e.g., Tedeschi et al., 2016, Degler et al., 2017, Heilbron et al., 2017) consideram esses dois orógenos como um sistema interligado, o Sistema Orogênico Araçuaí-Ribeira (AROS). Esta correlação é baseada principalmente na semelhança entre as unidades litológicas de alto grau metamórfico da zona interna dos dois orógenos e na ausência de estruturas marcantes que limitem diferentes

configurações tectônicas (Tupinambá., 2007), assim como pela continuidade cada vez mais detalhada em relação aos batólitos e plútons que compõem o Arco Ediacarano Rio Doce. Este arco magmático foi edificado em margem continental ativa, com características de arco “cordilheirano” (Heilbron et al., 2013; Gonçalves et al., 2016; Tedeschi et al., 2016; Soares et al., 2020), tais como dados isotópicos Sm-Nd e Rb-Sr que indicam grande contribuição continental antiga no magmatismo ($\varepsilon Nd_{(t)}$ = -5,7 a -7,8, e idades-modelo T_{DM} entre 1,3 e 1,7 Ga). Entretanto, uma característica marcante do Orógeno Ribeira é a presença de arcos magmáticos do Neoproterozoico inferior, os sistemas de arcos magmáticos Rio Negro (790-620 Ma) e Serra da Prata (856-838 Ma), que mostram grande importância de contribuição mantélica juvenil ($\varepsilon Nd_{(t)}$ = -3 a +5 e idades-modelo T_{DM} com modas principais em 1,0, 1,3 e 1,8 Ga para o Arco Rio Negro e $\varepsilon Nd_{(t)}$ = −3 a +5 e T_{DM} = 1,7–0,9 Ga para o Arco Serra da Prata; Tupinambá et al., 2011; Peixoto et al., 2017), representando arcos de ilhas intra-oceânicos a transicionais que evoluíram do Toniano ao Criogeniano (Tupinambá et al., 2012; Peixoto et al. 2017; Decol et al., 2021).

As diferentes idades, composições geoquímicas e isotópicas, e diferentes graus de contribuição mantélica juvenil *versus* crustal retrabalhada de cada uma destas unidades as tornam peças-chave para o entendimento da evolução destes orógenos e podem servir de parâmetro para a reconstrução paleogeográfica da zona de conexão Araçuaí/Ribeira, ainda mal delineada. Especificamente, a continuação ou não dos arcos magmáticos Tonianos/Criogenianos do Orógeno Ribeira no sul do estado do Espírito Santo é um dos maiores problemas paleogeográficos e tectônicos neste contexto.

Assim, esta tese tem como foco de estudo a região sul do Estado do Espírito Santo, zona de conexão dos orógenos Araçuaí-Ribeira, concentrando principalmente na investigação dos arcos magmáticos de diferentes assinaturas geoquímicas e ambientes tectônicos radicalmente diferentes descritos nos dois orógenos, e suas possíveis bacias sedimentares associadas. Para tanto, um estudo detalhado dos granitos e paragnaisses aflorantes nesta região, quanto à sua petrografia, litoquímica e características isotópicas é apresentado.

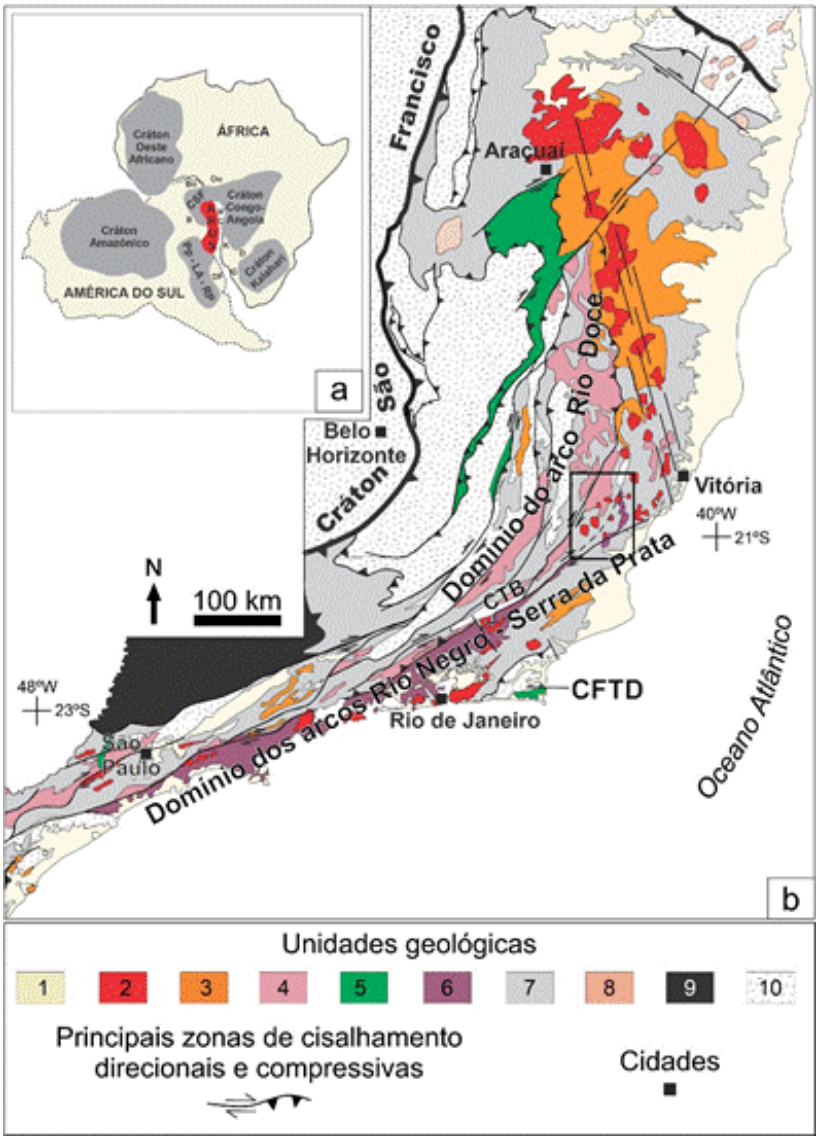

Fig I. 1 - Mapa geológico simplificado do Sistema Orogênico Araçuaí-Ribeira (AROS) e (a) sua localização no Gondwana Ocidental (modificado de Silva et al., 2005). Coberturas cenozóicas: 1. Unidades do AROS: 2 - Plutonismo pós-colisional; 3 - Plutonismo colisional; 4 - Arco magmático do Rio Doce e correlatos; 5 - Conjuntos rochosos contendo ofiolitos; 6 - Domínio do arco Serra da Prata - Rio Negro; 7 - Sucessões metassedimentares e metavulcânicas neoproterozóicas; 8 - Rochas magmáticas relacionadas ao rifte toniano e criogeniano; 9 - Faixa Sul Brasília; 10 - Unidades pré-neoproterozóicas. CTB - Limite Tectônica Central; CFTD - Domínio Tectônico de Cabo Frio; CSF - Cráton do São Francisco; Pp-LA-RP - Blocos cratônicos Paranapanema-Luiz Alves-Rio de La Plata.

I.2. Questões em aberto e relevância do estudo

A área de pesquisa (Fig. I.1) corresponde à zona de transição entre o núcleo cristalino de alto grau e granítico do Orógeno Araçuaí e o Terreno Oriental (Heilbron et al., 2004, Heilbron et al., 2017) do Orógeno Ribeira. Essa zona de transição foi estabelecida arbitrariamente pelo paralelo 21º S, que baliza uma grande inflexão da

tendência estrutural brasiliana em relação à extremidade sul do Cráton São Francisco (Pedrosa-Soares et al., 2001). Entretanto, a continuidade entre os dois orógenos é cada vez mais sugerida e adotada, principalmente devido à extensão dos batólitos e plutons que constituem o arco Rio Doce nas regiões compreendidas a ambos orógenos, e pela ausência de descontinuidades metamórficas e estruturais importantes, sustentando a interpretação de um sistema orogênico integrado. Apesar disso, algumas diferenças ainda dificultam a correlação entre os diversos componentes dos orógenos, tais como: o maior volume de unidades supracrustais das fácies xisto verde a anfibolito baixo no Orógeno Araçuaí; a aloctonia de terrenos descrita para a fase colisional principal do Orógeno Ribeira, não identificada no Orógeno Araçuaí; a presença do Domínio Tectônico Cabo Frio no Orógeno Ribeira, que representaria uma borda do Cráton de Angola fortemente retrabalhada durante a colagem Brasiliano/Pan-Africana (Heilbron et al., 2004, Heilbron et al., 2017).

Portanto, esta zona de transição, apesar de sua significativa importância na compreensão da evolução destas duas regiões orogênicas e para a reconstrução da evolução geodinâmica da Província Mantiqueira e da orogênese Brasiliano/Pan-africano, ainda carece de informação geológica sistemática e estudos detalhados. Nesse sentido, alguns pontos que demandam elucidação nesta região são:

I - Como se dispõem as litotipos e os componentes geotectônicos na zona de transição entre os Orógenos Araçuaí e Ribeira?

II - Qual a influência e extensão dos arcos magmáticos de diferentes assinaturas geoquímicas e ambientes tectônicos radicalmente diferentes descritos nos dois orógenos na área?

III - Qual é a idade, proveniência e significado geotectônico das rochas metassedimentares no sul do Espírito Santo? Estas rochas podem representar bacias relacionadas aos arcos Serra da Prata, Rio Negro ou Rio Doce?

IV - Como e quando ocorre a interação tectônica dos componentes dos dois orógenos nesta área no processo evolutivo do Gondwana Ocidental?

A região estudada, situada na porção meridional do Orógeno Araçuaí e provavelmente englobando a terminação norte das estruturas do Orógeno Ribeira, é marcada por paragnaisses e rochas metassedimentares de alto grau mapeados de forma indistinta na zona interna dos dois orógenos e cuja idade e significado geotectônico são ainda pouco conhecidos; por corpos ígneos intrusivos genericamente correlacionados às supersuites G1 a G5 do Orógeno Araçuaí, com

base nas relações pré, sin e pós-cinemáticas com as grandes zonas de cisalhamento do sul do Espírito Santo e com a foliação regional; e pelas zonas de Cisalhamento Guaçuí e Batatal, de expressão regional por dezenas de quilômetros na direção NE-SW (Silva, 2010). Dados geocronológicos, geoquímicos e isotópicos são necessários para investigar a possibilidade de que parte dos corpos graníticos intrudidos nas rochas metassedimentares de alto grau e hoje mapeados como G1 a G5 possam na realidade ser mais antigos e, possivelmente, representar a continuação norte dos arcos Rio Negro e/ou Serra da Prata na região.

Esta possibilidade vem sendo sugerida em alguns trabalhos recentes. Por exemplo, Decol et al. (2021) interpretaram, a partir de dados geoquímicos de rocha total, a presença de adakitos além de rochas típicas da série cálcio-alcalina expandida, toleiítica de arco e granitóides do tipo-A na região de Castelo – ES, englobando o que é chamado neste trabalho de batólito Caxixe. No Capítulo III da presente tese, são apresentados novos dados de campo, geoquímicos, geocronológicos e isotópicos que confirmam a presença de remanescentes dos arcos de ilha juvenis do Orógeno Ribeira na área de estudo; no Capítulo IV, um estudo da proveniência, idade e ambiente tectônico das sucessões metassedimentares paragnáissicas encaixantes; e no Capítulo V, uma caracterização geoquímica, isotópica e geocronológica das massa granítica principal do batólito Caxixe e plútons adjacentes.

I.3 Objetivos

A presente tese tem como objetivo principal o entendimento do processo evolutivo dos orógenos Araçuaí e Ribeira em sua zona limítrofe, na porção sul do Estado do Espírito Santo. Desta forma, o foco é sobretudo na identificação da ocorrência e delimitação de rochas dos diversos arcos magmáticos, principalmente os Arcos Serra da Prata e Rio Negro, cuja terminação na região é ainda mal compreendida, além de sua relação com as rochas paragnáissicas de alto grau. Especificamente, os objetivos são:

- Determinar a possível extensão para norte dos arcos magmáticos do Orógeno Ribeira e a outras prováveis presença do Arco Rio Doce na área de estudo;

- Determinar a proveniência sedimentar, idade, natureza das fontes e ambiente tectônico das rochas metassedimentares na área de estudo;

- Determinar as condições de preservação de remanescentes de sistemas acrescionários dentro dos grandes complexos batolíticos sin- a pós-colisionais em orógenos pré-cambrianos.

I.4. Metodologia

Para se atingir os objetivos propostos, os seguintes métodos foram utilizados:

1. Revisão bibliográfica do Orógeno Araçuaí e Orógeno Ribeira, focando sobre a compartimentação e evolução tectônica do segmento meridional da Orógeno Araçuaí e setentrional da Orógeno Ribeira.
2. Elaboração da base geológica de campo a partir da compilação de folhas dos projetos PRONAGEO/UFMG, PRONAGEO/UFES, PRONAGEO/UERJ, PLGB/CPRM (Folha Cachoeiro de Itapemirim (SF.24-V-A), escala 1:250.000);
3. Mapeamento geológico da região, com ênfase nos principais corpos graníticos já delimitados e na identificação de corpos semelhantes, além de suas rochas metassedimentares encaixantes. Ao todo, 102 pontos foram descritos e investigados.
4. Análise e classificação petrográfica macroscópica e microscópica dos diversos litotipos identificados na etapa de mapeamento. Lâminas delgadas das amostras coletadas em campo foram preparadas nos laboratórios do CPMTC-IGC-UFMG, e a descrição petrográfica foi realizada nos laboratórios de microscopia destes mesmos laboratórios.
5. Análises químicas de rocha total das diversas rochas graníticas e gnáissicas da área de estudo, para a caracterização de sua petrogênese e ambiência tectônica. As amostras foram preparadas através de procedimentos clássicos (moagem, pulverização) nos laboratórios de preparação de amostras do CPMTC-IGC-UFMG, e os teores de óxidos de elementos maiores e de elementos traços foram determinados em laboratório comercial (SGS-Geosol) através de ICPMS (*Induced Coupled Plasma – Mass Spectrometry*).
6. Análise U-Pb e Lu-Hf de zircões ígneos das rochas graníticas, buscando caracterizar sua idade (U-Pb) de cristalização e sua possível correlação aos diversos arcos magmáticos dos orógenos Araçuaí e Ribeira; e possível contribuição mantélica versus crustal em sua petrogênese (Lu-Hf). As análises U-Pb foram realizadas por SHRIMP (*Sensitive High-Resolution Ion Microprobe*) nos laboratórios do John de

Laeter Centre, University of Western Australia; e por LA-ICPMS (*Laser Ablation – Induced Coupled Plasma Mass Spectrometry*) nos laboratórios de Geocronologia e Geoquímica Isotópica das Universidade de Brasília e da Universidade Federal de Ouro Preto, respectivamente. As análises Lu-Hf foram realizadas por LA-ICPMS nestas duas últimas universidades.

7. Análise U-Pb e Lu-Hf de zircões detríticos das rochas paragnáissicas encaixantes, buscando caracterizar sua idade máxima de deposição e sua proveniência. A análise do espectro de idades U-Pb em zircão detrítico é uma técnica bastante utilizada e bem estabelecida para a análise de proveniência e idade das fontes de rochas sedimentares e metassedimentares (Fedo et al., 2003). As análises foram realizadas por LA-ICPMS no Laboratório de Geoquímica Isotópica da Universidade Federal de Ouro Preto.

8. Análises isotópicas dos sistemas Sm-Nd e Rb-Sr de amostras das diversas rochas graníticas da região, para auxiliar na determinação de sua petrogênese, ambiência tectônica e natureza das fontes dos magmas. Estas análises são particularmente significativas devido ao fato dos diversos arcos magmáticos da região apresentarem características isotópicas radicalmente distintas nos dois sistemas, o que os torna uma ferramenta importantíssima para a identificação e compreensão da evolução dos arcos nesta região. Para o Arco Serra da Prata, Peixoto et al. (2017) apresentaram dados de $\varepsilon Nd_{(t)}$ = -3 a +5 e T_{DM} = 1,7–0,9 Ga, com $^{87}Sr/^{86}Sr(t)$ entre 0,7061 e 0,7113; para o arco Rio Negro, Tupinambá et al. (2011) apresentaram dados de $\varepsilon Nd_{(t)}$ = -3 a +5 e idades-modelo T_{DM} principalmente em 1,0, 1,3 e 1,8 Ga, com $^{87}Sr/^{86}Sr_{(t)}$ abaixo de 0,705; e para o Arco Rio Doce, Tedeschi et al. (2016) compilaram dados de diversos autores que mostram $\varepsilon Nd_{(t)}$ entre -5,7 e -7,8, idades-modelo T_{DM} entre 1,28 e 1,68 Ga, e $^{87}Sr/^{86}Sr_{(t)}$ entre 0,7059 e 0,7118. As análises apresentadas nesta tese de doutorado foram realizadas no Laboratório de Geocronologia da Universidade de Brasília.

9. Redação da tese e dos artigos a serem submetidos para publicação, além da apresentação de trabalhos em eventos científicos.

I.5 Estrutura da tese

Este trabalho apresenta novos dados U-Pb (09 amostras LA-ICPMS e 05 amostras SHRIMP), Hf em zircão (109 análises), Nd-Sr em rocha total (13 amostras)

e geoquímicos de rocha total (72 amostras) que baseiam novas interpretações e modelos sobre a evolução geotectônica de rochas graníticas e paragnáissicas de alto grau encontradas na região sul do Estado do Espírito Santo, relacionadas ao Sistema Orogênico Araçuaí-Ribeira (AROS). A partir de dados de campo, petrográficos, geoquímicos, isotópicos e geocronológicos, procurou-se esclarecer questões sobre a constituição, gênese e interação dos diversos componentes tectônicos na zona de transição entre estes dois orógenos. Os resultados destes estudos são apresentados nesta tese principalmente sob a forma de artigos científicos. A tese se estrutura da seguinte forma:

Capítulo I: Introdução: Caracterização do problema e motivação da pesquisa, questões em aberto e relevância, os objetivos e a área de estudos.

Capítulo II: Contexto geológico do Sistema Araçuaí-Ribeira, com uma breve revisão sobre a geologia e evolução tectônica das duas unidades orogênicas.

Capítulo III: “Tonian island arc remnants in the northern Ribeira orogen of Western Gondwana: The Caxixe batholith (Espírito Santo, SE Brazil)”. Esse capítulo contempla o primeiro artigo da tese de doutorado, publicado no periódico *Precambrian Research* em 2020 (DOI: 10.1016/j.precamres.2020.105944)

Capítulo IV: “Detrital zircon U-Pb constraints on the age, provenance and tectonic setting of arc-related paragneissic units of the Araçuaí-Ribeira Orogenic System (AROS) high-grade core in the southern Espírito Santo State, Eastern Brazil”. Esse capítulo contempla o segundo artigo da tese de doutorado, submetido ao periódico *Journal of South American Earth Sciences*.

Capítulo V: “Preservation of pre-collisional accretionary systems as megaxenoliths and roof pendants through multiple partial melting episodes: 360 Ma of orogenic magmatism in the composite Caxixe batholith, Araçuaí-Ribeira orogenic system of western Gondwana”. Este capítulo contempla o terceiro artigo da tese, que será submetido para periódico especializado após as considerações da banca.

Capítulo VI: Conclusões gerais: apresenta a síntese das conclusões encontradas nos estudos apresentados.

I.6. Fontes financiadoras da tese

Os trabalhos de campo e análises desenvolvidas nesta tese foram possíveis devido ao apoio financeiro e logístico das seguintes fontes: Laboratório de

Geotectônica, Geodiversidade e Mapeamento Geológico (Geo3) do CPMTC-IGC-UFMG, Projeto MOBILE (geolifemobile.com), Instituto Serrapilheira (Serra-1912-31510), bolsas de produtividade em pesquisa do orientador e do co-orientador no CNPq.

CAPÍTULO II

SÍNTESE DO CONTEXTO GEOLÓGICO DO SISTEMA OROGÊNICO ARAÇUAÍ-RIBEIRA (AROS)

II.1. Descrição geral do segmento norte da Província Mantiqueira

A Província Mantiqueira desenvolveu-se durante o Ciclo Orogênico Brasiliano/Panafricano, cuja evolução é principalmente caracterizada por episódios diacrônicos de subducção e de colisão do tipo arco-continente e continente-continente (ex. Heilbron et al., 2004). O segmento setentrional da Província Mantiqueira é composto pelo Sistema Orogênico Araçuaí - Ribeira (AROS), caracterizado por um magmatismo pré-colisional de arco magmático juvenil (860 a 620 Ma – arcos Serra da Prata e Rio Negro; Tupinambá et al., 2011; Peixoto et al., 2017; Santiago et al., 2020b; Decol et al., 2021) e por um arco magmático continental (ca. 630 - 580 Ma – Arco Rio Doce; Heilbron et al., 2013; Gonçalves et al., 2016; Tedeschi et al., 2016; Corrales et al., 2020; Soares et al., 2020). A área de estudo (Fig. II.1) também é caracterizada por granitos e leucogranitos tipo S, associados ao estágio sin-colisional, em torno de 560 Ma (Pedrosa-Soares et al., 2008; Vieira e Menezes, 2015; Heilbron et al., 2016), além de um volumoso magmatismo pós-colisional, com idades entre 530 Ma e 490 Ma (Pedrosa-Soares et al., 2008). Unidades metassedimentares estão relacionadas ao arco Rio Doce, correspondendo a uma sequência metavulcano-sedimentar (Grupo Rio Doce; Vieira, 2007; Novo, 2013; Novo et al., 2018) e complexos metamórficos de alto grau (fácies anfibolito alto a granulito) compostos por paragnaisses migmatíticos (complexos Jequitinhonha e Nova Venécia; Noce et al., 2004; Vieira, 2007; Gradim et al., 2014; Moraes et al., 2015; Richter et al., 2016; Gonçalves-Dias et al., 2016; Pacheco et al., 2020).

Outras sequências metassedimentares são interpretadas como relacionadas ao arco toniano Serra da Prata (ca. 860-840 Ma; Peixoto et al., 2017) e ao arco criogeniano Rio Negro (ca. 790-600 Ma; Tupinambá et al., 2012). O Grupo Italva (ca. 848 Ma; Heilbron & Machado 2003, Sad & Dutra 1988, Peixoto & Heilbron 2010, Peixoto et al. 2017) consiste em gnaisses intercalado com mármores e anfibolitos, associado ao desenvolvimento do arco magmático Toniano da Serra da Prata (Peixoto et al. 2017). O Grupo São Fidelis (Tupinambá et al., 2012; Lobato et al.,2015;

Fernandes et al., 2015; Heilbron et al., 2017) representa outra sequência supracrustal que compreende paragnaisses migmatíticos a silimanita, granita e biotita, localmente com cordierita e grafita, com lentes e boudins de rocha calcissilicática, quartzitos puros ou feldspáticos e anfibolito.

O sistema orogênico apresenta estruturas tectônicas em tramas de direções NE-SW a N-S (Pedrosa-Soares e Wiedemann-Leonardos, 2000), registrando fases deformacionais relacionadas ao evento orogênico Brasiliano/Pan Africano. A zona de transição entre o orógeno Ribeira setentrional, ao sul, e o orógeno Araçuaí, ao norte, é marcada por uma mudança na tendência estrutural brasiliana de NE-SW para N-S (Heilbron et al., 2004, 2008). Os principais elementos tectônicos da região são as zonas de cisalhamento transcorrentes a transpressivas de direções NE-SW a NNE-SSW, como as zonas de Cisalhamento Guaçuí, Batatal e Além Paraíba, que estão associadas a uma foliação milonítica relacionada a escape lateral orogênico no estágio colisional tardio (Cunningham et al., 1998; Alkmim et al., 2006; Heilbron et al., 2004, 2008). Juntamente com as estruturas brasilianas ocorrem lineamentos de direções NW-SE a NNW-SSW relacionados a zonas de fraturas ou a falhas como os lineamentos Alegre, Colatina e Piúma (Novais et al., 2003; Calegari et al., 2016; Lourenço et al., 2016). Ao longo desses lineamentos são documentados diques toleíticos e alcalinos de idade cambriana a mesozoica (Santiago et al., 2020a).

II.2. Orógeno Araçuaí

O Orógeno Araçuaí situa-se entre o limite leste do Cráton do São Francisco e o Oceano Atlântico, entre os paralelos 15º e 21º S, e tem a Faixa Congo Ocidental como contraparte no sudoeste africano (Pedrosa-Soares et al. 2001, 2008) (Fig. II.2) englobando um conjunto de componentes geotectônicos que caracterizam um orógeno colisional sucessor de um orógeno acrescionário de margem continental ativa. Estes componentes são, por exemplo, depósitos de margem passiva, lascas ofiolíticas, zona de sutura, arco magmático, granitos sin-colisionais e plutonismo pós-colisional (Pedrosa-Soares et al., 2007).

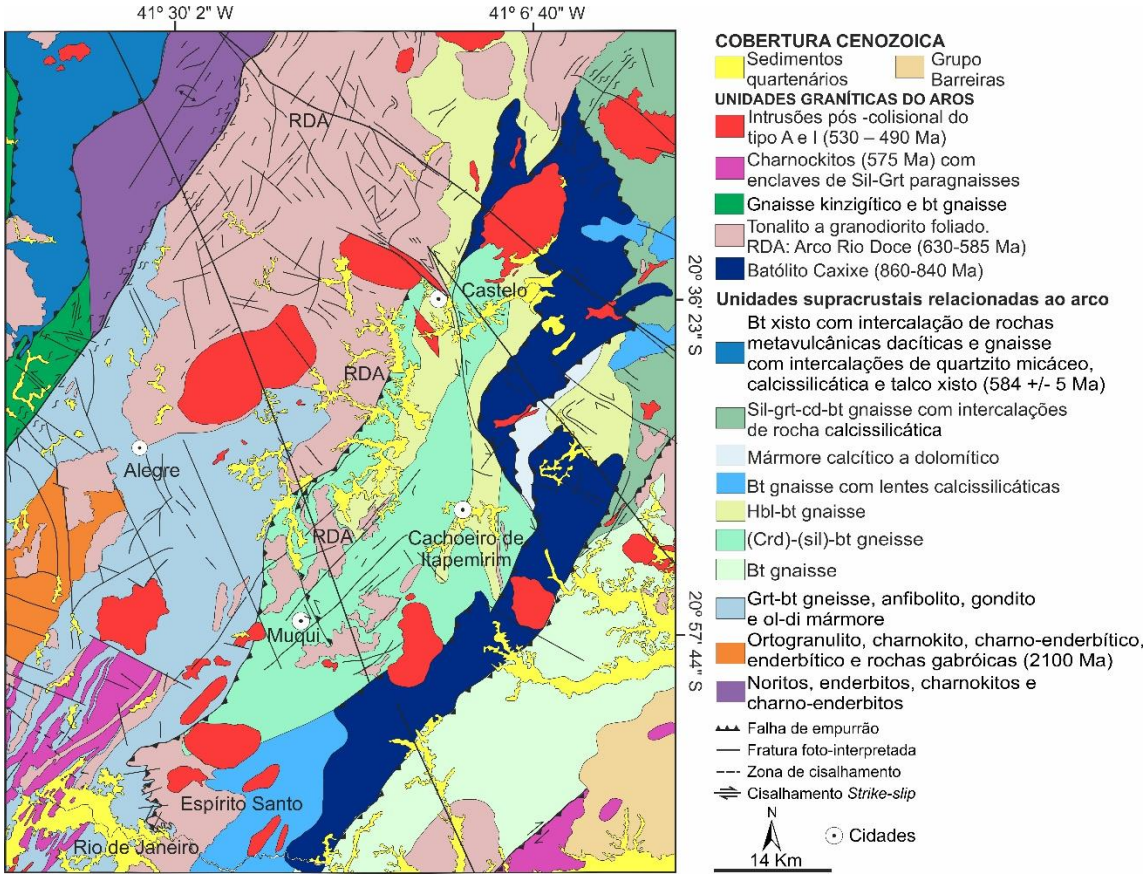

Fig. II. 1- Mapa geológico (modificado de Vieira et al., 2014 e Santiago et al., 2020b) da área de estudo, com foco no batólito Caxixe e suas unidades vizinhas. Arco Rio Doce (RDA); Sillimanita (Sil); Granada (Grt); Cordierita (Crd); Biotita (Bt); Hornblenda (Hbl); Olivina (ol); Diopsídio (di).

Após descobertas de remanescentes ofiolíticos neoproterozoicos por Pedrosa-Soares et al. (1992, 1998), de rochas plutônicas interpretadas como parte de um arco magmático Ediacarano da “Suíte Galiléia” e correlatos (Nalini, 1997; Pinto et al., 1997; Aracema, et al., 2000; Novo, 2009), além de outros componentes tectônicos característicos, adotou-se a concepção de orógeno confinado, no qual a bacia precursora do orógeno formou-se por uma reentrância parcialmente oceanizada no Cráton São Francisco (Pedrosa-Soares & Wiedemann-Leonardos, 2000). Esse confinamento decorre do fato de terem os crátons do São Francisco e do Congo permanecido ligados desde o Paleoproterozóico até a abertura do Atlântico Sul, no Cretáceo, por meio de uma “ponte continental”, posicionada na altura da Bahia (Brasil) e do Gabão (África) (Pedrosa-Soares et al., 2007). Em função do seu confinamento, o mecanismo determinado para a evolução do Orógeno Araçuaí-Congo Ocidental durante o Brasiliano seria semelhante ao do fechamento de um quebra-nozes, dinamizado por colisões à distância (Alkmim et al., 2007).

Fig. II. 2 - Orógeno Araçuaí na região central do Paleocontinente Gondwana. FA, traços estruturais da Faixa de Dobramentos Araçuaí; ZI, zona de interferência do Orógeno Araçuaí com o Aulacógeno do Paramirim (Pedrosa-Soares, et al. 2007). A região de estudo é indicada aproximadamente pelo retângulo preto.

A partir dessa configuração, Alkmim et al. (2006) propuseram um modelo de evolução tectônica composto por cinco estágios: i) formação da bacia precursora Macaúbas; ii) convergência inicial; iii) colisional; iv) escape lateral da porção sul; e v) colapso gravitacional.

Estágio i: abertura da bacia precursora do Orógeno Araçuaí teve início com o magmatismo da fase rifte, representado pelos diques máficos da Suíte Pedro Lessa (906 ± 2 Ma, U-Pb TIMS, zircão e badeleíta; (Machado et al., 1989) e granitos do tipo-A da Suíte Salto da Divisa (875 ± 9 Ma, U-Pb SHRIMP, zircão; Silva et al., 2002, 2007). Tal evento extensional foi uma reativação do sistema rifte Espinhaço de ca. 1,75 Ga, abrindo a bacia Macaúbas progressivamente de sul para norte (Figura II.3A) configurando um golfo oceanizado na metade meridional (Fig. II.3B) e ensiálico na contraparte setentrional do orógeno (Fig. II.3C).

Posteriormente, Pedrosa-Soares e Alkmim (2007) refinaram o modelo de abertura da bacia Macaúbas e propuseram seis eventos principais de rifteamento na região onde o orógeno Araçuaí se formaria: os eventos E1 (Estateriano, 1,77-1,7 Ga), E2 (Calimiano, 1,57-1,5 Ga), E3 (Esteniano, 1,18 - ? Ga), E4 (no limite Esteaniano-Toniano, ca. 1 Ga), E5 (Toniano, 930-850 Ma) e E6 (Criogeniano, 750-670 Ma). Desta

forma, o evento Toniano de abertura de bacias discutido por Alkmim et al. (2006) seria seguido por um evento criogeniano, E6, evidenciado pela Província Alcalina do Sul da Bahia entre 735 e 675 Ma, e pelo vulcanismo félsico La Louila (≤ 713 Ma) do sudoeste do Gabão

Nesta fase seguiu-se o preenchimento da pilha sedimentar da margem continental passiva, com extensos registros no domínio externo do orógeno Araçuaí, representados pelas unidades proximais do Grupo Macaúbas, como a unidade superior da Formação Chapada Acauã, a Formação Ribeirão da Folha, e lascas tectônicas de rochas máficas e ultramáficas ofiolíticas (Pedrosa-Soares et al., 2007). Estas lascas foram recentemente datadas pelo método U-Pb SHRIMP em zircões recuperados de plagiogranitos oceânicos em 645 ± 10 Ma (Amaral et al., 2020).

Estágio ii: dado o caráter confinado do orógeno e a configuração restrita da bacia Macaúbas, a força motriz para proporcionar subducção e consequentemente seu fechamento, se proveniente apenas das forças gravitacional e de arrasto astenosférico localizado, seria insuficiente. Segundo Alkmim et al. (2006), tal fechamento foi forçado, induzido à distância em consequência de colisões envolvendo a península São Francisco e a placa Paraná ou Rio de La Plata, por volta de ca. 630 Ma.

Considera-se, também, que a rotação e o fechamento do “quebra-nozes” foram facilitados por vários pontos pivô fixos situados nos aulacógenos (Paramirim, Pirapora e Sangha) gerados na etapa de abertura (Fig.II.3A) Estes aulacógenos serviram como eixos de rotação na etapa de fechamento e passaram por vários níveis de inversão tectônica durante esse processo.

A instalação do arco magmático pré-colisional representado pela suíte G1 (Arco Rio Doce; 630 - 580 Ma) e as rochas vulcânicas do Grupo Rio Doce caracterizam o início da fase de convergência e subducção no setor meridional (Fig. II.4A e B). A norte instalou-se uma frente de empurrões dos sedimentos de margem passiva distal e posteriormente, acumulação de leques turbidíticos da Formação Salinas (Fig. II.4C). A Suíte G1 é constituída majoritariamente por tonalitos e granodioritos, com fácies e autólitos dioriticos e máficos, portadores de xenólitos de rochas metassedimentares (Pedrosa-Soares et al., 2007; Tedeschi et al., 2016; Soares et al., 2020).

Estágio iii: Com o contínuo fechamento iniciando-se a norte e avançando progressivamente para o sul, tem-se a inversão tectônica da bacia oceânica e a formação de um cinturão de dobramentos e cavalgamentos com vergência para leste

do lado africano e para oeste do lado sul-americano. Nesta fase é impresso o metamorfismo relacionado às paragêneses que materializam a foliação regional (Pedrosa-Soares et al., 2001, 2008; Alkmim et al., 2006, 2007). É gerado grande volume de granitos do tipo S (com granada onipresente e cordierita e/ou sillimanita frequentes), a partir da fusão parcial de protólitos sedimentares aluminosos pertencentes ao golfo Macaúbas (suíte G2 - Pedrosa-Soares et al., 2007; Alkmim et al., 2007).

Posteriormente, no estágio tardi-colisional, tem-se a granitogênese G3. As rochas típicas desta suíte são leucogranitos resultantes da fusão autóctone e parautóctone da suíte G2 com granada e/ou cordierita, pobres em mica e livres da foliação regional (Pedrosa-Soares et al., 2008).

Estágio iv: nesta etapa (Fig. II.5A) tem-se a máxima aproximação entre o extremo sul da península São Francisco e a margem do continente do Congo. Devido ao grande espessamento crustal e a conformação do fechamento em formato de quebra-nozes, o resultado foi o escape de material para sul por grandes zonas de cisalhamento destrais.

Estágio v: o estágio pós-colisional é marcado por granitogênese oriunda do colapso gravitacional, livre de foliação regional, representada pelas suítes G4 e G5. Tal mecanismo é explicado através da ação da força peso exercida pela litosfera muito espessa com grandes elevações com alto potencial gravitacional. Estes elementos levam ao fluxo lateral da sua porção basal e posterior abatimento das porções superiores, acomodado por sistemas de zonas de cisalhamento (Fig. II.5B). A suíte G4 é composta por granitos a duas micas que, localmente, preservam cúpulas de granito pegmatoide ou raízes de biotita granito (Pedrosa-Soares et al., 2007). As rochas da suíte G5 são plútons zonados com evidências de mistura magmática (*mingling* e *mixing*). Possuem foliação de fluxo ígneo bem marcada e composição granítica a charno-enderbítica, além de termos noríticos e gabróicos (Wiedemann-Leonardos et al., 2000; Pedrosa-Soares & Wiedemann-Leonardos, 2000, 2001).

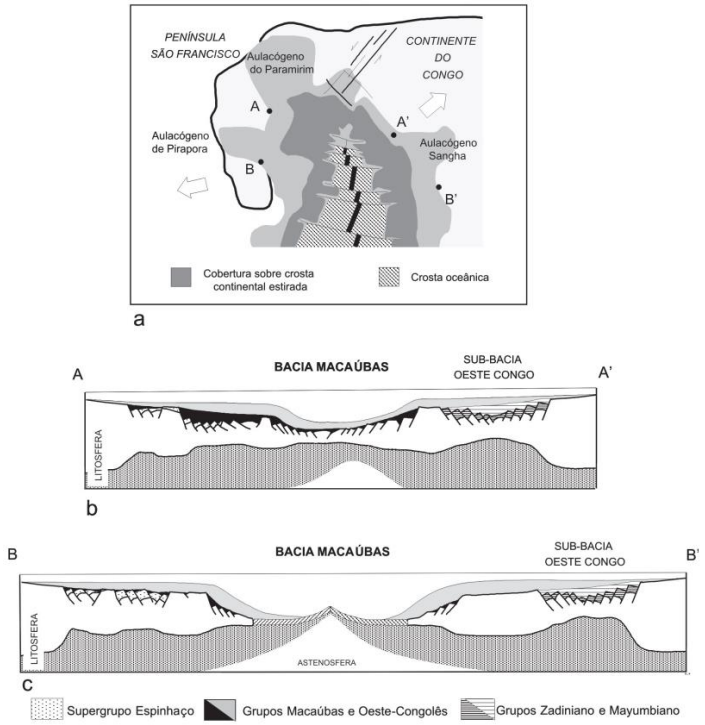

Fig. II. 3 - Configuração da bacia Macaúbas, precursora do Orógeno Araçuaí a ca. 700 Ma. Legenda: A - Elementos tectônicos visto em mapa. B - Seção através do setor setentrional ensiálico. C - Seção através do setor meridional oceânico (Alkmim et al., 2007).

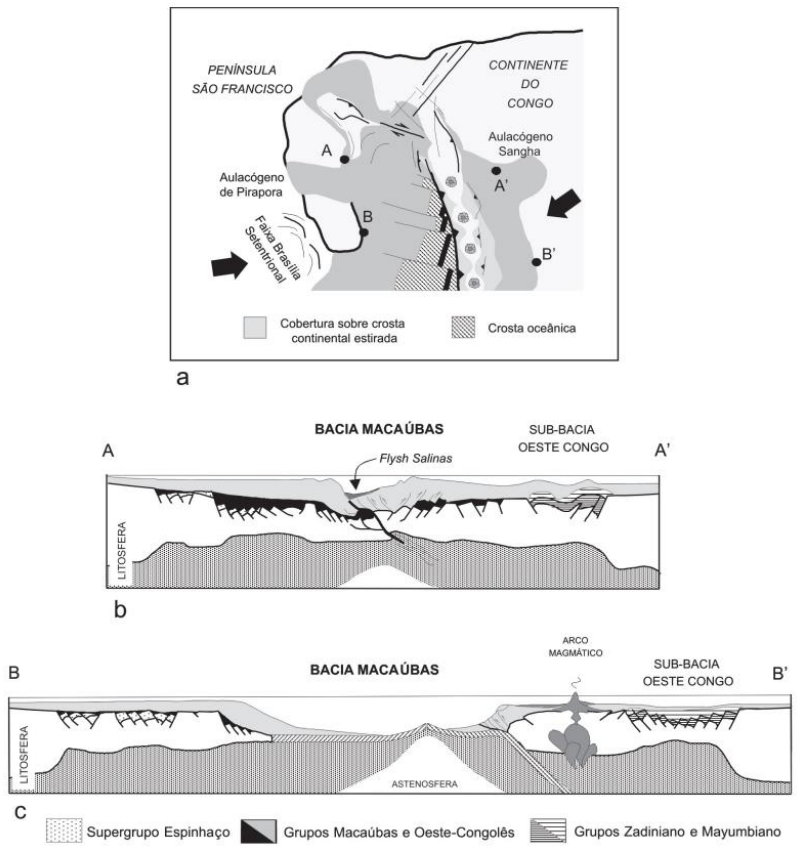

Fig. II. 4 - Configuração da bacia Macaúbas, precursora do Orógeno Araçuaí por volta de 600 Ma na fase de convergência inicial. Legenda: A - Elementos tectônicos visto em mapa. B -

Seção através do setor setentrional ensiálico. C - Seção através do setor meridional oceânico (Alkmim et al., 2007).

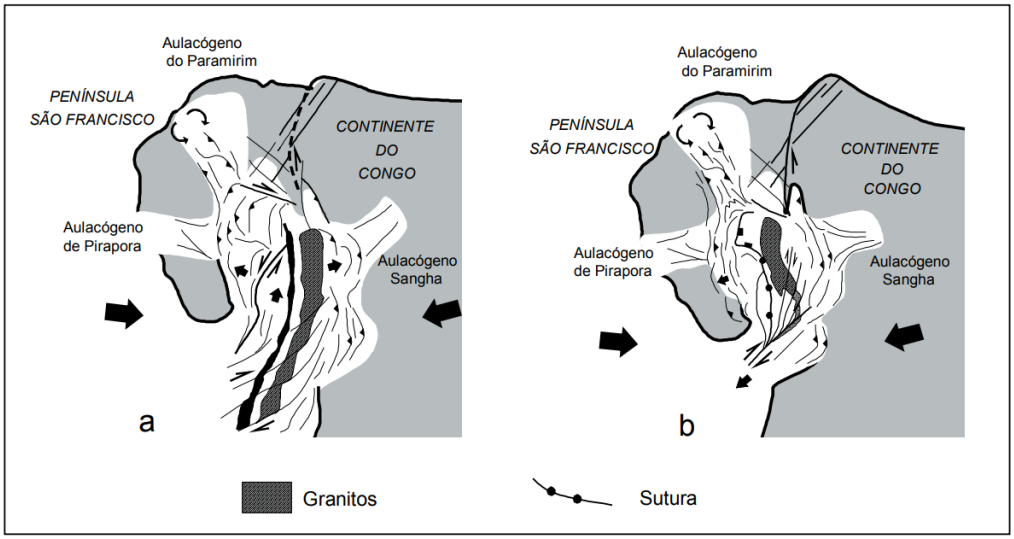

Fig. II. 5 - Estágios (a) colisional, por volta de ca. 560 Ma e (b) de colapso gravitacional após escape lateral da porção sul do Orógeno por volta de 500 Ma (Alkmim et al., 2007).

Alkmim et al. (2007) subdividiram o Orógeno Araçuaí em dez compartimentos tectônicos (Fig. II.6), os quais se distinguem em função da orientação espacial, significado cinemático e história de nucleação das estruturas dominantes. A área de estudo desta tese é inserida no Núcleo Cristalino, que é o mais extenso e o mais complexo compartimento do Orógeno Araçuaí e também, o que carece de mais estudos (Alkmim et al., 2007). O Núcleo Cristalino é constituído por: i) embasamento paleoproterozóico (Complexo Juiz de Fora), com metamorfismo na fácies anfibolito alto a granulito, ii) suítes graníticas pré a pós-colisionais (G1 a G5), iii) complexos paragnáissicos (ex.: Complexo Paraíba do Sul) e iv) o Grupo Rio Doce, ambos relacionados aos sedimentos oriundos do arco magmático acrescionário do orógeno (Alkmim et al., 2007). A porção meridional deste compartimento é caracterizada por extensas zonas de cisalhamento destrógiras de direção NNE (Trompette et al., 1993) dentre elas as zonas de cisalhamento de Abre Campo, Manhuaçu, Guaçuí e Batatal, sendo a zona de Abre Campo considerada uma zona de sutura tanto paleoproterozoica quanto neoproterozoica (Campos Neto & Figueiredo, 1995; Cunningham et al., 1998; Brueckner, 2000; Pedrosa-Soares et al., 2007).

A zona de Cisalhamento Guaçuí (ZCG), formada entre 560-530 Ma, é a mais expressiva estrutura nas adjacências da área de estudo. Constitui-se praticamente de um segmento único e se estende por um total de 350 km na direção NE-SW, com

foliação milonítica verticalizada. A movimentação é dextral, indicada por porfiroclastos milimétricos de feldspato. Na porção sul da ZCG, esta passa a se confundir com a Zona de Cisalhamento Além Paraíba do Orógeno Ribeira. Na mesma porção, esta ZC foi desenvolvida nas condições metamórficas de fácies anfibolito a granulito. Outra zona de cisalhamento também característica da área é a Zona de Cisalhamento Batatal, que se constitui, também, de um único segmento com cerca de 70 km de extensão. A norte, ela desaparece ao interceptar o lineamento de Vitória e ao sul, ela está truncada pelo pluton de Rio Novo. Foi desenvolvida sob condições metamórficas da fácias xisto verde a anfibolito, entre 560-520 Ma. Essas zonas de regime destral teriam sido geradas pela reativação de zonas reversas pré-existentes (Silva, 2010), sob a atuação da tectônica do tipo “Quebra-Nozes” (Alkmim et al., 2006, 2007).

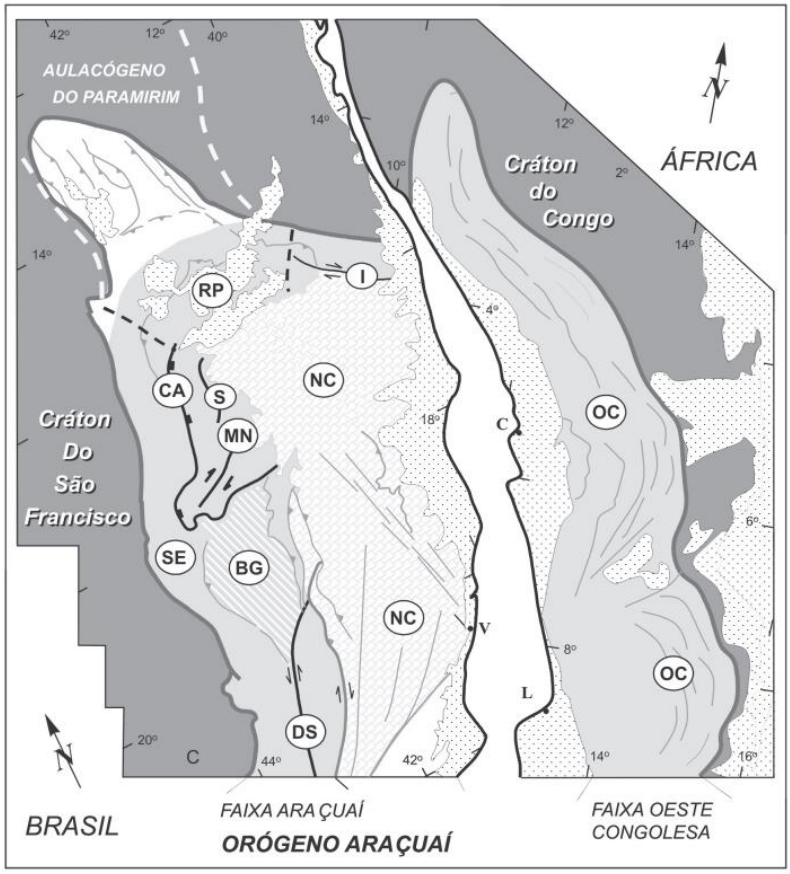

Fig. II. 6 - Compartimentos tectônicos do Orógeno Araçuaí-Congo Ocidental. V - Vitória, L - Luanda e C - Cabinda. SE - Cinturão de Cavalgamentos da Serra do Espinhaço Meridional; CA - Zona de Cisalhamento da Chapada Acauã; S - zona de dobramentos de Salinas; MN - Corredor Transpressivo de Minas Novas; RP - saliência do Rio Pardo e sua zona de interação com o Aulacógeno Paramirim; BG - Bloco Guanhães; DS - Zona de Cisalhamento Dom Silvério e estruturas associadas; I - Zona de Cisalhamento Itapebi e estruturas associadas; NC - núcleo cristalino (i.e., a zona interna, de alto grau, que representa o núcleo do orógeno); e OC - Cinturão Oeste-Congolês (Alkmim et al.,2007).

II.3. Orógeno Ribeira

O Orógeno Ribeira (Fig. II.7, Fig. II.8) é definido como um sistema de tendência estrutural marcante NE-SW, que resultou da interação colisional entre o paleocontinente São Francisco-Congo com a parte sudoeste do Cráton de Angola (Campos Neto 2000; Trouw et al., 2000; Heilbron et al., 2000).

A compartimentação tectônica proposta para o Orógeno Ribeira na sua porção setentrional compreende quatro terrenos tectono-estratigráficos (*sensu* Howell, 1995) desenvolvidos durante as várias etapas da Orogênese Brasiliana. São eles: (i) Terreno Ocidental, representando a margem retrabalhada do Cráton São Francisco; (ii) Terreno Paraíba do Sul; (iii) Terreno Oriental e (iv) Terreno Cabo Frio (Heilbron et al. 2000, 2004a; Trouw et al. 2000). Estes terrenos e seus respectivos domínios estão separados por importantes zonas de cisalhamento dúcteis com componente transpressivo destral. Para Heilbron & Machado (2003), a compartimentação tectônica no início da convergência brasiliana teria resultado em transporte tectônico em direção ao cráton do São Francisco, com a formação de dobras associadas à formação de foliação penetrativa. Esta compartimentação tectônica regional foi modificada pelas fases de deformação tardias, através de megadobramento em escala regional, destacando-se aí a Megassinforma do Rio Paraíba do Sul (Heilbron et al., 1991) e a Megantiforma do Rio de Janeiro, ou através de zonas de cisalhamento verticais importantes como a do Rio Paraíba do Sul (Chrispim & Tupinambá, 1989; Almeida, 2000).

Os terrenos e seus domínios estruturais são separados por importantes zonas de cisalhamento dúcteis com componente inverso e transpressivo destral, geradas durante a deformação principal (Heilbron 1993; Heilbron et al. 1998, 2000, 2004a; Almeida 2000). A deformação possui um padrão complexo, e muitas vezes uma mesma zona de cisalhamento passa de empurrão para zona transcorrente destral ao longo do strike, indicando convergência oblíqua (Heilbron 1993).

O Contato Tectônico Central (CTB – *Central Tectonic Boundary*) é uma grande descontinuidade que separa o terreno Oriental do terreno Ocidental, sendo considerada a zona de sutura entre estes terrenos. Está associado à convergência destas duas unidades com subducção e consumo de litosfera oceânica para leste levando ao desenvolvimento do Arco Magmático Rio Negro e a posterior colisão continental. O CTB (Almeida et al., 1998) é uma zona de cisalhamento dobrada que

apresenta uma complexa evolução estrutural (Heilbron et al., 2013).

O Terreno Ocidental, constituído pelos os domínios tectônicos Juiz de Fora e Andrelândia, apresenta intercalação tectônica entre as rochas do embasamento pré-1,8 Ga (Complexo Juiz de Fora) e as rochas metassedimentares neoproterozóicas da Megasseqüência Andrelândia, ambos metamorfisados em fácies granulito. O domínio Juiz de Fora compreende granulitos gnaissificados de origem ígnea com composição variando entre termos gabróicos a granodioríticos cujos protólitos incluem granitoides cálcio-alcalinos representantes de arco magmático cordilheirano e de arco de ilhas, e granitos colisionais (2,14 e 2,07 Ga, Heilbron et al.; 2003). O domínio Andrelândia é representado por uma sequência metassedimentar composta por rochas de composição pelítica a semipelítica com intercalações de lentes de quartzitos e de rochas calcissilicáticas e apresenta idades U-Pb em zircão detrítico entre 1,0 e 0,79 Ga (Ribeiro et al., 1995; Söllner & Trouw, 1997).

O terreno Paraíba do Sul é uma estrutura sinformal que se encontra sobre o domínio de Juiz de Fora e é composto por ortognaisses paleoproterozoicos e rochas metassedimentares, ambos em fácies anfibolito médio. Os primeiros compreendem hornblenda-biotita gnaisses de composição tonalítica a granodiorítica, enquanto as unidades metassedimentares incluem mármore dolomítico, biotita-granada gnaisse (com camadas de mármore, biotita-sillimanita xisto, rochas de cálcio-silicáticas e raro quartzito feldspático) e biotita-moscovita xisto comumente com granada e sillimanita. O mármore é característico desta unidade, em contraste com os domínios Andrelândia e Juiz de Fora, que incluem principalmente quartzitos e raramente rochas calcissilicáticas (Heilbron et al., 2003). Segundo Heilbron (2008) a colisão deste terreno com a placa São-franciscana ocorreu por volta de 620-580 Ma.

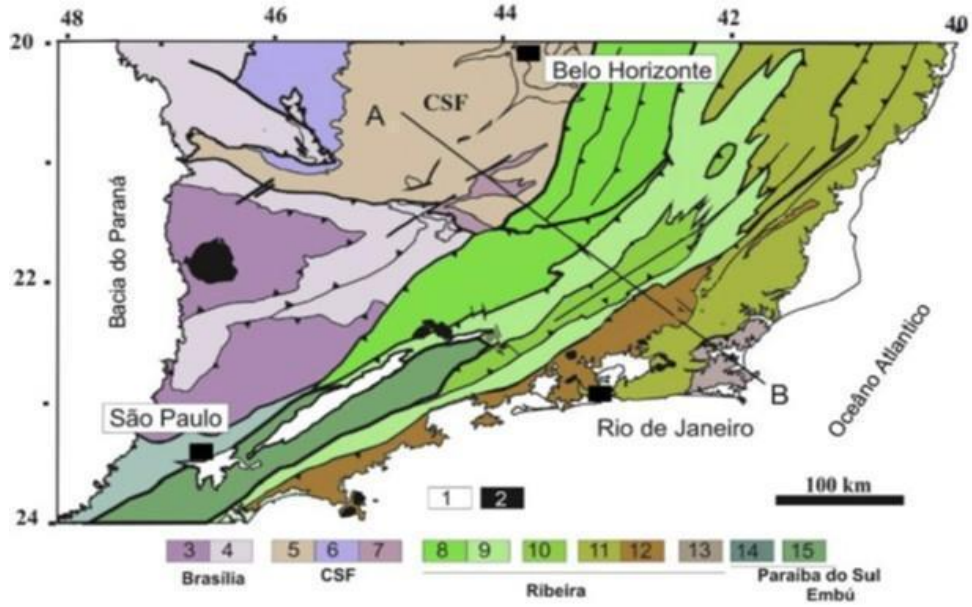

Fig. II. 7 - Organização tectônica do Orógeno Ribeira. 1 – Cobertura Cenozoica; 2 – Rochas alcalinas Cretáceo-Paleogênicas; 3 e 4 – Cinturão Brasília Sul; 5 a 7 – Cráton São Francisco: 5 – Embasamento, 6 – Grupo Bambuí, 7 – Rochas metassedimentares autóctones; 8 a 15 – Orógeno Ribeira: 8 e 9 – terreno Ocidental, domínios Andrelândia e Juiz de Fora; 10 – terreno Paraíba do Sul; 11 e 12: terreno Oriental, 11 – rochas de arco magmático; 12 – rochas metassedimentares; 13 – terreno Cabo Frio; 14 – terreno Embú; 15 – terreno Apiaí. Retirado de Heilbron et al. (2013).

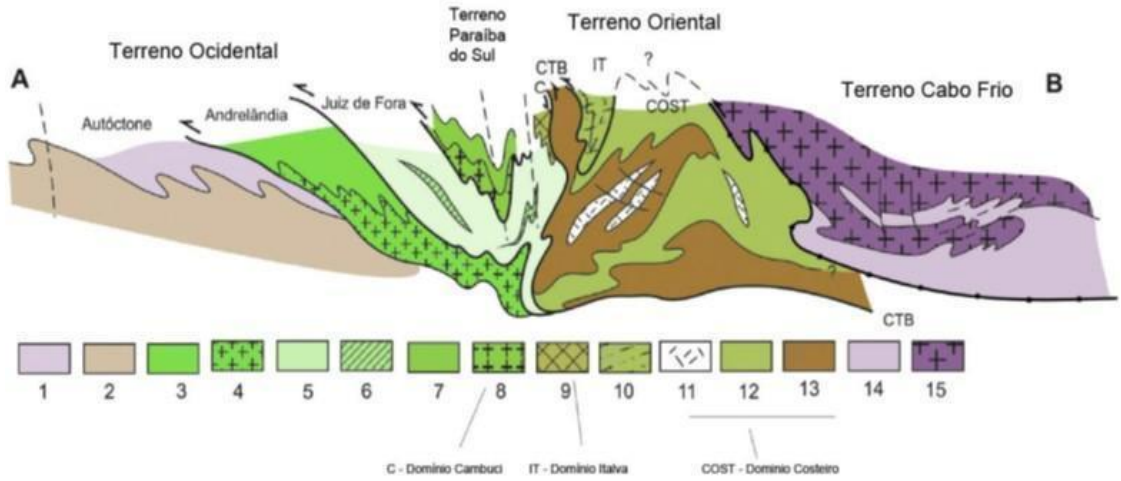

Fig. II. 8 - Seção transversal regional contendo os domínios do Terreno Oriental. 1 – Rochas metassedimentares neoproterozoicas autóctones; 2 – embasamento autóctone; 3 a 6: terreno Ocidental: 3 a 5 – Grupo Andrelândia (alóctone); 4 e 6 – embasamento alóctone, ortognaisses e ortogranulitos; 7 e 8 – terreno Paraíba do Sul: 7 – rochas metassedimentares do Complexo Paraíba do Sul; 8 – ortognaisses do complexo Quirino; 9 a 13 – terreno Oriental: 9 – rochas relacionadas ao arco Serra da Bolívia no domínio Cambuci; 10 – Grupo Italva com rochas relacionadas ao arco Serra da Prata; 11 – leucogranitos; 12 – rochas metassedimentares; 13 – rochas relacionadas ao arco Rio Negro no domínio Costeiro; 14 – rochas metassedimentares da orogenia Búzios; 15 – rochas do embasamento da Região dos Lagos no terreno Cabo Frio; CTB – Contato Tectônico Central. Retirado de Heilbron et al. (2013).

O terreno Oriental consiste em três domínios estruturais imbricados para NW, caracterizados por um conjunto de três arcos magmáticos Neoproterozóicos: a) o arco magmático Serra da Bolívia associado ao Domínio Cambuci (Tupinambá et al., 2007; Heilbron et al., 2013); b) o arco magmático Rio Negro alojado no Domínio Costeiro (Tupinambá et al., 2000b; Tupinambá et al., 2012) e; c) o complexo Serra da Prata pertencente ao Domínio Italva (Peixoto, 2010; Peixoto et al., 2017).

O domínio Cambuci é interpretado como uma sucessão metassedimentar correspondente a uma associação de antearco, relacionado ao arco magmático Serra da Bolívia, que tem sido correlacionado ao arco magmático Rio Doce do orógeno Araçuaí (Supersuite G1, Nalini-Junior et al., 2000, 2005; Pedrosa Soares et al., 2008; Heilbron et al., 2013; Tedeschi et al., 2016; Degler et al., 2017, Soares et al., 2020, Corrales et al., 2020), bem como ao arco magmático Socorro do orógeno Brasília Sul (Hackspacher et al., 2003; Campos Neto, 2000; Janasi et al., 2001), sendo considerados como integrantes do Terreno Paraíba do Sul-Embu.

O Domínio Costeiro compreende sucessões metassedimentares de alto grau metamórfico pertencentes ao Grupo São Fidélis, intrudidas por ortognaisses do arco magmático Rio Negro, bem como por várias gerações de granitoides mais jovens (Heilbron & Machado, 2003; Heilbron et al. 2003; Tupinambá et al., 2007, 2012). O Grupo São Fidélis é constituído por uma unidade basal, composta de silimanita-granada-biotita gnaisse em fácies granulito, relativamente homogêneo, e uma unidade superior que consiste em gnaisses pelíticos com lentes de quartzito, calciossilicáticas e anfibolitos, ambas intrudidas por ortognaisses do arco Rio Negro (Tupinambá et al., 2012; Lobato et al., 2015; Fernandes et al., 2015). A distribuição geográfica do arco magmático Rio Negro se estende por mais de 500 Km entre a região serrana do Rio de Janeiro e sul Espírito Santo. Este consiste em hornblenda-biotita ortognaisses de composição tonalítica, diorítica e gabroica pertencentes a série calcialcalinos de baixo, médio, alto-K, além de associações shoshoníticas (Heilbron & Machado, 2003; Tupinambá et al., 2012; Martins et al., 2016).

O Domínio Italva, sobreposto ao Domínio Costeiro, se estende por cerca de 225 Km a partir da porção norte da região serra do estado do Rio de Janeiro seguindo para o estado do Espírito Santo. Sua estrutura interna compõe um sinformal com eixo com caimento para NE e superfície axial subvertical. Seu flanco norte é caracterizado por intensa deformação e interdigitação tectônica entre as rochas dos dois domínios (Heilbron et al., 2003). Este domínio inclui ortognaisses do Complexo Serra da Prata

associados a paragnaisses e a anfibolitos intercalados com mármores calcíticos (Menezes, 1975) do Grupo Italva, além de intrusões de leucogranito-gnaisses (Machado Filho et al., 1983; Sad & Donadello, 1980; Heilbron & Machado, 2003; Peixoto, 2008, 2010; Peixoto & Heilbron, 2010). O complexo Serra da Prata consiste em hornblenda-biotita ortognaisse de composição diorítica a tonalítica, frequentemente com enclaves máficos, intercalado com biotita ortognaisse granodiorítico (Peixoto, 2010; Peixoto & Heilbron, 2010; Peixoto et al., 2017). Dados geocronológicos publicados por Heilbron & Machado (2003) e Heilbron et al. (2012) datam 848 ± 11 Ma para um ortognaisse tonalítico do complexo Serra da Prata e cerca de 860 Ma para um anfibolito intercalado com mármores, respectivamente. Esta última é estimada como a idade mínima para a deposição carbonática do Grupo Italva. Posteriormente, Peixoto et al. (2017) apresentaram novos dados U-Pb indicando cristalização do complexo Serra da Prata entre 856–838 Ma. Estes dados demostram uma evolução tectônica Toniana para o Domínio Italva, em ambiente de subducção, precedendo o desenvolvimento do Domínio Costeiro e a evolução do arco magmático Rio Negro (Peixoto, 2010; Peixoto & Heilbron, 2010; Heilbron et al., 2012, 2013; Moraes, 2006; Ragatky et al., 2007; Sad & Dutra, 1988).

O estágio colisional há ca. 530-510 Ma foi responsável pela aglutinação do terreno Cabo Frio na porção leste do terreno Oriental e desencadeou o redobramento da foliação principal a partir de zonas de cisalhamento transpressivas destrais (Machado et al., 1996; Heilbron e Machado, 2003). Granitos tardios e pós-colisionais e as estruturas transpressivas registram um estágio de colapso tectônico do edifício orogênico entre ca. 513 e 480 Ma (Heilbron et al., 2013).

Ao longo dos anos, a partir dos estudos sistemáticos para a caracterização evolutiva do Orógeno Ribeira, diversas propostas de modelos de evolução tectônica foram apresentadas, como propostas de estrutura em flor positiva (Ebert et al., 1993), endentação, semelhante a cadeia Himalaiana (Vauchez et al., 1994), zona de subducção para NW com formação de arco magmático (Campos Neto & Figueiredo, 1990, 1995) e colisão continental oblíqua seguida de transcorrência destral (Heilbron et al., 2000; Trouw et al., 2000, Almeida, 2000; Heilbron & Machado 2003). Embora cada proposta tenha suas particularidades, a maioria advoga sobre colisões continentais com componente transpressivo seguido de transcorrência e escape lateral e/ou vertical. O modelo de Campos Neto & Figueiredo (1995) e Machado (1997) defende a ocorrência de dois sistemas orogênicos superpostos: um mais antigo (entre

700 e 600 Ma), denominado “Orogênese Brasiliana I”, e outro, mais novo (entre 590 e 480 Ma), denominado “Orogênese Rio Doce” com estágio colisional entre 560 a 530 Ma, na região entre os estados do Rio de Janeiro e Espírito Santo. Este modelo ainda prevê a formação de arcos magmáticos com crescente alcalinidade de SE para NW, sugerindo a existência de zona de subducção pra NW.

Heilbron & Machado (2003) postulam a colisão de pelo menos dois terrenos sobre a margem retrabalhada da placa São Franciscana e consequente formação de arco magmático. Nesse sentido o terreno Oriental, onde se encontra o arco magmático Rio Negro, foi o primeiro terreno a ser anexado à placa São Franciscana por volta de 580 Ma, tendo como sutura o CTB. Esta estrutura passa por reativações durante a evolução do Orógeno Ribeira, resultando em uma complexa zona milonítica dobrada. A arquitetura gerada a partir desses processos (localização do arco Rio Negro e polaridades estruturais e metamórficas) indicam zona de subducção para leste. Posteriormente, por volta de 535-510 Ma, tem-se a docagem do terreno Cabo Frio representando a segunda etapa de colisão, denominada orogenia Búzios (Schmitt et al., 2004).

O modelo tectônico evolutivo mais atual é proposto por Heilbron et al. (2013) e faz menção à amalgamação de três terrenos e seus respectivos arcos magmáticos (Heilbron et al., 2020): arco Serra da Bolívia (Heilbron et al., 2013) no domínio Cambuci, arco Rio Negro (Tupinambá et al., 1998; Tupinambá, 1999; Tupinambá et al., 2011) e arco Serra da Prata (Peixoto et al., 2017; Peixoto & Heilbron, 2010) no domínio Italva.

O arco Serra da Bolívia, diferentemente das outras duas associações de arcos, apresenta um caráter menos primitivo com assinaturas de arco cordilheirano. Possui idades U-Pb entre 623-575 Ma e é correlacionado ao arco magmático Rio Doce do orógeno Araçuaí (Supersuite G1, Nalini-Junior et al., 2000, 2005; Pedrosa Soares et al., 2008; Heilbron et al., 2013; Tedeschi et al., 2015; Degler et al., 2017; Soares et al., 2020; Corrales et al., 2020), bem como ao arco magmático Socorro do orógeno Brasília Sul (Hackspacher et al., 2003; Campos Neto, 2000; Janasi et al., 2001), formando um extenso conjunto de arcos cordilheiranos que intrudiram crosta paleoproterozoica (Heilbron et al., 2013). A associação dos arcos Rio Negro e Serra da Prata apresenta assinaturas juvenis, idades entre 860 e 620 Ma e longo período de geração crustal a partir de consumo de crosta oceânica (Heilbron et al., 2013; Peixoto et al., 2017). Os principais episódios colisionais que amalgamaram estes

arcos intraoceânicos e cordilheiranos além de seus respectivos terrenos ocorreram a ca. 650-620 Ma, ca. 620-580 Ma e ca. 580-560 Ma. A combinação de arcos magmáticos Tonianos com os arcos magmáticos mais novos de evolução Criogeniana/Ediacarana sugerem mais de 200 milhões de anos de subducção ao redor dos blocos cratônicos mais antigos que compunham o Gondwana Ocidental o que, por sua vez, é indicativo de um amplo e longo período de consumo de litosfera oceânica.

Com base na compilação detalhada dos estudos realizados por Heilbron & Machado (2003), Schmitt (2000), Peixoto & Heilbron (2010), Tupinambá et al., (2011), Heilbron et al., (2013), entre outros, a sequência evolutiva proposta para o segmento setentrional do orógeno Ribeira é descrita a seguir:

a) Rifte a Margem Passiva: a partir de 1,0 Ga, desenvolveram-se as sequências deposicionais nas margens leste do Terreno Ocidental (Grupo Andrelândia e correlatos) e na margem oeste do Terreno Oriental (sucessões metassedimentares do Domínio Costeiro).

b) Subducção da Placa São Franciscana: consumo de crosta oceânica e geração de magmatismo de caráter juvenil. Registros de arcos intraoceânicos a ca. 860 Ma (Serra da Prata - Peixoto & Heilbron, 2010; Peixoto et al., 2017) e ca. 790 - 620 Ma (Rio Negro - Tupinambá et al., 2011) intrudindo as sucessões metassedimentares do domínio Italva e Costeiro, respectivamente. Os autores sugerem polaridade da subducção para leste com consumo da placa São Franciscana sob o Terreno Oriental. À medida em que os arcos se instalavam, sucessões sedimentares eram depositadas nas bacias antearco (domínios Paraíba do Sul, em parte, e Cambuci) e retroarco (domínios Italva e Búzios) (Fig. II.9A).

c) Primeiro e segundo evento colisional (ca. 650-620 Ma e ca. 620-580 Ma) entre o paleocontinente São Francisco e o Terreno Oriental, com início da amalgamação dos arcos intraoceânicos e instalação do CTB. A deformação principal é transpressiva e está associada ao metamorfismo principal impresso nos litotipos dos dois terrenos (Neves, 2004). Contemporaneamente tem-se a geração do arco cordilheirano Serra da Bolívia (ca. 623-590 Ma) (Fig. II.9B).

d) Etapa colisional principal (ca. 580-560 Ma): amplo registro metamórfico nos dados U-Pb, magmatismo expressivo com geração de granitoides sin- a tardi-colisionais. Inicialmente predominam granitoides derivados da fusão do pacote metassedimentar, seguidos por granitoides metaluminosos derivados do

embasamento ortoderivado.

e) Fechamento da Bacia retroarco e Colagem do Terreno Cabo Frio (535-510 Ma). Desenvolvimento da orogenia Búzios (Schmitt et al., 2004). Os dados geológicos disponíveis sugerem que este episódio pode representar o registro do fechamento da bacia retroarco Italva-Búzios, que resultou no cavalgamento destes segmentos crustais sob o Terreno Oriental.

f) Colapso do Orógeno (510-480 Ma): evidenciado por granitoides livres de foliação regional, por vezes de composição bimodal, zonas de cisalhamento transtrativas subhorizontais, zonas de cisalhamento normais e dobras com vergência para leste (Heilbron & Machado 2003).

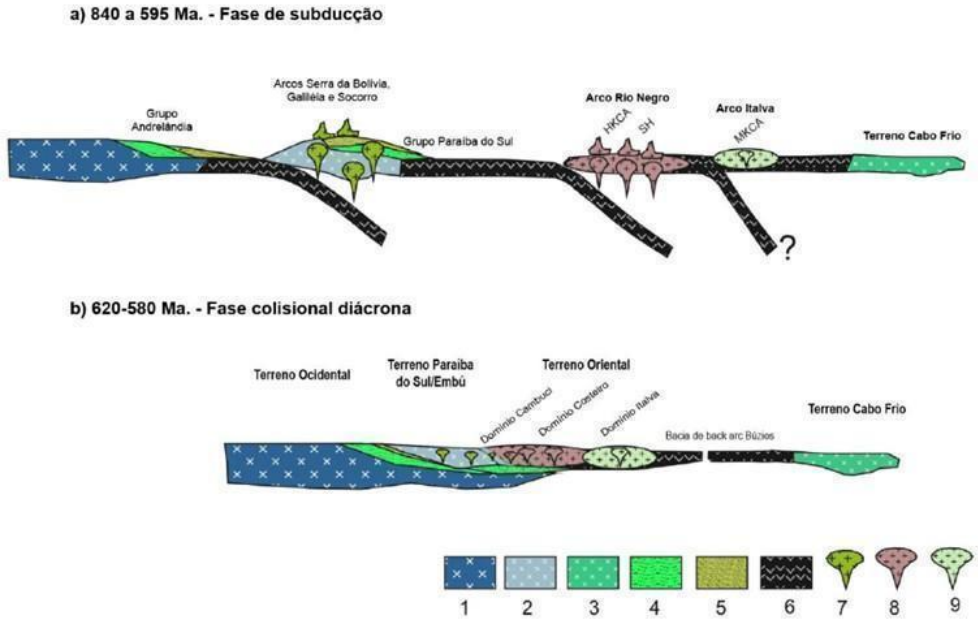

Fig. II. 9 - Modelo mostrando as fases de subducção e colisional diácrona do Orógeno Ribeira (Heilbron et al., 2013).

CAPÍTULO III

TONIAN ISLAND ARC REMNANTS IN THE NORTHERN RIBEIRA OROGEN OF WESTERN GONDWANA: THE CAXIXE BATHOLITH (ESPÍRITO SANTO, SE BRAZIL)

(artigo publicado no periódico *Precambrian Research*, Volume 351, Dezembro 2020, n. 105944, https://doi.org/10.1016/j.precamres.2020.105944)

Raíssa Santiago[a,*], Fabrício de Andrade Caxito[a,1], Antônio Carlos Pedrosa-Soares [a,1], Mirna Aparecida Neves[b], Elton Luiz Dantas[c,1]

a – Programa de Pós-graduação em Geologia and Centro de Pesquisas Manoel Teixeira da Costa, Universidade Federal de Minas Gerais (CPMTC-IGC-UFMG), Campus Pampulha, Av. Antônio Carlos 6627, 31270-901, Belo Horizonte, MG, Brazil.
b – Centro de Ciências Exatas, Naturais e da Saúde, Universidade Federal do Espírito Santo, Alto Universitário, s/nº - Guararema, 29500-000, Alegre, ES, Brazil.
c – Laboratório de Geocronologia, Instituto de Geociências, Universidade de Brasília, Asa Norte, 70910-900, Brasília, DF, Brazil.
* Corresponding author.
E-mail addresses: raissa.smendes@gmail.com (R. Santiago), caxito@ufmg.br (F.A. Caxito), pedrosasoares@gmail.com (A.C. Pedrosa-Soares), mirnaan@gmail.com (M.A. Neves), elton@unb.br (E.L. Dantas).
[1] Research fellow of the Brazilian Scientific Council (CNPq).

III.1 Abstract

The Tonian Serra da Prata magmatic arc is part of an association of several magmatic arcs of the Ribeira orogenic system in Southeastern Brazil. Along with the Cryogenian Rio Negro arc, the Serra da Prata arc represents an intra-oceanic arc system while the Ediacaran Rio Doce arc represents an active continental margin arc. Here, we characterize the northernmost segment of the Serra da Prata arc, based on lithochemical and isotopic (whole-rock Sm-Nd and Rb-Sr, and zircon U-Pb and Lu-Hf) data from the Caxixe batholith, located in Espírito Santo State. The Caxixe batholith mostly consists of granodioritic to granitic and minor tonalitic to gabbroic

rocks, with calc-alkaline, metaluminous to slightly peraluminous, magnesian, I-type signature and magmatic arc affinity. The rocks display LREE enrichment, positive to slightly negative Eu and negative Nb-Ta anomalies. Zircon U-Pb (LA-ICP-MS and SHRIMP) data reveal magmatic crystallization ages from 859±7 Ma to 847±8 Ma (for zircon cores) and a probably metamorphic age of 834±9 Ma (for zircon rims). Hf Isotopic data yield positive $\varepsilon Hf_{(t)}$ values between +10 and +14, and T_{DM} Hf model ages from 1.01 Ga to 0.84 Ga, in agreement with whole-rock Nd and Sr data, with $\varepsilon Nd_{(t)}$ values from +0.9 to +6.4and T_{DM} Nd model ages between 1.2 Ga and 0.8 Ga, and $^{87}Sr/^{86}Sr_{(i)}$ of 0.6979-0.7035. Our data characterize a juvenile magmatic arc with striking mantle contribution, formed on a supra-subduction intra-oceanic setting similar to modern island arcs. As a whole, the Serra da Prata juvenile arc points to a large ocean that underwent intra-oceanic subduction in the Early Tonian. As a corollary, the Angola, Congo – São Francisco and Paranapanema paleocontinental blocks should be far from each other during the Early Tonian, separated by that large ocean. In a broad scenario, involving ophiolites and juvenile arcs of southern and central Brazil, several cratons of Western Gondwana once had been parts of paleocontinental pieces separated by very extensive Tonian-Cryogenian oceanic realms, including the Neoproterozoic Goiás–Pharusian and Adamastor oceans.

Keywords: LA-ICPMS and SHRIMP U-Pb geochronology; Hf-Nd-Sr isotope geochemistry; Magmatic Arc; Adamastor Ocean; Brasiliano Orogeny; Plate tectonics.

III.2 Introduction

Magmatic arcs are important tectonic components to understand the geodynamic evolution of orogenic areas and paleocontinental reconstitutions. Neoproterozoic magmatic arcs of intra-oceanic or continental margin settings, as well as related ophiolite bodies, occur in several orogenic belts formed during the long-lasting Brasiliano – Pan-African event (Fig. 2.1; e.g., Pimentel & Fuck 1992; Pedrosa-Soares et al., 1998, 2001; Heilbron et al., 2004; Tupinambá et al., 2012; Caxito et al., 2014b; Brito-Neves et al. 2014; Basei et al., 2018; Tedeschi et al., 2016; Peixoto et al., 2017; Hartmann et al., 2019; Amaral et al., 2020; Brown et al., 2020), like in the Araçuaí – Ribeira orogenic system of Southeastern Brazil (AROS, Fig. 2.2), an extensive segment of the orogenic framework developed during Western Gondwana assembly

(e.g., Heilbron et al., 2004; Silva et al., 2005; Tedeschi et al. 2016; Degler et al., 2017). Comprising the AROS southern segment, the Ribeira orogenic system includes the Tonian Serra da Prata and the Cryogenian Rio Negro intra-oceanic magmatic arcs. Those are followed by the Ediacaran Rio Doce arc formed on an active continental margin, and at last, by collisional to post-collisional Ediacaran-Cambrian plutonic rocks (Fig.III.1). The arrangement of distinct geotectonic components in time and space suggests a complex geodynamic evolution, following a Phanerozoic-style plate tectonics cycle (Heilbron et al., 2004, 2013; Tupinambá et al., 2012; Peixoto et al., 2017; Corrales et al., 2020).

The studied area is located in the transition zone between the Ribeira and Araçuaí orogens, approximately on the 21°S meridian. The Caxixe batholith located in the southern Espírito Santo State was characterized as a candidate for a new segment of the Tonian Serra da Prata magmatic arc (Fig.III.2 and Fig.III.3), hence could be to redefine the northernmost portion of the Ribeira orogenic system. For this purpose, we present the first petrographic, lithochemical, isotopic (whole-rock Sm-Nd and Rb-Sr, and Lu-Hf in zircon) and geochronological (zircon U-Pb) results of a systematic study of the Caxixe batholith. The new data support the main objectives of the paper, which are: (a) to understand the tectonic environment of the igneous bodies in this region and (b) to determine the petrogenetic nature (mantellic x crustal) and contributions of distinct sources into the igneous rocks through use isotopic and elemental geochemistry data. Moreover, the integration of the new data with data available on the literature of the Mantiqueira Province provides new arguments: (c) to improve the models for the Neoproterozoic evolution of the Ribeira orogenic system in the scenario of an Early Tonian ocean where intra-oceanic subduction formed island arcs and (d) to discuss the implications for Western Gondwana crustal building, as well as and paleogeographic and paleotectonic models involving Angola, Paranapanema and Congo - São Francisco paleocontinental blocks amalgamated in Western Gondwana.

III.3. Geological Context

The Ribeira orogenic system developed from the collision of the Angola, Paranapanema and Congo - São Francisco paleocontinental blocks and the southernmost part of the Brasília orogen (Fig. III.1), during the Brasiliano – Pan-African event that finally led to Western Gondwana amalgamation from the Ediacaran to

Cambrian (Heilbron et al., 2000, 2008; Trouw et al., 2000; Schmitt et al., 2004). It is a NE-trending orogenic belt extending from the transition zone with the Araçuaí orogen, around the latitude of the southern tip of the São Francisco craton, to the Luiz Alves cratonic block (Fig. III.2).

The northern Ribeira orogenic system is here described according to its main geotectonic components of Neoproterozoic and Cambrian age (Fig. III.2), although there are previous divisions into tectono-stratigraphic terranes including both basement and younger units (Heilbron et al., 2000, 2008). Accordingly, the Ribeira orogenic system includes rift to passive margin metasedimentary successions, representing Mesoproterozoic to Neoproterozoic precursor basins, and metamorphosed sedimentary and magmatic rocks formed during orogenic stages, as well as a number of post-collisional intrusions (Trouw et al., 2000; Heilbron et al., 2008; Valeriano et al., 2011; Caputo Neto et al., 2018; Degler et al., 2017).

Among the earliest orogenic manifestations related to ancient plate convergence recorded in the study region, the Tonian to Cryogenian Serra da Prata and Rio Negro plutonic complexes form an extensive juvenile arc system apparently free of continental basement rocks (Tupinambá et al., 2012; Peixoto et al., 2017; Heilbron et al., 2020), extending along the Atlantic coastal region from São Paulo to Espírito Santo states, between the Rio Doce arc domain, to the west, that comprises a continental-margin arc system (Heilbron et al., 2020), and the Cabo Frio tectonic domain, to the east (Fig. III.2). The Serra da Prata Complex, comprising an expanded series from granite to gabbro with calc-alkaline, magnesian, volcanic arc signature, is the oldest magmatic arc association (856 Ma – 838 Ma) with previous Nd isotopic data (εNd_t = +5 to -3; T_{DM} Nd model ages at ca. 1 Ga, 1.3 Ga and 1.8 Ga), showing important juvenile mantle contribution (Peixoto and Heilbron, 2010; Peixoto et al., 2017). The Nd and Sr isotopic data of the Rio Negro magmatic arc (790 – 630 Ma) suggest a progressive evolution, characterized by an early stage of juvenile rocks ($\varepsilon Nd_{(t)}$ from +5 to −3; $^{87}Sr/^{86}Sr$ initial ratios between 0.705 and 0.710), followed by a mature stage with evolved isotopic signature ($\varepsilon Nd_{(t)}$ ratios from -3 to -14; $^{87}Sr/^{86}Sr$ initial ratios <0.705) (Cordani et al., 1973; Heilbron and Machado, 2003; Tupinambá et al., 2000, 2012). Associated with those magmatic arcs, the Italva and São Fidélis groups include sedimentary and volcanic rocks metamorphosed from the amphibolite to granulite facies at ca. 602 to 570 Ma, interpreted as back-arc deposits related to those two accretionary stages (Heilbron & Machado, 2003; Lobato et al., 2015; Peixoto et al.,

2017), all of them involved in a thrust-to-northwest structural domain (Heilbron et al., 2008).

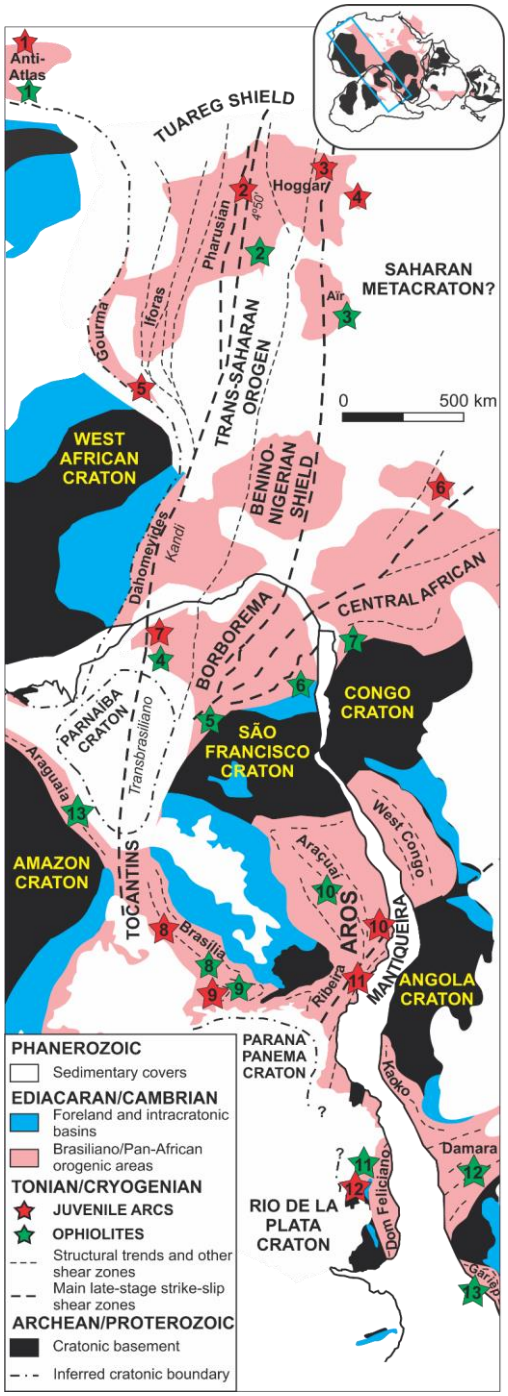

Fig. III. 1 - Schematic geology of central Western Gondwana showing the main orogenic and cratonic features. Location of Tonian-Cryogenian magmatic arcs (red stars): 1) Saghro (ca. 760 Ma – Saquaque, 1992; Walsh et al., 2012); 2) Silet (Iskel) (ca. 870 Ma - Caby et al., 1982, 2003; Béchiri-Benmerzoug et al., 2011); 3) Serouenout (unknown age - Adjerid et al., 2012, 2015); 4) Aouzegueur (ca. 730 Ma - Liégeois et al., 1994, 2019); 5) Amalaoulaou (ca. 790 Ma - Berger et al., 2011; Liégeois et al., 1994, 2019); 6) Mayo Kebbi (ca. 740 Ma - Penaye at al., 2006); 7) Lagoa Caiçara (ca. 880 Ma - Ganade de Araújo et al., 2014a); 8) Mara Rosa and 9) Arenópolis segments of the Goiás magmatic arc (ca. 890-860 Ma - Pimentel et al., 1992, 1997;

Laux et al ., 2005; Fuck et al., 2017); 10) Caxixe Batholith (860-840 Ma - this study); 11) Serra da Prata (ca. 860-840 Ma) - Rio Negro arc system (ca. 790-620 Ma) (Heilbron et al., 2003, 2008; Tupinambá, 2012; Peixoto et al., 2017); 12) Passinho (ca. 890-860 Ma) and São Gabriel (ca. 770-680 Ma) (Chemale Jr., 2000; Hartmann et al., 2011; Philipp et al., 2018). Ophiolites (green stars): 1) Bou Azzer (ca. 760 Ma – Saquaque et al., 1989; Hefferan et al., 2002; Samson et al., 2004; Bousquet et al., 2008); 2) Laouni (ca. 680 Ma - Black et al., 1994; Liégeois et al., 2003); 3) Aouzegueur (ca. 730 Ma - Boullier et al., 1991; Liégeois et al., 1994, 2019); 4) Novo Oriente (TDM model age < 1.4 Ga - Ganade de Araújo et al., 2010); 5) Monte Orebe (ca. 820 Ma Sm-Nd whole-rock isochron – Caxito et al., 2014b); 6) Canindé (ca. 700 Ma - Oliveira et al., 2006; Ancelmi et al., 2015); 7) Boumnyebel (Unknown age - Interpretation based on geochemical and petrographic data - Toteu et al., 2006; Nkoumbou et al., 2006 and Nkoumbou et al., 2006); 8) Abadiânia (ca. 800 Ma - Brown et al., 2020); 9) Araxá (ca. 800 Ma - Seer et al., 2001; Piuzana et al., 2003; Brown et al., 2020); 10) Ribeirão da Folha – São José da Safira (ca. 645 Ma - Amaral et al., 2020); 11) Bossoroca, Cambaizinho, Passo do Ivo, Palma, Palma Leste, Ibaré, Cerro Mantiqueiras and Arroio Grande (ca. 920-720 Ma - Hartmann et al., 2011, 2019; Ramos & Koester, 2015; Arena et al., 2016, 2017; Cerva-Alves et al., 2020); 12) Matchless (ca. 700 Ma – Meneghini et al., 2017); 13) Marmora (TDM model age ca. 800 Ma – Will et al., 2014); 14) Quatipuru (ca. 750 Ma - Sm-Nd whole-rock isochron - Paixão et al., 2008). Figure modeled after Caxito et al. (2020), where data sources are discussed.

The Rio Doce arc domain includes batholiths and stocks mostly composed of calc-alkaline, magnesian, I-type, tonalitic to granodioritic plutons displaying dioritic to mafic enclaves, and minor gabbro-noritic bodies. The Hf-Sr-Nd isotopic signatures and zircon inheritance from Paleoproterozoic continental basement, associated with arc-related supracrustal successions composed of metasedimentary and metavolcanic rocks, suggest a magmatic arc developed on a continental margin setting (Tedeschi et al., 2016; Gonçalves et al., 2016; Degler et al. 2017; Novo et al., 2018; Corrales et al., 2020).

The Cabo Frio tectonic domain (CFTD, Fig. III.2) was amalgamated onto the eastern border of the Rio Negro – Serra da Prata arc domain around 535 Ma, during a collisional stage that reworked the Paleoproterozoic basement and deformed Neoproterozoic metavolcano-sedimentary successions with ophiolite bodies (Buzios and Palmital groups), generating large-scale folds and thrusts, as well as late orogenic dextral transpressional shear zones (Schmitt et al., 2004). The Cabo Frio tectonic domain has been interpreted as a fragment of the Angola craton (Heilbron et al., 1982, 2017; Schmitt et al., 2008).

NE-trending batholiths and stocks of S-type granites formed during the Ediacaran collisional stage, followed by late collisional to post-collisional Cambrian intrusions related to strike-slip structures associated with processes of docking and extensional collapse of the Ribeira orogenic system and, finally, marking its

stabilization within the Western Gondwana Supercontinent between ca. 515 Ma and 480 Ma (Heilbron et al., 2004, 2013, 2017; Valeriano et al., 2011).

The northern Ribeira orogenic system shows tectonic structures recording two major deformational phases related to the Brasiliano orogenic event (Fig. III.2 and Fig. III.3). The first was imprinted by a NW-verging thrust tectonics, assisting the main tectonic transport towards the southern Brasília and Araçuaí domains and the São Francisco craton (Heilbron et al., 2004, 2008). This phase is compatible with an early tectonic transport from south to north, recorded by the first deformation phase in the southern Araçuaí orogen (Peres et al., 2004). Cutting across the former thrust-related structures, an extensive set of dextral, high-angle oblique strike-slip to transcurrent shear zones characterizes a late deformational phase, related to the docking and gravitational collapse stages in both the northern Ribeira and southern Araçuaí orogens (Alkmim et al., 2006; Heilbron et al., 2004, 2008).

III.4. Materials and Methods

III.4.1 Field campaigns, sample preparation and petrography

Field campaigns were conducted in the Caxixe batholith to collect representative samples for petrographical analysis and geological mapping. Thin sections were prepared for 50 samples at the CPMTC Research Center labs, Federal University of Minas Gerais (UFMG), Brazil. Samples were prepared for geochemical, isotopic and geochronological analysis at CPMTC laboratories.

III.4.2 Whole-rock chemistry analyses

Lithochemical analyses of 30 samples were conducted at SGS-Geosol Laboratory, Brazil (Supplementary Material SIII - 1). Element grades were analyzed via ICP-MS (Induced Coupled Plasma – Mass Spectrometry) after fusion with lithium metaborate/tetraborate and digestion with diluted nitric acid. Analytical errors are within 2% for major oxides and 5% for trace elements. The detection limit for major elements is of 0.01%. For the trace elements, the limits are of 10 ppm (Ba, Sr, Zr), 5 ppm (Zn, V, Cu, Ni), 0.5 ppm (Co), 0.3 ppm (Sn), 0.2 ppm (Rb), 0.1 ppm (Ce, Ga, La, Nd, Sm, Th, W, Yb) and 0.05 ppm (Cs, Dy, Er, Eu, Gd, Hf, Ho, Lu, Nb, Pr, Ta, Tb, Tm, U, Y).

Base and precious metal contents were determined by digestion in Aqua Regia followed by ICP-MS analysis. Loss on ignition (LOI) was determined by the weighing difference after ignition at 1000 °C. The CIPW norm of the standard mineral components, from the whole-rock analyses, was based on Johannsen (1931). Since the whole-rock chemical analyses considered only Fe_2O_3, the estimation of FeO and Fe_2O_3 was based on Gill (2010), who used the ratio 0.9, that is, FeO estimated = 0.9 × Fe_2O_3Total.

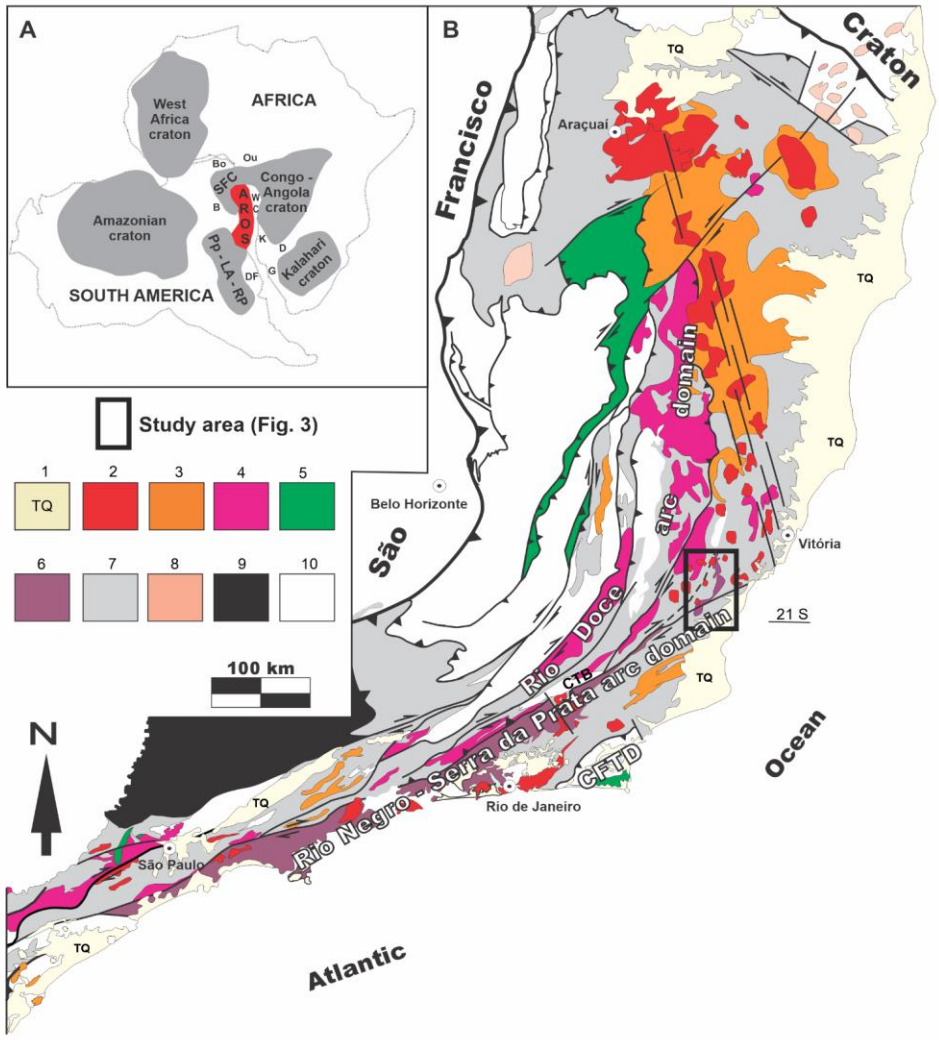

Fig. III. 2 - (A) Location of the Araçuaí-Ribeira orogenic system (AROS) in Western Gondwana (modified from Brito-Neves et al., 1999) and position of the Brasiliano - Pan-African orogenic belts (B: Brasília; Bo: Borborema; D: Damara; DF: Dom Feliciano; G: Gariep; K: K: Kaoko; WC: West Congo) and cratons (SFC: São Francisco; PP-LA-RP: Paranapanema-Luís Alves-Rio de La Plata). (B) Simplified geological map of the AROS (modified from Tedeschi et al., 2016; and Degler et al., 2017, 2018 and Peixoto et al., 2017) showing 1: Cenozoic cover (TQ); 2: post-collisional intrusions (ca. 525 – 470 Ma); 3: collisional granitic rocks (ca. 590 – 535 Ma); 4: batholiths and stocks of the Rio Doce magmatic arc (ca. 630 – 585 Ma) and probable correlatives; 5: Neoproterozoic ophiolite-bearing rock assemblages; 6: Rio Negro – Serra da Prata arc domain (Rio Negro and Serra da Prata magmatic arcs, and related units; ca. 860 Ma

– 630 Ma); 7: Neoproterozoic metasedimentary and metavolcanic successions; 8: Tonian and Cryogenian rift-related magmatic rocks; 9: Southern Brasília belt; 10: Pre-Neoproterozoic units; CTB: Central Tectonic Boundary; CFTD: Cabo Frio tectonic domain.

III.4.3 Sm-Nd and Rb-Sr isotope analyses

The Sm-Nd and Rb-Sr isotope analyses were conducted at the Laboratório de Geocronologia (Laboratory of Geochronology) of the Brasília University (UnB), Brazil (Supplementary Material SIII - 2). Samples were dissolved in a HF-HNO_3 mixture in high-pressure Teflon vessels. A ^{150}Nd-^{149}Sm tracer was added to determine Nd and Sm concentrations. Rare Earth Elements (REE) were then purified by cation exchange chromatography, and Sm and Nd were subsequently separated following the procedure of Gioia and Pimentel (2000). Sm and Nd analyses used a double filament assembly in a Thermoscientific Triton Plus mass spectrometer operating in static mode. The Sm and Nd concentrations and the $^{147}Sm/^{144}Nd$ ratios have accuracy of 0.5% that corresponds to an ± 0.5 average error on the initial εNd values of based on repeated measurements of the JNdi-1 standard, with a long-term (year-round) average during the period of analysis of $^{143}Nd/^{144}Nd$ = 0.512230 ± 0.000006. Sr and Rb were separated using the conventional cation exchange procedure according to Pankhurst and O'Nions (1973). Samples were measured at 1250–1300 °C in dynamic multi-collection mode. The $^{87}Sr/^{86}Sr$ values of the samples were corrected for the offset relative to the certified NIST SRM 987 value of 0.710250. The long-term (year-round) average of this standard $^{87}Sr/^{86}Sr$ ratios measured in this machine during the period of analysis is 0.71028 ± 0.00004. Procedural blanks for Sr are less than 100 pg. All uncertainties are presented at the 2σ level. Both Nd and Sr initial ratios are calculated using the crystallization age from U-Pb data obtained in this work.

III.4.4 LA-ICP-MS U-Pb zircon dating

Sample 06 was crushed to the 50-500 μm size range and submitted to analysis through the U-Pb LA-ICP-MS (Laser Ablation – Induced Coupled Plasma Mass Spectrometry) method at Laboratório de Geocronologia, Brasília University (UnB) (Supplementary Material SIII - 3). Zircon crystals were separated through standard magnetic, hand-picking techniques, and mounted in an epoxy resin, ground and polished. Images were made in a Scanning Electron Microscopy (SEM) in a FEI

Quanta 450 microscope through the backscattering technique (BKS) and cathodoluminescence images were also obtained. The resulting images emphasize the internal structure of zircon grains (zoning, fracturing, etc.) and were used to locate the laser spots avoiding (fractures and inclusions). Analyzes were carried out by laser ablation in using a Finnigan Neptune ICP-MS machine coupled to a Nd-YAG 213 nm laser ablation system. The U-Pb analysis follows the procedures outlined in Bühn et al. (2009). Ablation was done using 25-30 μm spots at a frequency of 9-13 Hz and intensity of 0.19 - 1.02 J/cm^2 with 60 seconds of analysis per spot. The ablated material was carried by Ar (~0.90 L/min) and He (~0.40 L/min) in 40 cycles of 1 s each. Analysis was conducted with bracketing of three unknown samples between measurements of primary and secondary reference materials and a blank analysis. The primary reference material GJ-1 zircon yielded a mean $^{206}Pb/^{238}U$ ratio of 0.0967 ± 0.0028 (ref. value 0.09761 ± 0.00011; Jackson et al., 2005), corresponding to a mean $^{206}Pb/^{238}U$ age of 595 ± 16 Ma (mean $^{206}Pb/^{238}U$ age of GJ-1 = 599.75 Ma; Jackson et al., 2005, Supplementary Material SIII - 3). Accuracy was controlled using the secondary reference material 91500 zircon, which yielded a Concordia age of 1057.7 ± 9.1 (n=7). Raw data were reduced using an in-house program and corrections were done for background, instrumental mass bias and common Pb. U-Pb ages were calculated using Isoplot 3.6 (Ludwig, 2008). All uncertainties are presented at the 2σ level.

III.4.5 SHRIMP U-Pb zircon dating

U-Pb (SHRIMP – Sensitive High-Resolution Ion Microprobe) analysis (Supplementary Material SIII - 3) was performed in zircon crystals separated through standard crushing, sieving, magnetic and gravimetric methods from homogeneous portions (i.e, bearing no veins, fractures or alteration fronts) of samples 25 and 38 in the SEPURA – Laboratório de Separação Mineral de Alta Pureza at CPMTC, Federal University of Minas Gerais (UFMG), Brazil.

After mounting in epoxi and polishing, zircon crystals were imaged through standard SEM (Scanning Electron Microscopy) techniques such as Secondary Electrons (SE), Back-Scattered Electrons (BSE) and Cathodoluminescence (CL) in a TESCAN Vega SEM at the Centre for Microscopy and Microanalysis (CMCA) at the University of Western Australia, Perth. The images were used for spot positioning based on the study of crystal features such as cores and rims, zones of damage by U

radioactive decay, zones of inclusions, etc. The sample mounts were analyzed for U-Pb at the SHRIMP II Laboratory of the John de Laeter Centre, Curtin University, Perth, Australia. The mounts were cleaned following internal standards of the Centre and coated with gold for SHRIMP analyses, with a microprobe spot size of 20 µm. Six scans were performed for each spot, with nine peaks analyzed at masses $^{196}Zr_2O$, ^{204}Pb, background, ^{206}Pb, ^{207}Pb, ^{208}Pb, ^{238}U, ^{248}ThO and ^{254}UO. The NBS611 glass standard was used to identify the peak position of mass ^{204}Pb, whereas the calibration of the U contents and Pb/U ratios were conducted using zircon standard Temora II (417 Ma; Black et al., 2004), which analysis was bracketed after each three or four unknows, yielding a Concordia Age of 416.4 ± 3.3 Ma (2σ; MSWD = 1.5; n = 25). The $^{207}Pb/^{206}Pb$ zircon standard used to monitor both instrument-induced mass fractionation and accuracy was OGC (3467 ± 3 Ma; Stern et al., 2009) yielding a Concordia Age of 3462.1 ± 6.8 Ma (2σ; MSWD = 0.73; n = 7) and a $^{207}Pb/^{206}Pb$ mean age of 3464.3 ± 6.6 Ma. SHRIMP data were reduced using SQUID 2.5 software (Ludwig, 2009) and plots were prepared using ISOPLOT 4.15 (Ludwig, 2008).

III.4.6 Lu-Hf isotope analyses

Hf isotope ratios were determined on four selected zircon crystals of sample 06 (Supplementary Material SIII - 4). Spots were located at the same zircon domain where U-Pb analyses were previously performed for this sample and also conducted at Laboratório de Geocronologia, Brasília University (UnB). G1-J zircon standard was monitored as reference material and yielded $^{176}Hf/^{177}Hf$ ratios of 0.281962 ± 0.000029 and 0.281985 ± 0.000038, at the beginning and at the end of the analysis, respectively, in agreement with published values for this standard (Morel et al. 2008). Blank signal intensities are corrected for the isobaric interference of ^{176}Yb and ^{176}Lu on ^{176}Hf, considering the signal intensity of interference-free ^{171}Yb, ^{173}Yb and ^{175}Lu. Internal mass bias was corrected using $^{179}Hf/^{177}Hf = 0.7325$ (Patchett and Tatsumoto, 1980) and the exponential law.

Hf isotope ratios were determined on six selected zircon crystals of sample 25 and ten zircon crystals of sample 38 (Supplementary Material SIII - 4). Hf-isotope analyses were carried out in a Thermo-Finnigan Neptune multicollector ICPMS coupled to a Photon-Machines laser system that delivers a beam of 193 nm UV light from a frequency-quintupled Nd:YAG laser hosted in Laboratório de Geoquímica

Isotópica, Federal University of Ouro Preto (UFOP) . The analyses were achieved with a beam diameter of 50 μm, a repetition rate between 4 and 6 Hz and 50% of laser output. Depending on the conditions and Hf contents, the Hf signals were between 1 to $6x10^{-11}$ A and the ablation time lasted 60 s. Ar carrier gas transported from the ablated sample from the laser ablation cell via mixing chamber to the ICPMS torch. To correct for the isobaric interferences of ^{176}Lu and ^{176}Yb on ^{176}Hf, masses 172, 173 and 175–180 were measured in static- collection mode and simultaneously monitored. The ^{177}Hf signal intensity was ca. 10 V. LA-ICP-MC data were reduced using In-house Excel Spreadsheets.

The accuracy and external reproducibility of the Lu–Hf results from samples 25 and 38 were monitored through the analysis of zircon standards Temora ($^{176}Hf/^{177}Hf$ = 0.282680 ± 0.000031; Black et al., 2003; Wu et al., 2006), Blue Berry ($^{176}Hf/^{177}Hf$ = 0.281674 ± 0.000018; Santos, M.M. et al., 2017), Mud Tank ($^{176}Hf/^{177}Hf$ = 0.282504 ± 0.000044; Black and Gulson, 1978; Woodhead and Hergt, 2005), GJ-1 ($^{176}Hf/^{177}Hf$ = 0.282000 ± 0.000005; Jackson et al., 2004) and Plešovice ($^{176}Hf/^{177}Hf$ = 0.282482 ± 0.000013; Sláma et al., 2008),which yielded $^{176}Hf/^{177}Hf$ average ratios of 0.282654 ± 0.000014 (n = 1), 0.281673 ± 0.000017 (n = 8), 0.282519 ± 0.000015 (n = 9), 0.282006 ± 0.000019 (n = 7) and 0.282485 ± 0.000014 (n = 9), respectively (±2SD); all values within the uncertainties and in good agreement with the accepted standard ratios.

Initial Hf isotope ratios were recalculated to the $^{206}Pb/^{238}U$ age of each zircon crystal. For the calculation of the $\varepsilon Hf_{(t)}$ values, the chondritic values reported by Bouvier et al. (2008) of $^{176}Hf/^{177}Hf$ = 0.282785 ± 11 and $^{176}Lu/^{177}Hf$ = 0.0336 ± 1 were used. To calculate the model ages (T_{DM}) based on a depleted mantled source, the present-day ratios of $^{176}Hf/^{177}Hf$ = 0.28325 and $^{176}Lu/^{177}Hf$ = 0.0388 were used (Griffin et al., 2000; updated by Andersen et al., 2009). The λ decay constant for ^{176}Lu used is $1.867x10^{-11}$/yr (Söderlund et al., 2004).

III.5. Results

III.5.1. Geology of the Caxixe batholith

Besides local Cenozoic covers and Cretaceous mafic dykes (Santiago et al., 2020), the study area shows Neoproterozoic and Cambrian lithological units (Fig. III.3), comprising:

i) Cambrian (530-490 Ma) post-collisional intrusions, encompassing A- and I-type granitic to charnockitic bodies generally displaying mafic cores, cutting across the regional SE-dipping ductile foliation but related to late NE-SW-trending strike-slip shear zones (e.g., De Campos et al., 2016; Santiago et al., 2020; Araujo et al., 2020);

ii) Ediacaran to Cambrian, syn-collisional to late collisional, peraluminous granitic to charnockitic rocks, forming leucosomes in migmatitic paragneisses and encompassing plutons, recording the regional ductile foliation and cut by late strike-slip shear zones (e.g., De Campos et al., 2004, 2016; Vieira et al., 2014);

iii) foliated tonalites to granodiorites and tonalitic-granodioritic orthogneisses, locally migmatized, generally with foliated and stretched dioritic to mafic enclaves, related to the pre-collisional G1 supersuite (ca. 630-585 Ma) of the Rio Doce magmatic arc in the western sector of the study area (to the west of the Caxixe batholith in Fig. 2.3), and possibly recording the presence of the Rio Negro magmatic arc along the coastal zone (e.g., De Campos et al., 2004; Pedrosa-Soares et al., 2011; Tupinambá et al., 2012; Vieira et al., 2014; Tedeschi et al., 2016);

iv) several supracrustal units mostly composed of migmatitic Al-rich paragneisses with minor calc-silicate intercalations, locally with thick marble layers, and probable intermediate to felsic metavolcanic (s.l.) rocks represented by hornblende gneisses; all of them currently interpreted as arc-related deposits with detrital zircon grains as young as ca. 600 Ma, and zircon age spectra representing main provenances from the Neoproterozoic arcs found in the Araçuaí – Ribeira orogenic system (e.g., Gradim et al., 2014; Vieira et al., 2014; Richter et al., 2016; Degler et al., 2017; Araujo et al., 2020); and

v) the Caxixe batholith (Fig. III.3), focus of the present work, comprising the Alto Guandu tonalite and the Cachoeiro orthogneiss (Vieira et al., 2014), extending from ca. 20 km to the north of Castelo city to the boundary between the Espírito Santo and Rio de Janeiro states, as described in more detail ahead.

The main rocks of the Caxixe batholith are medium- to coarse-grained mesocratic biotite-rich, granitic to tonalitic orthogneisses, with prevailing granodioritic composition, and dioritic to gabbroic enclaves. The rocks show mainly porphyroblastic and subordinated mylonitic textures. Eventually, they are associated with leucocratic granitic orthogneisses and cut by late-stage granitic veins discordant to the regional tectonic fabrics (Fig. III.4a). The regional foliation (modal maximum: 146/38; n = 27), imprinted by the orientation of biotite and hornblende, as well as by stretched quartz-

feldspar clusters (Fig. III.4b) is generally weakly-developed in the orthogneisses, except in the vicinities of ductile shear zones.

Despite the contacts of the Caxixe batholith with the country rocks being largely covered by soil, some contact segments are marked by NW-verging thrust shear-zones, locally displaced by NNW-to-NW-trending sinistral, strike-slip shear zones (Fig. III.3). Accordingly, the Caxixe batholith displays a roughly lens-shaped format in map view, defining a sigmoidal thrust slice (maximum 120 km long and 21 km wide), transported onto the Rio Doce arc domain, and tectonically overlain by the coastal tectonic domain. All of those domains are cut by late-stage, NE-SW-trending, dextral strike-slip shear zones.

The main mineralogy of the granodioritic to granitic orthogneiss of the Caxixe batholith consists of oligoclase-andesine, quartz, K-feldspar (microcline and orthoclase), dark brown to greenish biotite, and minor dark to light green hornblende. Accessory phases are titanite, apatite, allanite, zircon, opaque minerals, and rare garnet (Fig. III.4). Muscovite is the main alteration mineral, although rather scarce. Textures generally vary from granolepidoblastic, with the ductile foliation mainly outlined by oriented biotite and stretched quartz (Fig. III.4c), to granoblastic polygonal (Fig. 2.4d), with quartz showing undulatory extinction.

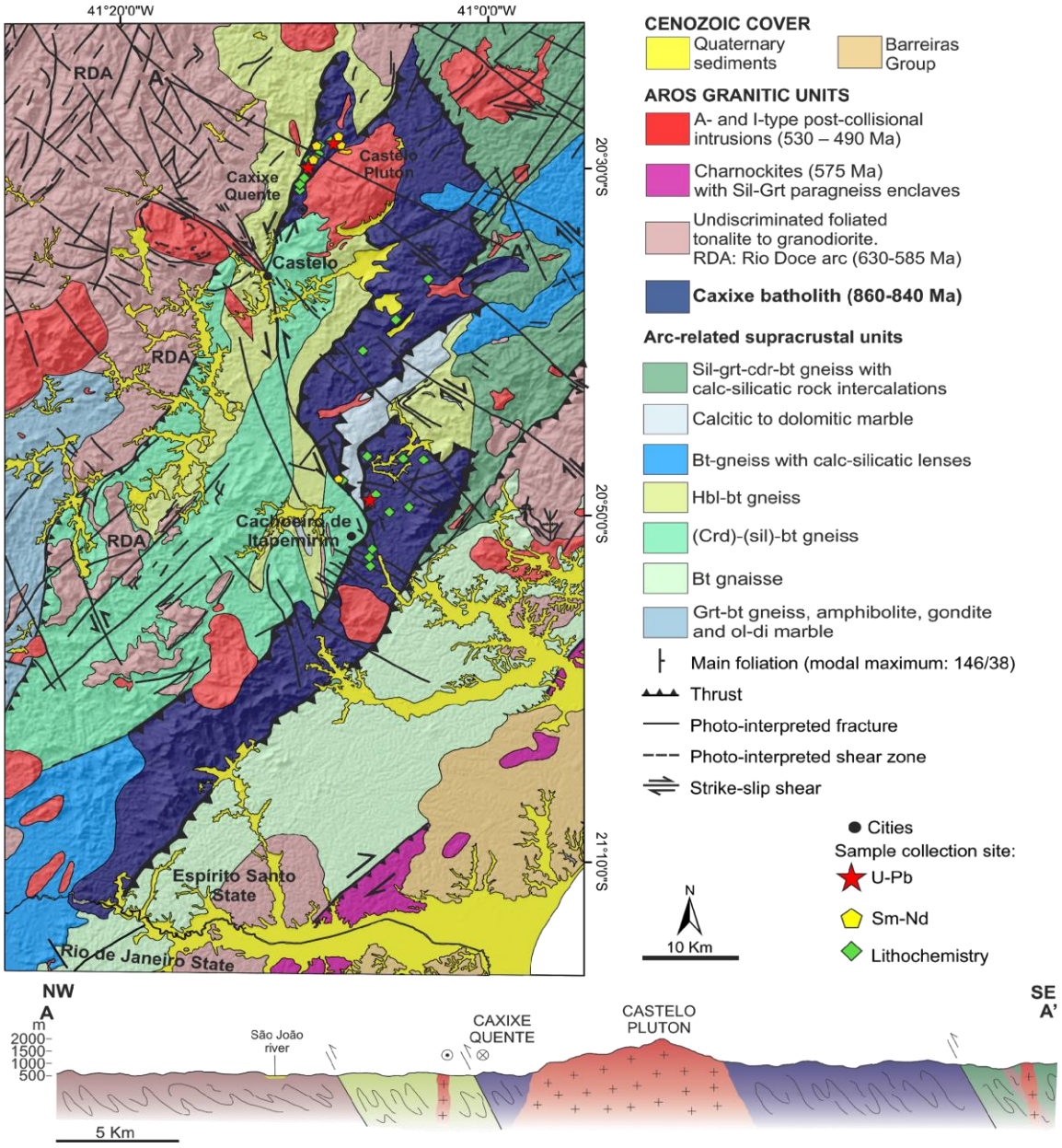

Fig. III. 3 - Geological map (modified from Vieira et al., 2014) and cross-section of the study area, focusing the Caxixe batholith and its neighboring units. Rio Doce arc (RDA); Sillimanite (Sil); Garnet (Grt); Cordierite (Crd); Biotite (Bt); Hornblende (Hbl); Olivine (Ol); Diopside (Di).

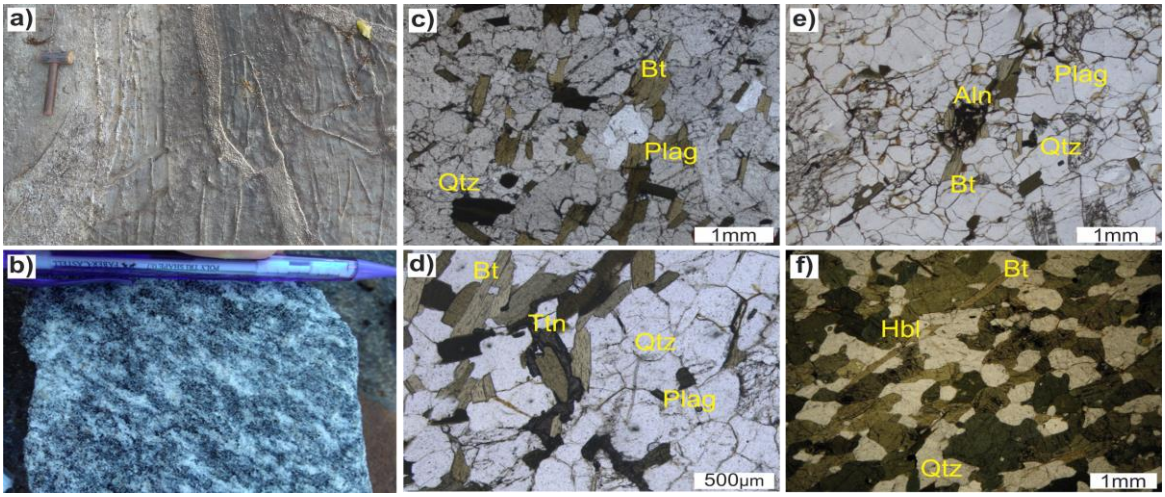

Fig. III. 4 - Features from the main rocks of the Caxixe batholith. Photos of outcrop showing a) biotite orthogneiss with the regional tectonic fabric cut by late granitic veins and b) displaying the regional foliation given by biotite orientation and stretched quartz-feldspars clusters that characterize predominant orthogneisses. Photomicrographs (c-f) on thin sections under non-polarized light, showing the mineralogical association (Aln, allanite; Bt, biotite; Hbl, hornblende; Plag, plagioclase; Qtz, quartz; Ttn titanite) and textures varying from granolepidoblastic (c, f) to granoblastic polygonal (d, e) in Caxixe orthogneisses.

III.5.2. Lithochemistry

Lithochemical data from samples of the Caxixe batholith (including six samples from mafic enclaves) characterize a roughly expanded series from granite to gabbro, with most rocks clustering on granodiorite and granite chemical compositions (Fig. III.5). For only whole-rock orthogneiss samples, excluding the mafic enclaves, the major elements data (wt%) show SiO_2 contents between 65.2% and 77.6% (with the exception of a quartz-rich vein sample reaching 86.8%), Al_2O_3 from 7.7% to 19.6%, average K_2O + Na_2O of 3.5%, and CaO ranging from 0.3% to 4.9% (Supplementary Material SIII - 1). Harker diagrams show negative correlations of Al_2O_3, MgO, TiO_2, CaO and Fe_2O_3 in relation to SiO_2, somewhat scattered Na_2O and K_2O values, and positive linear correlation of P_2O_5 with silica (Fig. III.7). The samples outline a general calc-alkaline trend in the AFM and FeO_t/MgO versus SiO_2 diagrams (Fig. III.5). Most of them are slightly peraluminous (< 1.1 A/CNK) to metaluminous, similarly to I-type peraluminous granites (Chappell et al., 2012), and much more calcic to calc-alkaline and magnesian than alkali-calcic to alkaline and ferroan (Fig. III.6). The chondrite-normalized (Sun and McDonough, 1989) patterns of rare-earth elements (REE) indicate slight enrichment in light REE (LREE) relative to heavy rare earth elements (HREE) ((La/Yb)N = 3.08 – 84.91; average = 19.01), and variable Eu anomalies

((Eu/Eu*)$_N$ = 0.60 – 3.12; average = 1.06), ranging from weakly negative anomalies to positive anomalies. The HREE show flat patterns (Tb/Yb)$_N$ ratios from 0.80 to 5.19; average = 1.82). The incompatible elements diagram, normalized to the primitive mantle (Sun and McDonough, 1989), generally shows negative anomalies of Th, Nb, Ta, Sr, P and Ti (Fig. III.9). On tectonic setting discrimination diagrams (Brown et al., 1984; Pearce et al., 1984), the studied samples show clear affinities with volcanic arcs formed on plate margins (Fig. III.8a, b), suggesting evolution from primitive to mature island arc settings (Fig. III.8c).

Enclaves and more mafic facies of the orthogneisses comprise rocks from gabbro and diorite to granodiorite in chemical composition. Their SiO_2 contents range between 50.31% and 70.72%, Al_2O_3 from 14.63% to 17.79%, average K_2O of 2.70%, average Na_2O of 3.77%, and CaO from 1.24% to 10.19% (Supplementary Material SIII - 1). The samples are metaluminous to slightly peraluminous, and calcic to calc-alkaline (Fig. III.6). The REE patterns show fractionation of LREE relatively to HREE ((La / Yb)$_N$ = 2.46 - 27.11; average = 12.29) and weak negative Eu anomalies ((Eu / Eu *)$_N$ = 0.49 - 2.25; average = 1.16), except for two samples that stand out for the prominent positive or negative anomalies. As the orthogneisses, the enclaves and more mafic facies show flat HREE patterns. The incompatible elements diagram displays negative anomalies of Nb, Ta, P, Zr and Ti (Fig. III.9).

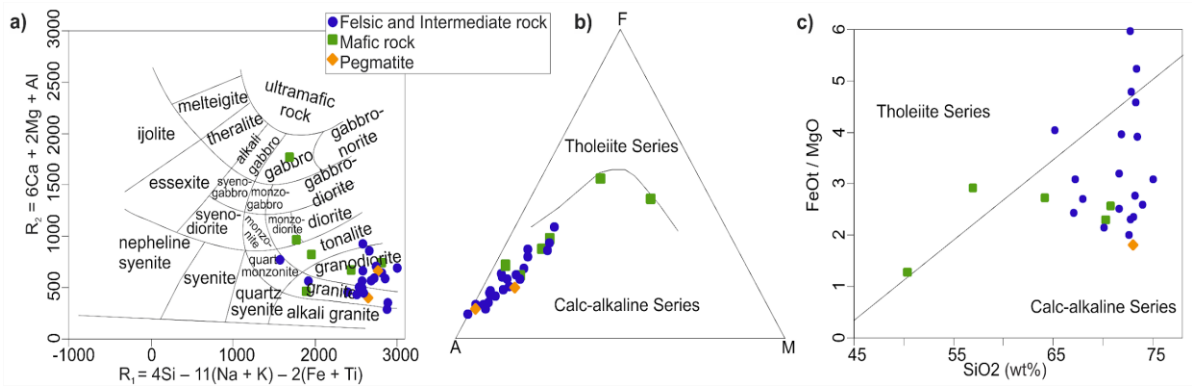

Fig. III. 5 - Geochemistry classification diagrams for Caxixe batholith samples: a) Classification diagram (R1–R2) of De la Roche et al. (1980); b) AFM diagram (Irvine and Baragar, 1971); c) FeOt/MgO versus SiO_2 plot (Miyashiro, 1974).

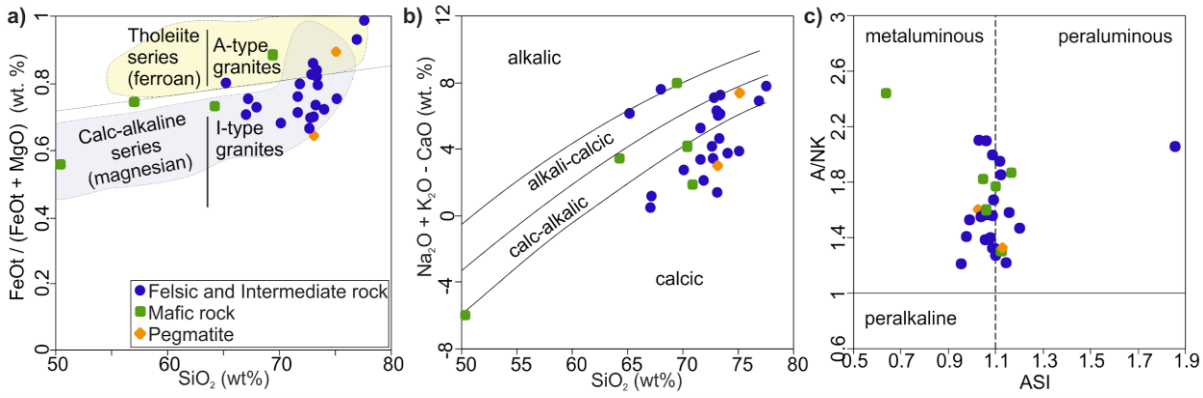

Fig. III. 6 - Plots for Caxixe batholith samples: a) FeOt/ (FeOt + MgO) versus SiO2 (wt%); b) Plot of $Na_2O + K_2O$ - CaO (wt%) versus SiO_2 (wt%); c) Discrimination diagram A/CNK – A/NK. All diagrams from Frost et al. (2001).

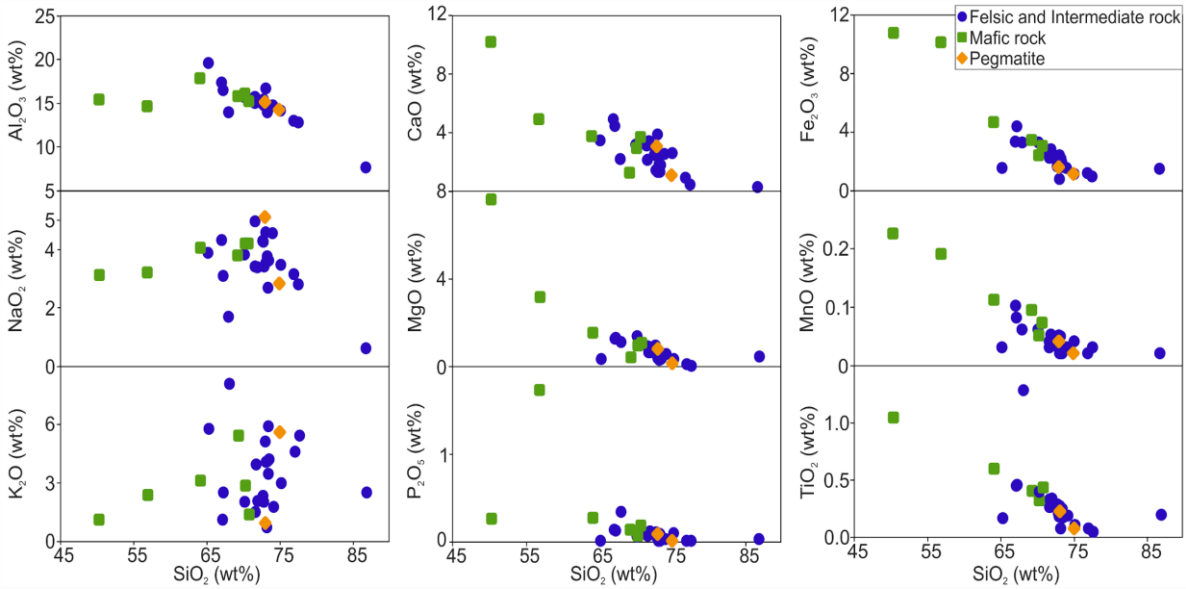

Fig. III. 7 - Binary diagrams show SiO_2 (wt%) versus major elements (wt%) for Caxixe batholith samples.

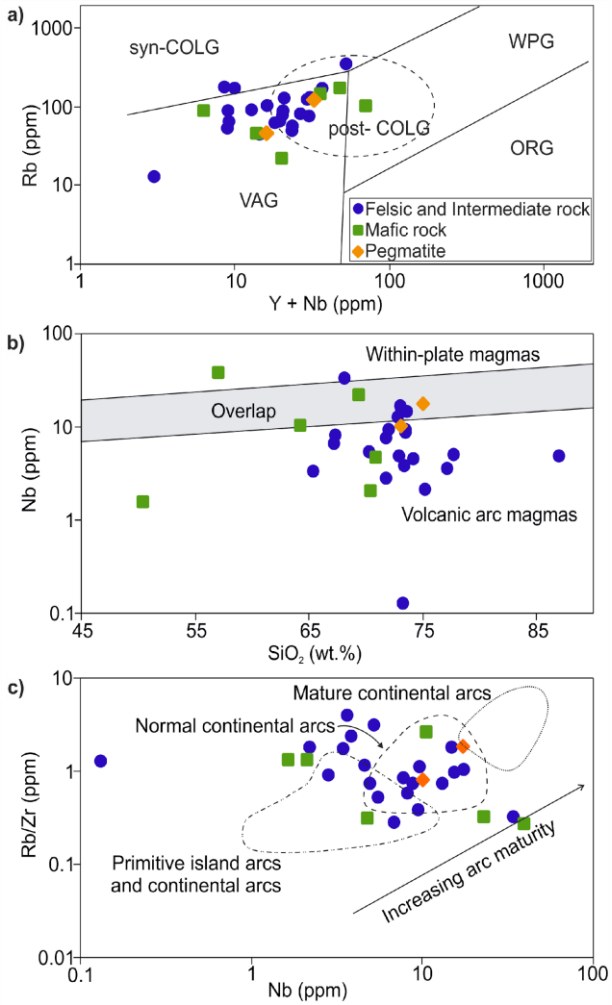

Fig. III. 8 - Tectonic discrimination diagrams for Caxixe batholith rocks. a) Rb versus Y+Nb diagram (Pearce et al., 1984, 1996), VAG: volcanic arc granite, ORG: ocean ridge granite, WPG: within-plate granite, syn-COLG: syn-collision granite; b) Nb versus SiO_2 diagram (Pearce and Gale, 1977); c) Rb/Zr versus Nb diagram (after Brown et al., 1984).

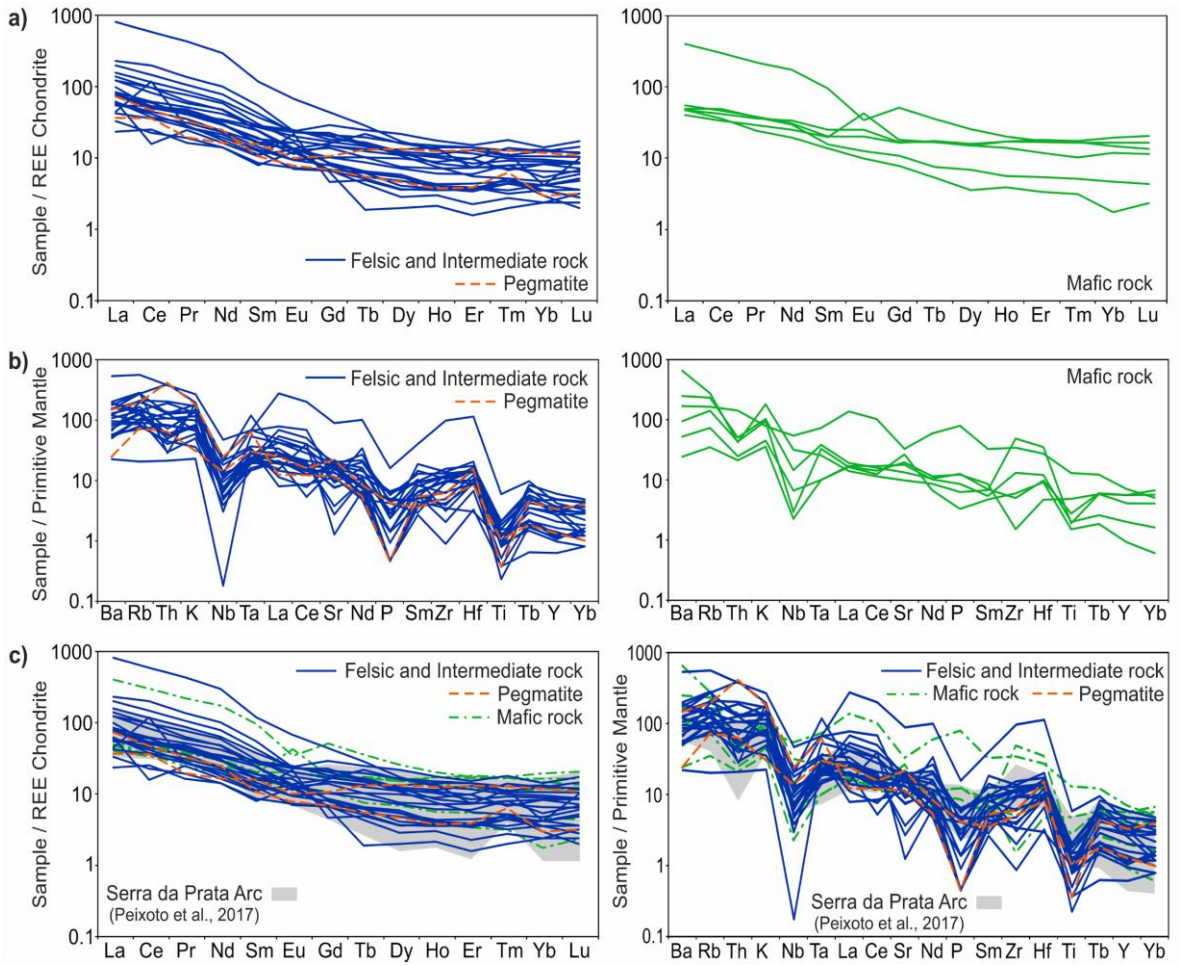

Fig. III. 9 - a) Chondrite-normalized REE patterns (Sun and McDonough, 1989); b) multi-element spidergrams normalized to the Primitive Mantle (element ordering after Thompson et al., 1984; normalizing values after Sun and McDonough, 1989) for the Caxixe batholith samples. c) Chondrite-normalized REE patterns and Primitive Mantle-normalized multi-element spidergram (Sun and McDonough, 1989) comparing the Caxixe batholith samples with Serra da Prata arc (Peixoto et al., 2017).

III.5.3 U-Pb geochronology and Hf-in-zircon data

The samples of the Caxixe batholith collected for U-Pb and Hf-in-zircon isotope analysis (see sampling location in Fig. III.3 and Supplementary Material SIII - 3 and SIII - 4) consist of fine-grained to medium-grained foliated biotite orthogneisses. Their lithochemical data show granodiorite composition with magnesian, metaluminous and calcic to calc-alkaline affinity.

III.5.3.1. Sample 06 (LA-ICP-MS)

Recovered zircon crystals are clear and translucid, inclusion-free, needle-like,

elongated euhedral prisms with length/width ratios of 5:1 and less than 200 μm long, showing conspicuous concentric internal zoning (Fig. III.10). The zircon crystals show typically igneous Th/U ratios from 0.3 to 0.9 (Rubatto, 2002; Hoskin and Schaltegger, 2003). The U/Pb isotope ratios of the analyzed zircon crystals cluster in a single coherent population in the Concordia diagram, yielding an upper intercept age of 858 ± 11 Ma (Fig. III.11).

Four of the most concordant zircon crystals were selected for Hf isotope analysis (Supplementary Material SIII - 4). Those yielded homogeneous initial $^{176}Hf/^{177}Hf_{(t)}$ ratios of 0.282512-0.282639, corresponding to highly juvenile $\varepsilon Hf_{(t)}$ from +13.9 to +9.3 (Fig. III. 12), with corresponding T_{DM} Hf model ages between ca. 0.84 and ca. 1.01 Ga.

III.5.3.2. Sample 25 (SHRIMP)

Zircon crystals are euhedral bipyramidal prisms and needle-like (up to 5:1 aspect ratio), less than 200 μm long, clear and translucid, normally with no inclusions. Cathodoluminescence (CL) images show well-defined igneous internal zoning (Fig. III.10). All zircon crystals show high Th/U ratios between 0.34 and 0.98, typical of igneous zircons (Rubatto, 2002; Hoskin and Schaltegger, 2003). The U/Pb isotope ratios of the analyzed zircon crystals cluster in a single coherent population, yielding a Concordia age of 847.4 ± 7.9 Ma (Fig. III.11).

Six of the most concordant zircon crystals were selected for Hf isotope analysis (Supplementary Material SIII-4). Those yielded homogeneous initial $^{176}Hf/^{177}Hf_{(t)}$ ratios of 0.282514-0.282566, corresponding to highly juvenile $\varepsilon Hf_{(t)}$ from +11.0 to +9.2 (Fig. III.12) with T_{DM} Hf model age of ca. 0.8 Ga.

III.5.3.3. Sample 38 (SHRIMP)

Zircon crystals consist of euhedral-subhedral bipyramidal prisms with length/width ratios of 5:1 and less than 200 μm long. The crystals are colorless and translucid, without inclusions, bearing typical igneous internal zoning, and Th/U ratios between 0.12 and 0.51 (Fig. III.10). However, CL images of some zircon crystals show light-colored core (low U) and dark rim (rich in U and low Th/U ratios), but apparently the transition between the two domains is normally not abrupt. Thus, the U/Pb isotope

ratios of the analyzed zircon crystals yielded two distinct Concordia ages. The first age of 859.4 ± 7.0 Ma, from the zircon crystals light-colored core (low U), is considered the crystallization age. The second age of 834.2 ± 9.5 Ma, from the zircon crystals dark rim (rich in U and low Th/U ratios) (Fig. III.11).

Ten of the most concordant zircon crystals were selected for Hf isotope analysis (Supplementary Material SIII-4). The zircon crystals with light core yielded initial $^{176}Hf/^{177}Hf_{(t)}$ ratios of 0.282480 – 0.282518, corresponding to highly juvenile $\varepsilon Hf_{(t)}$ from +10.31 to +8.6 (Fig. 2.12). The three dark rims analyzed yielded initial $^{176}Hf/^{177}Hf_{(t)}$ ratios of 0.282464 – 0.282500, corresponding to juvenile $\varepsilon Hf_{(t)}$ from +8.4 to +7.2. The Hf TDM models ages of the zircon crystals are around 1.0 Ga.

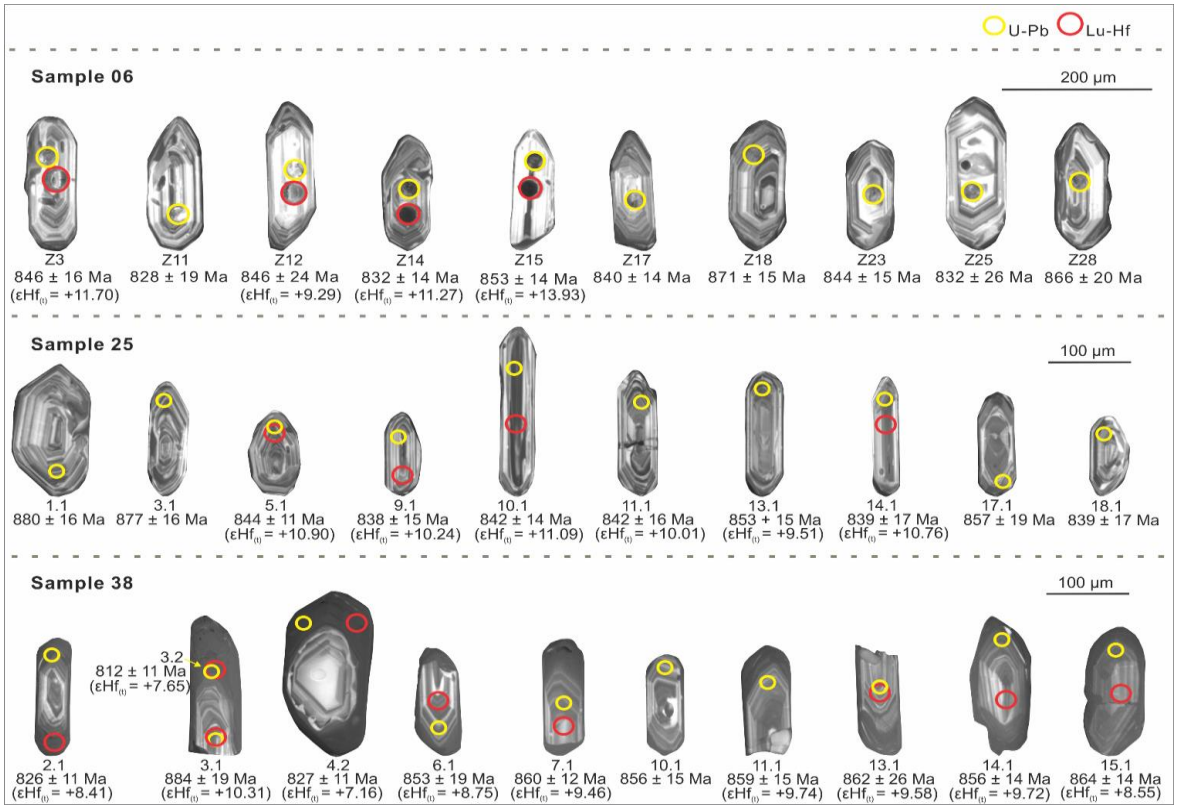

Fig. III. 10 - Representative cathodoluminescence (CL) images with U-Pb and Lu-Hf spots of analyzed zircons crystals from the Caxixe batholith.

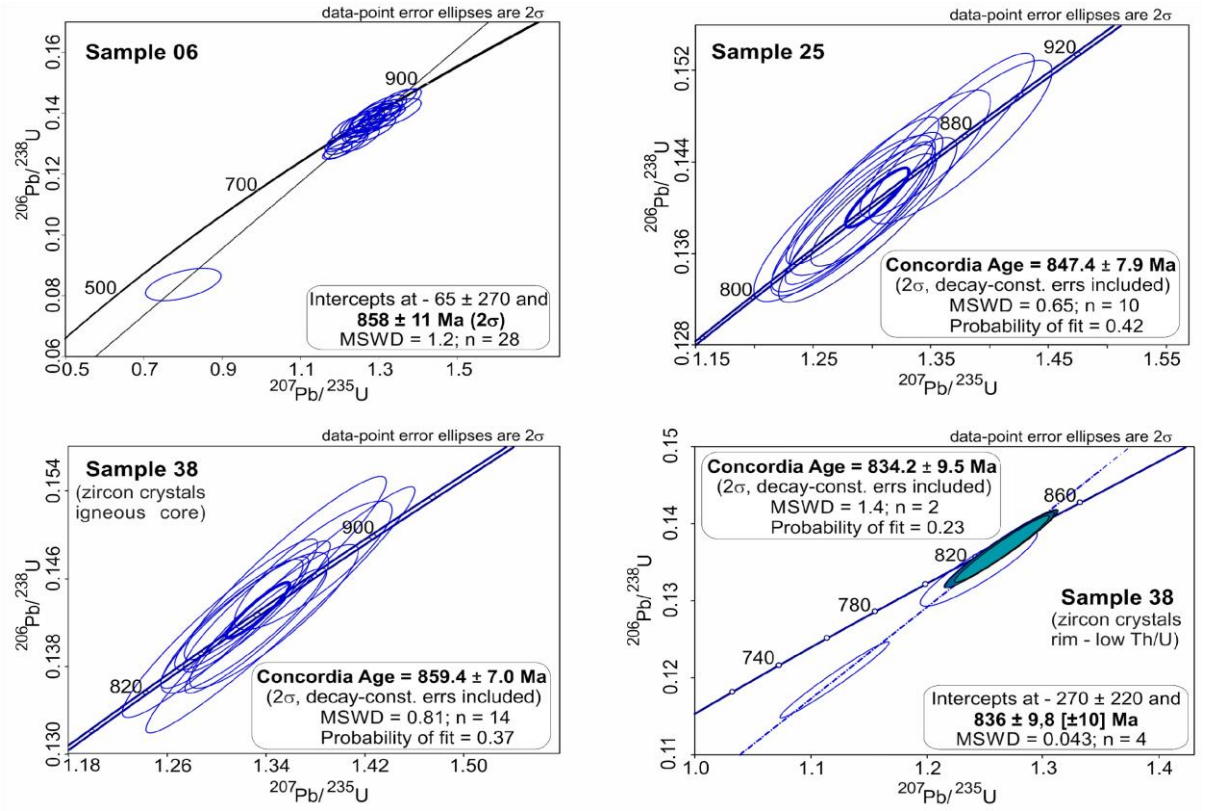

Fig. III. 11 - Concordia diagrams for samples of the Caxixe batholith. LA-ICP-MS U-Pb zircon dating for sample 06 and SHRIMP U-Pb zircon dating for samples 25 and 38.

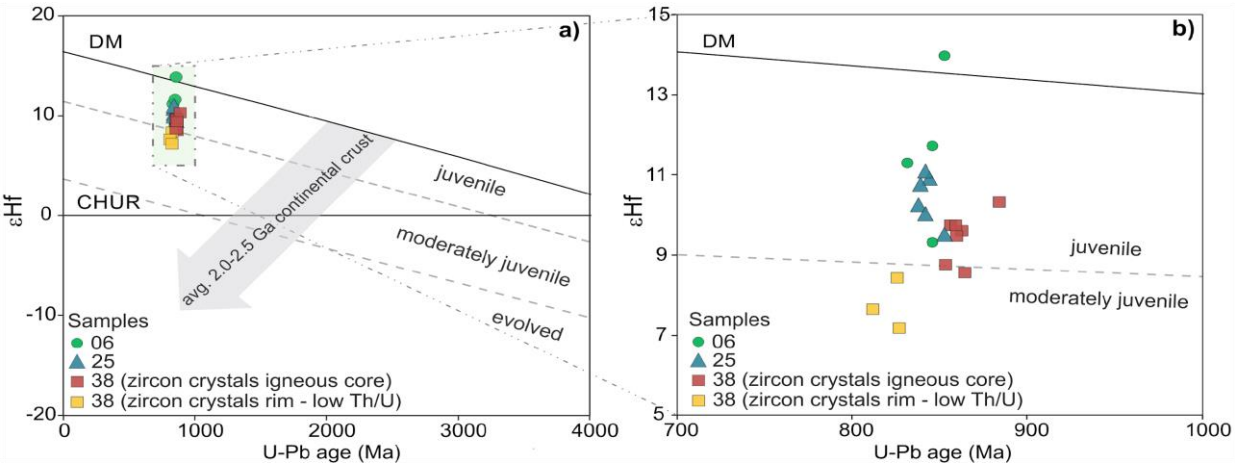

Fig. III. 12 - a) Plots of $\varepsilon Hf_{(t)}$ versus U-Pb age for analyzed zircon crystals; b) expanded view in the 700-1000 Ma interval. Grey dashed lines classify fields of juvenile (5 – 12 ε-units below DM) and evolved (> 12 ε-units below DM; Bahlburg et al., 2011) composition. The grey band represents the average evolution of typical continental crust generated around 2.0-2.5 Ga, with a $^{176}Lu/^{177}Hf$ = 0.010 for felsic and $^{176}Lu/^{177}Hf$ =0.022 for mafic crust (Pietranik et al., 2008). Model depleted mantle with present day $^{176}Hf/^{177}Hf$ ratio of 0.28325 and $^{176}Lu/^{177}Hf$ ratio of 0.0388 (Griffin et al., 2000; updated by Andersen et al., 2009).

III.5.4 Sm-Nd and Rb-Sr isotopes

Orthogneisses of the Caxixe batholith are characterized by Tonian to Stenian T_{DM} Nd model ages, ranging between ca. 0.8 Ga to ca. a1.2 Ga. The initial $^{143}Nd/^{144}Nd$ ratios show values between 0.5116 and 0.5119, which correspond to significantly positive $\varepsilon Nd_{(t)}$ values from +6.4 to +0.9. Initial $^{87}Sr/^{86}Sr$ ratios are between 0.6979 and 0.7035 (Fig. III.13 and Fig. III.14).

III.6 Discussion

III.6.1 Tectonic setting

The Caxixe batholith mostly includes biotite-rich granitic to tonalitic orthogneisses, with mafic and dioritic enclaves and facies, belonging to an expanded calcic to calc-alkaline series, with magnesian and I-type metaluminous to slightly peraluminous signature. The rocks show enrichment of highly mobile large ion lithophile elements (LILE) relative to high field strength elements (HFSE) and negative Nb-Ta-P-Ti anomalies, indicating classic features of arc-related igneous rocks. This signature is also corroborated by the negative Nb-Ta anomalies that are typical of subduction-related settings (Briqueu et al., 1984; Brown et al. 1984; McMillan et al., 1989; Pearce & Peate, 1995; Stern, 2002). The samples show positive to slightly negative anomalies of Eu, indicating minor plagioclase fractionation during magmatic differentiation. In addition, they present positive correlation between Na_2O and K_2O with SiO_2 but negative correlation for the other elements, according to fractionation of calc-alkaline magmas in subduction zones (Winter, 2010). Furthermore, lithochemical attributes plotted on tectonic discrimination diagrams are consistent with arc-related magmas, evolving from primitive (juvenile) to mature island arc settings (Fig. III.8).

The obtained geochronological and isotopic data supports the interpretation of arc-related juvenile magmatism, especially the robust isotopic (Hf in-zircon and whole-rock Nd and Sr) data, such as i) T_{DM} model ages for mantle extraction varying from 0.8 Ga to 1.01 Ga (Hf T_{DM}) and from 0.8 Ga to 1.2 Ga (Nd T_{DM}), very close to the U-Pb crystallization ages (ca. 840–860 Ma); and ii) highly positive values of $\varepsilon Hf_{(t)}$ (+13.9 to +7.2) and $\varepsilon Nd_{(t)}$ (+6.4 to +0.9). Altogether, the data point out to a striking contribution from the mantle wedge in magma genesis, thus ascribing the juvenile character for the

igneous protoliths of Caxixe orthogneisses. Furthermore, analyzed samples show isotopic Nd-Sr relations ranging from MORB (Mid-Ocean Ridge Basalt) up to BABI (Basaltic Achondritic Best Initial; Papanastassiou and Wassemburg, 1969) signatures, representing a rather undifferentiated mantle wedge component at the source (Fig. III.14). These features suggest that the juvenile Caxixe batholith (860–840 Ma) configures a very primitive segment of the Serra da Prata island arc.

The low Th/U rims of zircon crystals from sample 38, with Concordia age around 834 Ma, also display juvenile $\varepsilon Hf_{(t)}$ values but less positive (+8.4 to +7.2) than the related crystal cores with $\varepsilon Hf_{(t)}$ from +10.3 to +8.6 and magmatic age around 860 Ma, suggesting typical HT-LP intra-arc metamorphism (cf. Brown, 2009).

III.6.2 Regional correlations

Neoproterozoic juvenile magmatic arcs developed in the southeast and central Brazil during the Tonian. These juvenile arcs share a remarkable primitive nature and island arc setting related to intra-oceanic subduction in both the Goiás-Pharusian and Adamastor paleo-oceans (Fig. III.13 and Fig. III.14; Supplementary Material S3-2). For instance, the ca. 900-804 Ma Goiás Magmatic Arc (Pimentel and Fuck, 1992) of the Brasília Belt (Fig. III.1), that includes the Mara Rosa and Arenópolis arc segments, shows isotopic data with $\varepsilon Nd_{(t)}$ values of +0.37 to +6.0 and T_{DM} Nd model ages of ca. 1.2-0.8 Ga (Pimentel and Fuck, 1992). The rocks present metaluminous, calcic to calc-alkaline character with low Rb, Nb, Y, Zr and LREE concentrations (Pimentel and Fuck, 1992).

The main segment of the Serra da Prata arc (ca. 856-838 Ma) in the Ribeira belt (Peixoto et al., 2017) comprises orthogneisses with $\varepsilon Nd_{(t)}$ values of +3 to +5, T_{DM} Nd model ages of ca. 1.09-0.92 Ga and $^{87}Sr/^{86}Sr$ initial ratios between 0.7061 and 0.7113. Moreover, the geochemical characteristics of these rocks show calc-alkaline, metaluminous affinity, negative Eu anomalies and flat HREE patterns (Fig. III.9c) (Peixoto et al., 2017). Further arc system development in the Ribeira belt is represented by the oldest rocks of the Rio Negro arc (ca. 790 Ma) that comprises low- to medium-K compositions (Tupinambá et al., 2012) with $\varepsilon Nd_{(t)}$ if −3 to +5 and T_{DM} Nd model ages of ca. 0.99 Ga (Tupinambá et al., 2012).

Therefore, the Caxixe batholith shows both elemental and isotope (Nd-Sr-Hf) signatures and U-Pb crystallization ages very similar to other juvenile magmatic arcs

in the Brasiliano orogenic system. In addition, the robust dataset presented here strongly suggests that the juvenile batholith (860–840 Ma) represents the northern segment of the Serra da Prata intra-oceanic arc, much probably its northernmost tip that was tectonically emplaced in the transition zone between the Ribeira and Araçuaí orogens.

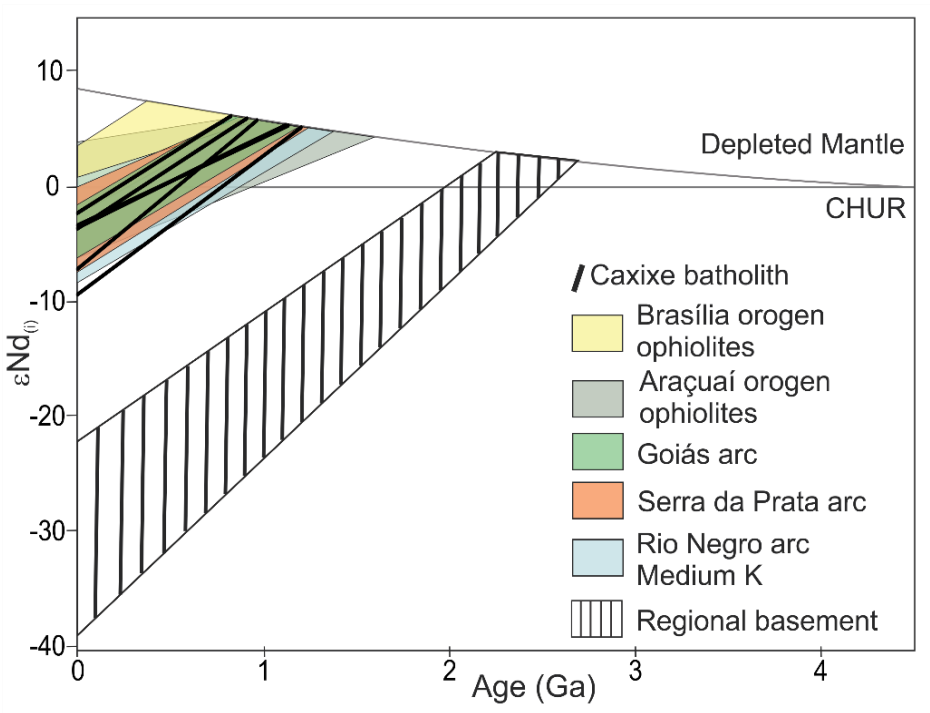

Fig. III. 13 - Nd isotopic signature of the Caxixe batholith orthogneisses compared to magmatic arcs and ophiolites of the Araçuaí, Ribeira and Brasília belts. Basement Paleoproterozoic basement rocks from São Francisco Craton and Quirino Complex (Ribeira belt basement) are presented for comparison. The compilation is based on Pimentel and Fuck (1992); Pedrosa-Soares et al. (1998); Machado et al. (2010); Queiroga (2010); Pimentel et al., (2000); Sato and Siga Junior (2000); Heilbron et al., (2013); Tupinambá et al., (2000, 2012); Peixoto et al., (2017) and Brown et al., (2020).

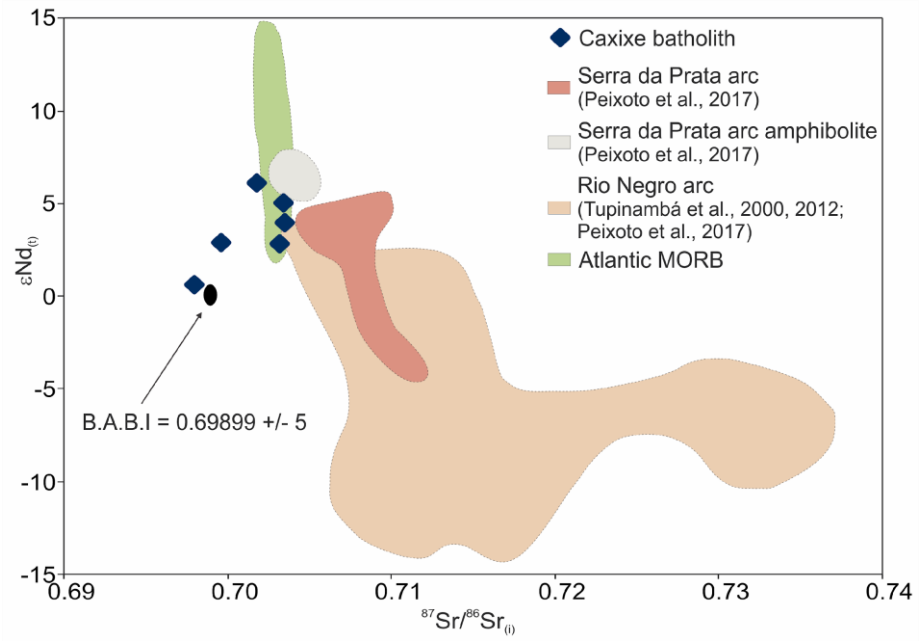

Fig. III. 14 - Initial $^{87}Sr/^{86}Sr$ versus $\varepsilon Nd_{(t)}$ suggesting the juvenile character of the original magmas and an important contribution of the mantle wedge in the genesis of the Caxixe batholith. Initial values are recalculated to 860 Ma. The amphibolites and orthogneisses of the Serra da Prata and Rio Negro complexes, Atlantic MORB and the BABI (Basaltic Achondritic Best Initial composition according to Papanastassiou and Wassemburg, (1969)) are presented for comparison. The compilation is based on Tupinambá et al., (2000, 2012) and Peixoto et al., 2017. Figure modified after Peixoto et al., (2017).

III.6.3. Implications for Western Gondwana crustal building, and paleogeographic and paleotectonic reconstructions

Island arcs are formed by processes related to intra-oceanic subduction within large oceanic realms that may endure from 50 Ma up to 300 Ma, comprising the most important records and reservoirs of juvenile (i.e., mantle-derived) continental crust in Earth's history (e.g., Condie, 2007; Cawood and Kröner, 2009). Modern island arcs provide the essential comparative tools to characterize Precambrian igneous rocks as parts of juvenile magmatic arcs that potentially represent ancient island arcs, such as classical arc-related rock assemblages, and their typical lithochemical and isotopic signatures (e.g., Rollinson, 1993; Pearce, 1996; Dickin, 2005; Allègre, 2012; White, 2013).

Accordingly, the geological-geochemical approach based on lithochemical and isotopic data has led to the discovery of Neoproterozoic juvenile arcs and ophiolites in Brazil (and elsewhere), such as the Goiás (Pimentel and Fuck, 1992; Laux et al., 2005), Rio Negro (Tupinambá et al., 2012) and Serra da Prata (Peixoto et al., 2017) island

arcs (Fig. III.1). As a corollary, the Serra da Prata and Goiás magmatic arcs, representing Early Tonian island arcs, require intra-oceanic subduction systems within large ocean realms that, in turn, would be located far south and west of the Congo - São Francisco paleocontinent (in relation to the present-day geography; Fig. III.15). Indeed, most paleogeographic reconstructions based on paleomagnetic data shows the Congo - São Francisco paleocontinent completely or in major part surrounded by large Tonian oceans (e.g., Cordani et al., 2003; Pisarevsky et al., 2003; Evans et al., 2015; D'Agrella-Filho and Cordani, 2017; Oriolo et al., 2017). In such scenario (Fig. III.15), the Caxixe batholith, characterized by clearly juvenile and rather primitive isotopic signatures, represents the northernmost tip of the Serra da Prata island arc around 860-840 Ma. This brings more solid evidence for the paleotectonic and paleogeographic scenarios long before the amalgamation of Western Gondwana, in which Neoproterozoic juvenile magmatic arcs (such as island arcs) developed over subduction zone systems within a paleo-ocean around the Angola, Congo – São Francisco, Paranapanema and Kalahari paleocontinental blocks. Another recent reconstruction also suggests intra-oceanic arcs outboard of the Congo - São Francisco paleocontinent, such as that from Merdith et al. (2017). In this reconstruction, the subduction zone dips northward, different from the model presented here where the arcs are oriented in a roughly N-S direction with both eastward and westwards subduction systems.

The present-day position of the Caxixe batholith resulted from complex structural interactions during the Brasiliano – Pan-African orogenic event some 300 Ma after the juvenile arc formation. Thus, this batholith represents an arc slice which now lies far from the original paleogeographic location (in relative terms to the other geotectonic components such as the Congo - São Francisco and Angola paleocontinental margins). The general tectonic transport from south-southeast to north-northwest, recorded by ductile structures related to the early deformation phases of both the northern Ribeira and southern Araçuaí orogens (Heilbron et al., 2004, 2008; Peres et al., 2004; Alkmim et al., 2006), together with relative displacements between blocks bounded by late-stage strike-slip shear zones can explain the present-day position of the Caxixe batholith in the transition zone between the Ribeira and Araçuaí orogens (Fig. III.2 and III.3).

Paleogeographic reconstructions based on paleomagnetic data suggest that the Congo - São Francisco paleocontinent drifted as a separated piece during the

Neoproterozoic, surrounded by large Tonian – Cryogenian oceans (e.g., Cordani et al., 2003; Pisarevsky et al., 2003; Evans et al., 2015; D'Agrella-Filho and Cordani, 2017; Oriolo et al., 2017). Besides, the reconstitutions of Heilbron et al. (2008) and Frimmel et al. (2011) suggest that the Angola block represents a distinct paleocontinental piece detached from the Congo paleocontinent during the Tonian and Cryogenian, leaving thus plenty of oceanic space for the formation of the Serra da Prata and Rio Negro island-arcs. Heilbron et al. (2008) suggested that the Luanda (or Malange) shear zone, a major E-W trending structure along the 9º S parallel south of Luanda (Angola) could be a main tectonic boundary which would separate the Angola craton, to the south, from the Congo craton, to the north. In any case, the present-day ridge-to-trench distance between the Mid-Atlantic Ridge and the Lesser Antilles and South Sandwich subduction zones, both around ca. 1300 km, suggest that there could have been more than enough space for the development of island arcs in the Tonian-Cryogenian Adamastor ocean, especially considering that the Neoproterozoic mantle was 100-150 ºC hotter than today (Brown et al., 2014).

In summary, the Caxixe batholith provides robust lithochemical and isotopic evidence supporting a clearly juvenile and primitive segment of an Early Tonian island arc, the Serra da Prata island arc, thus requiring development of intra-oceanic subduction, and as a corollary, the existence of a Tonian-Cryogenian Adamastor oceanic realm at least ca. 1300-2600 km wide, if compared to modern-day island arcs (Fig. III.15).

III.7 Conclusions

The Caxixe batholith has geochemical characteristics and isotopic signatures (Nd, Sr and Hf) consistent with emplacement in a Tonian (860-840 Ma) island arc setting in the transition zone between the Ribeira and Araçuaí orogens, not previously reported in the geological literature. Hf data from zircon and Nd-Sr isotopic data from whole-rock samples attest to the juvenile character of the protoliths, owing to important contributions from the mantle wedge in magma genesis of those rocks. Indeed, the Caxixe batholith correlates with other island-arc systems of similar age and isotopic features found in southeast and central Brazil and developed during the Tonian, strongly suggesting that the juvenile batholith represents a rather primitive northern segment of the Serra da Prata intra-oceanic arc. For the first time, a zircon rim age of

834 ± 9 Ma was obtained, indicating an intra-arc metamorphic event, a common process found in volcanic arcs of any age around the world.

Western Gondwana was formed mainly by the closure of the major Goiás-Pharusian and Adamastor oceans through consumption of oceanic crust in ocean-ocean and ocean-continent subduction zones. Therefore, the lithochemical and isotope signatures of the Caxixe batholith rocks and similar rocks southwards (the Serra da Prata and Rio Negro arcs) indicate the consumption of large tracts of oceanic crust in subduction zones and the involvement of a large amount of juvenile melt coming from the mantle wedge in its genesis. Comparing with the present-day ridge-to-trench distance to developing island-arcs, the Adamastor oceanic realm, within which the Serra da Prata Arc developed, could have been at least 1300-2600 km wide in the Tonian and Cryogenian.

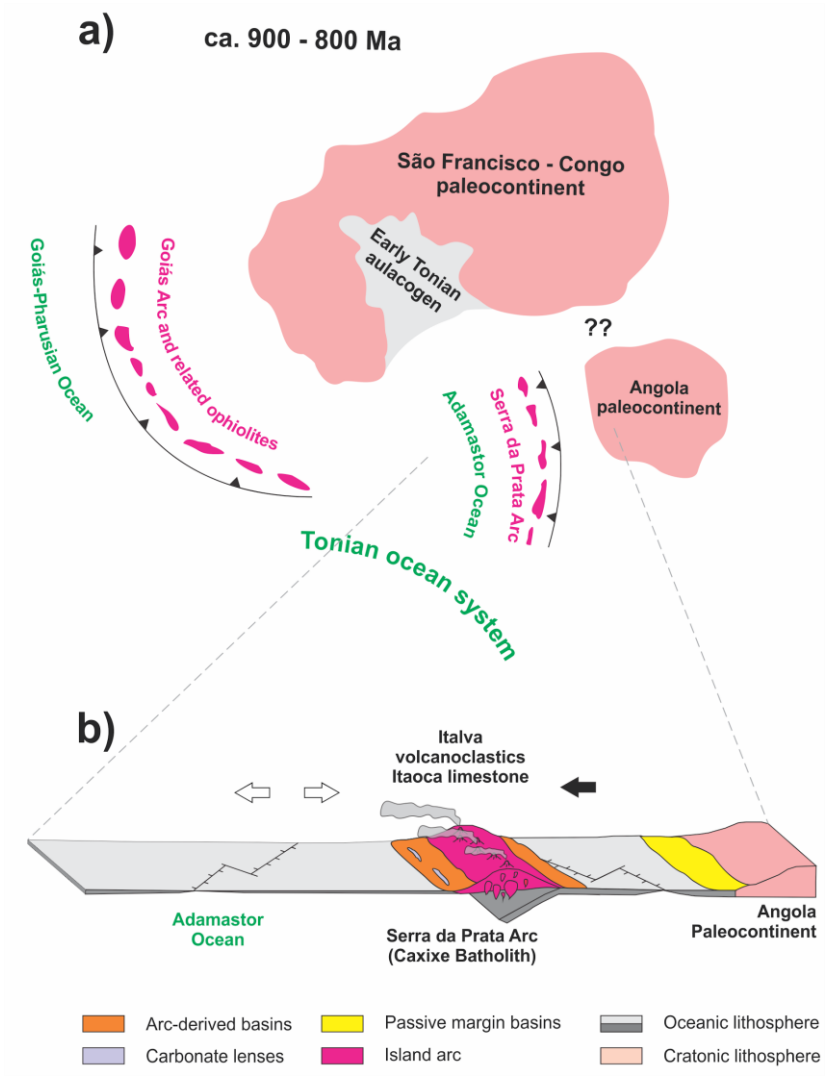

Fig. III. 15 - Cartoon suggesting a Tonian (900 – 800 Ma) paleotectonic-paleogeographic

scenario for the Serra da Prata island arc in map (a) and section (b).

III.8 Acknowledgments

The authors are grateful to the Brazilian research and development agencies (CNPq and CAPES) for financial support. SHRIMP work at the John de Laeter Center is enabled by NCRIS via AuScope. We thank Neal McNaughton, Allen Kennedy, Hao Gao and all of the John de Laeter staff for guidance and support during the analysis. FAC, ACPS and ELD are fellows of the Brazilian Scientific Council (CNPq), and acknowledge the financial support received, specially through grant 303566/2019-1 to FAC. An earlier version of this paper was greatly enhanced after comments and suggestions by Monica Heilbron and Donnelly Archibald. This paper is a contribution to Project MOBILE: Mountains Belts and the Inception of Complex Life on Earth (geolifemobile.com), supported by Instituto Serrapilheira (Serra-1912-31510).

CAPÍTULO IV

DETRITAL ZIRCON U-PB AND LU-HF CONSTRAINTS ON THE AGE, PROVENANCE AND TECTONIC SETTING OF ARC-RELATED HIGH-GRADE UNITS OF THE TRANSITION ZONE OF THE ARAÇUAÍ AND RIBEIRA OROGENS (SE BRAZIL)

(Artigo submetido ao periódico *Journal of South American Earth Sciences*)

Raíssa Santiago[a], Fabricio Andrade Caxito[a#], Antonio Pedrosa-Soares[a#], Mirna Aparecida Neves[b], Salomão Silva Calegari[b], Cristiano Lana[c#]

[a]Programa de Pós-graduação em Geologia and Centro de Pesquisas Manoel Teixeira da Costa, Universidade Federal de Minas Gerais (CPMTC-IGC-UFMG), Campus Pampulha, Av. Antônio Carlos 6627, 31270-901 Belo Horizonte, MG, Brazil

[b] Departamento de Geologia, Universidade Federal do Espírito Santo, Alto Universitário, s/n° – Guararema, 29500-000 Alegre, ES, Brazil

[c]Departamento de Geologia, Universidade Federal de Ouro Preto, Campus Morro do Cruzeiro, 35400-000 Ouro Preto, MG, Brazil

Fellow of the Scientific and Technologic Research Council of Brazil (CNPq)

IV.1. Abstract

Sedimentary basins with epiclastic and volcanoclastic components are important geotectonic components to understanding the complex evolution of orogenic systems. The age, provenance and tectonic setting of ancient basins are, however, often hard to constrain, especially in the high-grade core of ancient mountain belts where original sedimentary and stratigraphic relations have been largely obliterated by deformation and metamorphism. In this case, analytical tools such as whole-rock geochemistry and U-Pb and Lu-Hf analyses on detrital zircon grains can be deployed to unravel the provenance and tectonic setting of high-grade metasedimentary and metavolcaniclastic units. Here, we apply these analytical tools on samples from gneissic paleosomes of migmatites found in the eastern transition zone between the Neoproterozoic–Eopaleozoic Araçuaí and Ribeira orogens (southeastern Brazil). The studied paleosomes comprise peraluminous paragneisses rich in biotite, garnet and

sillimanite, metaluminous hornblende-bearing gneiss free of peraluminous silicates, and intermediate terms between these compositions, all of them with geochemical characteristics pointing to sources located in magmatic arc systems. Overall, U-Pb data from detrital zircon grains bracket a maximum sedimentation age for all samples between 600–627 Ma, and $\varepsilon Hf_{(t)}$: +5.7 to -18.7, and Hf T_{DM} model ages of 1.0 – 2.2 Ga) suggest moderately juvenile to evolved sources for the gneiss protoliths. However, despite the similarity in age range, the analyzed samples show contrasting isotope data indicating significant variability in the source areas. The first sample (7) only has grains with negative εHf (-5.9 to -18.7), most of them ranging in age from 708 Ma to 758 Ma, with very few older (1021-1143 Ma) and younger (642-651 Ma) zircons, indicating crustal evolved sources of distinct ages (e.g., the Late Tonian – Early Cryogenian South Bahia Alkaline Province, the Early Cryogenian magmatism found in the West Congo Belt, the Stenian to Early Tonian Espinhaço and Matadi-Noqui igneous rocks, and magmatic rocks of the early Rio Doce arc). Conversely, sample 13 has twenty grains with positive εHf values and ages between 602 – 758 Ma, suggesting sourcing from (meta)igneous rocks of the Rio Negro arc and their remelting products, and forty grains with negative εHf values with ages between 591 – 646 Ma suggesting magmatic sources from the Rio Doce arc. Additionally, the two youngest spot ages (553 Ma and 571 Ma) have highly negative εHf values (-11.1 and -16.4) suggesting their origin from collisional anatexis. Similarly, sample 12 shows detrital grains within the consistent time interval (ca. 596 Ma – 798 Ma) of the Rio Negro arc and Rio Doce arcs, reinforcing that the fragments of these arcs, or zircons crystals that were inherited from these arcs, are potential sources to the sedimentary protoliths of the paragneisses. The regional scenario together with our field and analytical data, compared with data available in the literature, suggest the sedimentary protoliths of the studied samples filled orogenic basins related to the Rio Doce magmatic arc. Most detrital zircon ages are close to the maximum depositional age, a classical signature of orogenic basins related to magmatic arcs. The studied paragneiss unit correlates with the Nova Venécia Complex, located from the intra-arc to back-arc zones of the Araçuaí orogen, and with the orogenic succession of the distal Andrelândia Group, shared by both the Araçuaí and Ribeira orogens. Furthermore, our data also suggest the juvenile Rio Negro - Serra da Prata arc system was either amalgamated with the Rio Doce arc, or that fragments of these arcs were incorporated as unmelted xenoliths and xenocrystals within the Rio Doce arc rocks before ca. 614 Ma, providing key hints

to unravel the evolution of the Araçuaí - Ribeira orogenic system (AROS) and its role in Gondwana assembly.

Keywords: Gondwana; sedimentary provenance; magmatic arc; Brasiliano Orogeny; detrital zircon; isotope geochemistry; back-arc basin; fore-arc basin; paragneiss; highgrade metamorphism.

IV.2. Introduction

Basins filled with sedimentary and volcaniclastic successions, found in orogenic systems, provide important records of plate margin evolution (Roeder, 2013). Therefore, the study of those basins can yield important information on the tectonic, magmatic, and thermal processes operating in the orogenic system to which they are related. However, owing to the different degrees of preservation, deformation, and metamorphism, the reconstruction of the sedimentary histories and tectonic settings of ancient basins becomes a challenge, especially in high-grade orogenic cores of ancient mountain belts (Erikson et al., 2001). As zircon generally preserves the initial isotopic compositions of the source magma at the time of crystallization and is particularly resistant to chemical weathering, detrital zircon grains can provide robust information on the ages of their sources, on magmatic and metamorphic events in the source areas, as well as data for paleogeographic reconstructions and tectonic analysis (e.g., Fedo et al., 2003, Griffin et al., 2004, Sun et al., 2008b; Fralick et al., 2009).

In southeastern Brazil, the Neoproterozoic-Eopaleozoic Araçuaí-Ribeira Orogenic System (AROS), extending for some 2,000 km in southeastern Brazil (Fig. IV. 1 a,b). It includes a northern segment, the Araçuaí orogen, developed to the east of the São Francisco craton (Pedrosa-Soares et al., 2001, 2008; Alkmim et al., 2006, 2017), and a southern segment, the Ribeira belt, a more complex orogenic system bordering the southern tip of the São Francisco craton and the eastern Paranapanema craton (Trouw et al., 2000; Heilbron et al., 2017). The Araçuaí and Ribeira orogens and their counterparts in Africa (from the West Congo to northern Kaoko belts), formed during the amalgamation of western Gondwana in the Ediacaran-Cambrian boundary, after a typical Wilson Cycle evolution, involving rift to passive margin basins, ophiolite slivers, intra-oceanic and continental-margin magmatic arcs and related orogenic

basins, and collisional to post-collisional processes and products (Cordani et al., 2003; Degler et al., 2017; Caxito et al., 2021). However, the border zone between the Araçuaí and Ribeira orogens is still a matter of debate, as the only well-known connection linking them is the Early Ediacaran Rio Doce magmatic arc (e.g., Tedeschi et al., 2016; Heilbron et al., 2020; Soares et al., 2020). While the Araçuaí orogen only shows one magmatic arc formed on an active continental margin, the Rio Doce arc (Pedrosa-Soares et al., 2011; Tedeschi et al., 2016; Gonçalves et al., 2017; Soares et al., 2020), the Ribeira orogen encompasses juvenile intra-oceanic arcs, the early Tonian Serra da Prata arc (Peixoto et al., 2017; Santiago et al., 2020b) and the Cryogenian to early Ediacaran Rio Negro arc (Tupinambá et al., 2012; Heilbron et al., 2020), and southern segments of the continental-margin Rio Doce arc (e.g., the Serra da Bolívia and Marceleza-Leopoldina batholiths and plutons; Heilbron et al., 2013, 2020; Corrales et al., 2020). Therefore, the arc-related basins, recorded by high-grade metasedimentary rocks, can provide important information on depositional ages, provenance and source of sedimentary successions, shedding light on the relations between those orogens in space and time.

The high-grade metasedimentary units of the high-grade core are thus of utmost importance for understanding the AROS tectonic evolution, especially those located in the transition zone between the Araçuaí and Ribeira orogens, around the 21°S parallel that has been considered as a reference divisor of the two orogens for a long time (Pedrosa-Soares and Wiedemann-Leonardos, 2000, Pedrosa-Soares et al., 2001, Heilbron et al., 2004). Nonetheless, recent studies have shown an increasingly precise continuity between units of both orogens in this area, especially in relation to the batholiths and plutons comprised by the Rio Doce arc (Tedeschi et al., 2016, Heilbron et al., 2020, Soares et al., 2020). Therefore, it is essential to investigate the focused metasedimentary unit by using tools such as whole-rock geochemical, U-Pb geochronology on detrital zircon grains, and Hf isotopic data, that have been widely used in the study of Precambrian sedimentary basins (e.g., Haughton et al., 1991).

In this paper, we present field observations, petrography, new whole-rock geochemical data, and the results of U-Pb and Hf isotope systematics on detrital zircon grains from gneissic paleosomes of migmatites found in the transition zone between the Araçuaí and Ribeira orogens, in the southern Espírito Santo state, eastern Brazil. The results shed light on the age, provenance, and tectonic setting of the high-grade gneisses within the internal zone of the AROS, and its relevance for western

Gondwana amalgamation processes.

IV.2. Geological Context

During the Neoproterozoic-Eopaleozoic Brasiliano – Pan-African cycle, the Araçuaí – Ribeira orogenic system (AROS) resulted from a series of subduction-to-collision processes, involving diachronic convergences of the São Francisco, Congo, Paranapanema and Angola cratons (Fig. IV. 1 a,b), and the closure of the northern Adamastor Ocean realm (e.g., Pedrosa-Soares et al., 2001, 2008; Cordani et al., 2003, Alkmim et al., 2006, 2017; Heilbron et al. 2017, 2020; Caxito et al., 2021). The AROS comprises Archean and Paleoproterozoic basement blocks and inliers, Tonian and Cryogenian rift-related to distal passive margin and oceanic sequences of the precursor basin system, and the orogenic core rich in granitic (s.l.) and high-grade metamorphic rocks (Pedrosa Soares et al., 2011; Heilbron et al., 2017, 2020; Caxito et al., 2021). The orogenic core includes pre-collisional magmatic arcs, collisional granitic batholiths and plutons, and post-collisional igneous intrusions, formed in several magmatic events since the Tonian to the Cambrian-Ordovician (Pedrosa-Soares et al., 2011; Tupinambá et al., 2012; Heilbron et al., 2013, 2020; Gradim et al., 2014; Tedeschi et al., 2016; De Campos et al., 2016; Gonçalves et al., 2017; Melo et al., 2017; Peixoto et al., 2018; Araujo et al., 2020, Corrales et al., 2020; Santiago et al., 2020b; Soares et al., 2020).

Along the eastern AROS region, the high-grade metamorphic complexes mostly comprise migmatitic paragneisses and peraluminous granulites, several of them with age spectra and isotopic Hf data from detrital zircon indicating sediment sources located in the Rio Doce, Rio Negro and Serra da Prata arcs (e.g., Gradim et al., 2014, Fernandes et al., 2015, Lobato et al., 2015, Gonçalves-Dias et al., 2016, Richter et al., 2016, Degler et al., 2017, Araujo et al., 2020, Pacheco et al., 2020).

Metasedimentary successions of the eastern Araçuaí Orogen include the Rio Doce Group, interpreted as an arc-related metavolcano-sedimentary sequence (Vieira, 2007; Novo, 2013; Novo et al., 2018); and the high-grade metamorphic complexes belonging to the Jequitinhonha and Nova Venécia complexes, composed of migmatitic paragneisses whose protoliths have been deposited in the distal passive margin and back-arc basin settings, respectively (Noce et al., 2004; Vieira, 2007; Gradim et al., 2014; Moraes et al., 2015; Richter et al., 2016; Gonçalves-Dias et al., 2016; Pacheco

et al., 2020).

Metasedimentary successions of the northern Ribeira Orogen adjacent to the study area are interpreted as related to the Serra da Prata (ca. 860-840 Ma; Peixoto et al., 2017, Santiago et al., 2020b) and Rio Negro (ca. 790–620 Ma; Tupinambá et al., 2012; Heilbron et al., 2020) intra-oceanic magmatic arcs. The Italva Group (ca. 860 – 840 Ma) consists of gneisses intercalated with marbles and amphibolites, associated with the development of the Tonian Serra da Prata magmatic arc, has been interpreted as a back-arc basin infill (Heilbron & Machado 2003, Sad & Dutra 1988, Peixoto & Heilbron 2010, Peixoto et al. 2017). The São Fidelis Group, comprising migmatitic graphite-cordierite-sillimanite-biotite-garnet paragneisses with lenses of orthoquartzite, feldspathic quartzite, amphibolite and calcsilicate rock, has also been interpreted as a back-arc basin but with detrital zircon provenance from the Rio Negro and Serra da Prata arcs, and from Mesoproterozoic to Orosirian (ca. 1.9 Ga) sources (Tupinambá et al., 2012; Lobato et al., 2015; Heilbron et al., 2017). Finally, the Andrelândia Group represents sedimentary rocks deposited in continental rift, passive margin and orogenic basins in the southeastern São Francisco Craton margin, encompassing both the southern Araçuaí, Brasília and Ribeira orogens (Paciullo et al., 2000; Heilbron et al., 2004; Belém et al., 2011; Trouw et al., 2013; Degler et al., 2017).

The AROS shows tectonic structures recording the deformational phases related to the Brasiliano orogenic event. Around the 21° S latitude (Fig.IV.1 b), the transition zone between the northern Ribeira orogen, to the south, and the southern Araçuaí orogen, to the north, is marked by a change in the Brasiliano structural trend from NE-SW to N-S (Pedrosa-Soares et al., 2001; Heilbron et al., 2004, 2008). The main tectonic elements in the region are dextral strike-slip shear zones trending NE-SW to NNE-SSW, such as the Guaçuí (GSZ) and the Batatal shear zones (BSZ) which are outlined by a prominent mylonitic foliation formed during the lateral escape tectonics at the late collisional stage (Cunningham et al., 1998; Alkmim et al., 2006; Heilbron et al., 2004, 2008).

The studied region, located in the AROS orogenic core between latitudes 20°S and 21°S (Fig.IV.1b), mainly encompasses pre-collisional orthogneisses (840-860 Ma) in the Caxixe batholith, recording the juvenile Serra da Prata arc (Santiago et al., 2020b), deformed and metamorphosed tonalitic to granitic batholiths and plutons of the G1 supersuite (630 - 580 Ma) representing the continental Rio Doce arc (Tedeschi et al., 2016; Soares et al., 2020), and post-collisional intrusions of the G5 supersuite

(525 - 480 Ma; De Campos et al., 2016). The collisional plutonism includes peraluminous (S-type) granitic leucosomes and small plutons mostly formed from the partial melting of high-grade paragneisses (De Campos et al., 2004; Pedrosa-Soares et al., 2011, Gradim et al., 2014).

In previous studies, the metasedimentary rocks in each side of the GSZ are variably interpreted as distinct regional stratigraphic units. For example, in the Cachoeiro de Itapemirim 1:250.000 sheet of the Brazilian Geological Survey (Vieira, 1995), to the west of the GSZ the rocks are mapped as “Paraíba do Sul Complex – metasedimentary and metavolcanosedimentary”, while to the east, they are mapped as “Paraíba do Sul Complex – metavolcanosedimentary”. In the Espera Feliz 1:100.000 geological sheet of the Brazilian Geological Survey (Horn, 2006), on the other hand, paragnaissic rocks to the west and east of the GSZ are mapped as “Andrelândia Group” and “Paraíba do Sul Complex”, respectively. In the newest geological map of the Espírito Santo state published by the Geological Survey of Brazil (Vieira et al., 2018), rocks to the east of the GSZ are mapped as part of the Rio Doce and Raposo groups, while to the west, the metasedimentary rocks are mapped as part of the Bom Jesus do Itabapoana, São Fidélis and Italva groups. Thus, there is currently no consensus on the stratigraphic positioning and correlation of the metasedimentary rock units in the studied area, being variably correlated to regional units interpreted as related to passive margin successions and to basins related to the Serra da Prata, Rio Negro and Rio Doce arc systems.

VI.3. Materials and Methods

VI.3.1 Field relationships, sample preparation and petrography

Field campaigns were conducted in the southern Espírito Santo State to collect representative samples for petrographic, geochemical, and geochronological analysis. Thin sections of 5 samples were prepared at the CPMTC Research Center labs, Federal University of Minas Gerais (UFMG), Brazil. Samples were prepared for geochemical and geochronological analysis at CPMTC laboratories. The studied samples include paragneiss with biotite, garnet and/or sillimanite, hornblende-bearing gneiss free of peraluminous minerals, and intermediate terms between them.

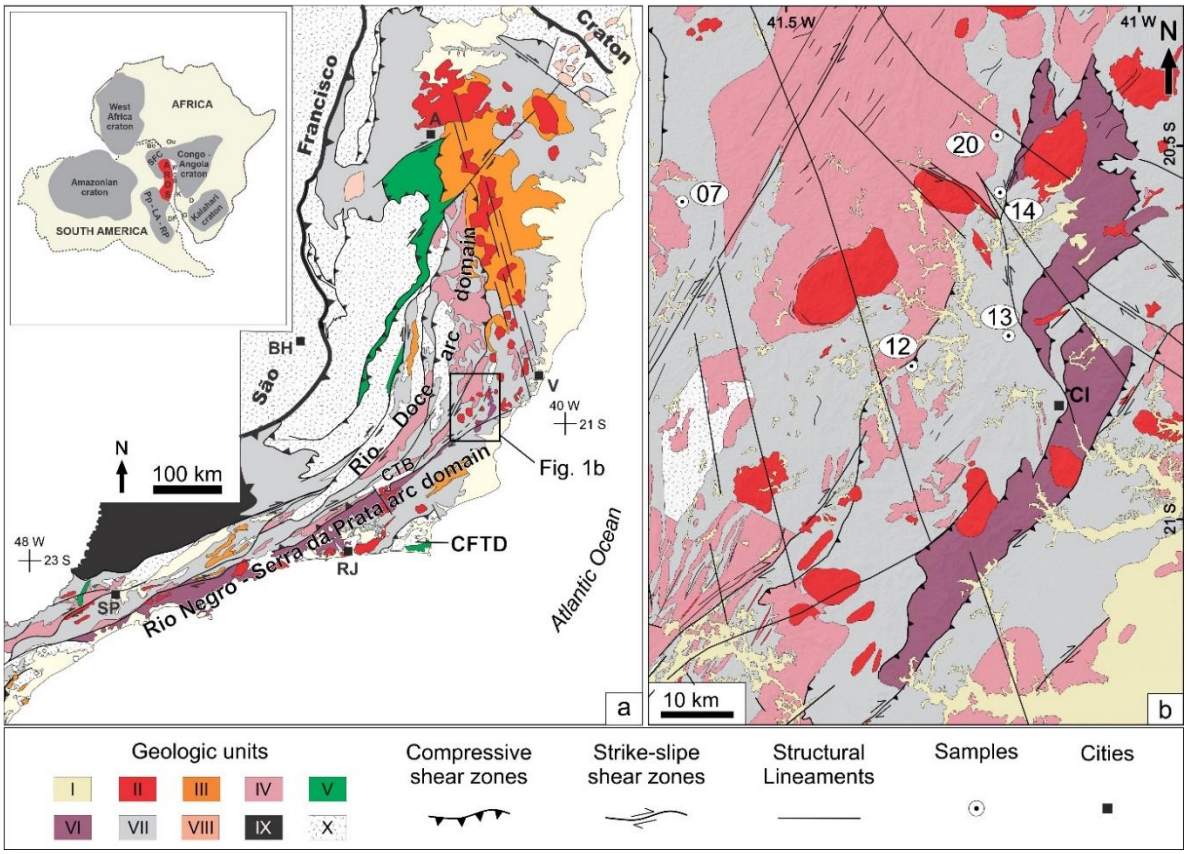

Fig. IV. 1 - a) Location sketch showing the Araçuaí-Ribeira orogenic system (AROS) in Western Gondwana. WCB, West Congo belt. CSF, Sao Francisco craton. Pp-LA-RP, Paranapanema-Luiz Alves-Rio de La Plata cratonic blocks; CI, Cachoeiro de Itapemirim. AROS geological map (modified and simplified from Silva et al., 2005) and b) Geological map of the study region (modified from Santiago et al., 2020b): I - Cenozoic covers; II - Post-collisional plutonism; III - Collisional plutonism; IV - Rio Doce magmatic arc; V - Ophiolite-bearing rock assemblages; VI - Serra da Prata - Rio Negro arc; VII - Neoproterozoic metasedimentary and metavolcanic successions; VIII - Tonian and Cryogenian rift-related magmatic rocks; IX - Southern Brasília belt; X - Pre-Neoproterozoic units and cratonic covers.

VI.3.2 Whole-rock chemistry analyses

Lithochemical analyses (Supplementary Material SIV-1) were conducted at SGS-Geosol Laboratory, Brazil. Element grades were analyzed by ICP-MS (Induced Coupled Plasma – Mass Spectrometry) after fusion with lithium metaborate/tetraborate and digestion with diluted nitric acid. Analytical errors are within 2% for major oxides and 5% for trace elements. The detection limit for major elements is 0.01%. For the trace elements, the limits are of 10 ppm (Ba, Sr, Zr), 5 ppm (Zn, V, Cu, Ni), 0.5 ppm (Co), 0.3 ppm (Sn), 0.2 ppm (Rb), 0.1 ppm (Ce, Ga, La, Nd, Sm, Th, W, Yb) and 0.05 ppm (Cs, Dy, Er, Eu, Gd, Hf, Ho, Lu, Nb, Pr, Ta, Tb, Tm, U, Y). Base and precious metal contents were determined by digestion in aqua regia followed by ICP-MS

analysis. Loss on ignition (LOI) was determined by the weighing difference after ignition at 1000 °C. The CIPW norm of the standard mineral components, from the whole-rock analyses, was based on Johannsen (1931). Since the whole-rock chemical analyses considered only Fe_2O_3, the estimation of FeO and Fe_2O_3 was based on Gill (2010), who used the ratio 0.9, that is, FeO estimated = 0.9 × Fe_2O_3Total.

VI.3.3 LA-ICP-MS U-Pb zircon dating

U-Pb and Hf LA-ICP-MS (Laser Ablation – Induced Coupled Plasma Mass Spectrometry) analysis (Supplementary Material SIV-2) were performed in zircon crystals separated through standard crushing, sieving, magnetic and gravimetric methods from homogeneous portions (i.e, bearing no veins, fractures or alteration fronts) of samples 07, 12 and 13 in the SEPURA – Laboratório de Separação Mineral de Alta Pureza at CPMTC, UFMG – Federal University of Minas Gerais, Brazil.

After mounting in epoxi and polishing, zircon crystals were imaged through standard SEM (Scanning Electron Microscopy) techniques such as Secondary Electrons (SE), Back-Scattered Electrons (BSE) and Cathodoluminescence (CL). The resulting images emphasize the internal structure of zircon grains (zoning, fracturing, etc.) and aid in the location of laser spots in the most homogeneous portions of zircon grains (e.g., free of fractures and inclusions).

Zircon U–Pb isotope analyses were performed by LA-ICP-MS at UFOP using a Thermo-Fisher Element II sector field ICP-MS coupled to a CETAC LSX-213 G2+ (λ = 213 nm) Nd:YAG laser. A detailed description of the method is given by Gerdes and Zeh (2006, 2009). Ablation was carried out in a low-volume cell with He as carrier gas; laser beam parameters used were a spot size of 20 µm, a repetition rate of 10 Hz, and a fluence of ~3 J cm-2. Time-resolved raw data were corrected offline for background signal, common Pb, laser-induced elemental fractionation, instrumental mass discrimination, and time-dependent elemental fractionation of Pb/U using the GLITTER® software package (Van Achterbergh et al., 2001). Common Pb correction was applied using the interference- and background-corrected ^{204}Pb signal and a model Pb composition (Stacey and Kramers, 1975). Laser induced elemental fractionation and instrumental mass discrimination were corrected by normalisation to the reference zircon GJ-1 (Jackson et al., 2004), which was routinely measured within each analytical session. The drift in inter-elemental fractionation (Pb/U) during 30s of

sample ablation was corrected individually before normalisation to GJ-1. Reported uncertainties (2σ) were propagated by quadratic addition of the external reproducibility obtained from the standard zircon GJ-1 during the analytical session (2SD in %) and the within-run precision of each analysis (standard error in %). In order to test the validity of the applied methods and the reproducibility of the data, multiple analyses of the reference zircon Plešovice (Sláma et al., 2008) were performed. Plešovice gave concordia ages of 338.6 ± 2.4 Ma (n = 10, MSWD = 0.29), 337.6 ±2.6 Ma (n = 6, MSWD = 1.5) and 339.8 ± 2.1 Ma (n = 14, MSWD = 0.03) during analysis of samples 07, 12 and 13, respectively. These are in agreement, within uncertainty, with the accepted ID-TIMS age reported for Plešovice (337.3 ± 0.4 Ma 2σ, Sláma et al., 2008). In addition, several analyses of the in-house reference zircon BB (Santos et al., 2017) were conducted. BB yielded Concordia ages of 563.2 ± 4.1 Ma (n = 10, MSWD = 0.05), 558.8 ± 4.4 Ma (n = 6, MSWD = 0.82) and 562.3 ±3.1 Ma (n = 14, MSWD = 0.04), respectively, which are consistent with the reported ID-TIMS age of this reference material (560.0 ± 0.4 Ma 2σ, Santos et al., 2017). U-Pb ages were calculated using Isoplot 3.6 (Ludwig, 2008). All uncertainties are presented at the 2σ level.

VI.3.4. Hf isotope analyses

Hf isotope ratios were determined on six selected zircon crystals of sample 07 and ten zircon crystals of sample 13 (Supplementary Material SIV-3). Hf isotope analyses were carried out in a Thermo-Finnigan Neptune multicollector ICPMS coupled to a Photon-Machines laser system that delivers a beam of 193 nm UV light from a frequency-quintupled Nd:YAG laser hosted in the *Laboratório de Geoquímica Isotópica*, Federal University of Ouro Preto (UFOP) . The analyses were achieved with a beam diameter of 50 μm, a repetition rate between 4 and 6 Hz and 50% of laser output. Depending on the conditions and Hf contents, the Hf signals were between 1 to 6x10-11 A and the ablation time lasted 60 s. Ar carrier gas transported from the ablated sample from the laser ablation cell via mixing chamber to the ICPMS torch. To correct for the isobaric interferences of ^{176}Lu and ^{176}Yb on ^{176}Hf, masses 172, 173 and 175–180 were measured in static- collection mode and simultaneously monitored. The ^{177}Hf signal intensity was ca. 10 V. LA-ICP-MC data were reduced using In-house Excel Spreadsheets.

The accuracy and external reproducibility of the Lu–Hf results from samples 07

and 13 were monitored through the analysis of zircon standards Temora ($^{176}Hf/^{177}Hf$ = 0.282680 ± 0.000031; Black et al., 2003; Wu et al., 2006), Blue Berry ($^{176}Hf/^{177}Hf$ = 0.281674 ± 0.000018; Santos, M.M. et al., 2017), Mud Tank ($^{176}Hf/^{177}Hf$ = 0.282504 ± 0.000044; Black and Gulson, 1978; Woodhead and Hergt, 2005), GJ-1 ($^{176}Hf/^{177}Hf$ = 0.282000 ± 0.000005; Jackson et al., 2004) and Plešovice ($^{176}Hf/^{177}Hf$ = 0.282482 ± 0.000013; Sláma et al., 2008), which yielded $^{176}Hf/^{177}Hf$ average ratios of 0.282654 ± 0.000014 (n = 1), 0.281673 ± 0.000017 (n = 8), 0.282519 ± 0.000015 (n = 9), 0.282006 ± 0.000019 (n = 7) and 0.282485 ± 0.000014 (n = 9), respectively (±2SD); all values within the uncertainties and in good agreement with the accepted standard ratios.

Initial Hf isotope ratios were recalculated to the $^{206}Pb/^{238}U$ age of each zircon crystal. For the calculation of the $\varepsilon Hf_{(t)}$ values, the chondritic values reported by Bouvier et al. (2008) of $^{176}Hf/^{177}Hf$ = 0.282785 ± 11 and $^{176}Lu/^{177}Hf$ = 0.0336 ± 1 were used. To calculate the model ages (TDM) based on a depleted mantled source, the present-day ratios of $^{176}Hf/^{177}Hf$ = 0.28325 and $^{176}Lu/^{177}Hf$ = 0.0388 were used (Griffin et al., 2000; updated by Andersen et al., 2009). The λ decay constant for ^{176}Lu used is $1.867x10^{-11}$/yr (Söderlund et al., 2004).

VI.4. Results

VI.4.1 Field and petrographic description

The studied samples include paragneiss with biotite, garnet and/or sillimanite, hornblende-bearing gneiss free of peraluminous minerals, and intermediate terms between them (Fig.IV. 2 and Fig.IV. 3). The paragneisses outcrops are typically banded and variably migmatized with bands varying in thickness from 4 mm to 20 cm, generally parallel to the low-angle east-dipping regional foliation. The predominant migmatitic structure is stromatic, but folded structure also occurs (Fig.IV. 2). The paragneisses containing aluminous minerals essentially consists of quartz, plagioclase, reddish-brown and green biotite, K-feldspar (both orthoclase and microcline), garnet and sillimanite, in decreasing order of content, while the hornblende-bearing gneisses are composed of quartz, plagioclase, biotite and hornblende. Accessory minerals are apatite, zircon, allanite and titanite. Down-dip mineral lineation is characterized by the stretching of the crystals of biotite, sillimanite and quartz. In addition, centimetric to decimetric isoclinal to closed intrafolial folds

verging WSW occur systematically (Fig.IV. 2). Discordant quartz-feldspar veins locally occur. The main studied outcrops, where samples were collected for geochronological and geochemical analysis, are described below.

Outcrop 07 consists of garnet-sillimanite-biotite gneiss, are mesocratic gray, fine- to medium-grained with millimeter to centimeter gneiss banding and garnet porphyroblasts (Fig.IV. 2 a) and b)). On thin section, plagioclase, quartz, biotite, K-feldspar, garnet, and sillimanite were identified, with titanite, and zircon as accessories (<1%), and secondary sericite and Fe-oxides. The dominant feldspar in the matrix is plagioclase, occurring with granoblastic texture and forming porphyroblasts. Biotite form subhedral crystals, defining the foliation. Quartz is present in the matrix with polygonal contacts. The total content of sillimanite is about 4–5 % in volume, forming subhedral crystals with granular habit. Garnet crystals are commonly euhedral to subhedral porphyroblasts ranging from 0.1 to 5.0 mm.

Outcrop 12 is a garnet-biotite gneiss from an outcrop of leuco- to mesocratic folded gneiss. The sample consists of garnet, plagioclase, quartz, biotite and zircon as the main accessory and Fe-oxides (Fig.IV. 3 c)). Subhedral to euhedral plagioclase crystals show typical polysynthetic twining, occurring with granoblastic texture. Sericite occur as an alteration product of plagioclase. Dark to light brown biotite form subhedral crystals, defining the foliation. Rare muscovite crystals are associated to biotite. Quartz is present in the matrix with polygonal contacts. Deformation microstructures of quartz include undulose extinction and sub-grains. Garnet crystals are commonly euhedral to subhedral porphyroblasts ranging in size from 0.2 to 2 mm.

Outcrop 13 shows portions with gneissic banding and portions with migmatized structure, revealing different partial melting intensity. In addition, there are mafic enclaves ranging from 10 to 80 cm, concordant with the fine-grained banding and foliated (Fig.IV. 2 d)). Foliation is locally interrupted by an L-type tectonite pattern (Fig.IV. 2 c) and d)) which the minerals of biotite, sillimanite and quartz are strongly elongated. The homogeneous banded portion (paleosome) consists of hornblende-biotite gneiss (Fig.IV. 3 d)). From this hornblende-bearing gneiss analyzes of whole-rock geochemistry, U-Pb and Lu-Hf in zircon were done. The minerals occur oriented yielding a nematolepidoblastic texture, and sometimes a granoblastic texture between quartz crystals with interlobate contacts. The quartz crystals show fine to medium granulation (0.25 to 3 mm) and granular habit, are xenoblastic, show interlocked contacts and usually presenting undulatory extinction. Hornblende is fine-grained with

a granular habit; the crystals vary from idioblastic to subdioblastic, with interlobed contacts and sometimes occur oriented associated with biotite. Biotite also occurs oriented, shows pleochroism ranging from light to dark brown and are fine-grained. The plagioclase, to a lesser proportion, presents fine to coarse granulation, granular habit, and usually shows a polysynthetic twin.

Other hornblende-biotite gneisses are leuco-mesocratic, fine- to medium-grained, and show millimeter to centimeter gneissic banding that can be folded (outcrops 14 and 20; Fig.IV. 2e)). The collected samples have plagioclase, quartz, biotite, hornblende and titanite as accessories and sericite and Fe-oxides as secondary minerals (Fig.IV. 3f)). The dominant feldspar in the matrix is subhedral to euhedral plagioclase crystals that show typical polysynthetic twining and form porphyroblasts. Quartz is present in the matrix with polygonal contacts. Brown and reddish biotite slats form subhedral crystals, defining the foliation, as well as hornblende, with medium-grained nematolepidoblastic texture and pleochroism varying in hues from dark to medium green.

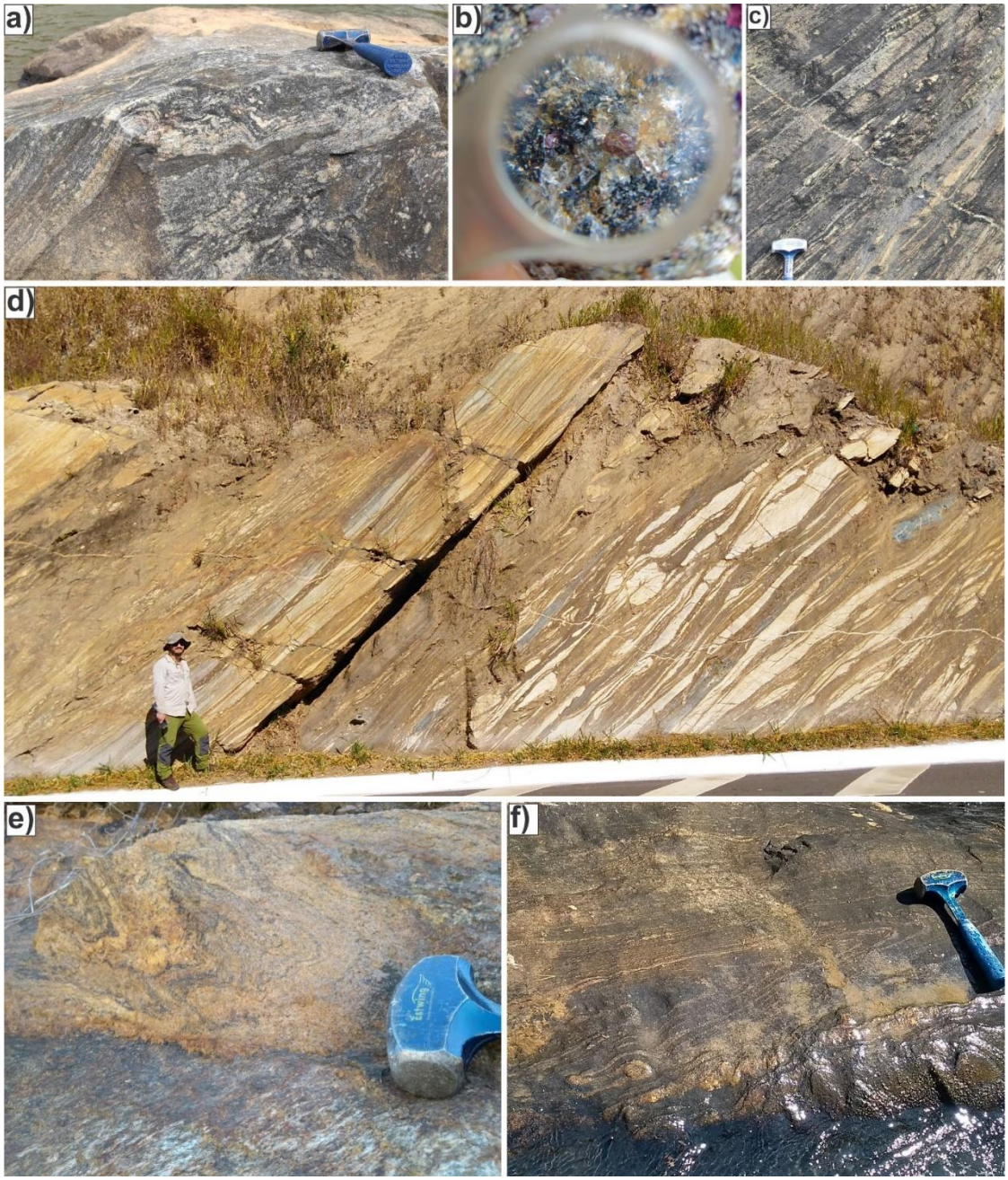

Fig. IV. 2 - Mesoscale aspects of the paragneisses from AROS inner core in the southern Espírito Santo state, Southeastern Brazil. (a) Garnet-sillimanite-biotite gneisses in outcrop 07 with (b) garnet porphyroblasts; (c) L-type tectonites pattern with strongly elongated biotite, sillimanite and quartz and (d) migmatitic structures and metamorphic banding with thickness varying from millimeters to centimeters in outcrop 13; isoclinal to tight intrafolial folds (with WSW vergence) in outcrops 12 (d) and 20 (e).

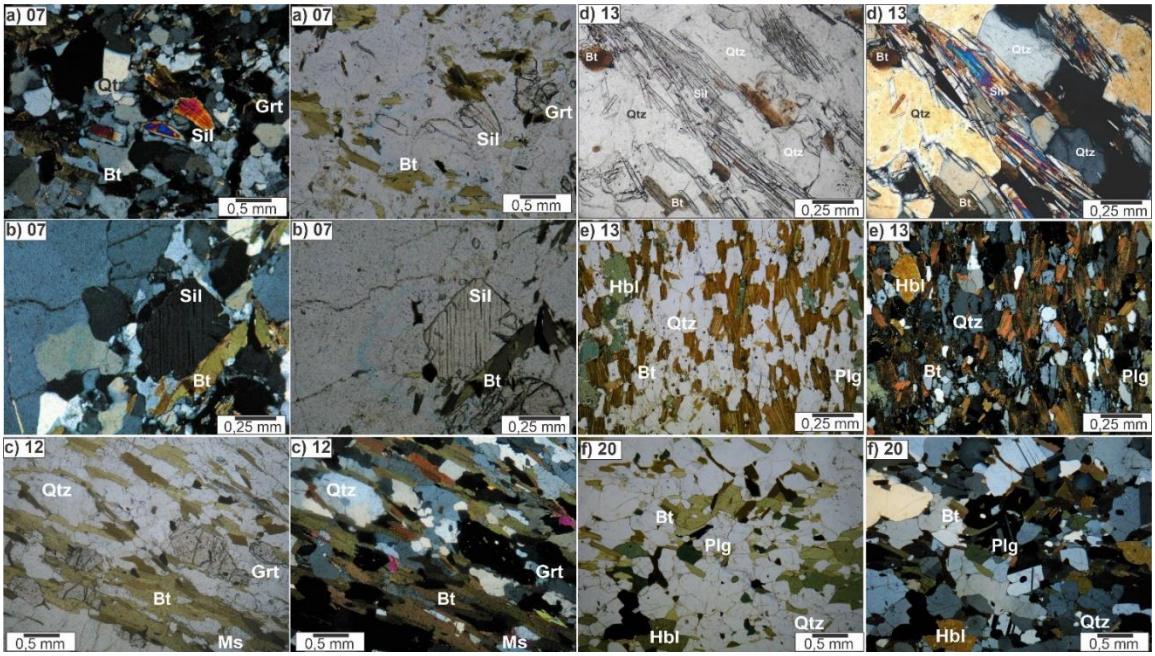

Fig. IV. 3 - Photomicrographs of thin sections of samples from AROS paragneisses in the southern Espírito Santo state, Southeastern Brazil showing the different mineralogical associations: a) and b) garnet-sillimanite-biotite gneiss (outcrop 07); c) garnet-biotite gneiss (outcrop 12); d) sillimanite-biotite gneiss with L-type tectonites pattern and e) hornblende-biotite gneisses, both in outcrop 13; and f) hornblende-biotite gneisses (outcrop 20). Legend: Qtz = Quartz, Sil = Sillimanite, Bt = Biotite, Plag = plagioclase, Grt = garnet, hbl = Hornblende, Ms = muscovite.

VI.4.2 Lithochemistry

Five whole-rock samples of gneissic paleosomes were analyzed for lithochemical data (Supplementary Material SIV-1). Only paleosome portions of migmatized samples were analyzed, in order to investigate the lithochemical signature as close as possible to the original protolith composition.

For whole-rock peraluminous gneisses rich in biotite, garnet and/or sillimanite samples (samples 7 and 12), the major elements data (wt%) show SiO_2 contents between 69.44% and 72.00%, TiO_2 from 0.65% to 0.76%, Al_2O_3 ranging from 13.46% to 14.32%, $FeO_{(t)}$ (5.03%–4.66%), MgO (0.81%–1.51%), CaO (1.83%–2.06%), Na_2O (2.49%–2.57%) and K_2O ranging from 3.04% to 3.72% (Fig.IV.4). In comparison, the hornblende-bearing metaluminous gneisses free of peraluminous silicates (samples 13, 14 and 20), the sample show contents of SiO_2 (51.36–61.81 wt%), TiO_2 (0.57–1.30 wt%), Al_2O_3 (14.06–17.62 wt%), $FeO_{(t)}$ (8.33–9.67 wt%), MgO (3.25–6.77 wt%), CaO (4.51-9.63 wt%), Na_2O (1.40–3.39 wt%), K_2O (1.64–2.24 wt%) (Fig.IV. 4).

Despite distinct alumina-saturation index (Fig.IV. 4a) and SiO_2/Al_2O_3 ratios

(Fig.IV. 4b), all samples plot in arc-related graywacke fields on the protolith discrimination diagram (cf. Rosen, 1992). Indeed, on the different diagrams that involve major and trace elements used to characterize the tectonic settings, as the diagrams of Bhatia (1983), Kroonenberg (1994) and Bhatia and Crook (1986), the samples plot in the oceanic island arc field with a few samples plotting in the continental arc and active continental margin field. Discriminant-function-based multi-dimensional diagrams are used in addition to these traditional diagrams of tectonic settings. These additional diagrams enable to discriminate between island/continental arc, continental rift and collision setting of high-silica (SiO_2 = 63 - 95 wt%) and low-silica (SiO_2 = 35 - 63 wt%) rocks (Verma and Armstrong-Altrin, 2013) (Fig.IV. 4 e) and f)). Both high-silica and low-silica samples plot in the arc tectonic setting, reinforcing the affinity of these samples for this tectonic setting.

The rare-earth element (REE) patterns among metaluminous to peraluminous gneiss are also distinguished, all normalized to the chondrite values of Taylor and McLennan, 1985. For the first rocks, indicate slight enrichment in light REE (LREE: $(La/Yb)_N$ = 2.08 – 6.62; average = 4.32), and variable Eu anomalies ($(Eu/Eu^*)_N$ = 0.77 – 1.21; average = 0.98), from negative anomalies to positive anomalies, compatible with sediments from active continental margins (0.65 - 1.0; McLennan et al., 1990) (Fig.IV. 5a). The heavy rare earth elements (HREE) show flat patterns ($(Tb/Yb)_N$ ratios from 1.20 to 1.43; average = 1.33). In relation to Rare Earth Elements (REE) Post-Archaean Average Shale (PAAS)-normalized show a similarity in the distribution patterns of samples with relatively flat patterns ($(La/Yb)_{PAAS}$ = 0.23–0.72; average = 0.47), and flat to positive Eu anomalies ($(Eu/Eu^*)_{PAAS}$ = 1.17–1.85; average = 1.50) (Fig.IV. 5b).

In contrast, peraluminous gneiss show slight enrichment in light REE (LREE: $(La/Yb)_N$ = 6.11 – 7.26; average = 6.69), and variable Eu anomalies ($(Eu/Eu^*)_N$ = 0.45 – 0.59; average = 0.52), from negative anomalies to flat anomalies, compatible with sediments from active continental margins (0.65 - 1.0; McLennan et al., 1990) (Fig.IV. 5a). The heavy rare earth elements (HREE) show flat patterns ($(Tb/Yb)_N$ ratios from 1.05 to 1.09; average = 1.07). Regarding the Rare Earth Elements (REE) Post-Archaean Average Shale (PAAS)-normalized the samples show a flat pattern ($(La/Yb)_{PAAS}$ = 0.23–0.72; average = 0.47), and negative Eu anomalies ($(Eu/Eu^*)_{PAAS}$ = 1.17–1.85; average = 1.50) (Fig.IV. 5b).

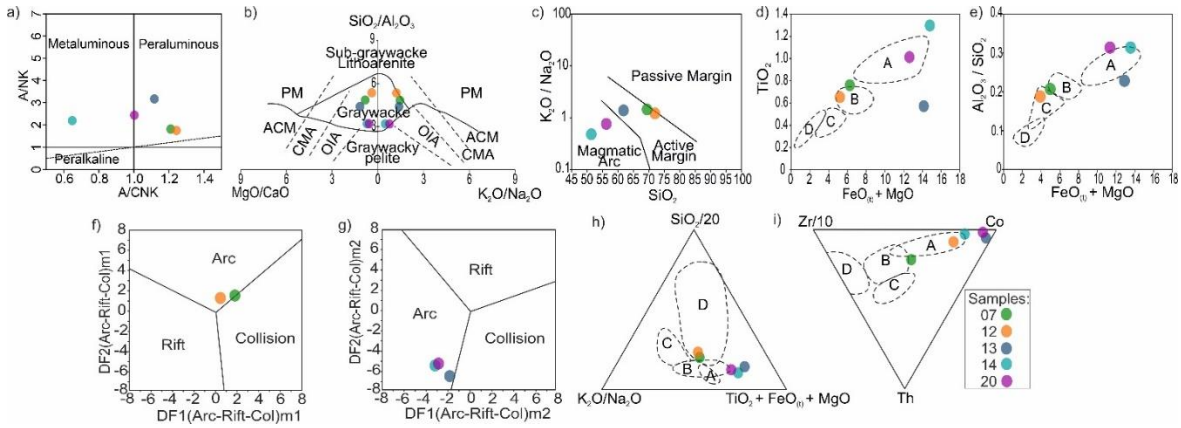

Fig. IV. 4 - Major and trace elements diagrams for provenance discrimination of protoliths for gneiss samples of the AROS transition zone. a) A/NK versus A/CNK diagram (Shand, 1943); b) Rosen (1992); c) Roser and Korsch (1986); d) and e) Bhatia (1983); f) Discriminant-function diagram for high-silica clastic sediments for three tectonic settings (arc, continental rift, and collision) and g) Discriminant-function diagram for low-silica clastic sediments for three tectonic settings (arc, continental rift, and collision) after Verma and Armstrong-Altrin (2013); h) Kroonenberg (1994); i) Bhatia and Crook (1986). ACM: active continental margin; CMA: continental magmatic arc; OIA: island arc. A: ocean island arc; B: Continental magmatic arc; C: active continental margin; D: passive margin.

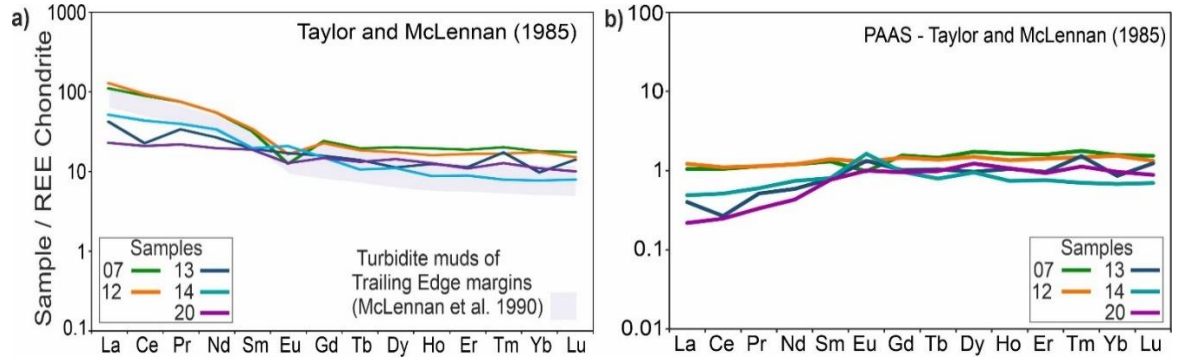

Fig. IV. 5 - Chondrite-normalized REE diagram (Taylor and McLennan, 1985) distribution for paragneiss samples of the AROS transition.

VI.4.3 Detrital zircon U-Pb analysis and Hf-in-zircon data

Three samples were collected for detrital zircon analyzes. To avoid neoformed crystals, only the paleosome portions of the samples were selected for zircon concentration. However, the millimetric banding of some samples makes it virtually impossible to avoid all of the neoformed zircons, as indicated by the presence of sparse grains with ages in the range of the regional metamorphism, as discussed below.

VI.4.3.1 Sample 07

This sample is a garnet-sillimanite-biotite gneiss collected near Ibitirama town. Recovered zircon crystals are clear and translucid, with colorless to brownish colors, localized inclusions, elongated to stubby euhedral-subhedral prisms with length/width ratios of 5:1 to 2:1 and less than 250 μm long (Fig.IV. 6). Cathodoluminescence (CL) images of most zircon crystals show typical patterns of igneous internal zoning and Th/U ratios between 0.10 and 2.03 with ages varying between 606 ± 20 Ma and 1196 ± 54 Ma. The Neoproterozoic grains (606 ± 20 Ma to 859 ± 21 Ma) represent the main age peaks. Two crystals show low Th/U ratios (spot 76 = 631 ± 13 and spot 59 = 642 ± 18 Ma; Th/U = 0.03), but typical igneous textures, with no metamorphic overgrowths, and are thus interpreted as not affected by regional metamorphism. Another zircon crystal is characterized by a metamorphic overgrowth and shows different ages and Th/U ratios of the core (spot 50 = 738 ± 15; Th/U = 0.59) and the rim (spot 51 = 624 ± 13; Th/U = 0.07). At last, a single Cambrian zircon crystal (spot 134 = 507 ± 16; Th/U = 0.07) also shows a metamorphic overgrowth with a perceptible transition to a dark rim. Therefore, the U/Pb isotopic ratios of the analyzed zircon crystals produced a spectrum with four main provenance peaks at ca. 630, 650, 720 and 740 Ma (Fig.IV. 7).

The analyzed grains yielded negatively fractionated $\varepsilon Hf_{(t)}$ values with the Neoproterozoic crystals clustering around -10 (Fig.IV. 8), while two Mesoproterozoic crystals yielded -18.7 and -5.9, with Hf T_{DM} model ages at 2.2 Ga and 1.9 Ga, and homogeneous initial $^{176}Hf/^{177}Hf_{(t)}$ ratios of 0.281610-0.281893, respectively.

VI.4.3.2 Sample 12

This outcrop consists of a folded garnet-biotite gneiss collected near Jerônimo Monteiro town. Zircon crystals consist of subhedral prisms, largely prismatic with sub-rounded edges and less than 200 μm long. CL images show a prevalence of cores, either non-zoned or with magmatic oscillatory zoning surrounded by structureless dissolution-recrystallization domains, convoluted zones and overgrowth rims (Fig.IV. 6). The Th/U ratios of these crystals are between 0.01 and 0.47 with ages varying between 950 ± 15 Ma and 556 ± 10 Ma. Most zircon grains show a low Th/U ratio (0.01 to 0.05), convoluted metamorphic features and an overgrowth rim. One of the youngest

zircon crystals with a Th/U ratio of 0.12 (spot 54 = 556 ± 10 Ma) shows typical igneous textures, however, this age corresponds to the range of regional high-grade metamorphism related to the Brasiliano Orogeny, and thus it probably represents a neoformed crystal. Moreover, seven zircon crystals also present Th/U ratios typical of igneous rock, however, the CL images show metamorphic overgrowth rims and convoluted zones. Thus, the U/Pb isotope ratios of the analyzed zircon crystals yielded a spectrum with two main peaks at ca. 600 and 640 Ma (Fig.IV. 7).

VI.4.3.3 Sample 13

This sample is from a hornblende-bearing gneiss, banded and folded concordant with the foliation, collected in a roadcut near Jerônimo Monteiro town. Zircon crystals consist of euhedral-subhedral bipyramidal prisms with length/width ratios of 5:1 and less than 250 μm long. The crystals are clear and translucid, colorless to brownish, with some inclusions, bearing typical igneous internal zoning (Fig.IV. 6). The Th/U ratios of these crystals are between 0.11 and 3.54 with ages varying between 1075 ± 41 Ma and 553 ± 11 Ma. The main populations are represented by Neoproterozoic grains (553 ± 11 Ma to 808 ± 16 Ma). One of the youngest zircon crystals presents a high Th/U ratio in the core (spot 215 = 3.35; 571 ± 12 Ma), but its CL image shows metamorphic overgrowth rims, reinforcing the suggestion that this might representing a neoformed zircon related to high-grade metamorphism during the Brasiliano Orogeny. In addition, four zircon crystals (spot 151 = 609 ± 12 Ma; spot 251 = 631 ± 13 Ma; spot 218 = 643 ± 13 Ma and spot 136 = 646 ± 13 Ma) present features as Th/U ratios from 0.03 to 0.08, but none shows metamorphic overgrowth rims. Thus, the U/Pb isotope ratios of the analyzed zircon crystals yielded a spectrum with two main detrital peaks at ca. 600 and 620 Ma (Fig.IV. 7).

Fig.IV. 8 shows the results of Hf isotope analysis which twenty-one of the Neoproterozoic zircons yielded positive $\varepsilon Hf_{(t)}$ values between +5.7 and +0.5, with Hf T_{DM} model ages at 1.03-1.3 Ga, and homogeneous initial $^{176}Hf/^{177}Hf_{(t)}$ ratios of 0.282504-0.282396. For the other 39 detrital grains all $\varepsilon Hf_{(t)}$ values are negative and range from −0.1 to −19.0, with Hf TDM model ages from 1.92 Ga to 1.20 Ga and initial $^{176}Hf/^{177}Hf_{(t)}$ ratios of 0.282389-0.281854.

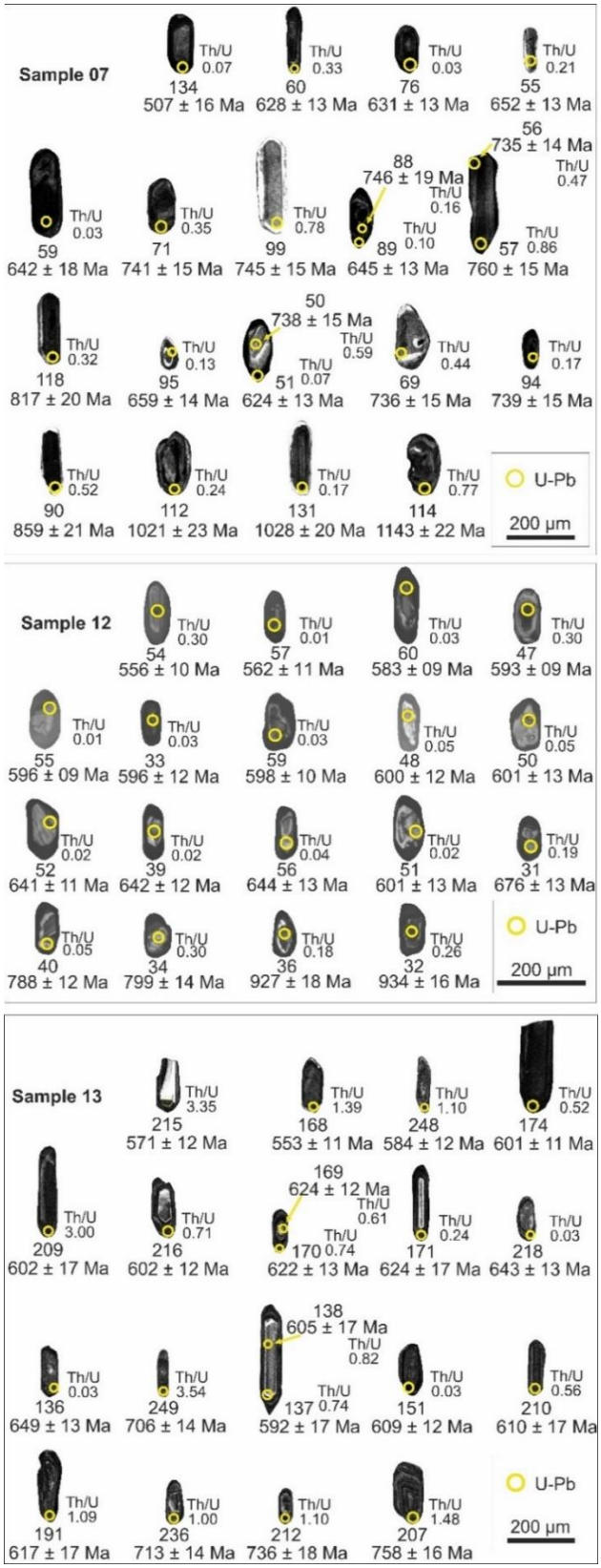

Fig. IV. 6 - Representative cathodoluminescence (CL) images with U-Pb spots of analyzed zircons crystals from the paragneiss samples.

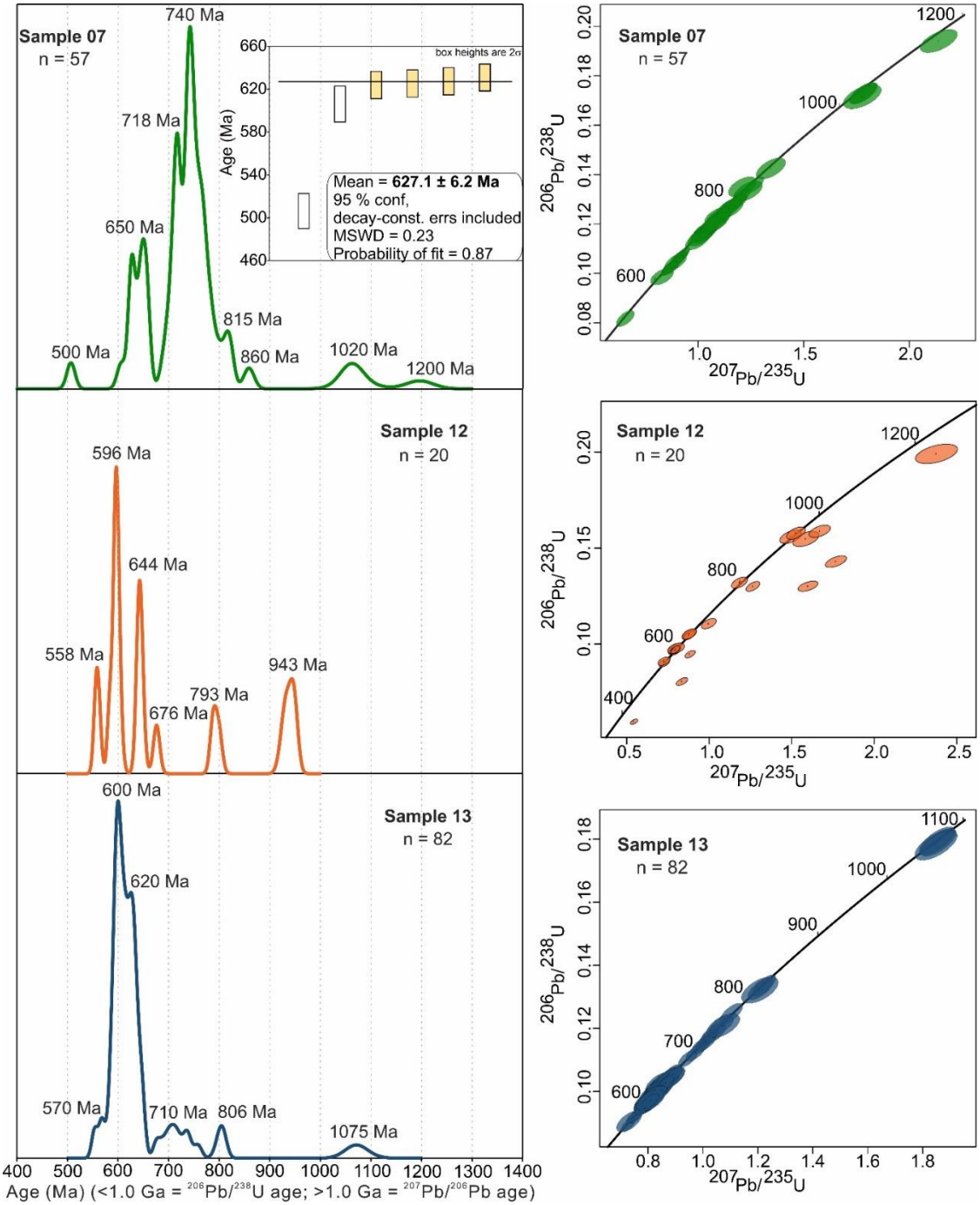

Fig. IV. 7 - Probability density plots for detrital zircon grains and Concordia diagrams from the paragneisses units samples. The youngest concordant zircon grains average $^{206}Pb/^{238}U$ age is indicated for sample 07.

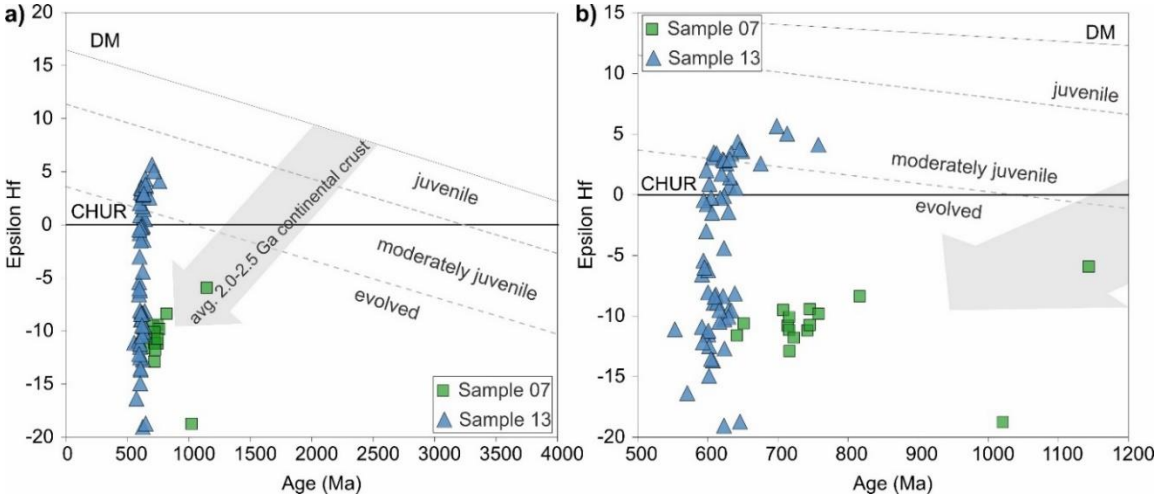

Fig. IV. 8 - a) Plots of $\varepsilon Hf_{(t)}$ versus U-Pb age for analyzed zircon crystals; b) expanded view in the 700-1000 Ma interval. Grey dashed lines classify fields of juvenile (5 – 12 ε-units below DM) and evolved (> 12 ε-units below DM; Bahlburg et al., 2011) composition. The grey band represents the average evolution of typical continental crust generated around 2.0-2.5 Ga, with a $^{176}Lu/^{177}Hf$ = 0.010 for felsic and $^{176}Lu/^{177}Hf$ =0.022 for mafic crust (Pietranik et al., 2008). Model depleted mantle with present day $^{176}Hf/^{177}Hf$ ratio of 0.28325 and $^{176}Lu/^{177}Hf$ ratio of 0.0388 (Griffin et al., 2000; updated by Andersen et al., 2009)

VI.5. Discussion

VI.5.1 Tectonic depositional setting and provenance of the sedimentary protoliths

The detrital zircon spectra and geochemical discrimination diagrams based on whole-rock major element compositions for the paragneisses collected in the AROS inner core made it possible to investigate their probable sources and tectonic settings. The studied samples represent the metamorphism of epiclastic (peraluminous paragneisses) and probable volcanoclastic (metaluminous, hornblende-bearing gneisses) greywackes, with intermediary terms. In tectonic discrimination diagrams, they show a clear trend toward magmatic arc (island arc or continental arc) and active continental margin fields (Fig.IV. 5). The Cryogenian-Ediacaran age peaks suggest that the main candidates of sediment sources are the distinct magmatic arc settings belonging to the AROS, as well as the chrono-correlated African units.

Although the samples show distinct age spectra, the predominance of grains with Neoproterozoic age is noticeable. The main age peaks are at ca. 600, 630, 720, 740 and 800 Ma with a minor Mesoproterozoic peak (1200 Ma).

Sample 07 shows 82% detrital grains within the consistent time interval (ca.

642 Ma – 859 Ma) of the juvenile Serra da Prata and Rio Negro arcs (Fig.IV. 7, 9 and 10). It implies that rocks derived from these arc terranes are potential sources of the sedimentary protoliths, emphasizing the ages correlated to the Rio Negro arc (790 - 600 Ma; Tupinambá et al., 2012). The contribution of this arc as a source of sediments is also recorded by the metamorphic ages found. Two zircon grains with low Th/U ratios (spot 76 = 631 ± 13 and spot 59 = 642 ± 18 Ma; Th/U = 0.03) might suggest intra-arc metamorphism or the record of the final stage of intra-oceanic subduction at 630 Ma (Tupinambá et al., 2012). Another interesting feature is registered by a zircon grain with a core age (738 ± 15 Ma) consistent with the Rio Negro arc and a rim metamorphic age at 624 ± 13 Ma. According to Degler et al. (2017), it is possible that the Rio Negro arc started to collide with the Rio Doce arc domain between 630 Ma and 614 Ma. Thus, the detrital zircon core age recovered would represent a Rio Negro arc magmatic age and the metamorphic age would be related to the collision of this terrane with the Rio Doce arc. The Ediacaran Rio Doce arc contributed as a sediment source reported by the three detrital zircons with ages of ca. 606 Ma, 625 Ma and 628 Ma. At last, a single Cambrian zircon crystal (ca. 507 Ma) indicates the influence of recrystallization processes and isotopic resetting related to post-collisional thermal events of the orogen, or Pb-loss. However, this younger single-grain age is an isolated occurrence in the cluster of older detrital zircons. Thus, we suggest the average of the youngest and most concordant detrital zircon grains as a realistic maximum depositional age for the protolith of these paragneisses, restricting the maximum sedimentation age to ca. 627.1 ± 6.2 Ma.

In comparison, sample 13 shows most detrital zircon grains (80%) within the interval of ca. 629 ± 12 Ma to 584 ± 12 Ma, consistent with main sourcing from the Rio Doce arc (Fig.IV. 7, 9 and 10). However, a considerable fraction of detrital zircon grains (20%) can be related to the Serra da Prata and Rio Negro arc terranes (ages varying between ca. 808 ± 16 Ma and 630 ± 13 Ma). Thus, fragments of these arcs, or zircon xenocrysts that were inherited from these terranes and incorporated in the Rio Doce arc magmas, are potential sources to the sedimentary protoliths of these paragneisses. The possible metamorphic grains recovered in this sample register metamorphic events related to the Rio Negro and Rio Doce arcs. The grains with the ages of ca. 643 ± 13 Ma and 646 ± 13 Ma indicate an origin from the Rio Negro intra-arc metamorphism. On the other hand, grains with the ages of ca. 631 ± 13 Ma and 609 ± 12 Ma could indicate both metamorphic events of the final stage of the Rio Negro arc

intra-oceanic subduction and initial collision with the Rio Doce arc or intra-arc metamorphism related to the Rio Doce arc. The youngest four recovered zircons (571 ± 12 to 553 ± 11 Ma) show typically igneous Th/U ratios (Th/U = 0.47 to 3.35), demonstrating the presence of neoformed syn-collisional crystals in the migmatitic paragneiss, with an age range consistent with the collisional phase of the AROS. Therefore, we suggest the age of the next youngest age peak as a realistic maximum depositional age for the protolith of the paragneisses, restricting the maximum sedimentation age at ca. 600 Ma.

Sample 12 shows detrital grains within the consistent time interval (ca. 596 Ma – 798 Ma) of the Rio Negro arc and Rio Doce arcs, reinforcing that the fragments of these arcs or zircons that were inherited from these terranes are potential sources to the sedimentary protoliths (Fig.IV. 6 and 7). Like sample 13, the two younger grains (556 ± 10 to 562 ± 11 Ma) show metamorphic characteristics recorded by zircon grain morphology and Th/U ratios, suggesting an association with the syn-collisional metamorphic peak in the AROS. Thus, for a realistic maximum age for the protolith of these paragneisses, we suggest the age of the next youngest age peak, restricting the maximum sedimentation age at ca. 596 Ma, very similar to sample 13.

Some detrital zircons yielded Mesoproterozoic ages (5%), showing a restricted oldest peak at ca. 1.2 Ga (Fig.IV. 7 and 9). These zircon grains could be provided from units of the African counterpart, as the West Congo Belt and the Angola Craton, in accordance with the interpretations of Lobato et al., (2015), Fernandes et al., (2015) and Degler et al., (2017). Possible sources of detrital sediments are the Mesoproterozoic Karagwe-Ankole-Kibaran belt and the Neoproterozoic Kaoko belt (Porada 1989; Seth et al., 1998, 2002, 2003; Kröner et al., 2004; Becker et al., 2006; Ernst et al., 2013). These zircon crystals could, alternatively, have been inherited when the youngest, transitional-stage magmas of the Rio Negro arc traversed thinned continental crust of the Angola craton. Thus, further reworking of Rio Negro arc rocks could have provided Mesoproterozoic grains as a secondary source.

The Hf isotope data provides further support for the involvement of sources related to both island arc terranes, with positively fractionated $\varepsilon Hf_{(t)}$ especially associated with Cryogenian grains, indicating the contribution of moderately juvenile Rio Negro arc rocks. However, in sample 07, the Cryogenian grains yielded evolved $\varepsilon Hf_{(t)}$ of ca -10 for the same age range (650-800 Ma), reinforcing the transitional nature of the Rio Negro arc involving both additions of juvenile material and the recycling of

older continental crust during its formation. The wide range of $\varepsilon Hf_{(t)}$ values on Ediacaran zircons, on the other hand, suggest the involvement of variably crustal rocks related to the Andean-type Rio Doce arc as the main source.

VI.5.2 Age of metamorphism

The detrital zircon age spectra indicate that the original sedimentary basins received sediments mainly from Neoproterozoic sources, but also record Neoproterozoic metamorphic overprints (igneous zircon cores with metamorphic rims and neoformed metamorphic zircon grains). Syn-collisional metamorphism in the Araçuaí Orogen is registered at ca. 575-550 Ma (Richter et al., 2016; Melo et al., 2017). However, Schannor et al. (2018) and Degler et al. (2017) also described metamorphic ages at ca. 630-625 Ma in the Araçuaí Orogen due to a regional metamorphic event. According to Degler et al. (2017), this age could be correlated with the pre-collisional stages (related to subduction) and with the initial collisional stages (630-585 Ma) of the Rio Doce arc domain. In addition, these authors also suggest a younger metamorphic age (ca. 540-480 Ma) owing to the recrystallization processes and isotopic resetting related to post-collisional thermal events. Even with few metamorphic detrital zircons recovered in the studied samples, we identified possible metamorphic events at ca. 609 Ma to 643 Ma, ca. 560 Ma and ca. 507 Ma, related to the pre-, syn-, and post-collisional events described in the AROS. Some of the older metamorphic ages present in these samples could represent zircon xenocrysts preserving intra-arc metamorphism of the Rio Negro and Rio Doce arcs.

VI.5.3. Correlation with other Neoproterozoic arc-related basins of the AROS

Neoproterozoic arc and passive margin-related basins were identified in the AROS by several studies on sedimentary provenance (*e.g.* Gradim et al., 2014; Lobato et al., 2015; Fernandes et al., 2015; Richter et al., 2016; Degler et al., 2017; Novo et al., 2018; Schannor et al., 2018; Araújo et., 2020; Pacheco et al., 2020). Some of these basins (Fig.IV. 9) present detrital zircon grains with ages older than 1.3 Ga, which were not recorded in our study. The lack of older detrital zircon grains removes the possibility of a source contribution from the Archean/Paleoproterozoic basement, such as the São Francisco Craton and reworked basement tracts within the AROS. This is coherent with the positioning of the studied samples, further away from the reworked

basement rocks and closer to the Neoproterozoic magmatism related to the magmatic arcs within the orogenic core.

Detrital zircons from the Ribeira Orogen have been interpreted to represent different tectonic settings for basin accommodation. According to Fernandes et al. (2015), the São Fidelis Group presents the main peak from Neoproterozoic sources (700–567 Ma) and a mainly crustal signature for their detrital zircon population in an active margin environment in the fore-arc basin. On the other hand, Lobato et al. (2015) describe detrital zircons in a large age spectrum, with the largest age peaks at ca. 1.2 Ga and 2.2 Ga and the youngest detrital zircon of ca. 613 Ma. These authors relate the provenance of Mesoproterozoic ages to the Kaoko Belt, also with some contribution from the Rio Negro arc, probably in a back-arc tectonic setting. Our data differ from that described by Lobato et al. (2015) due to the lack of a broad spectrum of Archean to Neoproterozoic ages.

The Italva Group stands out in the Ribeira Orogen for its U-Pb Tonian ages (ca.-860 – 840 Ma), which indicate that the Euclidelândia and São Joaquim units could represent basins related to the development of the Serra da Prata Arc (Heilbron & Machado 2003, Peixoto et al. 2017). Although our data do not register the most significant peaks in this age spectra, the whole-rock geochemistry data and the mineralogical composition of samples 13, 14 and 20 show similarity with this group considering that the samples are metaluminous hornblende-bearing gneiss free of peraluminous silicates. However, the obtained detrital zircon age spectra show clear youngest age peaks at 620-600 Ma, excluding the possibility that the paragneissic units located in the study area could be correlated to Tonian arc-related basins and suggesting instead their relation with the Ediacaran Rio Doce magmatic arc. Thus, older sedimentary basins related to the Tonian-Cryogenian arc systems of the Ribeira belt, if present at the study area, might only be preserved as smaller reworked remnants within the predominant Ediacaran successions.

U-Pb data of detrital zircon grains and Hf in zircon isotopic data of the Araçuaí Orogen metasedimentary rocks allow further characterization of the orogenic basins. The Nova Venécia Complex is a back-arc basin related to the pre-collisional magmatic arc showing detrital zircon ages ranging from 900 Ma to 700 Ma (Gradim et al., 2014; Richter et al., 2016) and $\varepsilon Hf_{(t)}$ values varying from +4.1 to -39.2 (Araujo et al., 2020), with metamorphic events registered at ca. 570 Ma and 540 Ma (Richter et al., 2016). Another similar age spectrum (900 Ma to 650 Ma) is presented by the

metavolcanosedimentary rocks of the Rio Doce Group, which present juvenile signatures ($\varepsilon Hf_{(t)}$ +1 and +15), also related to the Rio Doce magmatic arc (Vieira, 2007; Gonçalves et al., 2018; Novo et al., 2018; Schannor et al., 2019), just as the rocks of the Andrelândia Group, which are interpreted as fore-arc and intra-arc basins of the Rio Doce arc and present analogous age spectra. Therefore, these Neoproterozoic basins show similar provenance to the studied paragnaisses, with important detrital zircon age peaks of ca. 600 Ma to 630 Ma, which could indicate proximity to the continental Rio Doce magmatic arc (630-585 Ma; Gonçalves et al., 2016; Tedeschi et al., 2016). Likewise, they show a strong influence from rocks pertaining to the juvenile Rio Negro and Serra da Prata arcs (ca. 600 to 860 Ma; Tupinambá et al., 2012; Peixoto et al., 2017; Santiago et al., 2020b). Detrital zircon U-Pb ages and Lu-Hf data of mantellic signature on paragnaisses of the southern Araçuaí Orogen disclosed by Schannor et al. (2018) and Degler et al. (2017) also show these juvenile magmatic arcs as possible sources of detrital zircons in the metasedimentary protoliths.

The ca. 600 Ma to 630 Ma age peak suggests that the samples register similar age patterns to those attributed to trench volcanogenic and forearc basin sediments (Fig.IV. 10 b)). Such settings are characterized by more than 30% of detrital zircon ages being less than 100 Ma older than the depositional age, considering that forearc basins commonly have unimodal detrital zircon spectra with an age close to the deposition age of the strata, whereas back-arc basins have increasing input of older detritus from the adjoining craton (Cawood et al., 2012). Degler et al. (2017) suggest that the Rio Negro - Serra da Prata arc system was close, if not completely amalgamated with, the Rio Doce arc domain before ca. 614 Ma. Thus, the basin would have been formed during the convergence and amalgamation of the Rio Negro - Serra da Prata and the Rio Doce arc systems (Fig.IV. 10 a)). In addition, the isotopic data show mantle and crustal contribution ($\varepsilon Hf_{(t)}$ +5.6 to -18.7), which reiterates the contribution of the AROS Neoproterozoic arcs. Alternatively, the Tonian-Cryogenian peaks could have come from the reworking of unmelted xenoliths, xenocrystals and other remnants of the older arc systems that were incorporated in the Ediacaran Rio Doce arc. In any of those scenarios, the petrographic, lithochemical, isotopic, and geochronological data suggest that the sediments were deposited in an active continental margin basin, probably a forearc or intra-arc basin, related to the Ediacaran Rio Doce arc.

VI.6. Conclusions

The sedimentary protoliths of the paragneisses in the AROS inner core derived from magmatic arc systems (island arc or continental arc) of an Ediacaran active continental margin. The detrital zircon grains are predominantly Neoproterozoic, with maximum sedimentation ages of ca. 627.1 ± 6.2 Ma (sample 07) and ca. 600 Ma (samples 12 and 13). The main source areas of the sediments were rocks related to the transitional Rio Negro (620-790 Ma) and the continental Rio Doce (580-630 Ma) arc systems. The few Mesoproterozoic (1020 Ma to 1200 Ma) grains are inherited from the Angolan basement traversed by Rio Negro arc magmas, that were then further reworked as a secondary source to the AROS paragneisses protoliths. Furthermore, some Cryogenian-Ediacaran detrital zircon grains with metamorphic textures and chemical signatures suggest a relation to the intra-arc metamorphism of the Rio Negro and Rio Doce arcs, and sparse neoformed crystals at ca. 560 Ma and 507 Ma suggest a relation with the various metamorphic events (pre, syn- and post-collisional) of the AROS.

Most ages of detrital zircons are close to the depositional age of the sediments, a pattern similar to samples deposited in forearc or intra-arc basins in active continental margins (Cawood et al., 2012). This supports that the Rio Negro - Serra da Prata arc system was near, if not completely amalgamated with, the Rio Doce arc domain before ca. 614 Ma; or, alternatively, that reworked fragments, xenoliths, xenocrystals and other remnants of those arc systems were incorporated in the Rio Doce arc magmas and then sourced to the arc-related basins during the Ediacaran. It also reinforces the inferred convergent margin tectonic setting for the sedimentary succesions in this area.

Therefore, the studied meta-sedimentary rocks were deposited in a fore arc or intra-arc tectonic setting related to an Ediacaran continental arc system, the Rio Doce arc. They were later incorporated into the high-grade orogenic core in the transitional zone between the Araçuaí and Ribeira orogens, serving as excellent markers of accretionary and collisional processes in this portion of western Gondwana.

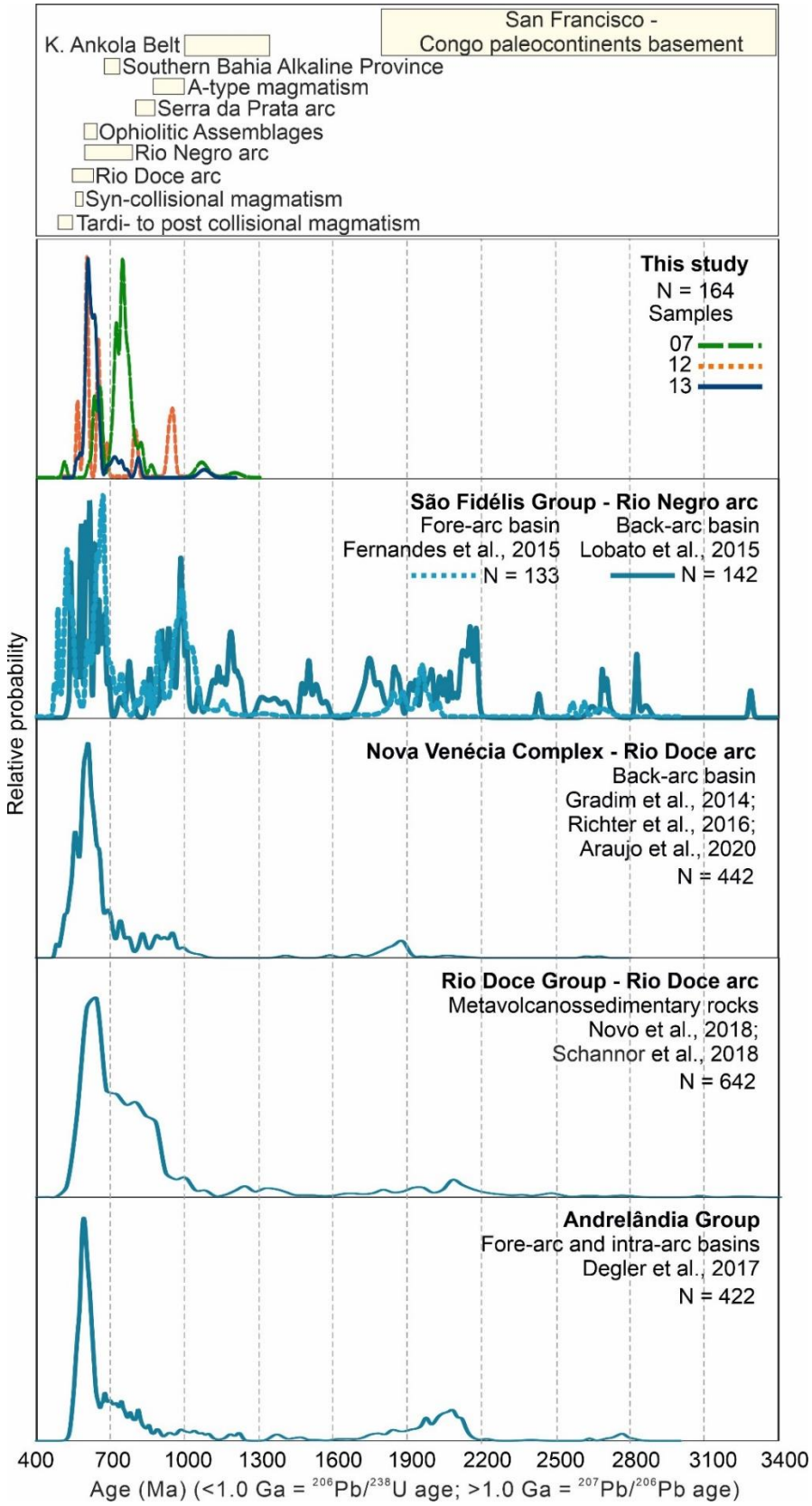

Fig. IV. 9 - Probability density plot for all detrital zircon grains of samples 7, 12 and 13. Comparison with another AROS basins and possible sources at the top of the diagram.

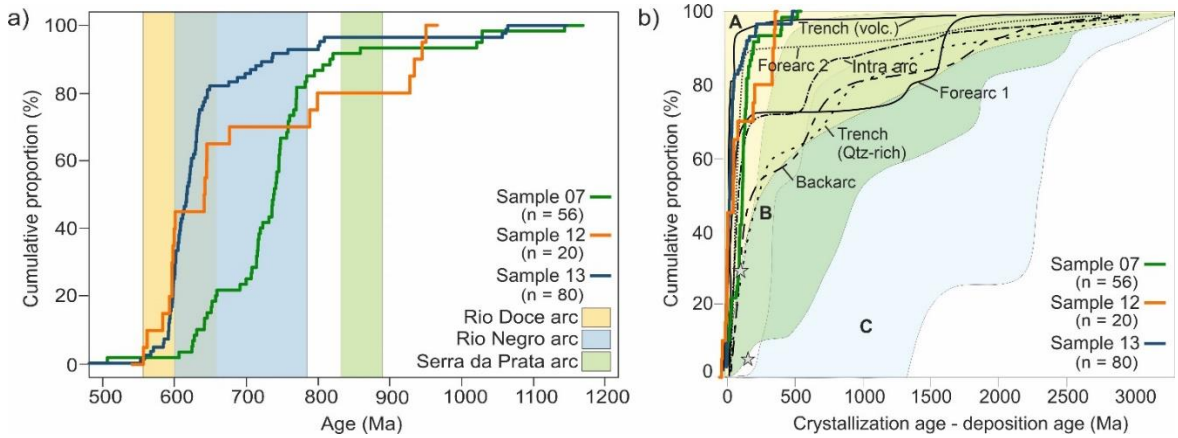

Fig. IV. 10 - a) Cumulative proportion curves from the detrital zircons of this study and their possible sources. b) (crystallization age – deposition age) versus cumulative proportion graph (after Cawood et al., 2012) for zircons from the paragneisses samples. Note that the samples plot in the active margin field similar to the fore-arc, intra arc and trench basins. (Star symbols CA-DA < 150 Ma with a cumulative proportion of 5% and CA-DA < 100 Ma with a cumulative proportion of 30%). Summary plot of the general fields for convergent (A), collisional (B) and extensional basins (C). Fore arc 1 and 2 data are from the southern California (United States) Margin and the Great Valley (California) fore arc basin, respectively; Trench (volc.) and Trench (Qtz-rich) curves from the Tablelands Complex (Terra Australis Orogen, Australia), from volcanogenic and quartz-rich sandstones data, respectively; Intra-arc data from the Macquarie Arc (Terra Australis Orogen); and backarc data from the Terra Australis Orogen (Cawood et al., 2012).

VI.7. Acknowledgements

This paper is a contribution to Project MOBILE: Mountains Belts and the Inception of Complex Life on Earth (geolifemobile.com), supported by Instituto Serrapilheira (Serra-1912-31510), and by CNPq, Brazil, through grant number 408815/2021-3. FAC, APS and CL are recipients of Research Productivity grants from CNPq and acknowledge the support received, especially through grant 304509/2021-3.

CAPITULO V

PRESERVATION OF PRE-COLLISIONAL ACCRETIONARY SYSTEMS AS MEGAXENOLITHS AND ROOF PENDANTS THROUGH MULTIPLE PARTIAL MELTING EPISODES: 360 MA OF OROGENIC MAGMATISM IN THE COMPOSITE CAXIXE BATHOLITH, ARAÇUAÍ-RIBEIRA OROGENIC SYSTEM OF WESTERN GONDWANA

(Artigo a ser submetido para periódico especializado)

V.1. Abstract

Plate tectonics characterize mountain building processes throughout Earth's history, mainly through the development of accretionary followed by collisional orogens. However, the high degree of partial melting, metamorphism and deformation attained specially in the high-grade crystalline core of ancient orogens often obliterates the remnants of pre-collisional systems, making it hard to unravel the accretionary history of Precambrian orogens. In western Gondwana, the high-grade orogenic core of the Araçuaí-Ribeira Orogenic System (AROS) is one such region where syn- to post-collisional magmatism has largely disrupted or even obliterated former structures and lithotectonic assemblages, hampering attempts to reconstruct the pre-collisional history of the Adamastor ocean realm. We investigated a key area of the transition zone between the Ribeira and Araçuaí orogens, in the southern Espírito Santo state of eastern Brazil, in order to clarify those issues. We demonstrate that formerly described remnants of a Tonian (ca. 840-860 Ma) juvenile island arc system actually occurs as kilometric roof pendants and megaxenoliths within the large, composite Caxixe batholith. Most of the pre- to syn-collisional granodiorites and granites composing the batholith formed, however, much later, at ca. 580-607 Ma. Garnet-bearing leucogranite dated at 575 Ma and a mafic intrusion at 560 Ma mark the syn-collisional and transition to tardi-collisional stages, and post-collisional A-type magmatism as undeformed granitic plutons intruded at ca. 500 Ma, finalizing ca. 360 Ma of orogenic magmatism in the same composite batholith and smaller adjacent plutons. Trace element geochemistry suggests that the 580-607 Ma magmatic pulses characterize calc-alkaline magmas probably developed in a continental volcanic arc setting, thus part of the Rio Doce continental arc of the Araçuaí Orogen, with evolved

$\varepsilon Hf_{(t)}$ around -6 to -10, $\varepsilon Nd_{(t)}$ of -4.9 to -9.5 and $^{87}Sr/^{86}Sr_{(i)}$ of 0.706-0.711. This is in contrast with the strikingly mantellic $\varepsilon Hf_{(t)}$ and $\varepsilon Nd_{(t)}$ of the juvenile Tonian roof pendants at ca. +14 and +6, respectively, with $^{87}Sr/^{86}Sr_{(i)}$ of 0.698–0.704. The post-collisional granites are the most evolved rocks in the composite batholith, with $\varepsilon Hf_{(t)}$ around -22 and $\varepsilon Nd_{(t)}$ of -5.6 to -13.2. Our results reinforce the importance of detailed mapping and petrological, geochemical and isotopic characterization of composite batholiths in high-grade orogenic areas, as those might preserve the remnants of former tectonic processes not easily recognizable otherwise, summarizing hundreds of million years of orogenic evolution of the pre-, syn- and post-collisional stages in a single, multi-intrusive batholithic complex.

V.2. Introduction

Interpretations of the tectonic evolution and geodynamic meaning of Precambrian orogenic belts are often complicated by the high degrees of deformation, metamorphism, partial melting and subsequent exhumation and erosion of the orogenic edifices. This has led to extensive debates of when and where modern-style plate tectonics began (Cawood et al., 2006), and on whether Precambrian orogenic belts represent or not classic Wilson Cycle tectonics, with rift-drift-subduction-collision and arc-continent or continent-continent collision (Heilbron et al., 2004, 2020). In southeastern Brazil, the Neoproterozoic-Eopaleozoic Araçuaí-Ribeira Orogenic System (AROS), extending for some 2,000 km in southeastern Brazil. The AROS comprises rocks related to magmatic arcs, supracrustal metamorphic sequences and voluminous syn- and post-collisional magmatism in the Ediacaran/Cambrian transition, which developed during Western Gondwana assembly.

Due to the strong reworking during evolution in the collisional and post-collisional periods, many records from the pre-collisional stages are fragmented along the Precambrian orogens, sometimes being found only as xenoliths and/or roof pendants in igneous bodies remelted during the syn- and post-collisional stages, composed of intrusions of different ages (e.g. de Toni et al., 2020). Tonian orthogneisses are found in the Ribeira Orogen as evidence of the Serra da Prata and Rio Negro juvenile and transitional arcs (Tupinambá et al., 2012; Peixoto et al., 2017). Recently, Tonian orthogneisses (860-840 Ma) were discovered within the Caxixe batholith (Santiago et al., 2020, Decol et al., 2021), located in the southern Espírito

Santo State of the southeastern Atlantic coast of Brazil. Those represent the northernmost remnants of island arc systems (part of the Serra da Prata magmatic arc) within the AROS, including adakites and slab window-related rocks (Decol et al., 2021).

In this paper, we present the results of a systematic study of the Caxixe batholith and surrounding minor plutons, involving geochronology (LA-ICPMS and SHRIMP U-Pb in zircon), elemental and isotopic geochemistry (whole-rock Nd-Sr and Hf-in-zircon). The results reveal that the ca. 860-840 Ma orthogneisses are in fact preserved as unmelted megaxenoliths and roof pendants of up to tens of square kilometers within a multi-intrusion batholith, composed of large pre- to syn-collisional (ca. 580-607 Ma), syn- to tardi-collisional (575-560 Ma) and post-collisional intrusions (ca. 503 Ma) with significant crustal contamination as demonstrated by isotope systematics. Thus, the 360 Ma of magmatic activity recorded within the Caxixe batholith preserves all stages of pre-, syn- and post-collisional evolution of the AROS and is a natural laboratory for the study of Precambrian orogens and the assembly of the western Gondwana.

V.3. Geological Context

The Araçuaí – Ribeira orogenic system (AROS) in southeastern Brazil formed during the amalgamation of western Gondwana in the late Neoproterozoic was intensely reworked during its development. Its formation resulted from a series of subduction-to-collision processes, involving diachronic convergences of the São Francisco, Congo, Paranapanema, and Angola cratons (Fig. IV. 1 a,b), and the closure of the northern Adamastor Ocean realm (e.g., Pedrosa-Soares et al., 2001, 2008; Cordani et al., 2003, Alkmim et al., 2006, 2017; Heilbron et al. 2017, 2020; Caxito et al., 2021). The high-grade (crystalline) core of this system is marked by a complex geodynamic evolution that encompasses both high-grade metamorphic supracrustal rocks, as well as tonalitic, granodioritic and granitic pre-collisional orthogneisses, syn-collisional garnet-bearing leucogranites, and post-collisional undeformed granites and gabbros.

The Caxixe batholith (Fig. V. 1; Santiago et al., 2020b) is located in the transitional zone of the AROS, encompassing the northern portion of the Ribeira Orogen and the southern portion of the Araçuaí Orogen. It is widely distributed, with about 110 km in length and width varying between 12 and 21 km. It is composed of four rock associations: (i) tonalitic to granitic biotite orthogneisses with mafic enclaves

and facies, representing juvenile Tonian rocks (Santiago et al. 2020b; Decol et al., 2021); (ii) the most volumetric in the composite batholith, comprising an association of leuco- to mesocratic biotite granite of fine to medium grain with foliation marked by biotite plates (135/40) with discordant granitic veins and mafic enclaves, and orthogneisses characterized by partial melting features in banded to foliated granitoid, rich in mafic enclaves and discordant granitic veins, that are interpreted as intimately linked in a migmatitic system. Furthermore, this association is composed of coarse-grained granite with dispersed to slightly oriented feldspar porphyries also occur in this association; (iii) garnet-bearing leucogranites and migmatitic neossomes, marking the peak of syn-collisional anatexis and melt generation; (iv) leucocratic isotropic fine-to-medium grained K-feldspar granites, representing late-stage intrusions. A localized deformed mafic intrusion was also recognized (outcrop 54C) and is probably related to rock association (iii), as discussed below.

Rock association (i) was studied by Santiago et al. (2020b) and Decol et al. (2021). It is composed of granodioritic to granitic and minor tonalitic to gabbroic rocks, with calc-alkaline, metaluminous to slightly peraluminous, magnesian, I-type signature and magmatic arc affinity. Zircon U-Pb (LA-ICP-MS and SHRIMP; Santiago et al., 2020b) data reveal magmatic crystallization ages from 859±7 Ma to 847±8 Ma (for zircon cores) and a probably metamorphic age of 834±9 Ma (for zircon rims). Hf Isotopic data yield positive $\varepsilon Hf_{(t)}$ values between +10 and +14, and T_{DM} Hf model ages from 1.01 Ga to 0.84 Ga (Santiago et al., 2020b). Whole-rock Nd and Sr data show $\varepsilon Nd_{(t)}$ values from +0.9 to +6.4and T_{DM} Nd model ages between 1.2 Ga and 0.8 Ga, and $^{87}Sr/^{86}Sr_{(i)}$ of 0.6979-0.7035 (Santiago et al., 2020b). Rocks with adakitic composition (Decol et al., 2021) are interpreted as formed by partial melting of subducted young and hot oceanic lithosphere under moderate to high pressures with stabilization of garnet in the residue. The petrographic, geochemical, isotopic and geochronologic data indicates that rock samples from association (i) were formed in a juvenile island arc setting, as the northernmost described portion of the Serra da Prata arc (Peixoto et al., 2017). In this study, we will focus on the characterization of rock associations (ii), (iii) and (iv).

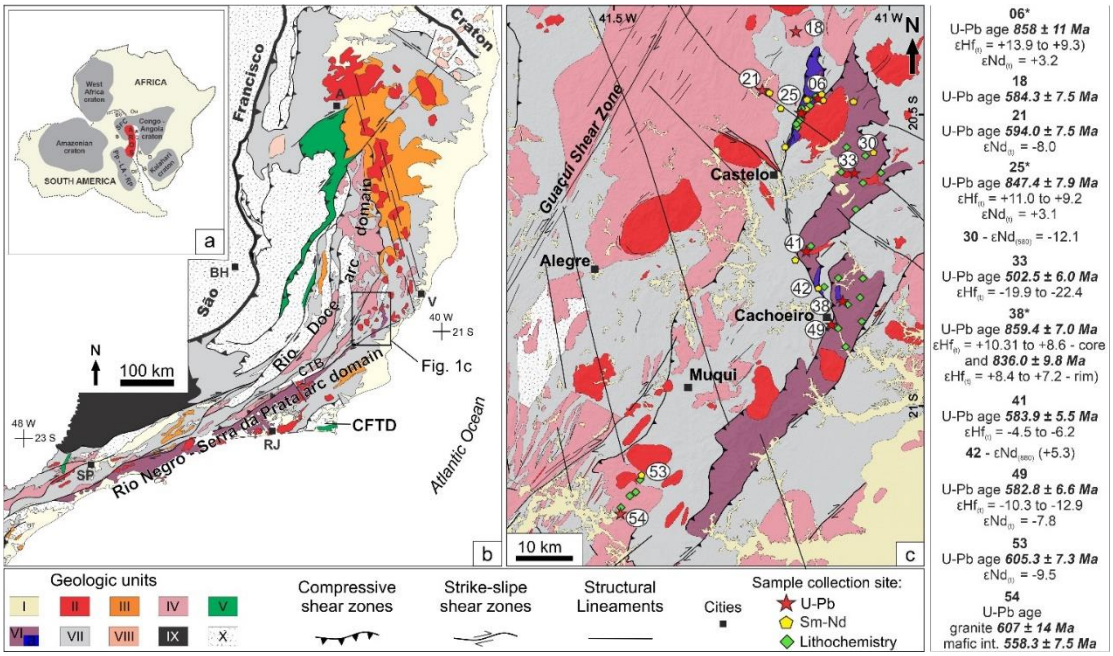

Fig. V. 1 - Simplified geological map of the Araçuaí-Ribeira orogenic system (AROS) (b) and its location in Western Gondwana (a) (modified from Silva et al., 2005); (c) Geological map (modified from Vieira et al., 2014) of the study area with respective age and isotopic results from this work, except for samples marked with * that are from Santiago et al. (2020b). 1 - Cenozoic covers. AROS units: 2 - Post-collisional plutonism; 3 - Collisional plutonism; 4 - Rio Doce magmatic arc and probable correlatives; 5 - Ophiolite-bearing rock assemblages; 6 - Serra da Prata -Rio Negro arc domain (Caxixe batholith Tonian xenoliths and roof pendants marked in blue in 6a); 7 - Neoproterozoic metasedimentary and metavolcanic successions; 8 - Tonian and Cryogenian rift-related magmatic rocks; 9 - Southern Brasília belt; 10 - Pre-Neoproterozoic units and cratonic covers. WCB, West Congo belt. CSF, Sao Francisco craton. Pp-LA-RP, Paranapanema-Luiz Alves-Rio de La Plata cratonic blocks.

Fig. V. 2 – Outcrops of the Caxixe batholith and adjacent smaller plutons. a) Biotite orgthogneiss of rock association (i) representing a xenolithic remnant of Tonian juvenile rocks within the Caxixe batholith, station 42 near Cachoeiro de Itapemirim city; b) pre-collisional foliated porphiry granite of rock association (ii) (Station 53 in the boundary with Rio de Janeiro state); c) syn-collisional foliated garnet-bearing leucogranite of rock association (iii) (Station 43 near Cachoeiro de de Itapemirim city); d) Biotite orthogneiss with mafic enclaves crosscut by granitic veins of rock association (ii) (station 41 near Cachoeiro de Itapemirim city); e) and f) various photos of migmatites of rock association (ii), with neosomes related to rock association (iii) (Station 49 at Cachoeiro de Itapemirim city and Station 54 in the border with Rio de Janeiro state); g) syn- to tardi-collisional mafic intrusion (Station 54C) related to rock association (iii).

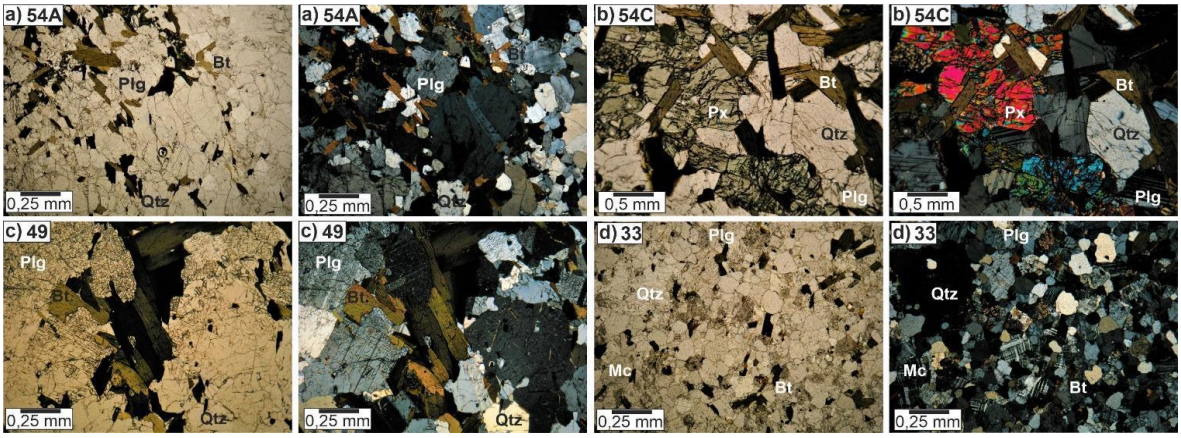

Fig. V. 3 - Photomicrographs of samples from the Caxixe batholith and adjacent smaller pluton showing their mineralogical associations (Bt, biotite; Hbl, hornblende; Plg, plagioclase; Qtz, quartz; Px, piroxene). All samples from rock association (ii) (foliated granites and orthogneisses), except for sample 33, from rock association (iv) (post-collisional granite) and sample 54C, from rock association (iii) (syn- to tardi-collisional mafic intrusion).

V.4. Methods

V.4.1. Field campaigns, sample preparation and petrography

Field campaigns were conducted to collect representative samples of the Caxixe batholith and surrounding plutons. Samples were then prepared for thin section, geochemical, isotopic and geochronological analysis at CPMTC Research Center labs, Federal University of Minas Gerais (UFMG), Brazil, through standard crushing, sieving, powdering and mineral separation techniques.

V.4.2. Whole-rock chemistry analyses

Lithochemical analyses were conducted at SGS-Geosol Laboratory, Brazil (Supplementary Material SV-1). Element grades were analyzed via ICP-MS (Induced Coupled Plasma – Mass Spectrometry) after fusion with lithium metaborate/tetraborate and digestion with diluted nitric acid. Analytical errors are within 2% for major oxides and 5% for trace elements. The detection limit for major elements is of 0.01%. For the trace elements, the limits are of 10 ppm (Ba, Sr, Zr), 5 ppm (Zn, V, Cu, Ni), 0.5 ppm (Co), 0.3 ppm (Sn), 0.2 ppm (Rb), 0.1 ppm (Ce, Ga, La, Nd, Sm, Th, W, Yb) and 0.05 ppm (Cs, Dy, Er, Eu, Gd, Hf, Ho, Lu, Nb, Pr, Ta, Tb, Tm, U, Y). Base and precious metal contents were determined by digestion in Aqua Regia followed by ICPMS analysis. Loss on ignition (LOI) was determined by the weighing difference after

ignition at 1000 °C. The CIPW norm of the standard mineral components, from the whole-rock analyses, was based on Johannsen (1931). Since the whole-rock chemical analyses considered only Fe_2O_3, the estimation of FeO and Fe_2O_3 was based on Gill (2010), who used the ratio 0.9, that is, FeO estimated = 0.9 × Fe_2O_3Total.

5.4.3. Sm-Nd and Rb-Sr isotope analyses

The Sm-Nd and Rb-Sr isotope analyses were conducted at the Laboratório de Geocronologia (Laboratory of Geochronology) of the Brasília University (UnB), Brazil (Supplementary Material SV-4). Samples were dissolved in a HF-HNO_3 mixture in high-pressure Teflon vessels. A ^{150}Nd-^{149}Sm tracer was added to determine Nd and Sm concentrations. Rare Earth Elements (REE) were then purified by cation exchange chromatography, and Sm and Nd were subsequently separated following the procedure of Gioia and Pimentel (2000). Sm and Nd analyses used a double filament assembly in a Thermoscientific Triton Plus mass spectrometer operating in static mode. The Sm and Nd concentrations and the $^{147}Sm/^{144}Nd$ ratios have accuracy of 0.5% that corresponds to an ± 0.5 average error on the initial εNd values of based on repeated measurements of the JNdi-1 standard, with a longterm (year-round) average during the period of analysis of $^{143}Nd/^{144}Nd$ = 0.512230 ± 0.000006. Sr and Rb were separated using the conventional cation exchange procedure according to Pankhurst and O'Nions (1973). Samples were measured at 1250–1300 °C in dynamic multi-collection mode. The $^{87}Sr/^{86}Sr$ values of the samples were corrected for the offset relative to the certified NIST SRM 987 value of 0.710250. The long-term (year-round) average of this standard $^{87}Sr/^{86}Sr$ ratios measured in this machine during the period of analysis is 0.71028 ± 0.00004. Procedural blanks for Sr are less than 100 pg. All uncertainties are presented at the 2σ level. Both Nd and Sr initial ratios are calculated using the crystallization age from U-Pb data obtained in this work.

5.4.4 LA-ICP-MS U-Pb zircon dating

Samples were crushed to the 50–500 μm size range and submitted to analysis through the U-Pb LA-ICP-MS (Laser Ablation – Induced Coupled Plasma Mass Spectrometry) method at both the Laboratório de Geocronologia, Universidade de Brasília (UnB), and at the Laboratório de Geoquímica Isotópica, UFOP, Brazil

(Supplementary Material SV-2). Zircon crystals were separated through standard magnetic, handpicking techniques, and mounted in an epoxy resin, ground and polished. Images were made in a Scanning Electron Microscopy (SEM) in a FEI Quanta 450 microscope through the backscattering technique (BKS) and cathodoluminescence images were also obtained. The resulting images emphasize the internal structure of zircon grains (zoning, fracturing, etc.) and were used to locate the laser spots avoiding (fractures and inclusions).

At UnB, analyzes were carried out by laser ablation using a Finnigan Neptune ICP-MS machine coupled to a Nd-YAG 213 nm laser ablation system. The U-Pb analysis follows the procedures outlined in Buhn et al. (2009). Ablation was done using 25–30 μm spots at a frequency of 9–13 Hz and intensity of 0.19–1.02 J/cm2 with 60 s of analysis per spot. The ablated material was carried by Ar (~0.90 L/min) and He (~0.40 L/min) in 40 cycles of 1 s each. Analysis was conducted with bracketing of three unknown samples between measurements of primary and secondary reference materials and a blank analysis. The primary reference material GJ-1 zircon yielded a mean $^{206}Pb/^{238}U$ ratio of 0.0967 ± 0.0028 (ref. value 0.09761 ± 0.00011; Jackson et al., 2004), corresponding to a mean $^{206}Pb/^{238}U$ age of 595 ± 16 Ma (mean $^{206}Pb/^{238}U$ age of GJ-1 = 599.75 Ma; Jackson et al., 2004, Supplementary Material S5-2). Accuracy was controlled using the secondary reference material 91500 zircon, which yielded a Concordia age of 1057.7 ± 9.1 (n = 7). Raw data were reduced using an in-house program and corrections were done for background, instrumental mass bias and common Pb. U-Pb ages were calculated using Isoplot 3.6 (Ludwig, 2008). All uncertainties are presented at the 2σ level.

Sample 43 was analyzed at UFOP using a Thermo-Fisher Element II sector field ICP-MS coupled to a CETAC LSX-213 G2+ (λ = 213 nm) Nd:YAG laser. A detailed description of the method is given by Gerdes and Zeh (2006, 2009). Ablation was carried out in a low-volume cell with He as carrier gas; laser beam parameters used were a spot size of 20 μm, a repetition rate of 10 Hz, and a fluence of ~3 J cm-2. Time-resolved raw data were corrected offline for background signal, common Pb, laser-induced elemental fractionation, instrumental mass discrimination, and time-dependent elemental fractionation of Pb/U using the GLITTER® software package (Van Achterbergh et al., 2001). Common Pb correction was applied using the interference- and background-corrected ^{204}Pb signal and a model Pb composition (Stacey and Kramers, 1975). Laser induced elemental fractionation and instrumental

mass discrimination were corrected by normalization to the reference zircon GJ-1 (Jackson et al., 2004). The drift in inter-elemental fractionation (Pb/U) during 30 s of sample ablation was corrected individually before normalization to GJ-1. Reported uncertainties (2σ) were propagated by quadratic addition of the external reproducibility obtained from the standard zircon GJ-1 during the analytical session (2SD in %) and the within-run precision of each analysis (standard error in %). For testing the validity of the applied methods and the reproducibility of the data, multiple analyses of the reference zircon Plešovice (Sláma et al., 2008) were performed, yielding a Concordia age of 338.1 ± 2.8 Ma (n = 4, MSWD = 0.01). This agrees, within uncertainty, with the accepted ID-TIMS age reported for Plešovice (337.3 ± 0.4 Ma 2σ, Sláma et al., 2008). In addition, several analyses of the in-house reference zircon BB (Santos et al., 2017) were conducted, yielding a Concordia age of 559.2 ± 4.7 Ma (n = 4, MSWD = 1.10), consistent with the reported ID-TIMS age of this reference material (560.0 ± 0.4 Ma 2σ, Santos et al., 2017). U-Pb ages were calculated using Isoplot 3.6 (Ludwig, 2008). All uncertainties are presented at the 2σ level.

5.4.5 SHRIMP U-Pb zircon dating

U-Pb (SHRIMP – Sensitive High-Resolution Ion Microprobe) analysis (Supplementary Material SV-2) was performed in zircon crystals separated through standard crushing, sieving, magnetic and gravimetric methods from homogeneous portions (i.e, bearing no veins, fractures or alteration fronts) of samples 33, 41 and 49 the SEPURA – Laboratório de Separacao Mineral de Alta Pureza at CPMTC, Federal University of Minas Gerais (UFMG), Brazil. After mounting in epoxi and polishing, zircon crystals were imaged through standard SEM (Scanning Electron Microscopy) techniques such as Secondary Electrons (SE), Back-Scattered Electrons (BSE) and Cathodoluminescence (CL) in a TESCAN Vega SEM at the Centre for Microscopy and Microanalysis (CMCA) at the University of Western Australia, Perth. The images were used for spot positioning based on the study of crystal features such as cores and rims, zones of damage by U radioactive decay, zones of inclusions, etc. The sample mounts were analyzed for U-Pb at the SHRIMP II Laboratory of the John de Laeter Centre, Curtin University, Perth, Australia. The mounts were cleaned following internal standards of the Centre and coated with gold for SHRIMP analyses, with a microprobe spot size of 20 µm. Six scans were performed for each spot, with nine peaks analyzed

at masses $^{196}Zr_2O$, ^{204}Pb, background, ^{206}Pb, ^{207}Pb, ^{208}Pb, ^{238}U, ^{248}ThO and ^{254}UO. The NBS611 glass standard was used to identify the peak position of mass ^{204}Pb, whereas the calibration of the U contents and Pb/U ratios were conducted using zircon standard Temora II (417 Ma; Black et al., 2004), which analysis was bracketed after each three or four unknows, yielding a Concordia Age of 416.4 ± 3.3 Ma (2σ; MSWD = 1.5; n = 25). The $^{207}Pb/^{206}Pb$ zircon standard used to monitor both instrument-induced mass fractionation and accuracy was OGC (3467 ± 3 Ma; Stern et al., 2009) yielding a Concordia Age of 3462.1 ± 6.8 Ma (2σ; MSWD = 0.73; n = 7) and a $^{207}Pb/^{206}Pb$ mean age of 3464.3 ± 6.6 Ma. SHRIMP data were reduced using SQUID 2.5 software (Ludwig, 2009) and plots were prepared using ISOPLOT 4.15 (Ludwig, 2008).

5.4.6. Hf isotope analyses

Hf isotope analyses were carried out in a Thermo-Finnigan Neptune multicollector ICPMS coupled to a Photon-Machines laser system that delivers a beam of 193 nm UV light from a frequency quintupled Nd:YAG laser hosted in Laboratorio de Geoquimica Isotopica, Federal University of Ouro Preto (UFOP) (Supplementary Material SV-3). The analyses were achieved with a beam diameter of 50 μm, a repetition rate between 4 and 6 Hz and 50% of laser output. Depending on the conditions and Hf contents, the Hf signals were between 1 and 6×10^{-11} A and the ablation time lasted 60 s. Ar carrier gas transported from the ablated sample from the laser ablation cell via mixing chamber to the ICPMS torch. To correct for the isobaric interferences of ^{176}Lu and ^{176}Yb on ^{176}Hf, masses 172, 173 and 175–180 were measured in static- collection mode and simultaneously monitored. The ^{177}Hf signal intensity was ca. 10 V. LA-ICP-MC data were reduced using In-house Excel Spreadsheets. The accuracy and external reproducibility of the Lu–Hf results were monitored through the analysis of zircon standards Temora ($^{176}Hf/^{177}Hf$ = 0.282680 ± 0.000031; Black et al., 2003; Wu et al., 2006), Blue Berry ($^{176}Hf/^{177}Hf$ = 0.281674 ± 0.000018; Santos et al., 2017), Mud Tank ($^{176}Hf/^{177}Hf$ = 0.282504 ± 0.000044; Black and Gulson, 1978; Woodhead and Hergt, 2005), GJ-1 ($^{176}Hf/^{177}Hf$ = 0.282000 ± 0.000005; Jackson et al., 2004) and Plešovice ($^{176}Hf/^{177}Hf$ = 0.282482 ± 0.000013; Slama et al., 2008), which yielded $^{176}Hf/^{177}Hf$ average ratios of 0.282654 ± 0.000014 (n = 1), 0.281673 ± 0.000017 (n = 8), 0.282519 ± 0.000015 (n = 9), 0.282006 ±

0.000019 (n = 7) and 0.282485 ± 0.000014 (n = 9), respectively (± 2SD); all values within the uncertainties and in good agreement with the accepted standard ratios. Initial Hf isotope ratios were recalculated to the $^{206}Pb/^{238}U$ age of each zircon crystal. For the calculation of the εHf(t) values, the chondritic values reported by Bouvier et al. (2008) of $^{176}Hf/^{177}Hf = 0.282785 \pm 0.000011$ and $^{176}Lu/^{177}Hf = 0.0336 \pm 0.0001$ were used. To calculate the model ages (T_{DM}) based on a depleted mantle source, the present-day ratios of $^{176}Hf/^{177}Hf = 0.28325$ and $^{176}Lu/^{177}Hf = 0.0388$ were used (Griffin et al., 2000; updated by Andersen et al., 2009). The λ decay constant for ^{176}Lu used is $1.867x10^{-11}$/yr (Soderlund et al., 2004).

V.5. Results

V.5.1. Whole-rock geochemistry

Samples from rock associations (ii), and (iv) were analyzed for whole-rock geochemistry. Rock association (iii) (syn-collisional garnet-bearing leucogranites) was not analyzed.

The whole rock elemental geochemistry data (Supplementary Material S5-1) of rocks pertaining to association (ii) as described above (*e.g.*, foliated biotite-granite and orthogneisses with mafic enclaves) characterize a series from granite to gabbro, with most rocks clustering in the granodiorite field and a general calc-alkaline trend (Fig. V.4). The rocks have metaluminous to slightly peraluminous, calcic to calc-alkaline and magnesian signatures (Fig. V.5), and characterize I-type granites.

The chondrite-normalized Rare Earth Element (REE) patterns show a slight enrichment in Light Rare Earth Elements (LREE) compared to the Heavy Rare Earth elements (HREE), less prominent in mafic rock that shows an almost flat pattern, and the HREE show a flat pattern on all samples. They have a slightly negative Eu anomaly with the exception of two samples that show a positive anomaly. Normalized incompatible element patterns show prominent negative anomalies of Th, Nb, Ta, P, and Ti (Fig. V.6).

For the post-collisional leucocratic granites (rock association (iv)), the chemical composition characterizes a series of granite to diorite, grouped in general in granite chemical compositions (Fig. V.7). The samples show metaluminous, calc-alkaline to alkaline affinity and are magnesian to ferroan (Fig. V.8). REE patterns show an

enrichment in LREE relative to HREE which have flat patterns in all rocks. The samples have negative Eu anomalies, with the exception of one sample that has a positive anomaly. The incompatible elements diagram shows negative anomalies of Ba, Nb, Ta, Sr, P, and Ti (Fig. V.9).

In most diagrams for discrimination of tectonic setting based on incompatible elements concentrations and ratios (Fig. V.10), both samples from rock associations (ii) and (iv) plot in ambiguous fields. There is however a clear preference for the undeformed samples of rock association (iv) to plot in the central “post-collisional granite” field of the Rb x Y+Nb diagram of Pearce et al. (1984, 1986) while the foliated samples of rock association (ii) tend towards the “volcanic arc granite” field. Further classification is attained with the Nb x SiO_2 diagram of Pearce and Gale (1977), where while the rock association (iv) samples plot in the overlapping field between within plate and arc magmas, most of the samples from rock association (ii) plot in the volcanic arc magmas field.

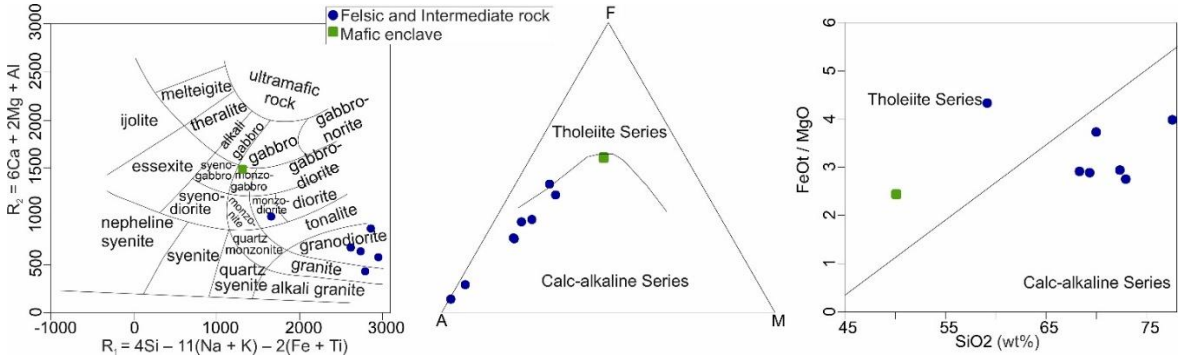

Fig. V. 4 - Geochemical classification diagrams for the foliated pre-collisional (rock association (ii)) rocks of the Caxixe batholith: a) R1-R2 classification diagram from De la Roche et al. (1980); b) AFM diagram (Irvine e Baragar, 1971); c) FeO_t/MgO versus SiO_2 diagram (Miyashiro, 1974).

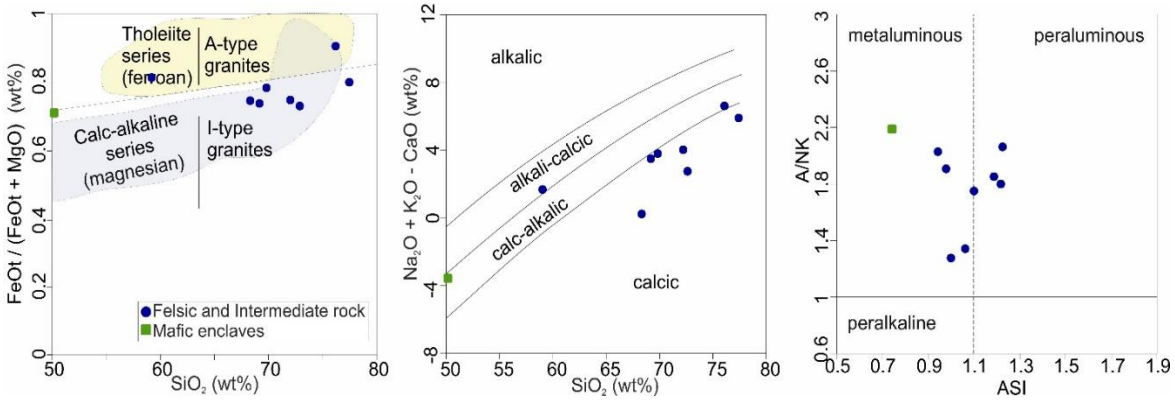

Fig. V. 5 - Geochemical characteristics of the foliated pre-collisional (rock association (ii)) rocks of the Caxixe batholith: a) FeO_t / (FeO_t + MgO) versus SiO_2 (%weight) diagram; b) Na_2O + K_2O - CaO (%weight) versus SiO_2 (%weight) diagram; c) A/CNK - A/NK diagram. All diagrams from Frost et al. (2001).

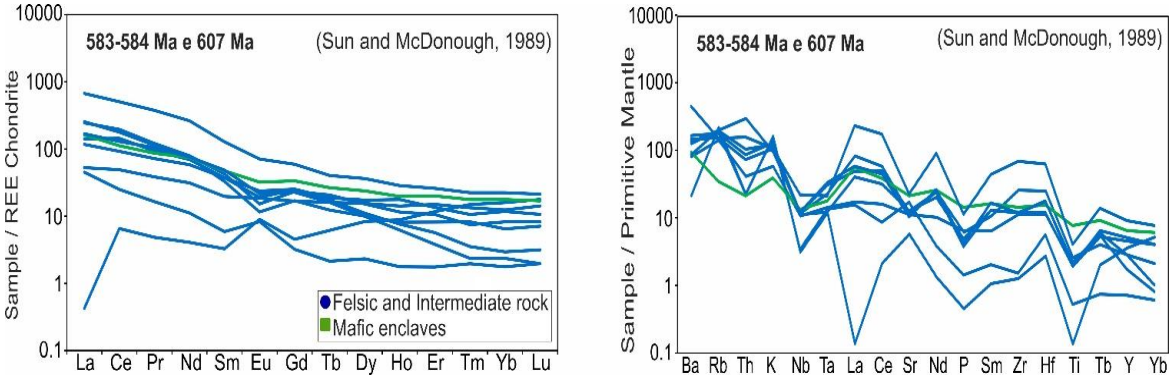

Fig. V. 6 - Chondrite-normalized Rare Earth Element (Sun and McDonough, 1989) and incompatible element plot (element ordering after Thompson et al., 1984; normalization values after Sun and McDonough, 1989) for the foliated pre-collisional (rock association (ii)) rocks of the Caxixe batholith.

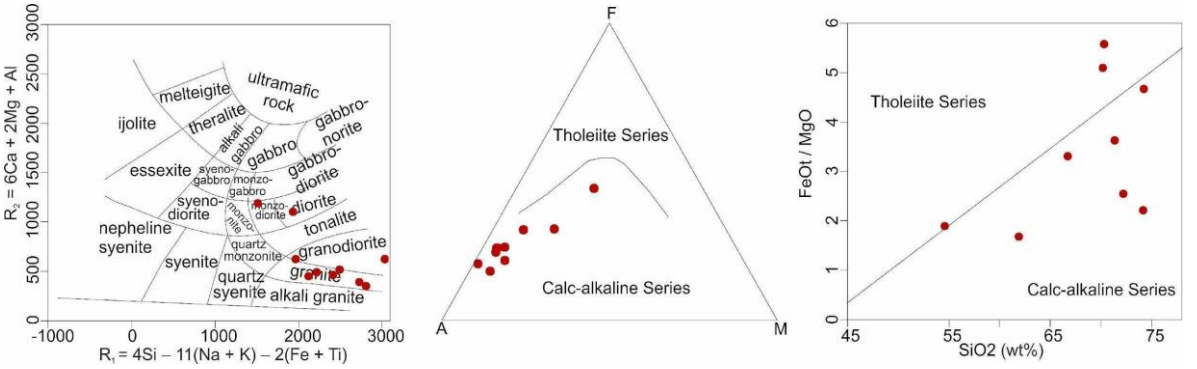

Fig. V. 7 - Geochemical classification diagrams for the post-collisional (rock association (iv)) rocks of the Caxixe batholith: a) R1-R2 classification diagram from De la Roche et al. (1980); b) AFM diagram (Irvine e Baragar, 1971); c) FeO_t / MgO versus SiO_2 diagram (Miyashiro, 1974).

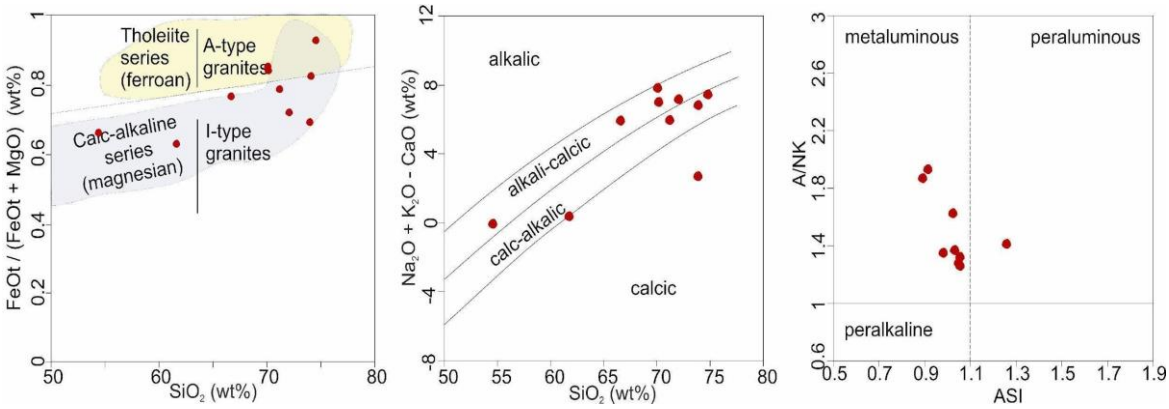

Fig. V. 8 - Geochemical characteristics of the post-collisional (rock association (iv)) rocks of the Caxixe batholith: a) FeO_t / (FeO_t + MgO) versus SiO_2 (%weight) diagram; b) Na_2O + K_2O - CaO (%weight) *versus* SiO_2 (%weight) diagram; c) A/CNK - A/NK diagram. All diagrams from Frost et al. (2001).

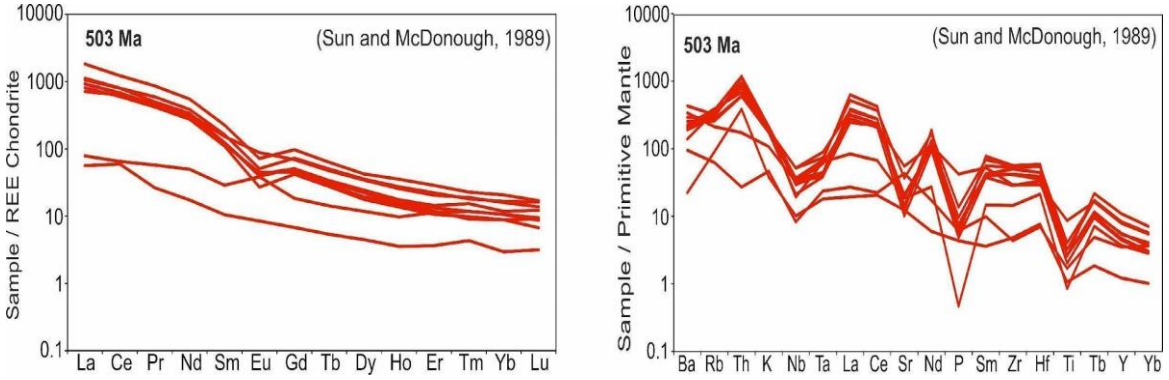

Fig. V. 9 - Chondrite-normalized Rare Earth Element (Sun and McDonough, 1989) and incompatible element plot (element ordering after Thompson et al., 1984; normalization values after Sun and McDonough, 1989) for the post-collisional (rock association (iv)) rocks of the Caxixe batholith.

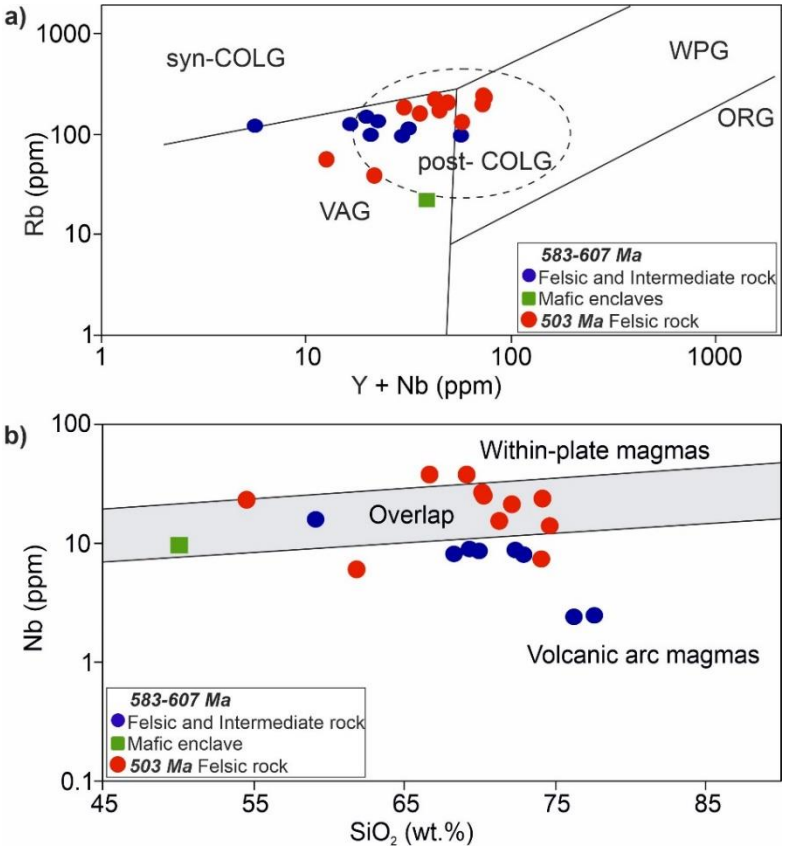

Fig. V. 10 - Tectonic discrimination diagrams for rocks of the Caxixe batholith. a) Rb versus Y+Nb diagram (Pearce et al., 1984, 1996), VAG: volcanic arc granite, ORG: ocean ridge granite, WPG: within-plate granite, syn-COLG: syn-collision granite; b) Nb versus SiO_2 diagram (Pearce and Gale, 1977).

V.5.2. U-Pb geochronology results

Six samples from rock association (ii), two from rock association (iii) and one sample from rock association (iv) were selected for geochronological analysis through the U-Pb method in zircon. Samples from the main body of the Caxixe batholith were analyzed by SHRIMP, while samples from smaller surrounding plutons were analyzed by LA-ICPMS.

V.5.2.1. U-Pb SHRIMP

Samples pertaining to rock association (ii) (49 and 41) and rock association (iii) (33) were analyzed by SHRIMP.

From outcrop 49, located near the southern exit of Cachoeiro de Itapemirim city, a sample taken from the paleosome of an orthogneiss with partial melting characteristics was dated. The paleosome is composed of biotite, plagioclase, quartz

and amphibole (Fig. V.3). Recovered zircon crystals are euhedral, elongated, translucent, inclusion-free, and <200 μm in length (Fig. V.11). They present typical zoning of igneous zircon and yielded a Concordia age of 582.8 ± 6.6 Ma (Fig. V.12).

Located nearby the Cachoeiro de Itapemirim town, outcrop 41 refers to a leucocratic granite of fine to medium grain and incipient foliation marked by biotite crystals. In addition to this mineral, the sample contains porphyritic plagioclase, quartz, microline and muscovite (Fig. V.3). The outcrop also presents mafic enclaves and discordant granitic veins. Elongated, euhedral, translucent, inclusion-free zircon crystals recovered from the homogeneous portion of the granite yielded a Concordia age of 583.9 ± 5.5 Ma (Fig. V.12).

Sample 33 is the only sample from rock association (iii) that was dated in this work. It was collected on the Ubá free flight runway in Castelo city. This sample refers to an isotropic, undeformed medium-grained granite composed of microcline, quartz, biotite, plagioclase, muscovite and titanite (Fig. V.3). The recovered zircon crystals and fragments are stubby, translucent, euhedral and mostly inclusion-free, and yielded a Concordia age of 502.5 ± 6 Ma (Fig. V.12).

V.5.5.2 LA-ICPMS

Samples of smaller granitic bodies located around the main body of the Caxixe batholith were analyzed by LA-ICPMS. Most of the samples are from rock association (ii), with the exception of sample 43, a garnet-bearing leucogranite of rock association (iii), and sample 54C, corresponding to a mafic intrusion emplaced during the syn- to tardi-collisional phase at ca. 560 Ma and this also pertaining to rock association (iii).

Sample 53 is from a porphyritic granite containing plagioclase, microcline, quartz and biotite (Fig. V.3). Recovered zircon crystals are homogeneous elongated prisms, translucent, euhedral and inclusion-free. These yielded an upper intercept age of 605.3 ± 7.3 Ma.

Samples 54A and 54C are from an outcrop composed of orthogneiss characterized by partial melting features grading to banded to foliated granitoid, rich in mafic enclaves and discordant granitic veins and crosscut by a mafic body. Zircons recovered from the orthogneiss (54A) composed of plagioclase, microline, quartz, biotite and titanite (Fig. V.3) are stubby, translucent, homogeneous and inclusion-free, and yielded an upper intercept age of 607 ± 14 Ma (Fig. V.13). Mafic intrusive body

(54C) is comprised of fine-grained crystals of plagioclase, quartz, biotite, pyroxene and hornblende (Fig. V.3). Recovered zircon crystals are stubby to elongated bipyramidal prisms, some with rounded edges, and yielded an upper intercept age of 558.7 ± 8.8 Ma (Fig. V.13).

Sample 18 is from a coarse-grained granite composed of plagioclase, microline, quartz and biotite. Recovered zircon crystals are large translucent bipyramidal prisms, yielding an upper intercept age of 584.3 ± 7.5 Ma (Fig. V.13).

Sample 21A is from a granite with fine to medium grain containing plagioclase, microcline, quartz and incipient foliation marked by biotite (135/40). Recovered zircons are stubby to elongated bipyramidal prisms and crystal fragments, and yielded an upper intercept age of ca. 594 ± 7.5 Ma (Fig. V.13).

Finally, sample 43 is from a syn-collisional garnet-bearing leucocratic granite near Cachoeiro de Itapemirim town. Unlike the other samples, this sample yielded zircons with variable amounts of common lead, defining a Discordia with a lower intercept at 574.4 ± 3.6 Ma (MSWD = 0.60).

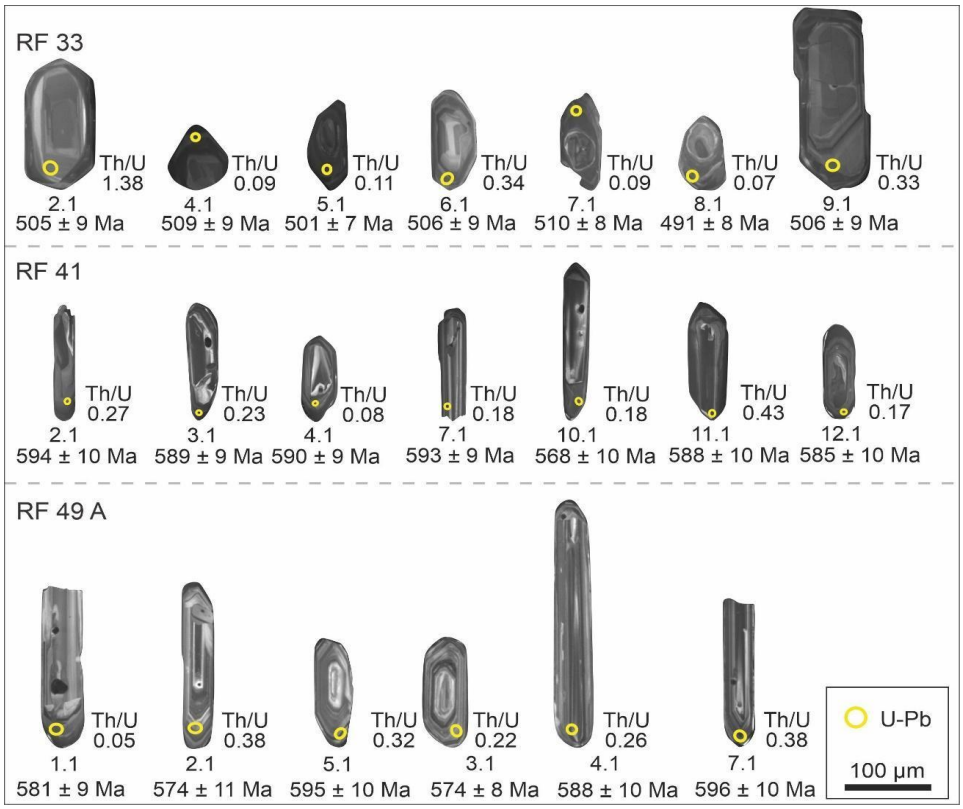

Fig. V. 11 - Representative cathodoluminescence (CL) images with indicated U-Pb spots of zircon crystals from the Caxixe batholith samples.

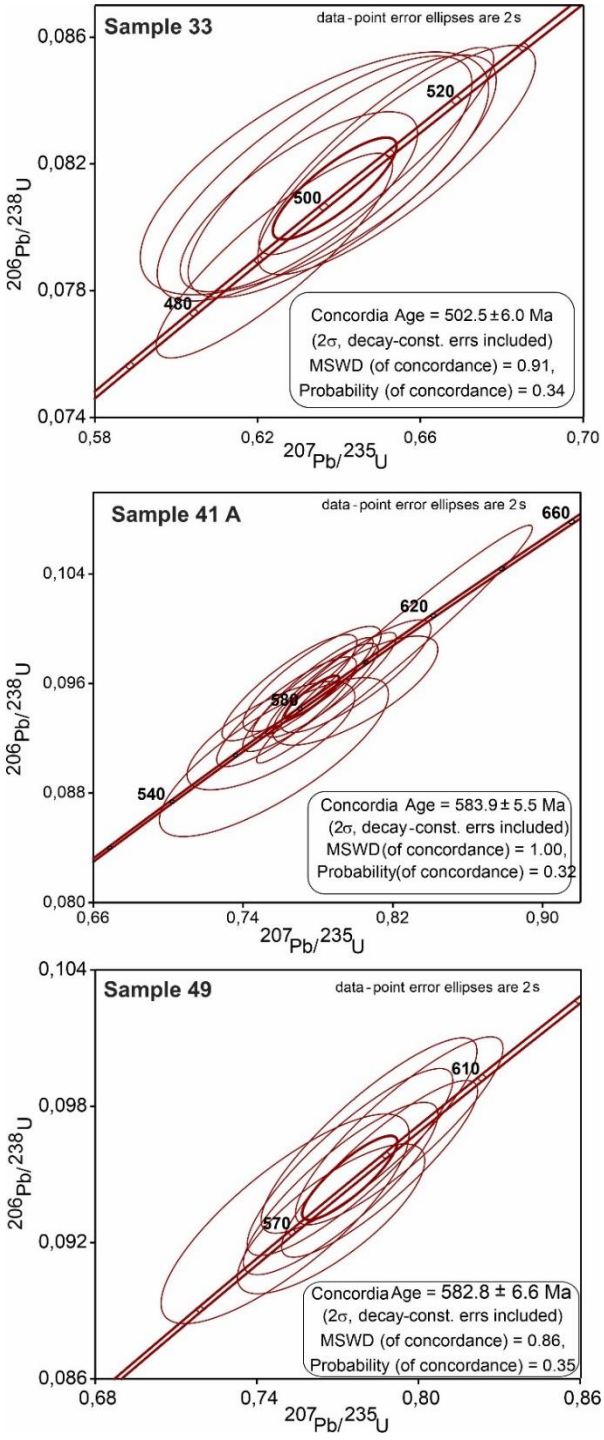

Fig. V. 12 - Concordia diagrams of SHRIMP U-Pb zircon analysis for Caxixe batholith samples.

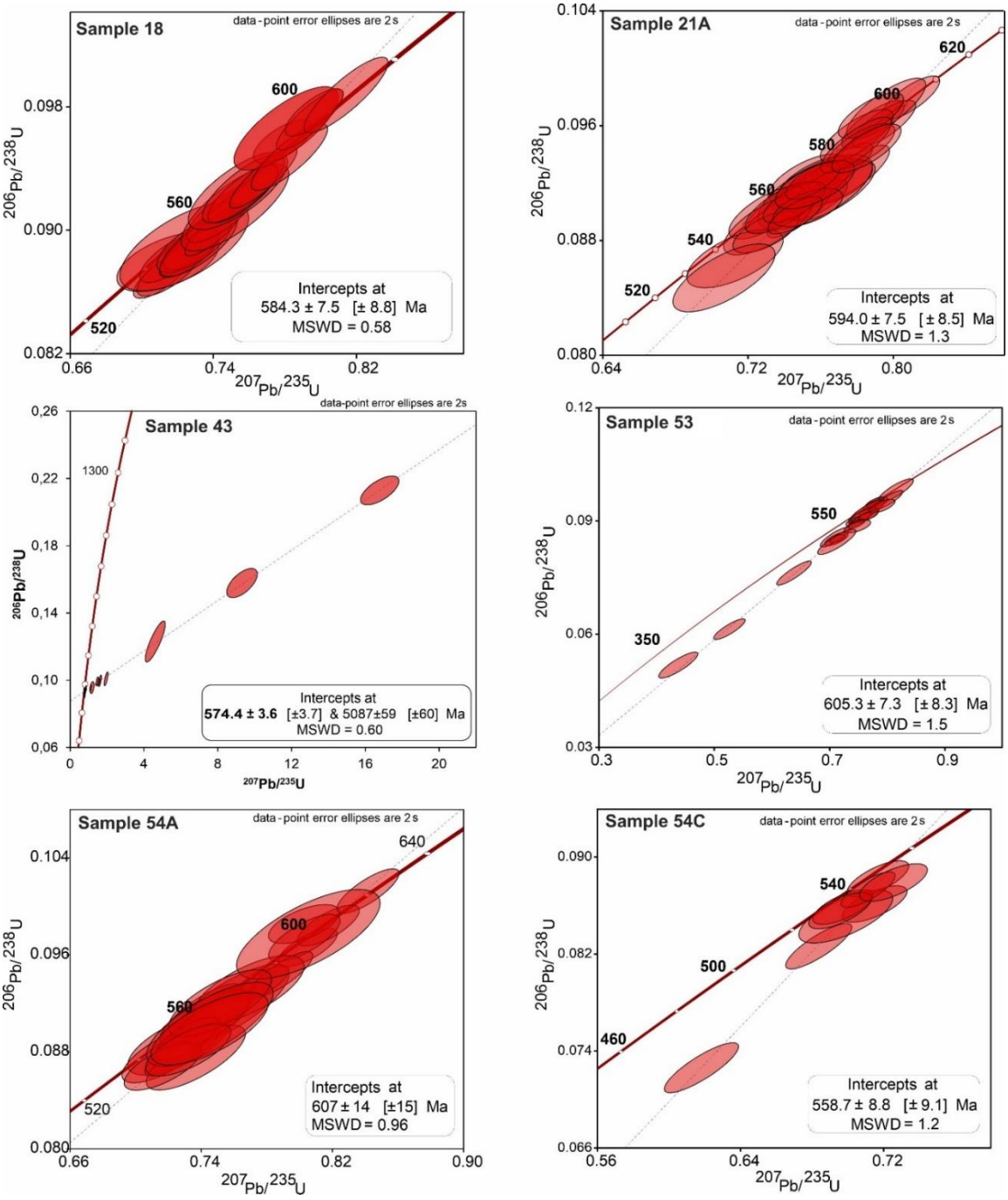

Fig. V. 13 - Concordia diagrams of LA-ICPMS analysis for Caxixe batholith and adjacent smaller pluton zircons.

V.5.3. Hf, Nd and Sr isotopes

Unlike the previously characterized Tonian orthogneiss megaxenoliths (Santiago et al., 2020b), zircons from the main granitic portions of the Caxixe batholith all yielded evolved, negatively fractionated $\varepsilon Hf_{(t)}$ (Supplementary Material SV-3). Zircons from rock association (ii) samples show values between -4 and -13 (Fig. V.

14), and TDM_{Hf} model ages from 1.33 Ga to 1.67 Ga. On the other hand, zircons from the 503 Ma rock association (iv) sample shows much more negative values between -20 and -22 and TDM_{Hf} model ages of 1.83 Ga to 1.93 Ga.

Similar patterns are unraveled in the whole rock Sm-Nd and Rb-Sr datasets (Fig. V. 15). Samples from granites emplaced from ca. 583 Ma to 607 Ma rock association (ii) provided $\varepsilon Nd_{(t)}$ data from -4.9 to -9.5 with TDM_{Nd} model ages ranging from 1.27 to 2.15 Ga, while the 503 Ma rock association (iv) samples provided $\varepsilon Nd_{(t)}$ data from -5.6 to -13.2 with T_{DMNd} model ages ranging from 1.48 to 1.83 Ga (Supplementary Material SV-4). Both sample sets are characterized by varied $^{87}Sr/^{86}Sr_{(i)}$ between 0.706 and 0.711. The Nd and Sr isotopic characteristics, as depicted in the diagrams of Fig. V. 15, indicate a clear affinity with rocks from the Rio Doce continental magmatic arc (Tedeschi et al., 2016).

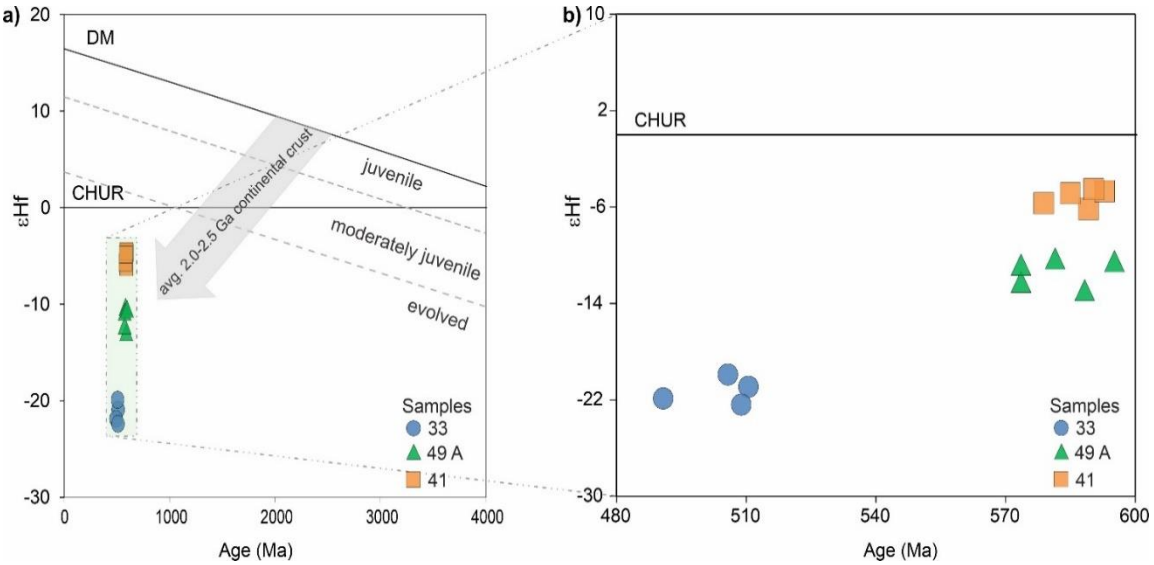

Fig. V. 14 - a) $\varepsilon Hf_{(t)}$ *versus* U-Pb age plots for the analyzed zircon crystals; in b) expanded view in the 480-600 Ma window. The gray band represents the average evolution of typical continental crust generated around 2.0-2.5 Ga, with $^{176}Lu/^{177}Hf$ = 0.010 for felsic and $^{176}Lu/^{177}Hf$ = 0.022 for mafic crust (Pietranik et al., 2008). Depleted mantle model using $^{176}Hf/^{177}Hf$ = 0.28325 and $^{176}Lu/^{177}Hf$ = 0.0388 (Griffin et al., 2000; updated by Andersen et al., 2009).

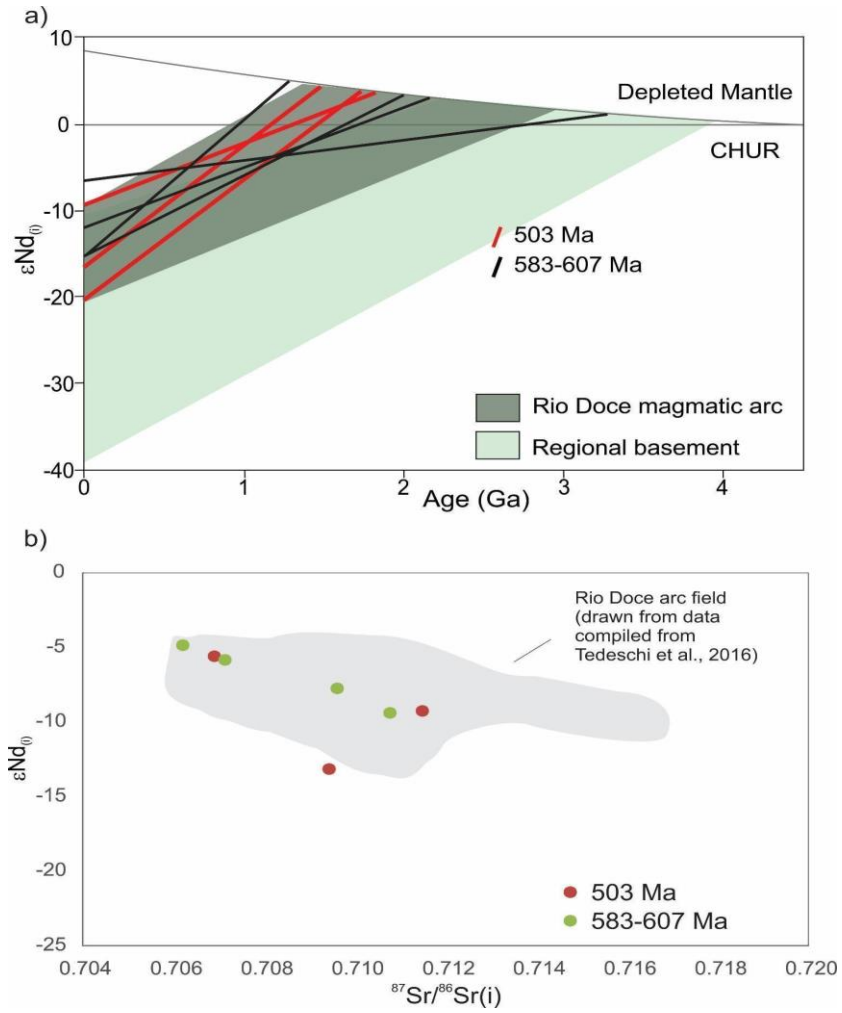

Fig. V. 15 - Nd and Sr isotopic characteristics of the 580-607 Ma (rock association (ii)) and 503 Ma (rock association (iv)) rocks in the southern Espírito Santo state, southeastern Brazil, compared to Rio Doce magmatic arc and Araçuaí Orogen basement. Initial values are recalculated for the respective ages. Fields drawn after data from Tedeschi et al. (2016).

V.6. Discussion

V.6.1. Interpretation of the Caxixe batholith as a composite igneous body

A batholith is understood as an area dominated by plutonic rocks with more than 100 km^2 that represent the deep magmatic portion of arc systems. The term is used both for a single body (pluton) and for areas with multiple intrusions (Paterson & Ducea, 2015). In this last sense, a batholith is not a homogeneous body, but composed of many smaller bodies (2-50 km^2) placed on time scales larger than millions of years, under different tectonic conditions and with distinct, evolving chemical and petrographic composition. The coastal batholith of Peru, for example, comprises about 800 plutons placed between 110 and 30 Ma (Sen & Stern, 2021). In the Sierra Nevada

batholith of western North America, multiple intrusions occurred both when the magma from earlier stages was not yet completely solidified and after it was completely solidified (e.g. Bateman and Chappel, 1979).

The new field, petrographic, geochemical, geochronological and isotopic data suggest that the Caxixe batholith characterizes a prime example of such composite batholith, composed of: (i) biotite-rich granitic to tonalitic orthogneisses with mafic facies and enclaves that occur as megaxenoliths and roof pendants and represent 840-860 Ma juvenile rocks; (ii) pre- to syn-collisional meso to leucocratic granite with a foliation marked by biotite and discordant granitic veins, in addition to orthogneisses with characteristics of partial melting in a banded to foliate granitoid, rich in mafic enclave and discordant granitic veins, both at ca. from 580-607 Ma; (iii) garnet-bearing leucocratic granite marking the peak of crustal anatexis at 575 Ma and mafic intrusions as young as ca. 560 Ma, marking the syn- to tardi-collisional stage; (iv) post-collisional intrusions of isotropic fine to medium-grained leucocratic granite, aged ca. 503 Ma.

The new isotopic and geochronological data disclosed here revealed that the formerly described Tonian orthogneisses of the Caxixe area (Santiago et al., 2020b), including adakitic terms (Decol et al., 2021), represent only small portions of the igneous body that is commonly mapped as a single batholith. Thus, the most parsimonious interpretation is that those portions represent unmelted megaxenoliths and roof pendants that were preserved from later anatexis events within the main batholith. Unfortunately, the contacts between the megaxenoliths and the surrounding igneous mass are not visible in the field, due to the advanced stage of weathering predominant in the area. Direct distinction between granodioritic and tonalitic orthogneisses that were crystallized during the Tonian and during the Ediacaran in this region is not an easy task as these rocks present very similar petrographic features, being distinguished only through application of isotopic and geochronological techniques. Thus, the shape of the igneous bodies and contact relationships (Fig. V.1) are inferred through the distribution of studied outcrops and the analytical data gathered in this work.

V.6.2. Tectonic setting of the Caxixe batholith and smaller plutons

Some geochemical features suggest that the igneous rocks of ca. 580-607 Ma in the Caxixe batholith and surrounding plutons are related to a continental magmatic

arc evolving to an arc-continent collision subduction setting, such as the negative anomalies of Nb-Ta-P-Ti and the slightly negative to positive anomalies of Eu (Fig. V. 9). Classification in some of the most classical diagrams for discrimination of tectonic setting is ambiguous, with samples plotting both in the post-collisional and VAG fields (Fig. V. 10); however, using more specific diagrams with incompatible elements such as Nb, the rocks are further classified in the volcanic arc field (Fig. V. 10). The petrographic, geochemical and isotopic signatures are similar to the continental Rio Doce arc (630-580 Ma - G1 Supersuite) of the Araçuaí Orogen, reinforcing an affinity with continental magmatic arc settings. Thus, the main igneous body of the Caxixe batholith and adjacent plutons, crystallized at ca. 607-583 Ma, probably corresponds to the continental Rio Doce magmatic arc of the Araçuaí Orogen.

Rocks of ca. 503 Ma, on the other hand, are related to a post-collisional environment, as indicated by the petrographic, geochronological and geochemical characteristics, such as negative Sr, Ba and Eu anomalies (Fig. V. 9). The latter indicates residual plagioclase in the magma source of these rocks. The age and isotopic signatures are similar to the plutons that make up the G5 Supersuite related to the collapse of the AROS orogenic edifice at 480-525 Ma (Pedrosa-Soares & Wiedemman-Leonardos, 2000; De Campos et al., 2016).

Thus, the 360 Ma of magmatic activity recorded in the Caxixe Batholith (Fig. V. 16) expose the pre-, syn- and post-collisional stages of the orogenic building in the high-grade core of the AROS. Conversely, this batholith and its surrounding plutons are key to unravelling the conjoined evolution of the two orogenic systems in their transitional area, as they contain rock units that characterize both the Araçuaí and Ribeira orogens.

Juvenile orthogneisses at 840-860 Ma pertain to remnants of the Serra da Prata juvenile arc (rock association (i)), a unit characteristic of the Ribeira Orogen (Peixoto et al., 2017; Heilbron et al., 2020), as unmelted xenoliths and roof pendants within the batholithic mass. The most prominent components of the batholith and surrounding plutons are 580-607 Ma pre-collisional rocks pertaining to the Rio Doce arc (rock association (ii)), which was developed at 580-630 Ma and show very similar geochemical and crustal isotopic signatures (Tedeschi et al., 2016; Soares et al., 2020) to the rocks described in this area, being typical representants of the G1 pre-collisional Supersuite (Pedrosa-Soares and Wiedemann-Leonardos, 2000).

Locally, syn-collisional garnet-bearing leucogranites and neossomes to

migmatites of the arc-related rocks were emplaced at ca. 575 Ma (rock association (iii)), corresponding to the regional peak in anatexis and metamorphism in the high-grade core of the Araçuaí Orogen, dated at ca. 575-550 Ma (Richter et al., 2016; Melo et al., 2017) and corresponding to the G2 syn-collisional Supersuite (Pedrosa-Soares and Wiedemann-Leonardos, 2000). This stage was also marked by deformed mafic intrusions emplaced at ca. 558.7 ± 8.8 Ma. Those are similar to the Córrego Taquari Suite, composed of metamafic dykes crosscutting the low-grade metasedimentary units of the external fold-and-thrust belt of the Araçuaí Orogen bordering the eastern São Francisco Craton margin, that was dated through U-Pb in zircon in an identical time frame within error, at 560 ± 6 Ma (Martins et al., 2011). As interpreted by Martins et al. (2011) for the Córrego Taquari Suite, the mafic intrusion of outcrop 54C was probably emplaced in a local transtensional setting in the transition between the syn- and tardi-collisional stages.

Finally, post-collisional intrusions (rock association (iv)) emplaced at ca. 503 Ma are correlative to similar plutons of the G5 Supersuite, spanning from ca. 525 to 480 Ma (De Campos et al., 2016). Post-collisional plutons of this age range characterize both the Ribeira and Araçuaí orogens (De Campos et al., 2016; Valeriano et al., 2016), providing important links between the two orogenic systems in their confluence zone.

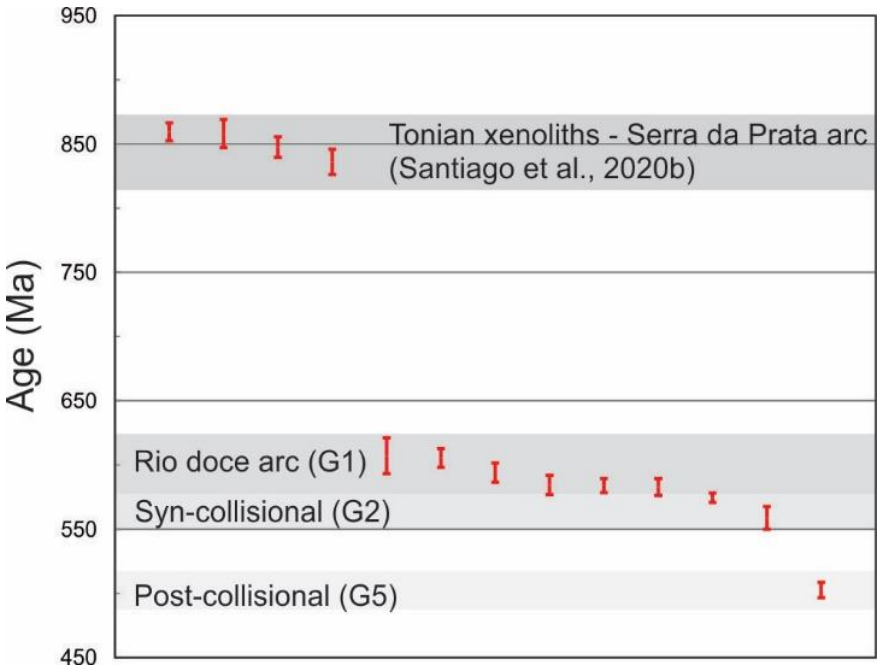

Fig. V. 16 – Distribution of crystallization ages for the various rocks of the Caxixe batholith and adjacent plutons of the AROS in the southern Espírito Santo state, compared to region igneous units and Supersuites. All data from this paper, except Tonian xenoliths from Santiago et al. (2020b).

V.6.3. Model for evolution of the Caxixe batholith and adjacent plutons and implications for western Gondwana amalgamation

The ca. 830-860 Ma rocks found as megaxenoliths and roof pendants formed in an intra-oceanic supra-subduction environment, characterizing remnants of a juvenile Tonian island arc (Santiago et al., 2020b; Decol et al., 2021). To understand how those rocks formed in an intra-oceanic environment and were later entrained within a continental magmatic arc system, and then all of those rocks developed in distinct accretionary settings were clumped together and involved in syn-collisional and post-collisional anatexis and metamorphism, we propose a five-stage model of evolution (Fig. V.17).

As a first step, we propose an oceanward-dipping subduction zone, to produce a purely intra-oceanic arc during the Tonian. The oceanward-dipping zone is proposed because it better explains how purely juvenile, intra-oceanic rocks could later be docked in a passive continental margin (with consumption of the small oceanic basin formed between the island arc and the continent) and then get involved, as an accreted terrane, in the development of an active continental margin arc. A distinct proposition, with an eastward-dipping subduction zone, is proposed by Peixoto et al. (2017) and Decol et al. (2021) for the main portion of the Serra da Prata arc, based mainly on the distribution of supracrustal sequences interpreted as developed in fore- and back-arc basins. In this respect, the paragnaissic units of the Southern Espírito Santo state that serve as host rocks for the Caxixe batholith and smaller plutons bear detrital zircons as young as ca. 600 Ma (Santiago et al., submitted), and thus, those basins are not related to the Tonian magmatic arc, but to the Ediacaran arc instead. In fact, the Tonian arc rocks themselves are preserved, in the study area, only as small remnants within the larger Ediacaran igneous mass. It is thus not probable that Tonian fore- and back-arc basins related to this juvenile arc system are well preserved as major paragnaissic units in this area, but only as small remnants reworked along the younger, Ediacaran basins.

Nevertheless, both eastward and westward subduction settings could be proposed for the Tonian island arc in the area. However, a westward (oceanward) subduction more easily explains the docking of the arc terranes in the passive continental margin of the Angola paleocontinent, which could them serve as a leading edge for the development of a continental magmatic arc during the Ediacaran. We

stress that the strong remelting and both deformational and metamorphic reworking strongly hampers the interpretation of former stratigraphic and structural relations in this area, with the Tonian accretionary systems being preserved only in restricted, localized areas within the Caxixe batholith.

Sometime during the Tonian-Cryonian, then, the island arc remnants were docked to the passive continental margin of the Angola paleocontinent. As a result, subduction polarity reversal occurred, with development of the Rio Doce continental arc in the Ediacaran by partial melting of the coupled continental margin + juvenile arc set at 580-607 Ma. The tectonic process evolves into the collision between the São Francisco and Angola paleocontinents, with the 860 Ma rocks being preserved as unmelted megaxenoliths and roof pendants incorporated in the extensive 607-580 Ma crustal rocks that were intensively remelted at ca. 575 Ma, generating garnet-bearing leucogranites and migmatite neosomes. At ca. 560 Ma, mafic intrusions were placed in local transtensional sites, probably in the transition from the syn- to tardi-collisional stages. Later, during the Cambrian, orogenic collapse and intrusion of post-collisional plutons ensued at ca. 500 Ma.

The occurrence of unmelted and variably preserved pre-collisional xenoliths and roof pendants within highly reworked composite igneous bodies seems to be a common feature of Brasiliano/Pan-African orogens in western Gondwana. For exemple, in the Dom Feliciano Orogen of the southern Mantiqueira Province, De Toni et al. (2020) recognized the Porto Belo Complex as a Tonian (ca. 800 Ma) arc remnant within a large anatectic granite belt, composing the Aiguá-Pelotas-Florianópolis batholith, along with many other unmelted pre-collisional remnants. The authors recognized a multi-stage evolution for this batholith, interpreted as reflecting changes in subduction style and plunge angle of the slab. The accretionary remnants are preserved only as megaxenoliths and roof pendants within the 660-640 Ma syn-collisional and 640-580 Ma post-collisional, shear belt-related main magmatic bodies.

Therefore, the search for testimonies of ancient accretionary systems preserved as fragments in later multi-intrusion plutonic bodies is a difficult task, but of enormous relevance for the understanding of the tectonic evolution of western Gondwana and Precambrian orogens in general. In this search, we emphasize the importance of detailed geochronological and isotopic data in order to differentiate between tonalitic and granodioritic orthogneisses of distinct ages and tectonic settings that might be preserved in the same major igneous bodies throughout the high-grade inner core of

Precambrian orogens.

V.7. Conclusions

The new field, petrographic, geochemical, geochronological and isotopic data presented for the southern Espírito Santo state plutonic rocks reveals a much more complex scenario than previously envisaged for this region, in the confluence between the Araçuaí and Ribeira orogens of the Mantiqueira Province. Tonian juvenile orthogneisses representing the northern termination of the Serra da Prata arc of the Ribeira Orogen, previously recognized in the area, are in fact preserved only as xenoliths and roof pendant remnants within a larger multi-intrusion, composite Caxixe batholith. Most of this batholith crystallized ca. 583-607 Ma as part of the Rio Doce continental magmatic arc, was remelted at ca. 575 Ma during the peak of crustal anatexis on the high-grade orogenic core, intruded by mafic magmas in localized transtensional sites at the syn- to tardi-collisional transition at ca. 560 Ma, and finally intruded by post-collisional bodies at ca. 503 Ma, finalizing the composition of the batholith and surrounding plutons. The amassed geochronological data indicates multi-temporal, multi-stage protracted evolution spanning ca. 360 Ma of orogenic magmatism preserved within this batholith and its vicinity.

Unlike in the juvenile Tonian xenoliths and roof pendants, elemental and isotopic geochemistry data obtained for the ca. 580-607 Ma rocks indicates the involvement of continental crust in the source magmas for the Rio Doce arc in this area. The ca. 503 Ma post-collisional intrusions yielded the most evolved Hf, Nd and Sr compositions, indicating intensive reworking of the orogenic core during the Cambrian collapse stage.

A model for the development of the AROS in the confluence zone between the Araçuaí and Ribeira orogens is presented, starting with the development of oceanward subduction zones and the development of a juvenile Tonian island arc at ca. 840-860 Ma. The arc terranes subsequently dock in the paleocontinental margin of Angola, and are remelted and reworked along with continental basement during the development of the Ediacaran Rio Doce arc in a typical active continental margin at ca. 580-607 Ma. Continental collision caused further remelting and anatexis of the whole orogenic core at ca. 575-560 Ma, and finally, at ca. 503 Ma, orogenic collapse caused the intrusion of post-collisional bodies. The previous accretionary rocks are preserved only as

unmelted xenoliths and roof pendants within the larger anatectic mass.

The preservation of pre-collisional rocks attesting for the accretionary phases of the Brasiliano Orogeny as unmelted remnants within larger, complex and multi-stage igneous bodies reinforces the importance of careful geological mapping allied with geochemical, isotopic and geochronological tools in order to unravel the previous tectonic history of ancient orogens, especially the chronology of oceanic opening and closure events as registered in the subduction phase. As the high-grade orogenic core of ancient orogens went through multiple intensive remelting, deformation and metamorphism events, those testimonies to events previous to continental collisional are key to reconstruct the history of ancient oceans and mountain belts, not only in western Gondwana but in the geological record in general.

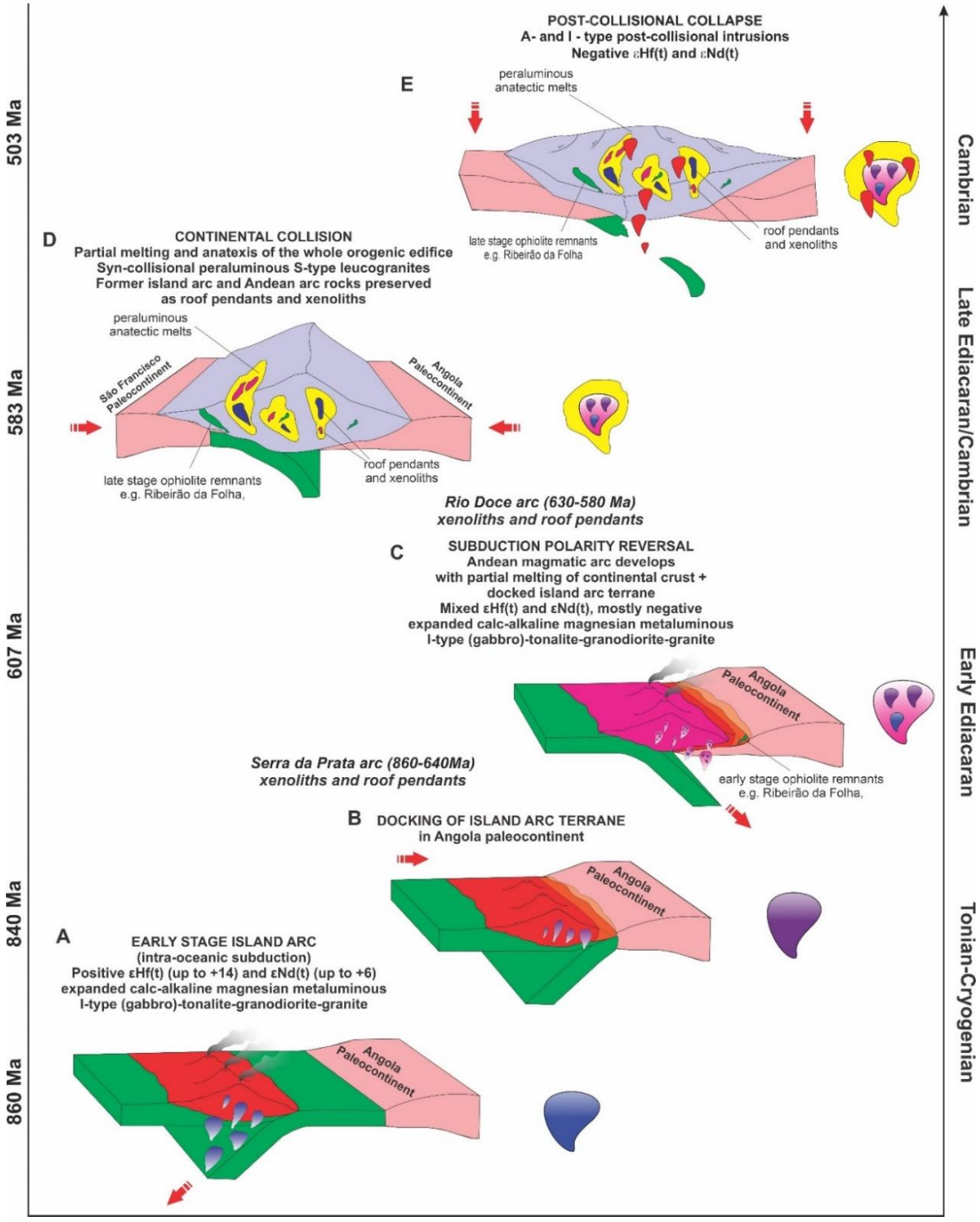

Fig. V. 17 - A model for the development of Brasiliano/Pan-African AROS with the preservation of unmelted pre-collisional xenoliths and roof pendants representing the ca. 860-840 Ma rocks of the Caxixe batholith.

CAPÍTULO VI

CONCLUSÕES GERAIS

A combinação entre dados de campo, petrográficos, isotópicos, geocronológicos e de geoquímica elementar das rochas do sul do Espírito Santo, especialmente do batólito Caxixe e das rochas metassedimentares e plutônicas adjacentes, permitiram chegar a algumas conclusões e à sugestão de modelos de evolução tectônica para a região. A seguir, estão sumarizados os principais resultados e conclusões desta tese de doutorado.

VI. 1 – Caracterização do batólito multi-intrusão Caxixe e plútons adjacentes

- O batólito Caxixe, localizado na zona de transição entre os orógenos Ribeira e Araçuaí, é um complexo batolítico multi-intrusão composto por rochas relacionadas ao Sistema Orogênico Neoproterozóico Araçuaí-Ribeira (AROS). Cerca de 360 Ma de magmatismo pré-, sin- e pós-colisional estão registrados neste batólito e plútons adjacentes, com quatro períodos principais de magmatismo, em 840-860 Ma (pré-colisional juvenil), 580-607 Ma (pré- a sin-colisional), 575-560 Ma (sin-colisional) e cerca de 500 Ma (pós-colisional).

- Ortognaisses tonianos (840-860 Ma) ocorrem neste complexo batolítico como megaxenólitos e *roof pendants*, e possuem características geoquímicas e assinaturas isotópicas (Nd, Sr e Hf) que atestam o caráter juvenil de seu protólito, com contribuições importantes da cunha mantélica na gênese do magma da qual estas rochas foram cristalizadas. Essas características tornam evidente que estas rochas são remanescentes de um arco de ilha Toniano, provavelmente representando o segmento norte, primitivo, do arco intra-oceânico Serra da Prata do Orógeno Ribeira.

- A maior parte do batólito Caxixe e dos plútons adjacentes é caracterizada por rochas graníticas e migmatíticas de ca. 580-607 Ma, com assinaturas geoquímicas semelhantes a rochas desenvolvidas em ambiente de arco magmático continental. Estas rochas fazem parte do arco magmático Ediacarano Rio Doce e apresentam dados isotópicos de Hf e Nd que indicam refusão crustal e assimilação de crosta antiga, provavelmente representada pela refusão da borda do continente Angola junto à crosta relacionada ao arco juvenil Serra da Prata docado em sua margem.

- Granitos leucocráticos ricos em granada e neossomas de migmatitos marcam o período sin-colisional e de anatexia crustal em ca. 575 Ma. Estes são seguidos por intrusões máficas colocadas localmente em sítios transtensionais, na transição entre os estágios sin- a tardi-colisional, a cerca de 560 Ma.

- Granitos pós-colisionais, indeformados, com ambiência geoquímica extensional e forte contaminação crustal, foram colocados em torno de 500 Ma, marcando o estágio de colapso orogênico do AROS com a intrusão de plutons da Supersuite G5.

VI. 2 – Idade, proveniência e ambiente tectônico das unidades paragnáissicas do sul do Espírito Santo

- Os paragnaisses encaixantes do batólito Caxixe e plútons menores na região possuem características geoquímicas que mostram que os protólitos sedimentares são derivados de arcos magmáticos (arco de ilha ou arco continental) em um ambiente de margem continental ativa. A proveniência destas rochas é caracterizada pela abundância de zircões detríticos neoproterozoicos, com idades mais novas em torno de 600 Ma. As unidades paragnáissicas aflorantes na região foram mapeadas anteriormente sob diversas denominações, variavelmente como parte dos complexos Andrelândia e Paraíba do Sul ou dos grupos Rio Doce, Raposo, São Fidélis, Italva e Bom Jesus do Itabapoana. As semelhantes idades das populações mais novas de zircão detrítico, porém, em cerca de 600-620 Ma, indicam que pelo menos parte das unidades metassedimentares e metavulcanosedimentares, tanto a leste quanto a oeste da Zona de Cisalhamento Guaçuí, se originaram de protólitos depositados em bacias aproximadamente contemporâneas, durante o Ediacarano inferior.

- A maioria das idades dos zircões detríticos está próxima à provável idade de deposição dos sedimentos, em torno de 600 Ma, um padrão semelhante a amostras de depósitos de bacias ante- ou intra-arco em margem ativa continental. Desta forma, a maioria das unidades metassedimentares da região representam bacias Ediacaranas relacionadas ao arco Rio Doce. Bacias relacionadas aos arcos mais antigos, Toniano-Criogenianos, se presentes, devem ter sido intensamente retrabalhadas, refundidas e seus detritos podem ter sido assimilados nas bacias mais recentes, Ediacaranas. Esta situação difere da interpretação que vem sendo apresentada para o domínio Italva, mais a sul no Orógeno Ribeira no estado do Rio

de Janeiro, onde as rochas metassedimentares são interpretadas como parte das bacias relacionadas ao arco Serra da Prata.

- Duas hipóteses podem ser colocadas para explicar a presença de zircões Tonianos e Criogenianos nas amostras de paragnaisses encaixantes, dominadas por picos em torno de 600 Ma. A primeira sugere que o sistema de arcos Rio Negro - Serra da Prata estava próximo, senão completamente amalgamado, com o domínio do arco Rio Doce antes de ca. 614 Ma. A segunda hipótese é que, como indicado pela presença de remanescentes Tonianos não-fundidos dentro da massa principal do batólito Caxixe, provavelmente parte do sistema de arcos Rio Negro-Serra da Prata foi refundido e envolvido na edificação do próprio arco Ediacarano Rio Doce. De acordo com esta segunda hipótese, a presença de zircões Tonianos e Criogenianos nas amostras de paragnaisses seria explicada pela erosão de todo o edifício magmático do arco Rio Doce, incluindo os megaxenólitos e *roof pendants* mais antigos, além de xenocristais não completamente fundidos assimilados durante a geração e ascensão dos magmas no ambiente de arco continental.

- A presença de zircões neoformados marca o metamorfismo regional das rochas paragnáissicas e sua migmatização a cerca de 560 Ma, coerente com o pico sin-colisional do AROS. Este dado também indica que a deposição dos protólitos dos paragnaisses na região ocorreu em um intervalo de tempo relativamente curto, entre 600 Ma (idade da população mais nova de zircão detrítico) e 560 Ma (idade do metamorfismo regional), uma situação típica de bacias sin-orogênicas. Um único zircão neoformado cristalizado a cerca de 507 Ma pode indicar a influência térmica das intrusões pós-colisionais na região.

VI. 3 – Modelo evolutivo e importância para a amalgamação do Gondwana Ocidental

- Os 360 Ma de atividade magmática registrados no Batólito Caxixe e nos plútons adjacentes expõem as etapas pré-, sin- e pós-colisionais do edifício orogênico na região sul do Espírito Santo. Inicialmente formaram-se as rochas de 840-860 Ma do arco magmático juvenil em um ambiente de supra-subducção intra-oceânica, seguido pela acoplagem do terreno de arco juvenil na margem continental passiva do paleocontinente Angola. Como resultado, há a inversão da polaridade da subducção e o desenvolvimento do arco continental Rio Doce no Ediacarano (580-607 Ma) por

fusão do conjunto margem continental + arco juvenil acoplado. O processo tectônico evolui para a colisão entre os paleocontinentes São Francisco e Angola há cerca de 575-560 Ma e pelo colapso orogênico em 500 Ma, sendo as rochas de 840-860 Ma preservadas como xenólitos e *roof pendants* pré-colisionais não fundidos em meio à massa batolítica pré-, sin- e pós-colisional.

- A ocorrência de xenólitos e *roof pendants* pré-colisionais não fundidos e preservados de forma variável dentro de corpos ígneos mais novos, que sofreram intensa refusão, metamorfismo e deformação no núcleo orogênico, parece ser uma característica comum dos orógenos Brasilianos/Pan-Africanos do Gondwana Ocidental, e muito bem representada no sul do Espírito Santo. A descrição pormenorizada deste fenômeno será de grande importância para a caracterização do edifício orogênico da costa Atlântica sudeste e sul brasileira, especialmente da sua porção interna de alto grau, menos conhecida do ponto de vista geológico e carente de dados e interpretações.

- A presença tanto de rochas juvenis relacionadas ao arco Serra da Prata do Orógeno Ribeira quanto de rochas de arco continental representadas pelo arco Rio Doce do Orógeno Araçuaí marca a conexão entre estes dois orógenos na região sul do Espírito Santo, indicando que esta é uma zona-chave para compreensão da zona de transição do AROS no Gondwana Ocidental.

- O Gondwana Ocidental se formou em um contexto que envolveu o consumo de oceanos e formação de arcos-de-ilha e continentais, muito semelhante aos processos de tectônica de placas do Fanerozoico.

CAPÍTULO VII

REFERÊNCIAS BIBLIOGRÁFICAS

Adjerid Z, Godard G, Ouzegane K. 2015. High-pressure whiteschists from the Ti-N-Eggoleh area (Central Hoggar, Algeria): a record of Pan-African oceanic subduction. Lithos 226:201–216

Adjerid, Z., Ouzegane, K., Godard, G., Bitam-Derridj, A., & Kienast, J. R. 2012. Le Sérouènout: un fragment de lithosphère océanique subducté à haute pression, exhumé puis granulitisé à haute température. Bulletin du Service Géologique National, 23(3), 199-217.

Alkmim, F.F., Marshak, S., Pedrosa-Soares, A.C., Peres, G.G., Cruz, S.C.P., & Whittington, A. (2006). Kinematic evolution of the Araçuaí-West Congo orogen in Brazil and Africa: nutcracker tectonics during the Neoproterozoic assembly of Gondwana. Precambrian Research, 149, 43–64

Alkmim, F.F., Pedrosa-Soares, A.C., Noce, C.M., Cruz, S.C.P., 2007. Sobre a evolução tectônica do orógeno Araçuaí- Congo Ocidental. 15(1). Revista Geonomos, pp. 25–43.

Alkmim, F.F., Kuchenbecker, M., Reis, H.L.S., Pedrosa-Soares, A.C., 2017. The Araçuaí Belt. Springer International Publishing Switzerland https://doi.org/10.1007/978-3-319-01715-0_14.

Allègre, C.J. 2012. Isotope Geology. Cambridge University Press. DOI (10.1017/CBO9780511809323).

Almeida F.F.M de, Amaral G., Cordani H.G., Kawashita K. 1973. The Precambrian evolution of South American cratonic margin, South of Amazon River. In: A.E.M. Nairs & F.G. Stehli (eds.) The ocean basins and margins. (vol. I), p. 411-446.

Almeida F.F.M. de, Hasui Y., Brito-Neves B.B de, Fuck R. A. (1977). As províncias estruturais do Brasil. In: SBG, Simp Geol. Nordeste, 8, Bol. Esp., 12p. Almeida F.F.M. de, Hasui Y., Brito-Neves B.B de, Fuck R. A. 1981. Brazilian Structural Provinces: an introduction. Earth-Sci. Rev., (17): 1-29.

Almeida F.F.M. de, Hasui Y., Brito-Neves B.B de, Fuck R. A. 1981. Brazilian Structural Provinces: an introduction. Earth-Sci. Rev., (17): 1-29.

Almeida J.C.H., Tupinambá M, Heilbron M., Trouw R. 1998. Geometric and kinematic analysis at the Central Tectonic Boundary of the Ribeira belt, Southeastern Brazil, In: SBG, Congr. Bras. Geol., 39, Anais, p. 32.

Almeida, J.C.H. (2000). Zonas de cisalhamento dúctil de alto grau do Médio Vale do Rio Paraíba do Sul. 190p. Tese de Doutoramento (inédito). IGCE-UNESP.

Amaral L. S. S., Caxito F. A, Pedrosa-Soares A.C., Queiroga G. M., Babinski M., Trindade R., Lana C., Chemale F. 2020. The Ribeirão da Folha ophiolite-bearing accretionary wedge (Araçuaí orogen, SE Brazil): New data for Cryogenian plagiogranite and metasedimentary rocks. Precambrian Research, 336, 105522. doi: https://doi.org/10.1016/j.precamres.2019.105522

Ancelmi, M. F., Santos, T. J. S. dos, Amaral, W. da S., Fuck, R. A., Dantas, E. L., & Zincone, S. A. (2015). Provenance of metasedimentary rocks from the Ceará Central Domain of Borborema Province, NE Brazil: implications for the significance of associated retrograded eclogites. Journal of South American Earth Sciences, 58, 82–99. doi:10.1016/j.jsames.2014.12.007

Andersen, T., Andersson, U.B., Graham, S., Åberg, G., Simonsen, S.L. 2009. Granitic magmatism by melting of juvenile continental crust: new constraints on the source of Palaeoproterozoic granitoids in Fennoscandia from Hf isotopes in zircon. Journal of the Geological Society 166, 233–247.

Aracema L.W., Neves, A.C., Ferreira J.C., Pedrosa-Soare, A.C., Lobato L.M. & Noce C.M. 2000. Novas evidências de remanescentes oceânicos na Faixa Araçuaí: As rochas

metaultramáficas de São José da Safira. Geonomos, (v. 8), n.1, p. 55-61.
Araujo, C., Pedrosa-Soaresa, A., Lana, C., Dussin, I., Queiroga, G., Serrano, P., Medeiros-Júnior, E. 2020. Zircon in emplacement borders of post-collisional plutons compared to country rocks: A study on morphology, internal texture, U–Th–Pb geochronology and Hf isotopes (Araçuaí orogen, SE Brazil) 352–353, 105252. https://doi.org/10.1016/j.lithos.2019.105252
Arena, K.R., Hartmann, L.A., Lana, C. 2016. Evolution of Neoproterozoic ophiolites from the southern Brasiliano Orogen revealed by zircon U-Pb-Hf isotopes and geochemistry. Precambrian Research 285, 299-314.
Arena, K.R., Hartmann, L.A., Lana, C. 2017. Tonian emplacement of ophiolites in the southern Brasiliano Orogen delimited by U-Pb-Hf isotopes of zircon from metasomatites. Gondwana Research 49, 296-332.
Babinski, M., Pedrosa-Soares, A.C., Trindade, R.I.F., Martins, M., Noce, C.M., Liu, D., 2012. Neoproterozoic glacial deposits from the Araçuaí orogen, Brazil: Age, provenance and correlations with the São Francisco craton and West Congo belt. Gondwana Res. 21, 451–465.
Bahlburg, H., Vervoort, J.D., DuFrane, S.A., Carlotto, V., Reimann, C., Cárdenas, J., 2011. The U-Pb and Hf isotope evidence of detrital zircons of the Ordovician Ollantaytambo Formation, southern Peru, and the Ordovician provenance and paleogeography of southern Peru and northern Bolivia. Journal of South American Earth Sciences 32, 196–209.
Basei M.A.S., Frimmel H.E., Campos Neto M..C., de Araujo C.E.G., de Castro N.A., Passarelli C.R. 2018. The Tectonic History of the Southern Adamastor Ocean Based on a Correlation of the Kaoko and Dom Feliciano Belts. In: Siegesmund S., Basei M., Oyhantçabal P., Oriolo S. (eds) Geology of Southwest Gondwana. Regional Geology Reviews. Springer, Cham
Bateman P.C. and Chappell B.W. 1979. Crystallization, fractionation, and solidification of the Tuolumne Intrusive Series, Yosemite National Park, California. Geological Society of America Bulletin, 90: 465-482.
Béchiri-Benmerzoug F., Liégeois J.P., Bonin B., Azzouni-Sekkal A., Bechiri H., Kheloui R., Matukov D.I., Sergeev S.A. 2011. The plutons from the cryogenian Iskel composite oceanic island arc (Hoggar, Tuareg Shield, Algeria): U–Pb on zircon SHRIMP geochronology, geochemistry and geodynamical setting. In: Hutton Symposium on Granites and Related Rocks, 7., 2011, Avila, Spain. Annals..., p. 17.
Berger J., Caby R., Liégeois J.P., Mercier J.C.C., Demaiffe D. 2011. Deep inside a Neoproterozoic intra-oceanic arc: growth, differentiation and exhumation of the Amalaoulaou complex (Gourma, Mali). American Mineralogist, 162:773-796. https://doi.org/10.1007/s00410-011-0624-5
Becker, T., Schreiber, U., Kampunzu, A.B., Armstrong, R., 2006. Mesoproterozoic rocksof Namibia and their plate tectonic setting. J. Afr. Earth Sci. 46, 112–140.
Belém, J., Pedrosa-Soares, A.C., Noce, C.M., da Silva, L.C., Armstrong, R., Fleck, A., Gradim, C.T., Queiroga, G.N., 2011. Bacia precursora versus bacias orogênicas: exemplos do Grupo Andrelândia com base em datações U-Pb (LA-ICP-MS) em zircão e analises litoquímicas. Geonomos 19, 224–243.
Bitencourt, C.N., Cruz, S.C.P., dos Anjos Cruz, V., Pedrosa-Soares, A.C., Paquette, J.L., Alkmim, A.R., Barbosa, J.S.F., 2019. Rifting events in the southern sector of the Paramirim Aulacogen, NE Brazil: new geochronological data and correlations for the São Francisco – Congo paleocontinent. Precambr. Res. 326, 417–446.
Bhatia, M.R., 1983. Plate tectonics and geochemical composition of sandstones. J. Geol. 91, 611–627.
Bhatia, M.R., Crook, K.A.W., 1986. Trace element characteristics of graywackes and tectonic setting discrimination of sedimentary basins. Contrib. Mineral. Petrol. 92, 181–193.
Black, L.P., Gulson, B.L., 1978. The age of the Mud Tank Carbonatite, Strangways range, Northern Territory. BMR J. Aust. Geol. Geophys. 3, 227–232.
Black, L.P., Kamo, S.L., Allen, C.M., Aleinikoff, J.N., Davis, D.W., Korsch, R.J., Foudoulis, C.,

2003. TEMORA 1: a new zircon standard for Phanerozoic U-Pb geochronology. Chem. Geol. 200, 155–170.

Black, L.P., Kamo, S.L., Allen, C.M., Davis, D.W., Aleinikoff, J.N., Valley, J.W., Mundil, R., Campbell, I.H., Korsch, R.J., Williams, I.S., Foudoulis, C. 2004. Improved Pb-206/U-218 microprobe geochronology by the monitoring of a trace-element-related matrix effect; SHRIMP, ID-TIMS, ELA-ICP-MS and oxygen isotope documentation for a series of zircon standards. Chemical Geology 205, 115-140.

Black, R., Latouche, L., Liégeois, J. P., Caby, R., & Bertrand, J. M. 1994. Pan-African displaced terranes in the Tuareg shield (central Sahara). Geology, 22(7), 641-644.

Boullier A.M., Rocci G., Cosson Y. 1991. La chaîne pan-africaine d'Aouzegueur en Aïr (Niger): un trait majeur du bouclier touareg. Comptes Rendus de l'Académie des Sciences de Paris, 313(2):63-68.

Bousquet R., El Mamoun R., Saddiqi O., Goffé B., Möller A., Madi A. 2008. Mélanges and Ophiolites during the Pan-African Orogeny: the Case of the Bou-Azzer Ophiolite Suite (Morocco). In: Ennih N., Liégeois J.-P. (Eds.). The Boundaries of the West African Craton. London, Geological Society, Special Publications, 297:233-247. https://doi.org/10.1144/SP297.11

Bouvier, A., Vervoort, J.D., Patchett, P.J., 2008. The Lu-Hf and Sm-Nd isotopic composition of CHUR: constraints from unequilibrated chondrites and implications for the bulk composition of terrestrial planets. Earth Planet. Sci. Lett. 273 (1-2), 48-57.

Briqueu L, Bougault H. and Joron J. L. (1984) Quantification of Nb, Ta, Ti and V anomalies in magrnas associated with subduction zones-petrogenetic implications. Earth Planet. Sci. Lerr. 68, 297-308.

Brito-Neves, B.B., Campos-Neto, M.C., Fuck, R.A. 1999. From Rodinia to western Gondwana: an approach to the Brasiliano-Pan African cycle and orogenic collage. Episodes 22, 155.

Brito Neves B.B., Fuck R.A., Pimentel M.M. 2014. The Brasiliano collage in South America: a review. Brazilian Journal of Geology, 44(3): 493-518.

Brown G.C., Thorpe R.S. & Webb P.C. 1984. The geochemical characteristics of granitoids in contrasting arcs and comments on magma sources. Journal of the Geological Society. London. 141: 413-426.

Brown, M. 2009. Metamorphic patterns in orogenic systems and the geological record. In: Cawood, P.A. and Kröner, A. 2009 (eds), Earth accretionary systems in space and time. Geological Society, Special Publication 318, DOI (10.1144/SP318.2).

Brown M.T., Fuck R.A., Dantas E.L. 2020. Isotopic age constraints and geochemical results of disseminated ophiolitic assemblage from Neoproterozoic mélange, Central Brazil. Precambrian Research. doi: https://doi.org/10.1016/j.precamres.2019.105581

Brown, M. 2014. The contribution of metamorphic petrology to understanding lithosphere evolution and geodynamics. Geoscience Frontiers, 5(4), 553–569. doi:10.1016/j.gsf.2014.02.005

Brueckner, H. K., Cunningham, D., Alkmim, F. F., & Marshak, S., 2000. Tectonic implications of Precambrian Sm–Nd dates from the southern Sao Francisco craton and adjacent Araçuaı and Ribeira belts, Brazil. Precambrian Research, 99(3-4), 255-269.

Bühn, B., Pimentel, M.M., Matteini, M., Dantas, E.L., 2009. High spatial resolution analysis of Pb and U isotopes for geochronology by laser ablation multi-collector inductively coupled plasma mass spectrometry (LA-MC-IC-MS). Anais da Academia Brasileira de Ciências. 81 (1), 1–16.

Caby R., Andreopoulos-Renaud U., Gravelle M. 1982. Cadre géologique et géochronologie U/Pb sur zircon des batholites précoces dans le segment pan-africain du Hoggar central (Algérie). Bulletin de la Société Géologique de France, 24:677-684.

Caby R. 2003. Terrane assembly and geodynamic evolution of centralwestern Hoggar: a synthesis. Journal of African Earth Sciences, 37(3):133-159. https://doi.org/10.1016/j.jafrearsci.2003.05.003

Calegari, S.S., Neves, M., A., Guadagnin, F., França, G., S., Vincentelli, M., G., C. 2016. The Alegre Lineament and its role over the tectonic evolution of the Campos Basin and adjacent continental margin, Southeastern Brazil. Journal of South American Earth

Sciences. (69) 226-242.
Castro, M.P., Queiroga, G., Martins, M., Alkmim, F., Pedrosa-Soares, A., Dussin, I., Souza, M.E., 2019. An Early Tonian rifting event affecting the São Francisco-Congo paleocontinent recorded by the Lower Macaúbas Group, Araçuaí Orogen, SE Brazil. Precambr. Res. 331.
Campos Neto, M.C. & Figueiredo, M. Evolução geológica dos terrenos Costeiro, Paraíba do Sul e Juiz de Fora. In: Cong. Bras. Geol, XXXVI, Natal, 1990, Natal, RN, SBG. v.6. p 2631-2648, 1990.
Campos Neto, M.C. & Figueiredo, M.C.H. (1995). The Rio Doce orogeny, Southeastern Brazil, Journal of South American Earth Sciences. (v. 8) n. 2, p. 143-162.
Campos Neto, M.C. (2000). Orogenic systems from southwestern Gondwana: an approach to Brasiliano – Pan-African cycle and orogenic collage in southeastern Brazil. In: Cordani, U.G., Milani, E.J., Thomaz-Filho, A., Campos, D.A. (Eds.), Tectonic Evolution of South America, Rio de Janeiro, 31st International Geological Congress, pp. 335–365.
Chappell, B., Colleen, B., Wyborn, D. 2012. Peraluminous I-type granites. Lithos, 153:142-153.
Chrispim, S. & Tupinambá, M.A. Observações sobre o caráter transpressivo da deformação entre as zonas de cisalhamento do Paraíba do Sul (RJ) e Guaçuí (ES). In: Simpósio de Geologia do Sudeste, I, Anais Rio de Janeiro, SBG/RJ, 1989.
Caputo Neto, V., Ribeiro, A., Nepomuceno, F. O., Dussin, I. A., & Trouw, R. A. J. 2018. The Pico do Itapeva Formation: A record of gravitational flow deposits in an Ediacaran intracontinental basin, southern Brasília Orogen, SE Brazil. Journal of South American Earth Sciences, 84, 34–47. doi: 10.1016/j.jsames.2018.03.006
Caxito F.A., Uhlein A., Stevenson R., Uhlein G.J. 2014b. Neoproterozoic oceanic crust remnants in northeast Brazil. Geology, 42:387-390.
Caxito, F.A., Santos, L.C.M.L., Ganade, C.E., Bendaoud, A., Fettous, E.H., Bouyo Houketchang, M., 2020. Towards an integrated model of geological evolution for NE Brazil–NW Africa: The Borborema Province and its connections to the Trans-Saharan (Benino-Nigerian and Tuareg shields) and Central African orogens. Brazilian Journal of Geology. 50(2): e20190122. DOI: 10.1590/2317-4889202020190122
Caxito, F.A.; Heilbron, M. ; Valeriano, C.M. ; Bruno, H. ; Pedrosa-Soares, A. ; Alkmim, F.F. ; Chemale, F. ; Hartmann, L.A. ; Dantas, E. ; Basei, M.A.S. 2021. Integration of elemental and isotope data supports a Neoproterozoic Adamastor Ocean realm. Geochemical Perspectives Letters, v. 17, p. 6-10. doi: 10.7185/geochemlet.2106.
Cerva-Alves, T., Hartmann, L. A., Remus, M. V. D., & Lana, C. 2020. Integrated ophiolite and arc evolution, southern Brasiliano Orogen. Precambrian Research, 105648. doi:10.1016/j.precamres.2020.105648
Chemale Jr. F. 2000. Evolução Geológica do Escudo Sul-RioGrandense. In: Holz M., De Ros L.F. (eds.) Geologia do Rio Grande do Sul. Editora UFRGS, Porto Alegre, p. 13-52.
Cawood, P., Kroner, A., Pisarevsky, S., 2006. Precambrian plate tectonics: criteria and evidence. GSA Today 16 (7), 4–11. http://dx.doi.org/10.1130/GSAT01607.1
Cawood, P.A., Kröner, A. (eds) 2009. Earth accretionary systems in space and time. Geological Society, London, Special Publications, 318 (DOI: 10.1144/SP318).
Cawood, P.A., Hawkesworth, C.J., Dhuime, B., 2012. Detrital zircon record and tectonic setting. Geology 40 (10), 875–878.
Condie, K.C., 2007. Accretionary orogens in space and time. In: Hatcher, R.D., Carlson, M.P., McBride, J H., Catalán, J.R. (eds), 4-D Framework of Continental Crust. Geological Society of America, Memoirs, 200, 1–14.
Cordani U.G., Amaral G., Kawashita K. 1973. The Precambrian evolution of South America. Geologische Rundschau, 62:309-317.
Cordani, U.G., D'Agrella-Filho, M.S., Brito-Neves, B.B., Trindade, R.I.F., 2003. Tearing up Rodinia: the Neoproterozoic paleogeography of South American cratonic fragments. Terra Nova 15, 350-359.
Corrales F.F.P., Dussin I.A., Heilbron M., Bruno H., Bersan S.A., Valeriano C.M., Pedrosa-Soares A.C., Tedeschi M. 2020. Coeval high Ba-Sr arc-related and OIB Neoproterozoic

rocks linking pre-collisional magmatism of the Ribeira and Araçuaí orogenic belts, SE-Brazil, Precambrian Research, doi: https://doi.org/ 10.1016/j.precamres.2019.105476.

Cunningham, D.; Alkmim, F.F. & Marshak, S. 1998. A structural transect across the coastal mobile belt in the Brazilian Highlands (latitude 20°S): the roots of a Precambrian transpressional orogen. Precambrian Research, 92(3): 251-275.

D'Agrella-Filho, M.S., Cordani, U.G., 2017. The Paleomagnetic Record of the São Francisco-Congo Craton. In: M. Heilbron et al. (eds.), São Francisco Craton, Eastern Brazil, Regional Geology Reviews, DOI 10.1007/978-3-319-01715-0_16

De Campos, C.P., Mendes, J.C., Ludka, I.P., Medeiros, S.R., Moura, J.C., Wallfass, C., 2004. A review of the Brasilian magmatism in southern Espírito Santo, Brazil, with emphasis on postcollisional magmatism. Journal of the Virtual Explorer 17, 1-35.

De Campos, C.P, Medeiros, S.R., Mendes, J.C, Pedrosa-Soares, A.C., Dussin, I., Ludka, I.P., Dantas, E.L., 2016. Cambro-Ordovician magmatism in the Araçuaí Belt (SE Brazil): Snapshots from a post-collisional event. Journal of South American Earth Sciences 68, 248-268.

Decol, J, Heilbron, M, Peixoto, C, Bruno, H, Bersan, S.M, Rodrigues, S. W. O, Corrales, F, Eirado, F. G, Tupinambá, M. 2021. Adakites and associated granitoids from the Serra da Prata Arc: Evidence for a Tonian subduction setting within the Araçuaí-Ribeira orogenic system (AROS), SE Brazil. Journal of South American Earth Sciences. V111 - 103481

Degler, R., Pedrosa-Soares, A.C., Dussin, I., Queiroga, G., Schulz, B., 2017. Contrasting provenance and timing of metamorphism from paragneisses of the Araçuaí-Ribeira Orogenic System, Brazil: Hints for Western Gondwana assembly. Gondwana Research, 51:30–50.

Degler, R., Pedrosa-Soares, A., Novo, T., Tedeschi, M., Silva, L. C., Dussin, I., & Lana, C. 2018. Rhyacian-Orosirian isotopic records from the basement of the Araçuaí-Ribeira orogenic system (SE Brazil): Links in the Congo-São Francisco palaeocontinent. Precambrian Research. doi:10.1016/j.precamres.2018.08.018

De La Roche, H., Leterrier, J., Grande Claude, P., Marchal, M. 1980. A classification of volcanic and plutonics rocks using R1-R2 diagrams and major element analyses - its relationships and current nomenclature. Chemical Geology, n. 29, p. 183-21.

DePaolo, D.J., 1981. Neodymium isotopes in the Colorado front range and crust-mantle evolution in the Proterozoic. Nature 291, 193-196.

De Toni, G.B., Bitencourt, M.F., Nardi, L.V.S., Florisbal, L.M., Almeida. B.S., Geraldes, M. 2020. Dom Feliciano Belt orogenic cycle tracked by its pre-collisional magmatism: The Tonian (ca. 800 Ma) Porto Belo Complex and its correlations in southern Brazil and Uruguay. Precambrian Research 342, 105702. https://doi.org/10.1016/j.precamres.2020.105702

Dickin, A.P. 2005. Radiogenic Isotope Geology. Cambridge University Press. 2nd ed. 488 p.

Ebert, H.D.; Hasui, Y.; Sartorato, G.; Almeida, S.H.; Costa, J.B.S. Arcabouço estrutural e tectônica transpressiva das faixas móveis das bordas sul a sudeste do Cráton de São Francisco e da Sintaxe de Guaxupé. In: IV Simp. Nac. de Estudos Tectônicos, 4, Salvador, p. 166-170, 1993.

Erikson, P.G., Martins-Neto, M.A., Nelson, D.R., Aspler, L.B., Chiarenzelli, J.R.,Catuneanu, O., Sarkar, S., Altermann, W., Rautenbach, C.J.W., 2001. An intro-duction to Precambrian basins: their characteristic and genesis. Sediment. Geol.141–142, 1–35.

Ernst, R.E., Pereira, E., Hamilton, M.A., Pisarevsky, S.A., Rodrigues, J., Tassinari, C.C.G.,Teixeira, W., Dunem, V.-V., 2013. Mesoproterozoic intraplate magmatic 'bar-code' record of the Angola portion of the Congo Craton: newly dated magmaticevents at 1505 and 1110 Ma and implications for Nuna (Columbia) superconti-nent reconstructions. Precambrian Res. 230, 103–118.

Evans, D., Trindade, R., Catelani, E., D'Agrella-Filho, M.S., Heaman, L.M., Oliveira, E.P., Söderlund U., Ernst, R.E., Smirnov, A.V. Salminen, J.M., 2015. Return to Rodinia? Moderate to high paleolatitude of the Sao Francisco-Congo craton at 920 Ma. In: Li, Z.X., Evans, D.A.D., Murphy, J.B. (Eds.), Supercontinent Cycles through Earth History.

Geological Society of London, London, Special Publication, 424, 167–190.
Faccenda, M., Gerya, T. V., & Chakraborty, S. (2008). Styles of post-subduction collisional orogeny: Influence of convergence velocity, crustal rheology and radiogenic heat production. Lithos, 103(1-2), 257-287
Fedo, C.M., Sicombe, K.N., Rainbird, R.H., 2003. Detrital zircon analysis of thesedimentary record. In: Hanchar, J.M., Hoskin, P.W.O. (Eds.), Zircon, vol. 53. Mineralogical Society of America Reviews in Mineralogy & Geochemistry, pp.277–303.
Fernandes, G.L.F., Schmitt, R.S, Bongiolo, E.M., Basei, M.A.S, Mendes, J.C., 2015. Unraveling the tectonic evolution of a Neoproterozoic–Cambrian active margin in the Ribeira Orogen (Se Brazil): U–Pb and Lu–Hf provenance data. Precambrian Research 266 (2015) 337–360
Fralick, P.W., Hollings, P., Metsaranta, R., Heaman, L.M., 2009. Using sediment geochemistry and detrital zircon geochronology to categorize eroded igneous units: an example from the Mesoarchean Birch-Uchi Greenstone Belt, Superior Province. Precambrian Research 168, 106–122.
Frimmel, H. E., Basei, M. S., & Gaucher, C. 2011. Neoproterozoic geodynamic evolution of SW-Gondwana: a southern African perspective. International Journal of Earth Sciences, 100(2-3), 323–354. doi:10.1007/s00531-010-0571-9
Frost, B. R., Barnes, C. G., Collins, W. J., Arculus, R. J., Ellis, D. J. & Frost, C. D. 2001. A geochemical classification for granitic rocks. Journal of Petrology 42: 2033–2048.
Fuck R.A., Pimentel M.M., Alvarenga C.J., Dantas E.L. 2017. The northern Brasília belt. In: Heilbron M., Cordani U.G., Alkmim F.F. (Eds.). São Francisco Craton, Eastern Brazil. Cham: Springer, p. 205-220.
Ganade de Araújo C.E., Pinéo T.R.G., Caby R., Costa F.G., Cavalcante J.C., Vasconcelos A.M., Rodrigues J.B. 2010. Provenance of the Novo Oriente Group, southwestern Ceará Central Domain, Borborema Province (NEBrazil): A dismembered segment of a magma-poor passive margin or a restricted rift-related basin? Gondwana Research, 18(2-3):497-513. https:// doi.org/10.1016/j.gr.2010.02.001
Ganade de Araújo C.E., Cordani U.G., Weinberg R.F., Basei M.A.S., Armstrong R., Sato K. 2014a. Tracing Neoproterozoic subduction in the Borborema Province (NE Brazil): clues from U-Pb geochronology and Sr- Nd-Hf-O isotopes on granitoids and migmatites. Lithos, 202-203:167-189. https://doi.org/10.1016/j.lithos.2014.05.015.
Gerdes, A., Zeh, A., 2006. Combined U-Pb and Hf isotope LA-(MC)ICP-MS analyses of detrital zircons: comparison with SHRIMP and new constraints for the provenance and age of an Armorican metasediment in Central Germany. Earth Planet. Sci. Lett. 249, 47–61.
Gerdes, A., Zeh, A., 2009. Zircon formation versus zircon alteration – new insights from combined U-Pb and Lu–Hf in situ LA-ICP-MS analyses, and consequences for the interpretation of Archean zircon from the Limpopo Belt. Chem. Geol. 261, 230–243.
Gill R. 2010. Igneous rocks and processes: a practical guide. New Jersey, Wiley-Blackwell.
Gioia, S.M.C.L., Pimentel, M.M., 2000. The Sm–Nd isotopic method in the Geochronology Laboratory of the University of Brasília. Anais da Academia Brasileira de Ciências. 72 (2), 219–245.
Gonçalves, L., Alkmim, F.F., Pedrosa-Soares, A.C., Dussin, I., Valeriano, C., Lana, C., Tedeschi, M., 2016. Granites of the intracontinental termination of a magmatic arc: an example from the Ediacaran Araçuaí orogen, southeastern Brazil. Gondwana Res. 36, 439–459.
Goncalves, L., Alkmim, F.F., Pedrosa, A., Goncalves, C.C., Vieira, V., 2017. From the plutonic root to the volcanic roof of a continental magmatic arc: a review of the Neoproterozoic Aracuai orogen, southeastern Brazil. Int. J. Earth Sci. 107, 337–358.
Gonçalves-Dias, T., Caxito, F.A., Pedrosa-Soares, A.C., Stevenson, R., Dussin, I., Silva, L. C., Alkmim, F.F., Pimentel, M., 2016. Age, provenance and tectonic setting of the high-grade Jequitinhonha Complex, Araçuaí Orogen, eastern Brazil. Braz. J. Genet. 46 (2), 199–219.
Gradim, C., Roncato, J., Pedrosa-Soares, A.C., Cordani, U., Dussin, I., Alkmim, F.F., Queiroga, G., Jacobsohn, T., Silva, L.C., Babinski, M., 2014. The hot back-arc zone of

the Araçuaí Orogen, Eastern Brazil: from sedimentation to granite generation. Brazilian Journal of Geology 44, 155-180.

Griffin, W.L., Pearson,N.J., Belousova, E., Jackson, S.E., van Achterbergh, E.,O'Reilly, S.Y., Shee, S.R., 2000. The Hf isotope composition of cratonicmantle: LAM-MC-ICPMS analysis of zircon megacrysts in kimberlites. Geochimica et Cosmochimica Acta 64, 133–147.

Griffin, W.L., Belousova, E.A., Shee, S.R., Pearson, N.J., O'Reilly, S.Y., 2004. Archeancrustal evolution in the northern Yilgarn Craton: U–Pb and Hf isotope evidencefrom detrital zircons. Precambrian Res. 131, 231–282.

Hackspacher, P.C., Fetter, A.H., Ebert, H.D., Janasi, V.A., Dantas, E.L., Oliveira, M.A.F., Braga, I.F., Negri, F.A. 2003. Magmatismo há ca. 660-640 Ma no Domínio Socorro: registros de convergência pré-colisional na aglutinação do Gondwana Ocidental. Geologia USP. Série Científica 3, 85-96.

Hartmann L.A., Philipp R.P., Santos J.O.S., McNaughton N.J. 2011. Time frame of 753-680 Ma juvenile accretion during the São Gabriel orogeny, southern Brazil. Gondwana Research, 19:84-99.

Hartmann L.A., Werle M., Michelin C.R.L., Lana C., Queiroga G.N., Castro M.P., Arena K. R. 2019. Proto-Adamastor ocean crust (920 Ma) described in Brasiliano Orogen from coetaneous zircon and tourmaline. Geoscience Frontiers, 10: 1623 – 1633.

Haughton, P.D.W., Todd, S.P., Morton, A.C., 1991. Sedimentary provenance studies. In: Morton, A.C., Todd, S.P., Haughton, P.D.W. (Eds.), Developments in Sedimentary Provenance Studies. Geological Society Special Publication, 57, pp. 1–11.

Hefferan K.P., Admou H., Hilal R., Karson J.A., Saquaque A., Juteau T., Bohn M.M., Samson S.D., Kornprobst J.M. 2002. Proterozoic blueschist-bearing mélange in the Anti-Atlas Mountains, Morocco. Precambrian Research, 118(3-4):179-194. https://doi.org/10.1016/S0301-9268(02)00109-2

Heilbron M., Simoes L.S.A., Alves R.P., Chrispim S.J. 1982. Geologia do Cabo dos Buzios. Anais da Academia Brasileira de Ciencias, Rio de Janeiro, 54: 553–562

Heilbron, M., Mohriak, W., Valeriano, C.M., Milani, E., Almeida, J.C.H., Tupinambá,M. 2000. From collision to extension: the roots of the South-eastern continen-tal margin of Brazil. In: Talwani, Mohriak (Eds.), Atlantic Rifts and ContinentalMargin. AGU Geophysical Monograph Series, vol. 115, 354 pp.

Heilbron, M., Machado, N., 2003. Timing of terrane accretion in the Neoproterozoic-Eopaleozoic Ribeira Orogen (SE Brazil). Precambr. Res. 125, 87–112.

Heilbron, M.L., Pedrosa-Soares, A.C., Campos Neto, M.C., Silva, L.C., Trouw, R. and Janasi, V.A., 2004. Brasiliano Orogens in Southeast and South Brazil. Journal of the Virtual Explorer 17, Paper 4.

Heilbron, M., Valeriano, C., Tassinari, C.C.G., Almeida, J.C.H., Tupinambá, M., Siga, O., Trouw, R., 2008. Correlation of Neoproterozoic terranes between the Ribeira Belt, SE Brazil and its African counterpart: comparative tectonic evolution and open questions. Geol. Soc., London, Spec. Publ. 294, 211–237.

Heilbron, M., Almeida, J.C.H., Silva, L.G.E., Tupinambá, M., Valente, S., Duarte, B. P., Corval, A., Guedes, E., Valeriano, C., Schmitt, R., Valladares, C., Ragatky, D., Geraldes, M., Peixoto, C.A. Arcabouço Regional. In Heilbron, M. Geologia e Recursos Minerais da Folha santo Antônio de Pádua. In: Monica Heilbron. (Org.). Geologia e Recursos Minerais da Folha Santo Antônio de Pádua-SF.26-X-D-VI, escala de 1:100.000. 1ed.Belo Horizonte: CPRM, 2012, v. 1, p. 22-36.

Heilbron, M., Tupinambá, M., Valeriano, C., Armstrong, R., Silva, L.G.E., Melo, R.S., Simonetti, A., Pedrosa Soares, A.C., Machado, N. 2013. The Serra da Bolívia complex: the record of a new Neoproterozoic arc-related unit at Ribeira belt. Precambr. Res. 238, 158–175.

Heilbron, M., do Eirado, L.G., Almeida, J., 2016. Geologia e Recursos Minerais do Estado do Rio de Janeiro: texto explicativo do mapa geológico e de recursos minerais. Belo Horizonte, CPRM, 2016. In: 01 mapa geológico, escala 1:400.000 e 01 mapa de recursos minerais, escala 1:400.000 (Série Programa de Geologia do Brasil, PGB, Coleção Mapas Geológicos Estaduais) versão em DVD, p. 182.

Heilbron, M., Ribeiro, A., Valeriano, C. M., Paciullo F., Almeida, J. C. H., Trouw, R., Tupinambá, M., Silva, L. G. E. 2017. The Ribeira belt. In: Heilnron, M., Cordani, U., Alkmim, F.F. (Org.). São Francisco Craton, Eastern Brazil Tectonic Genealogy of a Miniature Continent. 1ed.Cham: Springer, v. '1, p. 277-304.

Heilbron, M., Silva, L.G.E., Almeida, J.C.H., Tupinambá, M., Peixoto, C., Valeriano, C.M., Lobato, M., Rodrigues S.W.O., Ragatky, C.D, Silva, M.A., Monteiro, T., Freitas, N.C, Miguens, D., Girão R. 2020a. Proterozoic to Ordovician geology and tectonic evolution of Rio de Janeiro State, SE-Brazil: insights on the central Ribeira Orogen from the new 1:400,000 scale geologic map. Brazilian Journal of Geology. 50(2): e20190099. doi: 10.1590/2317-4889202020190099

Heilbron, M., de Morisson Valeriano, C., Peixoto, C., Tupinambá, M., Neubauer, F., Dussin, I., ... & do Eirado Silva, L. G., 2020b. Neoproterozoic magmatic arc systems of the central Ribeira belt, SE-Brazil, in the context of the West-Gondwana pre-collisional history: A review. Journal of South American Earth Sciences, 102710.

Horn, A., 2006. Folha Espera Feliz, SF.24-V-A-IV, escala 1:100.000. CPRM – Brazilian Geological Survey.

Hoskin, P.W.O., Schaltegger, U. 2003. The composition of zircon and igneous and metamorphic petrogenesis. In: Hanchar, J.M., Hoskin, P.W.O. (Eds.), Zircon. Reviews in Mineralogy and Geochemistry, pp. 27–62.

Howell, D.G. 1995. Principles of terrane analysis. Topics in Earth Sciences, vol. 8.

Irvine, T.N., Baragar, W.R.A., 1971. A guide to the chemical classification of the common volcanic rocks. Can. J. Earth Sci. 8, 523–548.

Jackson, S.E., Pearson, N.J., Griffin, W.L., Belousova, E.A., 2004. The application of laser ablation-inductively coupled plasma-mass spectrometry to in situ U–Pb zircon geochronology. Chemical Geology. 211(1-2), 47-69. https://doi.org/10.1016/j.chemgeo.2004.06.017

Janasi, V.A., Ulbrich, H.H.G.J. 1991. Late Proterozoic granitoid magmatism in the state of São Paulo, southeastern Brazil. Precambrian Research 51 (1), 351-374.

Johannsen A. 1931. A descriptive petrography of the igneous rocks. Geologiska Föreningen i Stockholm Förhandlingar. v. 1.

Kröner, S., Konopásek, J., Kröner, A., Passchier, C.W., Poller, U., Wingate, M.T.D., Hof-mann, K.H., 2004. U–Pb and Pb-Pb zircon ages for metamorphic rocks in theKaoko Belt of Northwestern Namibia: a Palaeo- to Mesoproterozoic basementreworked during the Pan-African orogeny. S. Afr. J. Geol. 7, 455–476.

Kroonenberg, S.B., 1994. Effect of provenance, sorting and weathering on the geochemistry of fluvial sands from different tectonic and climatic environments. Proceedings of the 29th International Geological Congress, Part A, 69–81.

Kuchenbecker, M., Pedrosa-Soares, A.C., Babinski, M., Fanning, M., 2015. Detrital zircon age patterns and provenance assessment for pre-glacial to post-glacial successions of the Neoproterozoic Macaúbas Group, Araçuaí Orogen, Brazil. Precambr. Res. 266, 12–26.

Laux J.H., Pimentel M.M., Dantas E.L., Armstrong R., Junges S.L. 2005. Two Neoproterozoic crustal accretion events in the Brasília Belt, central Brazil. Journal of South American Earth Sciences, 18:183-198.

Liégeois J.P., Black R., Navez J., Latouche L. 1994. Early and late Pan-African orogenies in the Aïr assembly of terranes (Tuareg shield, Niger). Precambrian Research, 67(1-2):59-88. https://doi.org/10.1016/0301-9268(94)90005-1

Liégeois, J. P., Latouche, L., Boughrara, M., Navez, J., & Guiraud, M. 2003. The LATEA metacraton (Central Hoggar, Tuareg shield, Algeria): behaviour of an old passive margin during the Pan-African orogeny. Journal of African Earth Sciences, 37(3-4), 161-190.

Liégeois J.P. 2019. A New Synthetic Geological Map of the Tuareg Shield: An Overview of Its Global Structure and Geological Evolution. In: Bendaoud A., Hamimi Z., Hamoudi M., Djemai S., Zoheir B. (Eds.). The Geology of the Arab World - An Overview. Berlin: Springer Geology, p. 83-107.

Lobato, M., Heilbron, M., Torós, B., Ragatky, D., & Dantas, E. 2015. Provenance of the Neoproterozoic high-grade metasedimentary rocks of the arc-related Oriental Terrane of

the Ribeira belt: Implications for Gondwana amalgamation. Journal of South American Earth Sciences, 63, 260–278. doi:10.1016/j.jsames.2015.07.019.

Lourenço, F.S.; Alkmim, F.F.; Araújo, M.N.C.; Romeiro, M.A.T.; Matos, G.C. & Crósta, A.P. 2016. The Piúma lineament, southern Espírito Santo: structural expression and tectonic significance. Brazilian Journal of Geology, 46(4): 531-546.

Ludwig, K.R., 2008. User's manual for Isoplot 3.6. A geochronological toolkit for Microsoft Excel. Special Publication, No. 4. Berkeley Geochronologic Center, Berkeley, USA.

Ludwig, K., 2009. SQUID 2: A User's Manual, rev. 12 Apr, 2009. Berkeley Geochron. Ctr. Spec. Pub. 5 110 p.

Machado, N.; Schrank, A.; Abreu, F.R.; de; Knauer, L.G.; Almeida-Abreu, P.A. 1989. Resultados preliminares da geocronologia U/Pb na Serra do Espinhaço Meridional. In: SBG, Simp. Geol. Minas Gerais, 5, Belo Horizonte, Anais, 171 –174.

Machado N., Valladares C., Heilbron M., Valeriano, C. 1996. U-Pb geochronology of the Central Ribeira Belt (Brazil) and implications for the evolution of the Brazilian Orogeny. Precambrian Res., (79) 347-361.

Machado Filho, L., Ribeiro, M.W., Gonzalez, S.R., Schemini, C.A., Santos Neto, A.S., Palmeira, R.C.B., Pires, I.L., Teixeira, W., Castro, H.F. Folhas SF 23/24 Rio de Janeiro e Vitória. 1983; Geologia. RADAMBRASIL, vol 32.

Machado, H.T., Valladares C., Valeriano, C., Medeiros, S., Duarte, B., 2010. Orthogneisses of the Quirino Complex, Central Ribeira belt, Se Brazil: Sr and Nd isotopic data. 2010. In: VII South American Symposium on Isotope Geology, Brasília, 25th–28th July 2010.

Martins, G.G., Mendes, J.C., Schmitt, R.S., Armstrong, R., Valeriano, C.M. 2016. 550–490 Ma pre-to post-collisional shoshonitic rocks in the Ribeira Belt (SE Brazil) and their tectonic significance. Precambrian Research 286: 352-369.

Martins, M., Babinski, M., Noce, C. M., Queiroga, G. N., Pedrosa-Soares, A. C., & Liu, D. 2011. A Suíte Córrego Taquari no Anticlinal de Itacambira, Bacia do Rio Macaúbas (MG): magmatismo básico tardi-ediacarano (ca. 560 Ma) no domínio externo do Orógeno Araçuaí. Geonomos, 19:2, 78-89.

Menezes S.O. As rochas Carbonáticas de Cantagalo-RJ. Mineração e Metalurgia. 1975, 39: 26-29.

McLennan S.M., Taylor S.R., McCulloch M.T., Maynard J.B. 1990. Geochemical and Nd-Sr isotopic composition of deep-sea turbidites: Crustal evolution and plate tectonic associations. Geochimica et Cosmochimica Acta, 54:2015-2050.

McMillan N. J., Harmon R. S., Moorbath S., Lopez-Escobar L., and Strong D. F. 1989. Crustal sources involved in continental arc magmatism: A case study of volcan Mocha-Choshuence, southern Chile. Geology 17, I 152-I 156.

Melo, M.G., Lana, C., Stevens, G., Pedrosa-Soares, A.C., Gerdes, A., Alkmin, L.A., Nalini Jr., H.A., Alkmim, F.F., 2017. Assessing the isotopic evolution of S-type granites of the Carlos Chagas batholith, SE Brazil: clues from U-Pb, Hf isotopes, Ti geothermometry and trace element composition of zircon. Lithos 284e285, 730e750.

Meneghini, F., Fagereng, A., & Kisters, A. (2017). The Matchless Amphibolite of the Damara belt, Namibia: unique preservation of a late Neoproterozoic ophiolitic suture. Ofioliti, 42(2), 129-145. Meneghini, F., Kisters, A., Buick, I., & Fagereng, Å. (2014). Fingerprints of late Neoproterozoic ridge subduction in the Pan-African Damara belt, Namibia. Geology, 42(10), 903-906.

Merdith, A. S., Collins, A. S., Williams, S. E., Pisarevsky, S., Foden, J. D., Archibald, D. B., Blades, M. L., Alessio, B. L., Armistead, S., Plavsa, D., Clark, C., and Müller, R. D., 2017. A full-plate global reconstruction of the Neoproterozoic: Gondwana Research, v. 50, p. 84-134.

Miyashiro, A., 1974. Volcanic rock series in island arcs and active continental margins. Am. J. Sci. 274, 321–355.

Moraes, J.M. Caracterização geoquímica dos ortoanfibolitos de Grupo Italva, Setor Central da Faixa Ribeira. Rio de Janeiro: Uerj; Monografia Final de Graduação, 2006.

Moraes R., Nicollet C., Barbosa J.H.F., Fuck R.A., Sampaio A.R. 2015. Applications and limitations of thermobarometry in migmatites and granulites using as an example rocks

of the Araçuaí Orogen in southern Bahia, including a discussion on the tectonic meaning of the current results. Brazilian Journal of Geology, 45(4):517-539.

Morel, M.L., Nebel, O., Nebel-Jacobsen, Y.J., Miller, J.S., Vroon, P.Z., 2008. Hf isotope characterization of the GJ-1 zircon reference material by solution and laserablation MC-ICPMS. Chem. Geol. 255, 231-235.

Nalini, H.A. (1997). Caractérisation des suites magmatiques néoprotérozoïques de la région de Conselheiro Pena et Galiléia (Minas Gerais, Brésil):étude géochimique et structurale dês suites Galiléia et Urucum et leur relation avec les pegmatites à éléments rares associées. École des Mines de Saint-Étienne et École des Mines de Paris, Thèse.

Nalini-Junior, H.A., Bilal, E., Paquette, J.L., Pin, C., Machado, R., 2000. Geochronolo-gie U–Pb et géochimie isotopique Sr–Nd des granitoides neoproterozoiques dessuites Galiléia et Urucum, vallée du Rio Doce, Sud-Est du Brésil. Compte RenduAcademie Science Paris 331, 459–466.

Nalini-Junior, H.A., Machado, R.M., Bilal, E., 2005. Geoquímica e petrogênese da SuíteGaliléia: exemplo de magmatismo tipo-I, metaluminoso, pré-colisional, neoproterozóico da região do Médio Vale do Rio Doce. Revista Brasileira de Geociências35 (4), 23–34.

Neves, A.C. Análise Estrutural do Contato Tectônico Central da Faixa Ribeira, entre os Municípios de Japeri e Paraty, RJ. 2004. 110p. Dissertação de Mestrado. PPGABFM-UERJ, 2004.

Nkoumbou, C., Goune, C. Y., Villiéras, F., Njopwouo, D., Yvon, J., Ekodeck, G. E., & Tchoua, F. 2006. Découverte des roches à affinité ophiolitique dans la chaîne panafricaine au Cameroun: les talcschistes de Ngoung, Lamal Pougue et Bibodi Lamal. Comptes Rendus Geoscience, 338(16), 1167-1175.

Nkoumbou, C., Njopwouo, D., Villiéras, F., Njoya, A., Yonta Ngouné, C., Ngo Ndjock, L., Tchoua, F.M., Yvon, J. 2006. Talc indices from Boumnyebel (Central Cameroon), physico-chemical characteristics and geochemistry. Journal of African Earth Sciences, 45(1), 61–73. doi:10.1016/j.jafrearsci.2006.01.007.

Noce, C.M., Pedrosa-Soares, A.C., Piuzana, D., Armstrong, R., Laux, J.H., de Campos, C.M., de Medeiros, S.R., 2004. Ages of sedimentation of the kinzigitic complex and a late orogenic thermal episode in the Aracuai orogen, northern Espirito Santo state, Brazil: zircon and monazite U-Pb SHRIMP and ID-TIMS data. Rev. Bras. Geociencias 34, 587–592.

Novais, L.C.C., Teixera, L.B., Neves, M.T., Rodarte, J.B.M., Almeida, J.C.H., Valeriano, C.M. 2004. Novas ocorrências de diques de diabásio na faixa Colatina-ES: estruturas rútpeis associadas e implicações tectônicas para as bacias de Campos e do Espírito Santo. Boletim de Geociências Petrobras 1(2(1)) 191-194

Novo, T., 2013. Caracterização do Complexo Pocrane, magmatismo básico Mesoproterozóico e unidades neoproterozóicas do Sistema Araçuaí-Ribeira, com ênfase em geocronologia U-Pb (SHRIMP e LA-ICP-MS). Tese de Doutorado. Instituto de Geociências, Universidade Federal de Minas Gerais, pp. 177.

Novo, T, Pedrosa-Soares, A.C., Vieira, V.S., Dussin, I, Silva, L.C. 2018. The Rio Doce Group revisited: An Ediacaran arc-related volcano-sedimentary basin, Araçuaí orogen (SE Brazil). Journal Of South American Earth Sciences, v. 85, p. 345-361.

Oliveira, E. P., Toteu, S. F., Araújo, M. N. C., Carvalho, M. J., Nascimento, R. S., Bueno, J. F., McNaughton, N., Basilici, G. 2006. Geologic correlation between the Neoproterozoic Sergipano belt (NE Brazil) and the Yaoundé belt (Cameroon, Africa). Journal of African Earth Sciences, 44(4-5), 470–478. doi:10.1016/j.jafrearsci.2005.11.014.

Pacheco, F. E. R. C., Caxito, F. A., Pedrosa-Soares, A. C., Dussin, I. A., Gonçalves-Dias, T. Detrital zircon U-Pb and Lu-Hf data for a kinzigitic gneiss (Jequitinhonha Complex, Araçuaí Orogen, SE Brazil) constrain the age of a huge storage of Ediacaran carbon. 2Journal of South American Earth Sciences 105(2):102709. https://doi.org/10.1016/j.jsames.2020.102709.

Paciullo, F.V.P., Ribeiro, A., Andreis, R.R., Trouw, R.A.J., 2000. The Andrelândia Basin, a Neoproterozoic intraplate continental margin, southern Brasília belt, Brazil. Revista

Brasileira de Geociencias 30, 200–202.
Paixão M.A.P., Nilson A.A., Dantas E.L. 2008. The Neoproterozoic Quatipuru ophiolite and the Araguaia fold belt, central-northern Brazil, compared with correlatives in NW Africa. In: Pankhurst R.J., Trouw R.A.J., de Brito Neves B.B., de Wit M.J. (Eds.). West Gondwana: Pre-Cenozoic Correlations Across the South Atlantic Region. London: Geological Society, Special Publications, 294(1):297-318. http://dx.doi.org/10.1144/SP294.16
Pankhurst, R.J. and O'Nions, R.K., 1973. Determination of Rb/Sr and 87Sr/86Sr ratios of some standard rocks and evaluation of X-ray fluorescence spectrometry in Rb-Sr geochemistry: Chem. Geol., 12, 127-136.
Papanastassiou, D. A. and Wasserburg, G. J. 1969. Initial strontium isotopic abundances and the resolution of small-time differences in the formation of planetary objects. Earth and Planetary Science Letters, 5, 361–376. doi:10.1016/s0012-821x(68)80066-4
Patchett, P.J., Tatsumoto, M., 1980. A routine high-precision method for Lu-Hf isotope geochemistry and chronology. Contrib. Mineral. Petrol. 75, 263-267.
Paterson, S. R & Ducea, M. N. 2015. Arc Magmatic Tempos: Gathering the Evidence. Elements, vol. 11, pp. 91–98. DOI: 10.2113/gselements.11.2.91.
Pearce, J.A., Gale, G.H., 1977. Identification of ore-depositional environment from trace-element geochemistry of associated igneous host rocks. In: Volcanic Processes in Ore Genesis, Geological Society of London Special Publication 7, pp. 14–24.
Pearce, J.A., Harris, N.B.W., Tindle, A.G., 1984. Trace element discrimination diagramsfor the tectonic interpretation of granitic rocks. Journal of Petrology 25, 956–983.
Pearce, J. A. & Peate, D. W. 1995. Tectonic implications of the composition of volcanic arc magmas. Annual Review of Earth and Planetary Sciences 23, 251–286.
Pearce J.A. 1996. Sources and settings of granitic rocks. Episodes, 19(4): 120-125.
Pedrosa-Soares, A. C., Noce, C. M., Vidal, P., Monteiro, R. & Leonardos, O. H. (1992) Toward a new tectonic model for the Late Proterzoic Araçuaí (SE Brazil) - West Congolian (SW Africa) Belt. Journal of South American Earth Sciences (v. 6) p. 33-47.
Pedrosa-Soares, A.C., Vidal, P., Leonardos, O.H., Brito-Neves, B.B., 1998. Neoprotero-zoic oceanic remnants in eastern Brazil: further evidence and refutation of anexclusively ensialic evolution for the Araçuaí–West Congo orogen. Geology 26,519–522.
Pedrosa-Soares, A.C., Noce, C.M., Wiedemann, C.M., Pinto, C.P., 2001. The Araçuaí–West Congo orogen in Brazil: an overview of a confined orogen formed during Gondwanland assembly. Precambrian Res. 110, 307–323.
Pedrosa-Soares A. C. Noce C. M., Alkmim F. F., Silva L. C., Babinsk, M., Cordani U., Castañeda C. (2007). Orógeno Araçuaí: Síntese do Conhecimento 30 anos após Almeida 1977. Geonomos (v. 15) p. 1-16.
Pedrosa-Soares, A.C., Alkmim, F.F., Tack, L., Noce, C.M., Babinski, M., Silva, L.C.,Martins-Neto, M.A., 2008. Similarities and differences between the Brazilianand African counterparts of the Neoproterozoic Arac¸ uaí–West Congo orogen. In:Pankhurst, R.J., Trouw, R.A.J., Brito Neves, B.B., de Wit, M.J. (Eds.), West Gond-wana: Pre-Cenozoic Correlations Across the South Atlantic Region. GeologicalSociety of London Special Publications 294, pp. 153–172.
Pedrosa-Soares, A.C. & Alkmim F.F. 2011. How many rifting events preceded the development of the Araçuaí-west Congo Orogen? Geonomos. Edição Especial - 30 Anos do CPMTC. 19(2).
Pedrosa-Soares, A.C., Campos, C.P.C., Noce, C., Silva, L.C., Novo, T., Roncato, J., Medeiros, S., Castañeda, C., Queiroga, G., Dantas, E., Dussin, I., Alkmim, F., 2011a. Late Neoproterozoic-Cambrian granitic magmatism in the Araçuaí orogen (Brazil), the Eastern Brazilian Pegmatite Province and related mineral resources. In: Sial, A.N., Bettencourt, J.S., De Campos, C.P., Ferreira, V.P. (Eds.), Granite-Related Ore Deposits. Geological Society, Special Publications, London, pp. 25–51.
Pedrosa-Soares, A.C., Babinski, M., Noce, C.M., de Martins, M.S., Queiroga, G.N., Vilela, F., 2011b. The Neoproterozoic Macaúbas Group (Araçuaí orogen, SE Brazil) with emphasis on the diamictite formations. Memoirs, London In: Arnaud, E., Halverson, G.P., Shields-Zhou, G. (Eds.), The Geological Record of Neoproterozoic Glaciations. Geological

Society, pp. 523–534.
Peixoto C., Heilbron M. 2010. Geologia da klippe Italva na região entre Cantagalo e Itaocara, nordeste do Estado do Rio de Janeiro. UNESP Geociências, 29:277-289.
Peixoto, C.A., Heilbron, M., Ragatky. D., Armstrong, R., Dantas, E., Valeriano, C.M., Simonetti, A. 2017. Tectonic evolution of the juvenile tonian serra da prata magmatic arc in the ribeira belt, se brazil: Implications for early west gondwana amalgamation. Precambrian Research. (302), 221-254.
Peres, G.G, Alkmim, F., Jordt-Evangelista, H. 2004. The southern Araçuaí belt and the Dom Silvério Group: geologic architecture and tectonic significance. Annals of the Brazilian Academy of Sciences 76(4): 771-790.
Philipp R.P., Pimentel M.M., Basei M.A.S. 2018. The Tectonic Evolution of the São Gabriel Terrane, Dom Feliciano Belt, Southern Brazil: The Closure of the Charrua Ocean. In: Siegesmund S., Basei M., Oyhantçabal P., Oriolo S. 2018. (eds) Geology of Southwest Gondwana. Regional Geology Reviews. Springer, Cham
Pietranik, A.B., Hawkesworth, C.J., Storey, C.D., Kemp, A.I.S., Sircombe, K.N., Whitehouse, M.J., Bleeker, W., 2008. Episodic, mafic crust formation from 4.5 to 2.8 Ga: new evidence from detrital zircons, Slave craton, Canada. Geology 36, 875–878.
Pimentel M.M., Fuck R.A. 1992. Neoproterozoic crustal accretion in central Brazil. Geology, 20:375-379.
Pimentel M.M., Whitehouse M.J., Viana M.G., Fuck R.A., Machado N. 1997. The Mara Rosa Arc in the Tocantins Province: further evidence for Neoproterozoic crustal accretion in Central Brazil. Precambrian Research, 81:299-310.
Pimentel, M.M., Fuck, R.A., Gioia, S.M.C.L., 2000. The Neoproterozoic Goiás Magmatic Arc, Central Brazil: a review and New Sm-Nd isotopic data. Revista Brasileira de Geociências (1), 035–039.
Pinto C.P., Drumond J.B.V., Féboli W.L. (coord.). Projeto Leste, Etapa 1. CPRM-COMIG, Belo Horizonte, 1997.
Pisarevsky, S.A., Wingate, M.T.D., Powell, C.M., Johnson, S., Evans, D.A.D., 2003. Models of Rodinia assembly and fragmentation. In: Yoshida, M., Windley, B., Dasgupta, S. (Eds.), Proterozoic East Gondwana: Supercontinent Assembly and Breakup. Special Publication Geological Society of London vol. 206, pp. 35– 55.
Piuzana, D., pimentel, M. M., fuck, R. A. & amstrong, R. 2003. SHRIMP U–Pb and Sm–Nd data for the Araxá Group and associated magmatic rocks: Constraints for the age of sedimentation and geodynamic context of the southern Brasília Belt, central Brazil. Precambrian Research, 125, 139–160.
Porada, H., 1989. Pan-African rifting and orogenesis in southern to equatorial Africa and eastern Brazil. Precambrian Research 44, 103–136.
Oriolo, S., Oyhantçabal, P., Wemmer, K., Siegesmund, S. 2017. Contemporaneous assembly of Western Gondwana and final Rodinia break-up: Implications for the supercontinent cycle. Geoscience Frontiers, 8: 1431-1445.
Queiroga, G., Pedrosa-Soares, A.C., Noce, C.M., Alkmim, F.F., Pimentel, M.M., Dantas, E., Martins, M., Castaneda, C., Suite, M.T.F., Prichard, H., 2007. Age of the Ribeirão da Folha ophiolite, Araçuaí Orogen: the U–Pb zircon dating of a plagiogranite. Geonomos 15 (1), 61–65.
Queiroga, G.N., 2010. Caracterização de restos de litosfera oceânica do Orógeno Araçuaí entre os paralelos 17º e 21ºS. Instituto de Geociências, Universidade Federal de Minas Gerais PhD thesis.
Ragatky, D., Maceira, J., Duarte, B.P., Valente, S., Parisotto, M. 2007. Geoquímica preliminar dos ortoanfibolitos da Bacia Italva, setor central da Faixa Ribeira. In: XI Congresso Brasileiro de Geoquímica: Atibaia;
Ramos, R. C., & Koester, E. 2015. Lithogeochemistry of the meta-igneous units from Arroio Grande Ophiolitic Complex, southernmost Brazil. Brazilian Journal of Geology, 45(1): 65-78
Ribeiro, A.; Andreis, R.R.; Trouw, R.A.J.; Paciullo, F.V.P.; Valença, J.G. (1995). Evolução das bacias proterozoicas e o termo-tectonismo brasiliano na margem sul do Cráton do São

Francisco. Revista Brasileira de Geociências (v. 25) p. 235-248.
Richter, F., Lana, C., Steven, G., Buick, I., Pedrosa-Soares, A.C., Alkmim, F.F., Cutts, K. 2016. Sedimentation, metamorphism and granite generation in a back-arc region: Records from the Ediacaran Nova Venécia Complex (Araçuaí Orogen, Southeastern Brazil). Precambrian Research 272, 78–100.
Roeder D.2013. 6 - Convergent margins and orogenic belts. Regional Geology and Tectonics: Principles of Geologic Analysis 112-177. doi: https://doi.org/10.1016/B978-0-444-53042-4.00006-6
Rollinson, H.R. 1993. Using geochemical data: Evaluation, Presentation, Interpretation. Prentice Hall. 352 p.
Rosen, O.M., 1992. Graywackes of the precambrian metamorphic complexes: composition and paleogeodynamic reconstructions. Int. Geol. Rev. 34 (12), 1169–1186.
Roser, B.P., Korsch, R.J., 1986. Determination of tectonic setting of sandstone-mudstone suites using SiO2 content and K2O/Na2O ratio. J. Geol. 94, 635–650.
Rubatto, D., 2002. Zircon trace element geochemistry: partitioning with garnet and the link between U-Pb ages and metamorphism. Chem. Geol. 184, 123–138.
Sad, J.H.G., Donadello, M.M., Figueiras, RR, Arantes, D. Projeto Carta Geológica do Estado do Rio de Janeiro. Escala 1:50.000. Folha Santa Maria Madalena (SF-23-X-D-VI-4): Texto Explicativo. 1980. GEOSOL LTDA. DRM-RJ.
Sad, J.H.G., Dutra, C., 1988. Chemical composition of supracrustal rocks from Paraíba do Sul Group, Rio de Janeiro State, Brazil. Geochim. Brasil 7 (2), 143–174.
Sato, K. & Siga Junior, O. 2000. Superproduction Evidence of the Continental Crust During Paleoproterozoic in South American Platform. Implications Regarding the Interpretative Value of the Sm-Nd Model Ages. Revista Brasileira de Geociências, Rio de Janeiro-Brazil, vol. 30, n. 1, pp. 147 160, 2000.
Samson S.D., Inglis J.D., D'lemos R.S., Admou H., Blichert-Toft J., Hefferan K. 2004. Geochronological, geochemical, and Nd–Hf isotopic constraints on the origin of Neoproterozoic plagiogranites in the Tasriwine ophiolite, Anti-Atlas orogen, Morocco. Precambrian Research, 135(1-2):133-147. https://doi.org/10.1016/j.precamres.2004.08.003
Santiago, R. et al. 2020a.Two generations of mafic dyke swarms in the Southeastern Brazilian coast: reactivation of structural lineaments during the gravitational collapse of the Araçuaí Ribeira Orogen (500 Ma) and West Gondwana breakup (140 Ma). Precambrian Research, 340, 105344.
Santiago, R. et al. 2020b.Tonian Island Arc Remnants in the Northern Ribeira Orogen of Western Gondwana: The Caxixe Batholith (ESPÍRITO SANTO, SE BRAZIL). Precambrian Research, p. 105944.
Santos, M.M., Lana, C., Scholz, R., Buick, I., Schmitz, M.D., Kamo, S.L., Gerdes, A., Corfu, F., Tapster, S., Lancaster, P., Storey, C.D., Basei, M.A.S., Tohver, E., Alkmim, A., Nalini, H., Krambrock, K., Fantini, C., Widenbeck, M., 2017. A new appraisal of sri lankan bb zircon as a reference material for LA-ICP-MS U-Pb geochronology and Lu-Hf isotope tracing. Geostand. Geoanal. Res., 41(3): 335-358.
Saquaque A., Admou H., Karson J., Hefferan K., Reuber I. 1989. Precambrian accretionary tectonics in the Bou-Azzer-El-Graara region, Anti-Atlas, Morocco. Geology, 17(12):1107-1110. https://doi.org/10.1130/0091-7613(1989)017%3C1107:PATITB%3E2.3.CO;2
Saquaque A. 1992. Un exemple de suture-arc: Le Precambrien de l'Anti-Atlas centre oriental (Maroc). PhD Dissertation, Université Cadi Ayyad, Marrakech, 366 p.
Schannor, M., Lana, C., Fonseca,M.A., 2018. São Francisco-Congo break-up delimited by UPb-Hf isotopes and trace-elements of zircon from metasediments of the Araçuaí Belt. Geosci. Front. 10, 611–628. https://doi.org/10.1016/j.gsf.2018.02.011.
Schmitt, R.S., Trouw, R.A.J., Van Schmus, W.R., Pimentel, M.M., 2004. Late amalgam-ation in the central part of Western Gondwana: new geochronologicalal dataand the characterization of a Cambrian collision orogeny in the Ribeira belt (SEBrazil). Precambrian Research 133, 29–61.
Schmitt, R. S., Trouw, R. A. J., Van Schmus, W. R., & Passchier, C. W. 2008. Cambrian

orogeny in the Ribeira Belt (SE Brazil) and correlations within West Gondwana: ties that bind underwater. Geological Society, London, Special Publications, 294(1), 279–296. doi:10.1144/sp294.15

Seer, H. J., Brod, J. A., Fuck, R. A., Pimentel, M. M., Boaventura, G. R., & Dardenne, M. A. 2001. Grupo Araxá em sua área tipo: um fragmento de crosta oceânica neoproterozóica na Faixa de Dobramentos Brasília. Revista Brasileira de Geociências, 31(3), 385-396.

Sem, G., and Stern, J. R. 2021. Subduction Zone Magmas. Encyclopedia of Geology (Second Edition). Pages 33-5. https://doi.org/10.1016/B978-0-08-102908-4.00086-2

Seth, B., Kronner, A., Mezger, K., Nemchin, A.A., Pidgeon, R.T., Okrusch, M., 1998. Archaean to neoproterozoic magmatic events in the Kaoko belt of Nw Namibia and their geodynamic significance. Precambrian Res. 92, 341e363.

Seth, B., Jung, S., Hoernes, S., 2002. Isotope constraints on the origin of Pan-African granitoids rocks in the Kaoko belt, NW Namibia. S. Afr. J. Earth Sci. 105, 179-192.

Seth, B., Armstrong, R.A., Brandt, S., Villa, I.M., Kramers, J.D., 2003. Mesoproterozoic U–Pb and Pb–Pb ages of granulites in NW Namibia: reconstructing a complete orogenic cycle. Precambrian Res. 126, 147–168

Shand, S. J. (1943). Classic A/CNK vs A/NK plot for discriminating metaluminous, peraluminous and peralkaline compositions.

Silva, L.C.; Armstrong, R.; Noce, C.M.; Carneiro, M.; Pimentel, M.; Pedrosa-Soares, A. C.; Leite, C.; Vieira, V. S.; Silva, M.; Paes, V. & Cardoso-Filho, J. 2002. Reavaliação da evolução geológica em terrenos pré-cambrianos brasileiros com base em novos dados U-Pb SHRIMP, parte II: Orógeno Araçuaí, Cinturão Móvel Mineiro. e Cráton São Francisco Meridional. Revista Brasileira de Geociências, v. 32, p. 513-528.

Silva, L.C., McNaughton, N.J., Armstrong, R., Hartmann, L., Fletcher, I. 2005. The Neoproterozoic Mantiqueira Province and its African connections. Precambrian Research 136, 203–240.

Silva L.C., Pinto C.P., Gomes A.C.B., Paes V. 2007. Geocronologia U-Pb (LA-ICP-MS) e a cronoestratigrafia granítica no segmento norte do Orógeno Araçuaí (MG). In: Simpósio de Geologia do Sudeste, 10, Diamantina. SBGMG, Resumos, 2007.

Silva, L.C., Pedrosa-Soares, A.C., Teixeira, L.R., Armstrong, R., 2008. Tonian rift-related, A-type continental plutonism in the Araçuaí Orogen, eastern Brazil: new evidence for the breakup stage of the São Francisco-Congo Paleocontinent. Gondwana Res. 13, 527–537

Silva, C. M.T., 2010. O sistema transcorrente da porção sudeste do orógeno Araçuaí e norte da faixa Ribeira: geometria e significado tectônico, 221 p. Tese (Doutorado em Evolução Crustal e Recursos Naturais) - Universidade Federal de Ouro Preto, Ouro Preto, 2010.

Sláma, J., Košler, J., Condon, D.J., Crowley, J.L., Gerdes, A., Hanchar, J.M., Horstwood, M.S.A., Morris, G.A., Nasdala, L., Norberg, N., Schaltegger, U., Schoene, B., Tubrett, M.N., Whitehouse, M.J., 2008. Plešovice zircon – a new natural reference material for U-Pb and Hf isotopic microanalysis. Chem. Geol. 249, 1–35.

Soares, C., Queiroga, G., Pedrosa-Soares, A., Gouvêa, L. P., Valeriano, C. M., de Melo, M. G., ... & Delicio, R. (2020). The Ediacaran Rio Doce magmatic arc in the Araçuaí–Ribeira boundary sector, southeast Brazil: Lithochemistry and isotopic (Sm–Nd and Sr) signatures. Journal of South American Earth Sciences, 104, 102880.

Söderlund, U., Patchett, J.P., Vervoort, J.D., Isachsen, C.E., 2004. The 176Lu decay constant determined by Lu–Hf and U-Pb isotope systematics of Precambrian mafic intrusions. Earth Planet. Sci. Lett. 219, 311–324.

Söllner, F.; Trouw, R. A. J. (1997). The Andrelândia depositional cycle (Minas Gerais/, Brazil), a postTransamazonic sequence south of the São Francisco craton: evidence from U-Pb dating on zircons of a metasediment. Journal of South American Earth Sciences, (v. 10), p. 21-28.

Souza, M. E., Martins, M. S., Queiroga, G. N., Leite, M., Oliveira, R. G., Dussin, I., Pedrosa-Soares, A. C. 2019. Paleoenvironment, sediment provenance and tectonic setting of Tonian basal deposits of the Macaúbas basin system, Araçuaí orogen, southeast Brazil. Journal of South American Earth Sciences, 96, 102393.

doi:10.1016/j.jsames.2019.102393.
Stacey, J.S., Kramers, J.D., 1975. Approximation of terrestrial lead isotope evolution by a two-stage model. Earth Planetary Science Letters 26, 207–221.
Stern, R. J. 2002. Subduction zones. Reviews of Geophysics, 40(4). doi:10.1029/2001rg000108
Stern, R.S., Bodorkos S., Kamo S. L., Hickman, A. H., and Corfu F. 2009. Measurement of SIMS instrumental mass fractionation of Pb-isotopes during zircon dating: Geostandards and Geoanalytical Research, v. 33, p. 145-168.
Sun, S.S., McDonough, W.F., 1989. Chemical and isotopic systematic of oceanicbasalts: implications for mantle composition and processes. In: Magmatism inthe Ocean Basins. Geol. Soe. Sp. Pub., 42, pp. 313–345.
Sun, W.H., Zhou, M.F., Yan, D.P., Li, J.W., Ma, Y.X., 2008b. Provenance and tectonic setting of the Neoproterozoic Yanbian Group, western Yangtze Block (SW China). Precambrian Research 167, 213–236.
Taylor, S.R., McLennan, S.M., 1985. The Continental Crust: Its Composition and Evolution. Blackwell Scientific.
Tedeschi, M., Novo, T., Pedrosa-Soares, A.C., Dussin, I., Tassinari, T., Silva, L.C., Gonçalves, L., Alkmim, F.F., Lana, C., Figueiredo, C., Dantas, E., Medeiros, S., De Campos, C., Corrales, F., Heilbron, M., 2016. The Ediacaran Rio Doce magmatic arc revisited (Araçuaí- Ribeira orogenic system, SE Brazil). J. S. Am. Earth Sci. 68, 167–186.
Thompson, R.N., Morrison, M.A., Hendry, G.L., Parry, S.J., Simpson, P.R., Hutchison, R., O'Hara, M.J., 1984. An assessment of the relative roles of crust and mantle in magma genesis: an elemental approach [and discussion]. Philos. Trans. R. Soc. London A: Math., Phys. Eng. Sci. 310 (1514), 549–590.
Toteu, S.F., Yongue Fouateu, R., Penanye, J. Tchakounté, J., Seme Mouangue, A.C., Van Schmus, W.R., Deloule, E., Stendal, H.2006. U–Pb dating of plutonic rocks involved in the nappe tectonic in southern Cameroon: consequence for the Pan-African orogenic evolution of the central African fold belt, J. Afr. Earth Sci. 44, 479–493
Trompette R. (1994). Geology of Western Gondwana (2000-500 Ma). Pan-African-Brasiliano aggregation of South America and Africa. Rotterdam, A.A. Balkema, 350 p.
Trouw, R.A.J., Heilbron, M; Ribeiro,A.; Paciullo, F.; Valeriano, C.; Almeida, J.H.; Tupinambá, M. & Andreis, R. 2000. The Central Segment of the Ribeira belt. In: Tectonic Evolution of South America. Special Publication for the 31 IGC. P. 287-310.
Trouw, R.A.J., Peternel, R., Ribeiro, A., Heilbron, M., Vinagre, R., Duffles, P., Trouw, C.C., Fontainha, M., Kussama, H.H., 2013. A new interpretation for the interference zone between the southern Brasília belt and the central Ribeira belt, SE Brazil. Journal of South American Earth Sciences 48, 43–57.
Tupinambá, M.; Teixeira, W.; Heilbron, M. & BaseI, M. The Pan-African/ Brasiliano arc-related magmatism at the Costeiro Domain ot the Ribeira Belt, southeastern Brazil. In: International Conference on Basement Tectonics, 14, Ouro Preto p. 12-14, 1998.Tupinambá, M.; Heilbron, M.; Duarte, B.P.; Nogueira, J.R.; Valladares, C.; Almeida, J.; Silva, L.G.E.; Medeiros, S.R.; Almeida, C.G.; Miranda, A.; Ragatky, C.D.; Mendes, J.; Ludka, I. (2007). Geologia da faixa Ribeira setentrional: estado da arte e conexão com a faixa Araçuaí. Geonomos, Belo Horizonte (v. 15) p. 67-79.
Tupinambá M., Teixeira W.,,Heilbron M. 2000. Neoproterozoic Western Gondwana assembly and subductionrelated plutonism: the role of the Rio Negro Complex in the Ribeira Belt. Revista Brasileira de Geociências. Volume 30.
Tupinambá M., Heilbron M., Duarte B.P., Nogueira J.R., Valladares C., Almeida J., Eirado Silva L.G., Medeiros S.R., Almeida C.G., Miranda A., Ragatky C.D., Mendes J.& Ludka I. 2007. Geologia da faixa Ribeira Setentrional: estado da arte e conexões com a Faixa Araçuaí. Geonomos: 15 (1): 67-79.
Tupinambá, M., Heilbron, M., Valeriano, C., Júnior, R.P., de Dios, F.B., Machado, N.,Eirado Silva, L.G., Almeida, J.C.H. (2011). Juvenile contribution of the Neoprotero-zoic Rio Negro Magmatic Arc (Ribeira Belt, Brazil): implications for Western Gondwana amalgamation. Gondwana Research, 1–30.

Tupinambá, M., Heilbron, M., Valeriano, C.M., Porto Jr., R., Blanco de Dios, F., Machado, N., Silva, L.G.E., Almeida, J.C.H. (2012). Juvenile contribution of the Neoproterozoic Rio Negro magmatic arc (Ribeira Belt, Brazil): implications for western Gondwana amalgamation. Gondwana Research (21), 422–438.

Valeriano, C.M., Tupinambá, M., Simonetti, A., Heilbron, M., Almeida, J.C.H., do Eirado, L.G., 2011. U-Pb LA-MC-ICPMS geochronology of Cambro-Ordovician post-collisional granites of the Ribeira belt, southeast Brazil: Terminal Brasiliano magmatism in central Gondwana supercontinent. Journal of South American Earth Sciences 32, 416-428.

Valeriano, C.M., Mendes, J.C., Tupinambá, M., Bongiolo, E., Heilbron, M., Junho, M.D.C.B. 2016. Cambro-Ordovician post-collisional granites of the Ribeira belt, SE-Brazil: a case of terminal magmatism of a hot orogen. Journal of South American Earth Sciences, 68, 269-281.

Van Achterbergh, E., Ryan, C.G., Jackson, S.E., Griffin, W., 2001. Data reduction software for LA-ICP-MS. In: Sylvester, P. (Ed.), Laser Ablation ICP-Mass Spectrometry in the Earth Science: Principles and Applications. Mineral. Assoc., Canada, pp. 239–243.

Vauchez, A.; Tommasi, A; Egydio-Silva M. Self-indentation of a heterogeneous continental lithosphere. Geology. v. 22. P. 967-970, 1994.

Verma, S.P., Armstrong-Altrin, J.S., 2013. New multi-dimensional diagrams for tectonic discrimination of siliciclastic sediments and their application to Precambrian basins. Chem. Geol. 355, 117–133.

Vieira, V.S., 1995. Folha Cachoeiro de Itapemirim, SF-24-V-A, escala 1:250.000. CPRM – Brazilian Geology Survey.

Vieira, V.S., 2007. Significado Do Grupo Rio Doce No Contexto Do Orógeno Araçuaí. Tese de Doutorado. Instituto de Geociências, Universidade Federal de Minas Gerais, pp. 117.

Vieira, V.S., Silva, M.A., Corrêa, T.R., Lopes, M.H.B. 2014. Mapa Geologico do Espírito Santo e Escala 1:400.000. In: VI Simexmin and Simposio Brasileiro de Exploração Mineral, Ouro Preto, Anais.

Vieira, V.S. & Menezes, R.G. (org.). 2015. Geologia e Recursos Minerais do Estado do Espírito Santo: texto explicativo do mapa geológico e de recursos minerais, escala 1:400.000. Belo Horizonte, CPRM, 289 p.

Vieira, V.S., Silva, M.A., Corrêa, T.R., Lopes, N.H.B., 2018. Mapa geológico do estado do Espírito Santo, escala 1:400.000. CPRM – Brazilian Geological Survey.

Walsh G.J., Benziane J.N., Aleinikoff F., Harrison R.W., Yazidi A., Burton W.C., Quick J.E., Saadane A. 2012. Neoproterozoic tectonic evolution of the Jebel Saghro and Bou Azzer-El Graara inliers, eastern and central Anti-Atlas, Morocco. Precambrian Research, 216-219:23-62. https://doi. org/10.1016/j.precamres.2012.06.010

White, W.M. 2013. Geochemistry. Wiley. 668 p.

Will, T. M., Frimmel, H. E., Gaucher, C., & Bossi, J. (2014). Geochemical and isotopic composition of Pan-African metabasalts from southwestern Gondwana: evidence of Cretaceous South Atlantic opening along a Neoproterozoic back-arc. Lithos, 202, 363-381.

Winter, J.D., 2010. Principles of Igneous and Metamorphic Petrology. 2nd ed. Prentice Hall.

Woodhead, J.D., Hergt, J.M., 2005. A preliminary appraisal of seven natural zircon reference materials for in situ Hf isotope determination. Geostand. Geoanal. Res. 29, 183–195.

Wu, F.Y., Yang, Y.H., Xie, L.W., Yang, J.H., XU, P., 2006. Hf isotopic compositions of the standard zircons and baddeleyites used in U-Pb geochronology. Chem. Geol. 234 (1–2), 105–126.

APÊNDICE - SUPPLEMENTARY MATERIALS

SUPPLEMENTARY MATERIAL III

CAPÍTULO III

TONIAN ISLAND ARC REMNANTS IN THE NORTHERN RIBEIRA OROGEN OF WESTERN GONDWANA: THE CAXIXE BATHOLITH (ESPÍRITO SANTO, SE BRAZIL)

(artigo publicado no periódico Precambrian Research, Volume 351, Dezembro 2020, n. 105944, https://doi.org/10.1016/j.precamres.2020.105944)

Supplementary Material SIII - 1

Lithochemical data of Caxixe batholith samples from the Espírito Santo state, Southeastern Brazil. Element ratios at the bottom of the table are normalized to the chondrite of Sun and McDonough (1989) (sampling location in Fig. III. 3). Samples analyzed at SGS Geosol (Brazil).

Sample	Felsic and Intermediate rock																					Mafic rock						Pegmatite	
	6	42B	25	4	37	24	38A	23	50B	1	48	45	36	34	5	39	46A	22B	44	15A	50A	22A	46B	38B	42A	15B	06A	06C	06B
Major Elements (%)																													
SiO2	71.33	70.91	73.65	76.71	82.04	72.54	72.75	71.20	64.20	75.43	65.39	71.23	65.33	70.68	72.26	68.18	74.37	71.03	69.16	71.62	66.49	65.72	68.58	49.03	68.28	62.92	53.62	74.92	70.62
TiO2	0.28	0.08	0.22	0.05	0.19	0.19	0.18	0.33	0.17	0.08	0.45	0.17	0.44	0.26	0.27	0.39	0.11	0.18	0.33	0.19	1.26	0.39	0.32	1.02	0.42	0.59	2.66	0.08	0.22
Al2O3	14.63	16.12	15.57	12.63	7.25	14.46	14.59	14.88	19.27	12.71	15.99	14.25	16.91	15.45	14.81	15.27	14.00	14.36	14.70	13.89	13.65	14.96	15.66	14.98	14.71	17.46	13.79	14.19	14.67
Fe2O3	2.03	0.71	1.68	0.91	1.36	1.50	1.59	2.46	1.51	1.17	4.23	1.56	3.23	2.17	2.38	3.16	1.09	1.76	2.71	1.87	3.20	3.25	2.32	10.47	2.95	4.58	9.57	1.13	1.54
MnO	0.04	0.02	0.04	0.03	0.02	0.03	0.05	0.04	0.03	0.02	0.08	0.03	0.10	0.03	0.05	0.06	0.04	0.03	0.05	0.02	0.06	0.09	0.05	0.22	0.07	0.11	0.18	0.02	0.04
MgO	0.91	0.27	0.66	0.01	0.40	0.52	0.52	0.88	0.33	0.08	1.24	0.36	1.20	0.61	0.36	1.32	0.32	0.33	0.62	0.32	1.07	0.38	0.91	7.41	1.03	1.51	2.95	0.12	0.76
CaO	2.38	3.73	2.89	0.40	0.25	2.48	1.80	3.05	3.41	0.88	4.29	1.72	4.77	2.07	1.26	3.03	2.56	1.37	3.23	1.24	2.12	1.18	2.83	9.93	3.54	3.66	4.59	1.05	2.96
Na2O	4.21	4.46	4.32	2.78	0.60	4.45	3.74	4.94	3.82	3.11	3.03	3.52	4.21	3.37	3.49	3.72	3.45	3.33	3.27	2.62	1.68	3.60	4.12	3.04	4.05	4.00	3.02	2.84	4.96
K2O	2.26	0.67	2.04	5.34	2.35	1.73	4.07	1.49	5.66	4.52	2.42	4.07	1.05	3.90	4.02	1.96	2.95	4.98	2.00	5.75	7.89	5.16	2.78	1.05	1.31	3.05	2.23	5.58	0.91
P2O5	0.09	0.01	0.11	0.01	0.03	0.03	0.01	0.10	0.01	0.01	0.13	0.03	0.14	0.07	0.02	0.06	0.10	0.05	0.12	0.05	0.34	0.13	0.07	0.26	0.18	0.27	1.63	0.01	0.09
Cr2O3	0.01	0.01	0.01	0.01	0.01	0.01	0.01	0.01	0.01	0.01	0.01	0.01	0.01	0.01	0.01	0.01	0.01	0.01	0.01	0.01	0.01	0.01	0.01	0.04	0.01	0.01	0.01	0.01	0.01
LOI	0.42	0.50	0.39	0.81	0.72	0.24	0.35	0.49	0.72	0.30	0.85	0.31	0.54	0.82	0.77	0.51	0.57	0.32	0.34	0.50	0.47	0.38	0.52	0.68	0.47	0.44	1.21	0.56	0.43
Sum	98.17	96.99	101.19	98.88	94.50	97.94	99.31	99.38	98.42	98.02	97.26	96.95	97.39	98.62	98.93	97.16	99.00	97.43	96.20	97.58	97.77	94.87	97.65	97.45	96.55	98.16	94.25	99.95	96.78
Trace Elements (ppm)																													
Ba	499.00	157.00	405.00	1243.00	556.00	610.00	903.00	388.00	140.00	747.00	136.00	469.00	373.00	131.80	104.50	351.00	825.00	847.00	669.00	105.40	372.60	455.30	662.00	170.00	366.00	173.70	117.90	104.00	172.00
Rb	79.20	13.00	45.00	174.00	82.10	53.90	104.50	65.60	179.60	90.10	77.00	125.50	50.10	92.20	130.40	66.20	63.00	133.40	57.60	173.10	354.90	175.50	89.90	22.20	46.50	147.40	104.00	123.00	46.50

Sr	239.00	415.00	344.00	27.00	79.00	288.00	280.00	368.00	338.00	58.00	340.00	159.00	384.00	460.00	164.00	414.00	313.00	194.00	424.00	204.00	1878.00	207.00	561.00	412.00	376.00	281.00	692.00	249.00	467.00
Ga	16.30	18.10	17.80	14.50	10.80	19.20	19.30	17.00	21.00	15.70	15.70	19.40	18.00	20.60	15.80	19.00	13.70	16.30	17.20	19.50	20.70	17.90	18.30	18.30	17.40	18.90	17.80	21.90	15.30
Ta	1.38	1.38	0.86	0.93	0.93	1.15	0.66	0.60	0.78	0.89	0.94	4.86	0.98	1.21	1.50	1.12	2.19	2.80	0.81	2.73	2.77	1.05	1.35	0.41	0.41	1.57	3.00	2.60	1.25
Nb	12.94	0.13	4.99	5.13	4.86	4.53	3.82	2.80	3.42	3.62	8.14	14.79	6.71	7.59	15.10	5.48	2.17	17.17	9.36	9.59	33.67	22.62	2.10	1.61	4.73	10.33	38.80	17.34	10.07
Hf	2.78	1.02	0.94	3.82	3.09	2.73	3.28	2.74	5.11	2.08	4.21	4.63	5.40	4.38	4.50	4.72	2.82	4.77	4.45	6.32	35.19	10.84	2.83	1.45	3.73	3.02	8.43	4.82	2.62
Zr	107.00	10.00	39.00	55.00	111.00	47.00	44.00	72.00	102.00	23.00	134.00	69.00	175.00	108.00	136.00	127.00	35.00	129.00	147.00	156.00	10907.00	547.00	67.00	17.00	147.00	56.00	385.00	69.00	58.00
Y	7.45	2.87	9.49	4.86	21.82	4.44	12.42	6.38	5.14	5.42	22.27	14.72	16.84	5.27	5.86	14.12	16.06	13.68	14.29	27.33	19.11	25.45	4.19	18.60	9.12	25.56	32.02	15.33	6.01
Th	4.70	1.80	6.90	10.90	5.00	3.40	6.10	2.50	2.40	4.10	4.20	11.50	3.80	16.10	10.80	10.80	9.10	17.20	7.00	33.30	32.00	3.60	3.70	1.80	2.10	4.30	12.10	35.30	5.50
U	1.42	0.66	5.27	1.17	1.76	0.61	0.72	0.48	6.02	0.48	1.27	3.35	1.53	3.09	1.62	3.00	1.91	20.21	1.04	9.11	5.10	3.04	0.41	1.63	0.53	1.17	3.42	21.82	1.69
Ni	22.00	7.00	10.00	5.00	6.00	8.00	11.00	11.00	8.00	5.00	7.00	10.00	9.00	7.00	8.00	14.00	7.00	7.00	8.00	<5	14.00	9.00	12.00	92.00	5.00	17.00	23.00	10.00	18.00
Co	49.10	224.40	53.50	98.10	178.60	128.00	97.00	82.30	72.20	114.50	63.40	124.30	107.30	85.60	151.20	106.50	139.60	80.20	49.70	116.20	96.50	66.40	109.80	67.30	87.70	67.80	58.40	105.90	128.60
V	36.00	<5	13.00	<5	23.00	<5	<5	52.00	<5	<5	71.00	<5	16.00	8.00	16.00	40.00	<5	18.00	13.00	<5	32.00	20.00	28.00	207.00	48.00	41.00	157.00	<5	23.00
Cu	20.00	<5	<5	<5	<5	32.00	5.00	<5	12.00	<5	<5	<5	52.00	26.00	<5	10.00	5.00	13.00	<5	<5	21.00	<5	7.00	160.00	6.00	11.00	31.00	<5	<5
Zn	44.00	6.00	43.00	8.00	30.00	23.00	24.00	48.00	20.00	33.00	64.00	27.00	53.00	26.00	58.00	51.00	<5	49.00	85.00	27.00	58.00	50.00	36.00	73.00	52.00	66.00	150.00	14.00	43.00
W	346.10	1509.90	386.60	696.70	1335.00	959.60	636.40	561.00	376.30	836.40	407.70	771.00	727.30	576.00	1065.60	688.20	924.80	561.50	352.80	868.80	548.80	430.70	665.00	156.20	603.30	386.30	245.90	793.90	799.50
Mo	4.00	4.00	3.00	3.00	4.00	4.00	2.00	2.00	2.00	2.00	2.00	6.00	4.00	2.00	3.00	2.00	2.00	2.00	2.00	4.00	3.00	3.00	2.00	2.00	3.00	3.00	2.00	3.00	3.00
Rare Earth Elements (ppm)																													
La	5.50	7.80	9.90	10.60	12.90	13.50	14.10	14.40	14.40	17.20	17.60	18.50	19.70	19.90	23.10	28.80	28.90	32.80	37.20	53.80	189.40	9.60	11.20	11.30	11.70	13.10	94.50	8.60	17.10
Ce	15.30	13.80	21.90	71.20	32.60	25.20	27.20	22.50	9.50	36.00	30.90	32.70	37.70	30.40	31.10	50.00	59.20	59.10	70.90	121.80	354.60	20.40	22.10	25.30	30.10	28.40	181.60	21.70	28.40
Pr	1.53	1.80	2.54	2.56	3.83	2.68	3.35	2.92	2.31	3.87	3.84	4.51	4.87	4.04	4.32	5.55	7.20	5.88	8.26	12.89	40.79	2.73	2.31	3.43	3.53	3.60	20.92	1.84	3.11
Nd	6.60	6.50	9.90	9.00	13.50	8.30	11.10	10.70	7.60	13.60	16.10	15.20	19.30	13.70	14.30	22.10	27.10	21.70	29.20	46.20	136.30	11.70	9.10	15.60	13.80	14.30	80.30	7.50	11.50
Sm	1.30	1.20	2.00	1.90	2.90	1.70	2.50	2.20	1.60	2.50	4.10	3.70	4.30	2.80	2.40	4.10	4.60	3.60	5.70	8.30	17.80	3.00	2.10	3.80	2.40	3.10	14.50	2.40	1.60
Eu	0.42	0.70	0.54	0.40	0.66	0.76	0.77	0.54	1.26	0.93	1.32	0.78	1.41	0.93	0.78	1.16	1.00	0.73	1.36	1.37	3.91	2.46	0.57	1.44	0.73	1.16	1.97	0.58	0.45
Gd	1.41	1.31	2.08	1.35	3.06	1.37	2.07	1.62	0.95	1.70	4.28	3.26	3.72	1.68	1.73	3.42	3.03	2.85	4.10	5.96	8.92	3.71	1.59	3.45	2.23	3.40	10.39	2.15	1.41

Tb	0.23	0.07	0.32	0.19	0.50	0.16	0.38	0.20	0.18	0.23	0.72	0.80	0.62	0.23	0.24	0.54	0.46	0.38	0.56	0.91	1.05	0.63	0.20	0.63	0.28	0.65	1.32	0.49	0.20
Dy	1.34	0.50	1.81	0.92	3.29	0.72	1.91	1.20	0.90	1.37	4.12	4.05	3.09	1.03	1.48	2.91	2.75	2.49	3.01	5.45	4.35	3.83	0.91	3.85	1.73	4.00	6.52	3.36	1.17
Ho	0.24	0.12	0.34	0.20	0.80	0.17	0.40	0.23	0.21	0.21	0.83	0.76	0.64	0.21	0.23	0.57	0.61	0.50	0.47	0.99	0.71	0.96	0.22	0.79	0.32	0.97	1.13	0.70	0.21
Er	0.72	0.26	0.98	0.59	2.30	0.37	1.20	0.56	0.64	0.63	2.32	1.20	2.12	0.56	0.64	1.37	1.59	1.61	1.24	2.49	1.90	2.79	0.56	1.97	0.90	2.98	2.89	2.10	0.63
Tm	0.12	<0,05	0.20	0.13	0.28	0.07	0.20	0.13	0.09	0.08	0.32	0.29	0.27	0.11	0.11	0.23	0.17	0.35	0.18	0.45	0.25	0.42	0.08	0.26	0.13	0.44	0.43	0.32	0.16
Yb	0.70	0.40	0.90	0.80	2.10	0.40	1.40	0.50	0.70	0.60	2.20	0.70	1.80	0.70	0.60	1.50	1.40	2.10	1.10	2.40	1.60	2.80	0.30	2.00	0.80	3.30	2.50	2.00	0.50
Lu	0.13	0.06	0.17	0.15	0.30	0.08	0.21	0.05	0.09	0.07	0.29	0.25	0.26	0.12	0.09	0.21	0.18	0.36	0.16	0.43	0.22	0.42	0.06	0.29	0.11	0.52	0.34	0.27	0.08
$\sum_{REE}$	35.54	34.52	53.58	99.99	79.02	55.48	66.79	57.75	40.43	78.99	88.94	86.70	99.80	76.41	81.12	122.46	138.19	134.45	163.44	263.44	761.80	65.45	51.30	74.11	68.76	79.92	419.31	54.01	66.52
Eu/Eu*	0.95	1.71	0.81	0.76	0.68	1.52	1.03	0.87	3.12	1.38	0.96	0.69	1.08	1.31	1.17	0.95	0.82	0.70	0.86	0.60	0.95	2.25	0.95	1.22	0.96	1.09	0.49	0.78	0.92
$(La/Yb)_N$	5.64	13.99	7.89	9.50	4.41	24.21	7.22	20.66	14.76	20.56	5.74	18.96	7.85	20.39	27.62	13.77	14.81	11.20	24.26	16.08	84.91	2.46	26.78	4.05	10.49	2.85	27.11	3.08	24.53

$Eu/Eu^* = Eu/(SmxGd)^{0.5}$

Supplementary Material SIII - 2
Sm–Nd and Rb-Sr isotope data of Caxixe batholith samples in the southern Espírito Santo state. Initial isotope ratios are calculated for t = 860 Ma. (m) – measured; (i) – initial (calculated). TDM model ages after DePaolo (1981).

Sample	Sm (ppm)	Nd (ppm)	$^{147}Sm/^{144}Nd$	$^{143}Nd/^{143}Nd_{(m)} \pm 2\sigma$ (abs)	$\varepsilon Nd_{(0)}$	$^{143}Nd/^{143}Nd_{(i)}$	$\varepsilon Nd_{(i)}$	T_{DM} (Ga)	Rb (ppm)	Sr (ppm)	$^{87}Rb/^{86}Sr_{(m)}$	$^{87}Sr/^{86}Sr_{(m)} \pm 2\sigma$ (abs)	$\varepsilon Sr_{(0)}$	$^{87}Sr/^{86}Sr_{(i)}$	$\varepsilon Sr_{(i)}$
6	1.30	6.60	0.134500	0.512449	-3.7	0.511690	3.2	1.14	79.2	239	0.959118	0.711410	98.083747	0.699625	-54.847478
06B	1.60	11.50	0.091900	0.512263	-7.3	0.511745	4.3	0.97	46.5	467	0.288066	0.707010	35.628105	0.703471	-0.189170
22B	3.60	21.70	0.102400	0.512151	-9.5	0.511573	0.9	1.22	133.4	194	1.992372	0.722430	254.506742	0.697950	-78.664024
23	2.20	10.70	0.116700	0.512512	-2.5	0.511854	6.4	0.84	65.6	368	0.515773	0.708100	51.100071	0.701763	-24.465616
25	2.23	9.84	0.137087	0.512459	-3.5	0.511686	3.1	1.15	45.0	344	0.378484	0.707870	47.835344	0.703220	-3.756383
42A	2.40	13.80	0.114100	0.512442	-3.8	0.511798	5.3	0.92	46.5	376	0.357812	0.707800	46.841732	0.703404	-1.141010

DePaolo, D.J., 1981. Neodymium isotopes in the Colorado front range and crust-mantle evolution in the Proterozoic. Nature 291, 193-196.

Supplementary Material SIII - 3

U-Pb (LA-ICP-MS and SHRIMP) results for magmatic zircon crystals from the Caxixe batholith.

Sample 06 - (LA-ICP-MS)

Spot Name	U (ppm)	Th/U	f206 (%)	$^{206}Pb/^{238}U$ Age	2s err	$^{207}Pb/^{206}Pb$ Age	2s err	4corr 207*/206*	% err	4corr 207*/235	% err	4corr 206*/238	% err	err corr	discordance (%)
046-ZR28		0.47		866	20	880	43	0.068391	1.04	1.3556	1.67	0.143745	1.25	0.75	1.66
030-ZR18		0.26		871	15	862	38	0.067785	0.93	1.3520	1.38	0.144649	0.94	0.69	-1.03
009-ZR4		0.25		846	22	915	58	0.069537	1.42	1.3443	2.01	0.140197	1.37	0.68	7.54
028-ZR16		0.51		844	12	898	35	0.068966	0.84	1.3301	1.20	0.139870	0.77	0.64	5.99
024-ZR15		0.64		852	15	857	37	0.067638	0.90	1.3184	1.36	0.141364	0.94	0.70	0.59
039-ZR23		0.39		844	15	862	44	0.067797	1.06	1.3085	1.48	0.139968	0.95	0.65	2.07
006-ZR3		0.35		844	17	861	42	0.067741	1.03	1.3059	1.54	0.139810	1.08	0.70	1.98
005-ZR2		0.48		821	39	914	110	0.069510	2.72	1.3026	3.74	0.135902	2.54	0.68	10.12
047-ZR29		0.36		835	20	877	49	0.068294	1.19	1.3015	1.79	0.138211	1.28	0.72	4.90
021-ZR12		0.51		846	27	846	59	0.067273	1.43	1.3010	2.24	0.140254	1.68	0.75	0.02
029-ZR17		0.62		840	14	851	34	0.067423	0.82	1.2942	1.26	0.139208	0.89	0.70	1.26
012-ZR7		0.38		844	20	829	42	0.066703	1.02	1.2864	1.66	0.139865	1.26	0.76	-1.86
041-ZR25		0.28		832	26	857	67	0.067625	1.62	1.2849	2.36	0.137796	1.68	0.71	2.90
011-ZR6		0.33		817	21	892	61	0.068761	1.49	1.2803	2.06	0.135032	1.37	0.67	8.42
004-ZR1		0.36		826	14	861	31	0.067749	0.75	1.2764	1.23	0.136634	0.90	0.73	4.10
022-ZR13		0.43		825	14	860	33	0.067735	0.81	1.2747	1.26	0.136474	0.90	0.71	4.16
023-ZR14		0.38		832	15	835	42	0.066917	1.01	1.2714	1.44	0.137788	0.96	0.67	0.37
033-ZR19		0.34		823	17	854	46	0.067536	1.13	1.2678	1.60	0.136138	1.08	0.67	3.70
015-ZR8		0.32		813	18	865	41	0.067868	1.00	1.2578	1.57	0.134404	1.15	0.73	5.97
016-ZR9		0.54		795	18	908	39	0.069321	0.96	1.2546	1.58	0.131249	1.20	0.76	12.48
018-ZR11		0.34		828	19	819	46	0.066384	1.11	1.2540	1.68	0.136997	1.20	0.72	-1.12
017-ZR10		0.32		821	18	797	43	0.065712	1.03	1.2301	1.60	0.135754	1.17	0.73	-2.94
045-ZR27		0.27		791	19	861	47	0.067763	1.13	1.2192	1.73	0.130482	1.25	0.72	8.21

036-ZR22	0.42		799	17	837	47	0.066984	1.13	1.2188	1.64	0.131953	1.14	0.69	4.57
042-ZR26	0.48		786	21	872	49	0.068102	1.20	1.2178	1.89	0.129681	1.41	0.75	9.82
010-ZR5	0.27		797	20	838	45	0.066995	1.10	1.2161	1.75	0.131645	1.31	0.75	4.82
040-ZR24	0.42		774	13	868	36	0.067979	0.88	1.1956	1.29	0.127548	0.86	0.67	10.84
035-ZR21	0.93		518	26	913	167	0.069470	4.16	0.8023	4.91	0.083748	2.59	0.53	43.20

Sample 25 - (SHRIMP)

Spot Name	ppm U	Th/U	f206(%)	$^{206}Pb/^{238}U$ Age	1s err	$^{207}Pb/^{206}Pb$ Age	1s err	4corr 207*/206*	% err	4corr 207*/235	% err	4corr 206*/238	% err	err corr	discordance (%)
25-01.1	209.87	0.53	0.000	880	16	857	20	0.067621	0.96	1.3641	2.22	0.146303	2.00	0.90	-2.90
25-03.1	202.57	0.49	0.064	877	16	882	24	0.068430	1.15	1.3753	2.31	0.145758	2.00	0.87	0.54
25-05.1	323.97	0.76	0.000	844	11	853	18	0.067508	0.85	1.3012	1.66	0.139797	1.43	0.86	1.24
25-09.1	248.27	0.79	0.031	838	15	839	22	0.067040	1.07	1.2839	2.22	0.138896	1.94	0.87	0.08
25-10.1	365.15	0.98	0.000	842	14	838	17	0.067001	0.80	1.2889	1.99	0.139523	1.82	0.92	-0.53
25-11.1	223.72	0.36	0.000	842	16	835	23	0.066904	1.09	1.2878	2.31	0.139599	2.04	0.88	-0.97
25-13.1	311.31	0.50	0.022	853	15	814	19	0.066237	0.89	1.2920	2.07	0.141469	1.87	0.90	-5.13
25-14.1	203.34	0.78	0.040	839	17	825	26	0.066581	1.26	1.2767	2.47	0.139072	2.13	0.86	-1.91
25-17.1	150.08	0.34	0.000	857	19	841	27	0.067107	1.28	1.3154	2.66	0.142168	2.33	0.88	-2.01
25-18.1	210.03	0.48	0.000	839	17	859	23	0.067672	1.11	1.2965	2.39	0.138951	2.12	0.89	2.46

Sample 38 - (SHRIMP)

Spot Name	ppm U	Th/U	f206(%)	$^{206}Pb/^{238}U$ Age	1s err	$^{207}Pb/^{206}Pb$ Age	1s err	4corr 207*/206*	% err	4corr 207*/235	% err	4corr 206*/238	% err	err corr	discordance (%)
38-01.1	540.10	0.51	0.000	885	13	866	20	0.067909	0.97	1.3784	1.89	0.147215	1.63	0.86	-2.42
38-02.1	1800.08	0.02	0.017	826	11	838	8	0.067002	0.39	1.2621	1.52	0.136621	1.47	0.97	1.57
38-03.1	470.64	0.49	0.075	884	19	835	17	0.066913	0.83	1.3558	2.47	0.146961	2.32	0.94	-6.26
38-03.2	1823.80	0.12	0.102	812	11	846	15	0.067271	0.70	1.2450	1.65	0.134223	1.49	0.91	4.31
38-04.2	1783.82	0.06	0.019	827	11	839	8	0.067038	0.37	1.2655	1.52	0.136913	1.47	0.97	1.50

38-05.2	2722.38	0.07	0.071	729	12	865	7	0.067880	0.35	1.1206	1.72	0.119730	1.69	0.98	16.61
38-06.1	421.68	0.37	0.050	853	19	831	17	0.066767	0.83	1.3027	2.49	0.141512	2.35	0.94	-2.92
38-07.1	420.52	0.40	0.000	860	12	837	15	0.066971	0.71	1.3179	1.60	0.142721	1.44	0.90	-2.96
38-10.1	427.04	0.28	0.000	856	15	855	21	0.067569	1.02	1.3226	2.11	0.141964	1.84	0.87	-0.05
38-11.1	276.24	0.32	0.000	859	15	884	18	0.068493	0.88	1.3462	2.08	0.142552	1.88	0.90	2.95
38-12.1	569.41	0.46	0.011	852	13	879	13	0.068357	0.62	1.3317	1.76	0.141292	1.64	0.94	3.33
38-13.1	322.39	0.44	0.000	862	26	883	17	0.068472	0.80	1.3515	3.30	0.143152	3.20	0.97	2.47
38-14.1	524.56	0.46	0.000	856	14	842	15	0.067137	0.71	1.3146	1.86	0.142013	1.72	0.93	-1.78
38-15.1	529.57	0.42	0.000	864	14	849	14	0.067355	0.66	1.3325	1.82	0.143482	1.69	0.93	-1.96

Supplementary Material SIII - 4

Lu-Hf isotope data of Caxixe batholith from the southern Espírito Santo state, Brazil.

Zircon	U-Pb age (Ma)	± 1σ	Isotope ratios				Initial ratios			
			$^{176}Hf/^{177}Hf$	±2σ	$^{176}Lu/^{177}Hf$	±2σ	$^{176}Hf/^{177}Hf_{(t)}$	$\varepsilon Hf_{(t)}$	±2σ	$T_{DM}Hf$ (Ga)
Sample 06										
ZR-15	853	14	0.282655	0.000057	0.001001	0.000060	0.282639	13.93	1.1	0.84
ZR-14	832	14	0.282590	0.000049	0.000817	0.000019	0.282577	11.27	0.4	0.92
ZR-12	846	24	0.282523	0.000041	0.000653	0.000023	0.282512	9.29	0.6	1.01
ZR-3	846	16	0.282596	0.000035	0.001016	0.000019	0.282580	11.70	0.4	0.92
Sample 25										
5.1	844	11	0.282570	0.000026	0.000690	0.000004	0.282559	10.90	0.2	0.95
9.1	838	15	0.282559	0.000024	0.000940	0.000007	0.282544	10.24	0.3	0.97
14.1	839	17	0.282569	0.000021	0.000690	0.000006	0.282558	10.76	0.3	0.95
13.1	853	15	0.282528	0.000018	0.000870	0.000011	0.282514	9.51	0.3	1.01
11.1	842	16	0.282548	0.000027	0.000810	0.000006	0.282535	10.01	0.3	0.98
10.1	842	14	0.282580	0.000027	0.000910	0.000006	0.282566	11.09	0.3	0.94
Sample 38										
13.1	862	26	0.282532	0.000014	0.001350	0.000016	0.282510	9.58	0.4	1.02
14.1	856	14	0.282542	0.000029	0.001480	0.000013	0.282518	9.72	0.2	1.01
11.1	859	15	0.282541	0.000022	0.001510	0.000010	0.282517	9.74	0.2	1.01
15.1	864	14	0.282512	0.000019	0.001980	0.000014	0.282480	8.55	0.2	1.06
2.1	826	11	0.282515	0.000020	0.000940	0.000006	0.282500	8.41	0.2	1.03
3.1	884	19	0.282533	0.000018	0.000970	0.000008	0.282517	10.31	0.3	1.01
3.2	812	11	0.282509	0.000013	0.001400	0.000019	0.282488	7.65	0.2	1.05
4.2	827	11	0.282485	0.000016	0.001330	0.000025	0.282464	7.16	0.2	1.08
6.1	853	19	0.282513	0.000019	0.001280	0.000009	0.282492	8.75	0.3	1.04
7.1	860	12	0.282533	0.000018	0.001530	0.000010	0.282508	9.46	0.2	1.02

SUPPLEMENTARY MATERIAL IV

CAPÍTULO IV

DETRITAL ZIRCON U-Pb AND Lu-Hf CONSTRAINTS ON THE AGE, PROVENANCE AND TECTONIC SETTING OF ARC-RELATED HIGH-GRADE UNITS OF THE TRANSITION ZONE OF THE ARAÇUAÍ AND RIBEIRA OROGENS (SE BRAZIL)

(artigo submetido ao Journal of South American Earth Sciences)

Supplementary Material SIV - 1

Lithochemical data of paragneiss samples from the southern Espírito Santo state, Southeastern Brazil. Element ratios at the bottom of the table are normalized to the chondrite of Sun and McDonough (1989) (sampling location in Fig. IV.1). Samples analyzed at SGS Geosol (Brazil).

Sample	7	12	13	14	20
Major Elements (%)					
Al2O3	13.93	13.38	13.48	15.62	17.20
CaO	1.78	2.05	4.32	9.34	5.51
Cr2O3	0.01	0.01	0.05	0.03	0.01
Fe2O3	5.44	5.15	9.78	8.98	10.49
K2O	3.62	3.02	1.86	1.59	2.19
MgO	1.47	0.81	5.06	6.57	3.17
MnO	0.10	0.09	0.13	0.13	0.15
Na2O	2.50	2.48	1.34	3.29	2.87
P2O5	0.13	0.19	0.05	0.38	0.15
SiO2	67.53	71.57	59.27	49.82	54.87
TiO2	0.74	0.65	0.55	1.26	0.99
LOI	0.33	0.64	2.66	0.95	1.31
Sum	97.58	100.04	98.55	97.96	98.91
Trace Elements (ppm)					
Ba	562.00	605.00	472.00	506.00	577.00
Ce	84.10	88.10	21.40	41.00	19.80
Co	34.60	105.70	71.80	46.10	84.30
Cs	0.65	3.22	3.83	8.83	9.28
Cu	17.00	33.00	47.00	37.00	34.00
Ga	17.80	17.20	14.50	18.90	24.10
Hf	6.46	7.54	2.94	3.57	2.58
Ho	1.64	1.35	1.05	0.74	1.07

Mo	2.00	3.00	2.00	2.00	4.00
Nb	10.87	12.72	7.26	9.02	7.79
Ni	21.00	20.00	71.00	54.00	9.00
Rb	139.00	121.70	69.80	67.70	112.90
Sn	3.40	2.50	2.40	0.80	2.80
Ta	0.46	1.55	4.13	2.03	1.07
Th	15.90	13.80	5.40	2.90	3.40
Tl	<0.5	<0.5	3.40	1.60	<0.5
U	1.19	3.02	1.57	0.59	1.42
W	184.50	658.80	208.50	112.60	370.90
Y	41.97	36.96	20.88	18.72	25.68
Ba	562.00	605.00	472.00	506.00	577.00
Sr	90.00	189.00	279.00	864.00	340.00
Zn	66.00	95.00	66.00	74.00	85.00
Zr	270.00	260.00	17.00	82.00	49.00
V	54.00	74.00	115.00	148.00	250.00
Rare Earth Elements (ppm)					
La	39.80	46.20	15.20	18.60	8.30
Ce	84.10	88.10	21.40	41.00	19.80
Pr	10.09	10.12	4.57	5.34	2.96
Nd	38.40	38.40	18.80	23.70	13.80
Sm	7.30	7.80	4.40	4.50	4.30
Eu	1.08	1.42	1.46	1.79	1.10
Gd	7.30	6.85	4.76	4.53	4.48
Tb	1.12	1.06	0.80	0.61	0.76
Dy	7.59	6.56	4.25	4.17	5.40
Er	4.62	4.10	2.80	2.20	2.70
Tm	0.71	0.59	0.61	0.28	0.45
Yb	4.40	4.30	2.40	1.90	2.70

Lu	0.66	0.57	0.53	0.30	0.38
$\sum_{REE}$	207.17	216.07	81.98	108.92	67.13
Eu/Eu*	0.452298	0.593908	0.975319	1.212052	0.766202
$(La/Yb)_N$	6.488301	7.7068	4.542897	7.021985	2.205032

$Eu/Eu^* = Eu/(SmxGd)^{0.5}$

Supplementary Material SIV - 2

U-Pb (LA-ICP-MS and SHRIMP) results for detrital zircon of paragneiss samples from the southern Espírito Santo state, Southeastern Brazil.

Sample 07 - (LA-ICP-MS)

Spot Name	U (ppm)	Th/U	f206c	$^{207}Pb/^{206}Pb$ Age	2s err	$^{206}Pb/^{238}U$ Age	2s err	4corr 207*/206*	% err	4corr 207*/235	% err	4corr 206*/238	% err	err corr	discordance (%)
1.sSMPABC118	1143	0.32	1.000	773	78	817	20	0.064958	3.72	1.209478	4.47	0.135040	2.47	0.55	2.71
1.sSMPABC098	1943	1.24	1.000	752	79	748	19	0.064316	3.76	1.090683	4.52	0.122992	2.51	0.56	1.05
1.sSMPABC115	672	0.28	0.062	730	49	723	15	0.063660	2.33	1.041389	3.10	0.118643	2.04	0.66	0.91
1.sSMPABC075	556	0.24	0.113	732	46	718	14	0.063718	2.19	1.034557	2.93	0.117758	1.95	0.66	0.66
1.sSMPABC099	485	0.78	0.061	761	46	745	15	0.064600	2.18	1.091689	2.97	0.122564	2.02	0.68	0.65
1.sSMPABC113	417	0.44	0.051	762	49	746	15	0.064617	2.33	1.092389	3.08	0.122611	2.02	0.66	0.64
1.sSMPABC048	583	0.57	0.233	787	46	769	15	0.065387	2.20	1.142910	2.98	0.126770	2.01	0.68	0.64
1.sSMPABC093	576	1.04	0.143	764	48	745	15	0.064667	2.30	1.092393	3.05	0.122516	2.00	0.66	0.57
1.sSMPABC132	1159	1.43	0.023	737	56	719	14	0.063865	2.63	1.039374	3.32	0.118034	2.03	0.61	0.55
1.sSMPABC127	406	1.14	0.354	790	57	770	17	0.065488	2.73	1.145607	3.52	0.126875	2.22	0.63	0.55
1.sSMPABC131	1317	0.17	0.030	1059	43	1028	20	0.074637	2.12	1.779872	2.95	0.172954	2.05	0.69	0.55
1.sSMPABC090	279	0.52	0.846	883	72	859	21	0.068466	3.46	1.344854	4.24	0.142463	2.45	0.58	0.54
1.sSMPABC091	754	0.35	0.275	768	53	747	15	0.064811	2.49	1.097883	3.22	0.122859	2.03	0.63	0.48
1.sSMPABC079	590	0.73	0.266	821	48	795	16	0.066472	2.31	1.202695	3.11	0.131224	2.08	0.67	0.37
1.sSMPABC087	1183	0.11	0.015	738	46	715	14	0.063901	2.19	1.033748	2.97	0.117330	2.01	0.68	0.37
1.sSMPABC129	643	0.74	0.075	1064	44	1028	21	0.074834	2.20	1.783971	3.02	0.172897	2.07	0.69	0.37
1.sSMPABC094	1234	0.17	0.047	763	44	739	15	0.064660	2.08	1.082679	2.89	0.121441	2.01	0.69	0.36
1.sSMPABC051	2373	0.07	0.065	644	47	624	13	0.061130	2.20	0.856737	3.01	0.101646	2.04	0.68	0.36

1.sSMPABC116	468	0.17	0.330	674	55	651	14	0.061985	2.56	0.908166	3.30	0.106262	2.09	0.63	0.30
1.sSMPABC088	1849	0.16	1.000	774	77	746	19	0.064993	3.67	1.099937	4.49	0.122745	2.58	0.58	0.26
1.sSMPABC071	651	0.35	0.110	768	44	741	15	0.064818	2.10	1.088313	2.89	0.121774	1.99	0.69	0.26
1.sSMPABC128	221	0.30	0.460	733	68	707	17	0.063746	3.23	1.018359	4.01	0.115864	2.37	0.59	0.25
1.sSMPABC076	1339	0.03	0.048	655	50	631	13	0.061450	2.35	0.871387	3.09	0.102845	2.00	0.65	0.22
1.sSMPABC089	1401	0.10	0.112	671	50	645	13	0.061901	2.32	0.898568	3.04	0.105282	1.96	0.65	0.20
1.sSMPABC119	521	0.44	0.371	772	53	742	16	0.064929	2.52	1.091951	3.32	0.121974	2.15	0.65	0.18
1.sSMPABC053	761	0.41	1.000	745	80	714	18	0.064090	3.77	1.035297	4.53	0.117158	2.51	0.55	0.13
1.sSMPABC069	360	0.44	0.231	768	47	736	15	0.064790	2.25	1.079929	3.01	0.120889	2.00	0.67	0.11
1.sSMPABC095	613	0.13	0.207	688	47	659	14	0.062391	2.22	0.925978	3.07	0.107642	2.12	0.69	0.11
1.sSMPABC109	557	0.28	1.000	745	84	714	18	0.064107	3.96	1.035157	4.74	0.117111	2.60	0.55	0.10
1.sSMPABC110	615	0.43	0.213	749	49	716	14	0.064213	2.34	1.040739	3.10	0.117549	2.04	0.66	0.07
1.sSMPABC077	262	1.32	0.065	858	43	821	17	0.067656	2.05	1.266628	2.90	0.135782	2.05	0.71	0.06
1.sSMPABC133	517	0.52	0.029	805	50	770	16	0.065961	2.37	1.153632	3.16	0.126846	2.10	0.66	0.05
1.sSMPABC120	561	0.48	0.012	793	49	758	16	0.065592	2.32	1.128329	3.13	0.124762	2.11	0.67	0.02
1.sSMPABC114	1197	0.77	0.071	1196	54	1143	22	0.079963	2.73	2.139372	3.38	0.194043	1.99	0.59	0.00
1.sSMPABC096	1244	0.45	0.042	689	45	657	13	0.062424	2.09	0.923522	2.91	0.107299	2.02	0.70	0.00
1.sSMPABC052	570	0.36	0.082	778	44	743	15	0.065127	2.10	1.096392	2.89	0.122097	1.98	0.69	-0.01
1.sSMPABC059	1818	0.03	1.000	673	82	642	18	0.061982	3.85	0.894700	4.73	0.104692	2.74	0.58	-0.02
1.sSMPABC056	815	0.47	0.087	772	46	735	14	0.064923	2.20	1.081727	2.95	0.120841	1.96	0.66	-0.04
1.sSMPABC050	716	0.59	0.145	775	45	738	15	0.065016	2.14	1.087018	2.92	0.121260	1.99	0.68	-0.06
1.sSMPABC074	1148	1.67	1.000	638	99	606	17	0.060957	4.59	0.828963	5.36	0.098630	2.76	0.51	-0.07
1.sSMPABC108	328	0.62	1.000	847	78	806	20	0.067299	3.75	1.236641	4.53	0.133270	2.54	0.56	-0.07
1.sSMPABC057	959	0.86	0.082	799	44	760	15	0.065756	2.08	1.134596	2.89	0.125143	2.00	0.69	-0.07
1.sSMPABC130	810	0.32	0.000	809	57	769	16	0.066070	2.72	1.154755	3.42	0.126761	2.07	0.61	-0.08
1.sSMPABC055	272	0.21	0.000	686	46	652	13	0.062350	2.15	0.915150	2.93	0.106452	1.98	0.68	-0.09
1.sSMPABC112	923	0.24	1.000	1072	69	1021	23	0.075138	3.44	1.777117	4.16	0.171536	2.33	0.56	-0.12
1.sSMPABC092	664	0.28	0.000	796	49	756	16	0.065680	2.31	1.127255	3.14	0.124477	2.13	0.68	-0.12
1.sSMPABC107	971	0.24	1.000	745	80	708	18	0.064116	3.79	1.025534	4.60	0.116007	2.60	0.57	-0.13

1.sSMPABC060	277	0.33	0.045	662	64	628	13	0.061652	2.99	0.869233	3.61	0.102255	2.03	0.56	-0.14
1.sSMPABC078	1020	0.43	0.191	660	48	625	13	0.061592	2.23	0.865235	3.02	0.101884	2.03	0.67	-0.15
1.sSMPABC049	1370	1.64	0.072	824	55	782	15	0.066552	2.65	1.183181	3.27	0.128940	1.91	0.58	-0.15
1.sSMPABC054	376	0.46	1.000	738	83	700	18	0.063895	3.93	1.010103	4.72	0.114656	2.62	0.55	-0.16
1.sSMPABC070	337	2.03	1.000	772	83	731	18	0.064925	3.93	1.075614	4.66	0.120156	2.51	0.54	-0.18
1.sSMPABC097	554	0.26	0.047	756	46	716	14	0.064430	2.18	1.043572	2.96	0.117472	2.01	0.68	-0.18
1.sSMPABC047	1141	0.26	0.009	827	43	784	15	0.066654	2.04	1.188492	2.85	0.129321	1.99	0.70	-0.18
1.sSMPABC080	763	0.45	0.041	801	55	758	15	0.065823	2.65	1.133161	3.29	0.124857	1.95	0.59	-0.20
1.sSMPABC100	416	0.79	1.000	809	79	766	19	0.066089	3.76	1.149964	4.52	0.126199	2.51	0.55	-0.21
1.sSMPABC134	2406	0.07	1.000	537	92	507	16	0.058203	4.19	0.656101	5.28	0.081757	3.21	0.61	-0.22
1.sSMPABC068	403	0.95	1.000	781	78	736	19	0.065202	3.73	1.087819	4.53	0.121003	2.57	0.57	-0.31
1.sSMPABC067	855	0.22	1.000	736	80	691	18	0.063826	3.79	0.996032	4.60	0.113180	2.61	0.57	-0.39
1.sSMPABC117	1706	0.13	0.060	688	45	642	13	0.062412	2.09	0.900586	2.91	0.104654	2.02	0.69	-0.54

Sample 13 - (LA-ICP-MS)

Spot Name	U (ppm)	Th/U	f206 (%)	$^{206}Pb/^{238}U$ Age	2s err	$^{207}Pb/^{206}Pb$ Age	2s err	4corr 207*/206*	% err	4corr 207*/235	% err	4corr 206*/238	% err	err corr	discordance (%)
1.sSMPABC196	1570	0.69	0.069	565	46	616	12	0.058939	2.12	0.814175	2.89	0.100187	1.97	0.68	2.06
1.sSMPABC193	1270	0.84	1.000	584	86	629	17	0.059470	3.96	0.840831	4.83	0.102544	2.77	0.57	1.86
1.sSMPABC173	600	0.37	0.082	626	44	649	13	0.060640	2.06	0.885735	2.90	0.105936	2.04	0.70	1.08
1.sSMPABC171	841	0.24	1.000	602	86	624	17	0.059961	4.00	0.839781	4.89	0.101577	2.82	0.58	1.04
1.sSMPABC216	1024	0.71	0.176	582	48	602	12	0.059395	2.20	0.801822	3.05	0.097909	2.10	0.69	1.00
1.sSMPABC187	1429	2.41	0.169	611	46	629	13	0.060218	2.13	0.851574	2.97	0.102563	2.06	0.70	0.92
1.sSMPABC200	1465	0.61	0.091	582	51	598	11	0.059406	2.34	0.796312	3.07	0.097219	1.98	0.64	0.84
1.sSMPABC207	1315	1.48	0.000	746	47	758	16	0.064140	2.25	1.103073	3.11	0.124731	2.15	0.69	0.72
1.sSMPABC210	361	0.56	1.000	598	91	610	17	0.059859	4.20	0.818583	5.06	0.099181	2.83	0.56	0.67
1.sSMPABC235	1107	0.38	0.272	596	50	606	12	0.059797	2.33	0.812936	3.11	0.098599	2.07	0.67	0.63
1.sSMPABC191	951	1.09	1.000	608	88	617	17	0.060111	4.06	0.833059	4.93	0.100512	2.79	0.57	0.63

1.sSMPABC229	673	2.01	1.000	624	87	633	18	0.060564	4.01	0.860991	4.94	0.103106	2.89	0.58	0.60
1.sSMPABC159	567	0.28	1.000	588	86	597	17	0.059584	3.97	0.797802	4.91	0.097110	2.90	0.59	0.59
1.sSMPABC230	1098	0.56	1.000	626	86	634	17	0.060625	4.01	0.863347	4.90	0.103283	2.82	0.58	0.56
1.sSMPABC238	821	0.49	1.000	609	86	616	17	0.060158	3.97	0.832322	4.87	0.100345	2.82	0.58	0.54
1.sSMPABC227	733	0.43	0.140	605	53	611	12	0.060026	2.44	0.823473	3.16	0.099497	2.00	0.63	0.53
1.sSMPABC237	1199	0.57	0.173	628	48	635	13	0.060685	2.25	0.865597	3.12	0.103451	2.16	0.69	0.52
1.sSMPABC211	1343	0.65	0.023	613	47	619	12	0.060256	2.16	0.837940	2.95	0.100858	2.01	0.68	0.52
1.sSMPABC220	645	0.31	0.227	587	52	594	12	0.059545	2.41	0.792014	3.19	0.096469	2.10	0.66	0.51
1.sSMPABC258	387	0.47	1.000	551	89	558	16	0.058579	4.07	0.730750	5.07	0.090474	3.02	0.60	0.51
1.sSMPABC169	1078	0.61	0.260	618	52	622	13	0.060403	2.41	0.843834	3.19	0.101321	2.09	0.65	0.43
1.sSMPABC131	1504	0.17	0.047	1065	41	1064	20	0.074855	2.03	1.852493	2.87	0.179489	2.02	0.70	0.41
1.sSMPABC167	715	0.47	1.000	615	87	618	17	0.060313	4.05	0.836264	4.92	0.100562	2.80	0.57	0.39
1.sSMPABC158	600	0.56	0.221	676	49	675	13	0.062052	2.31	0.944919	3.07	0.110442	2.02	0.66	0.29
1.sSMPABC132	801	1.36	0.373	739	57	737	14	0.063931	2.70	1.067490	3.36	0.121102	2.00	0.59	0.25
1.sSMPABC232	949	0.44	0.124	601	47	600	12	0.059935	2.18	0.806176	2.97	0.097554	2.02	0.68	0.24
1.sSMPABC151	1311	0.03	0.043	611	45	609	12	0.060204	2.10	0.821825	2.96	0.099004	2.09	0.71	0.20
1.sSMPABC251	627	0.05	0.157	634	50	631	13	0.060854	2.33	0.862966	3.12	0.102849	2.07	0.67	0.19
1.sSMPABC257	388	0.47	0.039	569	49	567	12	0.059057	2.24	0.748515	3.07	0.091924	2.10	0.68	0.19
1.sSMPABC236	584	1.00	0.084	717	47	713	14	0.063267	2.20	1.020447	2.98	0.116980	2.01	0.68	0.18
1.sSMPABC197	1124	0.21	0.163	616	50	612	12	0.060341	2.32	0.829195	3.05	0.099664	1.99	0.65	0.17
1.sSMPABC239	715	2.91	0.117	650	47	646	13	0.061318	2.19	0.890974	2.99	0.105384	2.03	0.68	0.14
1.sSMPABC170	845	0.74	0.141	628	47	624	12	0.060694	2.16	0.849885	2.96	0.101558	2.02	0.68	0.12
1.sSMPABC148	1013	2.11	0.000	605	48	600	12	0.060040	2.23	0.808074	3.02	0.097613	2.04	0.67	0.12
1.sSMPABC192	662	0.30	1.000	626	84	621	17	0.060632	3.88	0.845800	4.80	0.101173	2.83	0.59	0.12
1.sSMPABC157	1457	0.17	0.068	603	46	598	11	0.059979	2.11	0.803833	2.89	0.097199	1.97	0.68	0.11
1.sSMPABC152	1542	0.54	0.107	597	46	592	11	0.059826	2.14	0.793156	2.93	0.096154	2.00	0.68	0.09
1.sSMPABC177	785	0.26	0.260	619	49	613	12	0.060432	2.26	0.831677	3.08	0.099812	2.10	0.68	0.09
1.sSMPABC213	2010	1.29	0.147	591	44	585	12	0.059652	2.04	0.781688	2.98	0.095040	2.18	0.73	0.08
1.sSMPABC153	818	0.46	0.248	627	48	621	13	0.060649	2.23	0.845052	3.06	0.101055	2.09	0.68	0.07

1.sSMPABC231	833	0.62	0.070	628	49	622	13	0.060687	2.29	0.847151	3.14	0.101242	2.15	0.68	0.06
1.sSMPABC234	894	0.80	0.132	613	45	606	12	0.060261	2.07	0.819563	2.96	0.098639	2.12	0.71	0.06
1.sSMPABC133	482	0.55	0.229	811	48	802	17	0.066158	2.28	1.209106	3.16	0.132551	2.18	0.69	0.05
1.sSMPABC128	238	0.32	0.378	729	59	721	16	0.063629	2.78	1.038477	3.58	0.118371	2.26	0.63	0.05
1.sSMPABC178	1873	0.61	0.066	639	44	632	12	0.060989	2.04	0.865797	2.88	0.102958	2.03	0.71	0.05
1.sSMPABC179	510	0.68	0.000	707	48	698	13	0.062950	2.26	0.992996	3.01	0.114406	2.00	0.66	0.04
1.sSMPABC140	1217	0.58	1.000	601	85	594	17	0.059924	3.94	0.797309	4.92	0.096499	2.95	0.60	0.04
1.sSMPABC195	895	0.34	0.184	599	47	591	12	0.059860	2.19	0.793034	2.99	0.096085	2.03	0.68	0.03
1.sSMPABC176	961	1.28	0.135	615	46	608	12	0.060328	2.14	0.822783	2.95	0.098915	2.03	0.69	0.03
1.sSMPABC127	430	1.00	0.085	819	41	808	16	0.066393	1.97	1.223069	2.85	0.133606	2.06	0.72	0.01
1.sSMPABC175	1030	0.15	0.022	642	48	633	12	0.061067	2.23	0.869136	2.99	0.103224	1.99	0.67	0.01
1.sSMPABC129	681	0.76	0.080	1075	41	1061	20	0.075260	2.06	1.857402	2.87	0.178996	2.01	0.70	-0.01
1.sSMPABC247	782	0.52	1.000	601	87	593	17	0.059934	4.04	0.795890	4.97	0.096312	2.90	0.58	-0.02
1.sSMPABC194	1773	0.69	0.210	640	45	631	13	0.061022	2.08	0.864759	2.99	0.102780	2.15	0.72	-0.03
1.sSMPABC190	1079	0.86	0.039	611	45	602	12	0.060206	2.06	0.812440	2.91	0.097870	2.06	0.71	-0.03
1.sSMPABC233	1020	0.98	1.000	617	86	607	17	0.060371	3.97	0.822373	4.87	0.098797	2.82	0.58	-0.05
1.sSMPABC174	1033	0.52	0.037	610	47	601	11	0.060188	2.20	0.810227	2.94	0.097633	1.96	0.67	-0.06
1.sSMPABC218	973	0.08	0.128	653	44	643	13	0.061401	2.06	0.887589	2.97	0.104841	2.14	0.72	-0.07
1.sSMPABC219	1717	0.42	1.000	651	83	640	17	0.061333	3.89	0.883010	4.77	0.104417	2.77	0.58	-0.07
1.sSMPABC180	1687	1.19	1.000	649	84	639	17	0.061286	3.89	0.879925	4.75	0.104131	2.72	0.57	-0.07
1.sSMPABC208	701	0.46	1.000	627	85	617	17	0.060655	3.93	0.839447	4.84	0.100374	2.82	0.58	-0.07
1.sSMPABC147	740	1.06	1.000	611	84	601	17	0.060208	3.91	0.810659	4.85	0.097653	2.87	0.59	-0.08
1.sSMPABC130	778	0.33	1.000	814	78	800	20	0.066238	3.72	1.207153	4.53	0.132176	2.59	0.57	-0.10
1.sSMPABC136	642	0.03	0.032	657	44	646	13	0.061510	2.05	0.893261	2.89	0.105325	2.04	0.71	-0.10
1.sSMPABC150	772	0.65	0.037	640	42	629	12	0.061028	1.97	0.862188	2.84	0.102465	2.04	0.72	-0.10
1.sSMPABC189	894	0.11	0.027	638	44	627	12	0.060974	2.07	0.858109	2.91	0.102070	2.05	0.70	-0.12
1.sSMPABC135	835	0.17	1.000	603	85	591	17	0.059979	3.91	0.794700	4.86	0.096095	2.89	0.59	-0.12
1.sSMPABC209	651	3.00	1.000	613	86	602	17	0.060273	3.99	0.813100	4.91	0.097840	2.85	0.58	-0.12
1.sSMPABC217	3145	0.92	0.064	643	43	630	13	0.061101	2.01	0.865550	2.90	0.102741	2.10	0.72	-0.13

1.sSMPABC160	626	0.42	1.000	617	86	605	17	0.060372	3.97	0.818943	4.95	0.098382	2.95	0.60	-0.13
1.sSMPABC252	1107	0.66	0.227	607	56	595	12	0.060103	2.58	0.801651	3.29	0.096736	2.05	0.62	-0.14
1.sSMPABC256	1406	1.15	0.047	701	47	687	14	0.062790	2.20	0.974087	3.07	0.112513	2.14	0.70	-0.16
1.sSMPABC138	739	0.82	1.000	605	85	592	17	0.060051	3.92	0.796626	4.87	0.096213	2.88	0.59	-0.18
1.sSMPABC240	215	1.58	0.040	1076	53	1057	22	0.075290	2.63	1.848724	3.42	0.178088	2.18	0.64	-0.18
1.sSMPABC137	644	0.74	1.000	619	84	605	17	0.060434	3.89	0.819371	4.83	0.098333	2.86	0.59	-0.22
1.sSMPABC249	954	3.54	0.184	722	50	706	14	0.063403	2.34	1.011266	3.09	0.115679	2.02	0.65	-0.23
1.sSMPABC139	1328	0.45	0.000	613	49	598	12	0.060250	2.26	0.807214	3.05	0.097170	2.05	0.67	-0.23
1.sSMPABC168	859	1.39	0.060	567	46	553	11	0.059004	2.11	0.728512	2.91	0.089547	2.01	0.69	-0.24
1.sSMPABC215	461	3.35	0.000	586	47	571	12	0.059510	2.15	0.759514	3.06	0.092565	2.17	0.71	-0.26
1.sSMPABC248	1365	1.10	0.279	601	57	584	12	0.059942	2.64	0.784104	3.36	0.094872	2.08	0.62	-0.33
1.sSMPABC212	2004	1.10	1.000	756	80	736	18	0.064443	3.79	1.074018	4.58	0.120875	2.57	0.56	-0.36
1.sSMPABC154	938	1.86	1.000	616	84	597	17	0.060341	3.88	0.807288	4.83	0.097032	2.87	0.60	-0.38
1.sSMPABC214	1054	0.49	1.000	618	93	598	16	0.060392	4.30	0.809940	5.15	0.097268	2.82	0.55	-0.39
1.sSMPABC155	377	2.58	0.200	619	50	597	12	0.060429	2.31	0.808051	3.07	0.096982	2.01	0.66	-0.49

Sample 12 - (LA-ICP-MS)

Spot Name	U (ppm)	Th/U	f206c	$^{207}Pb/^{206}Pb$ Age	2s err	$^{206}Pb/^{238}U$ Age	2s err	4corr 207*/206*	% err	4corr 207*/235	% err	4corr 206*/238	% err	err corr	discordance (%)
1.sSMPABC031	148	0.19	0.644	788	66	676	13	0.0654	3.16	0.9976	3.73	0.1106	1.97	0.53	3.7
1.sSMPABC032	239	0.26	0.000	914	63	934	16	0.0695	3.08	1.4932	3.58	0.1558	1.84	0.51	-0.6
1.sSMPABC033	405	0.03	0.332	572	73	596	12	0.0591	3.34	0.7902	3.93	0.0969	2.08	0.53	-0.9
1.sSMPABC034	82	0.30	0.000	776	59	799	14	0.0651	2.83	1.1831	3.36	0.1319	1.80	0.54	-0.8
1.sSMPABC036	368	0.18	1.000	1051	72	927	18	0.0743	3.55	1.5861	4.12	0.1547	2.10	0.51	3.9
1.sSMPABC037	173	0.16	0.000	1103	55	950	15	0.0763	2.73	1.6699	3.19	0.1588	1.65	0.52	4.7
1.sSMPABC039	601	0.02	0.261	629	64	642	12	0.0607	2.99	0.8765	3.58	0.1047	1.97	0.55	-0.5
1.sSMPABC040	390	0.05	0.032	945	45	788	12	0.0706	2.18	1.2649	2.73	0.1300	1.63	0.60	5.1
1.sSMPABC047	1234	0.30	0.000	611	47	593	9	0.0602	2.16	0.7993	2.72	0.0963	1.66	0.61	0.6
1.sSMPABC048	347	0.05	0.267	565	77	600	12	0.0589	3.55	0.7920	4.15	0.0975	2.16	0.52	-1.2

1.sSMPABC049	489	0.47	0.102	933	53	944	15	0.0702	2.58	1.5264	3.08	0.1578	1.68	0.55	-0.4
1.sSMPABC050	266	0.05	0.000	579	102	601	13	0.0593	4.69	0.7992	5.23	0.0977	2.31	0.44	-0.8
1.sSMPABC051	236	0.02	0.000	628	73	645	13	0.0607	3.40	0.8803	3.98	0.1052	2.07	0.52	-0.6
1.sSMPABC052	239	0.02	0.060	639	57	641	11	0.0610	2.63	0.8793	3.20	0.1045	1.82	0.57	-0.1
1.sSMPABC054	438	0.12	0.000	550	68	556	10	0.0585	3.11	0.7275	3.61	0.0902	1.84	0.51	-0.2
1.sSMPABC055	381	0.01	0.075	574	52	596	9	0.0592	2.41	0.7905	2.93	0.0969	1.66	0.57	-0.8
1.sSMPABC056	288	0.04	0.294	625	74	644	13	0.0606	3.44	0.8787	4.05	0.1051	2.15	0.53	-0.7
1.sSMPABC057	429	0.01	0.252	525	80	562	11	0.0579	3.63	0.7264	4.13	0.0910	1.97	0.48	-1.3
1.sSMPABC059	475	0.03	0.000	584	47	598	10	0.0595	2.19	0.7968	2.76	0.0972	1.69	0.61	-0.5
1.sSMPABC060	482	0.03	0.044	859	49	583	9	0.0677	2.34	0.8841	2.86	0.0947	1.65	0.58	9.3

Supplementary Material – IV3
Lu-Hf isotope data for detrital zircon of paragneiss samples from the southern Espírito Santo state, Southeastern Brazil (Sampling location in Fig. IV. 1).

Zircon	U-Pb age (Ma)	± 1σ	Isotope ratios				Initial ratios			
			$^{176}Hf/^{177}Hf$	±2σ	$^{176}Lu/^{177}Hf$	±2σ	$^{176}Hf/^{177}Hf_{(t)}$	$\varepsilon Hf_{(t)}$	±2σ	TDMHf (Ga)
Sample 7										
1.sSMPABC107	708	18	0.282078	0.000057	0.000612	0.000060	0.282070	-9.5	1	1.6
1.sSMPABC109	714	18	0.282045	0.000057	0.001112	0.000060	0.282030	-10.8	1	1.7
1.sSMPABC110	716	14	0.281983	0.000057	0.001078	0.000060	0.281968	-12.9	1	1.8
1.sSMPABC112	1021	23	0.281621	0.000057	0.000593	0.000060	0.281610	-18.7	2	2.2
1.sSMPABC113	746	15	0.282066	0.000057	0.001310	0.000060	0.282048	-9.4	1	1.7
1.sSMPABC116	651	14	0.282084	0.000057	0.000733	0.000060	0.282075	-10.6	1	1.6
1.sSMPABC117	642	13	0.282069	0.000057	0.001358	0.000060	0.282052	-11.6	1	1.7
1.sSMPABC118	817	20	0.282053	0.000057	0.001361	0.000060	0.282032	-8.4	1	1.7
1.sSMPABC119	742	16	0.282019	0.000057	0.001293	0.000060	0.282001	-11.2	1	1.7
1.sSMPABC120	758	16	0.282043	0.000057	0.001004	0.000060	0.282029	-9.8	1	1.7
1.sSMPABC097	716	14	0.282030	0.000057	0.000913	0.000060	0.282018	-11.2	1	1.7
1.sSMPABC097	716	14	0.282061	0.000057	0.000948	0.000060	0.282048	-10.1	1	1.7
1.sSMPABC115	723	15	0.282003	0.000057	0.000558	0.000060	0.281996	-11.8	2	1.7
1.sSMPABC114	1143	22	0.281942	0.000057	0.002272	0.000060	0.281893	-5.9	0	1.9
1.sSMPABC99	745	15	0.282025	0.000057	0.000994	0.000060	0.282011	-10.7	1	1.7

Sample 13										
1.sSMPABC187	629	12.5	0.282133	0.000075	0.001249	0.000021	0.282118	-9.5	0	1.6
1.sSMPABC180	639	16.8	0.282168	0.000078	0.001298	0.000015	0.282152	-8.1	0	1.5
1.sSMPABC217	630	12.8	0.282427	0.000057	0.001566	0.000060	0.282408	0.8	0	1.2
1.sSMPABC216	602	12.3	0.282444	0.000057	0.001165	0.000060	0.282431	0.9	0	1.1
1.sSMPABC219	640	17.1	0.282422	0.000057	0.002174	0.000060	0.282396	0.5	0	1.2
1.sSMPABC220	594	12.1	0.282268	0.000057	0.000967	0.000060	0.282257	-5.4	0	1.4
1.sSMPABC215	571	12	0.281982	0.000057	0.001753	0.000060	0.281963	-16.4	1	1.8
1.sSMPABC227	611	11.8	0.282183	0.000057	0.001380	0.000060	0.282167	-8.2	1	1.5
1.sSMPABC228	623	12	0.282407	0.000057	0.001521	0.000060	0.282389	-0.1	0	1.2
1.sSMPABC231	622	12.9	0.282173	0.000057	0.001438	0.000060	0.282157	-8.4	1	1.5
1.sSMPABC179	698	13.4	0.282516	0.000057	0.000930	0.000060	0.282504	5.7	0	1.0
1.sSMPABC178	632	12.4	0.282448	0.000057	0.001791	0.000060	0.282427	1.4	0	1.1
1.sSMPABC168	553	10.8	0.282135	0.000057	0.001141	0.000060	0.282123	-11.1	1	1.6
1.sSMPABC167	618	16.7	0.282403	0.000057	0.001332	0.000060	0.282388	-0.3	0	1.2
1.sSMPABC169/170	624	12.2	0.282111	0.000057	0.000812	0.000060	0.282102	-10.3	1	1.6
1.sSMPABC173	649	13	0.282490	0.000057	0.001062	0.000060	0.282477	3.6	0	1.1
1.sSMPABC171	624	17	0.282045	0.000057	0.000966	0.000060	0.282033	-12.7	1	1.7
1.sSMPABC174	601	11	0.282096	0.000057	0.001374	0.000060	0.282081	-11.5	1	1.6
1.sSMPABC175	633	12	0.282491	0.000057	0.000736	0.000060	0.282482	3.4	0	1.1
1.sSMPABC176	608	12	0.282165	0.000057	0.001316	0.000060	0.282150	-8.9	1	1.5
1.sSMPABC177	613	12	0.282161	0.000057	0.001160	0.000060	0.282147	-8.9	1	1.5
1.sSMPABC218	643	13	0.282515	0.000057	0.001078	0.000060	0.282502	4.3	0	1.0
1.sSMPABC230	634	17	0.282129	0.000057	0.001158	0.000060	0.282115	-9.6	1	1.6
1.sSMPABC214	598	16	0.282401	0.000057	0.001432	0.000060	0.282385	-0.8	0	1.2
1.sSMPABC193	629	17	0.282364	0.000057	0.001333	0.000060	0.282348	-1.4	0	1.3

1.sSMPABC189	627	12.4	0.282473	0.000057	0.000926	0.000060	0.282462	2.6	0	1.1
1.sSMPABC190	602	12	0.282073	0.000057	0.001768	0.000060	0.282053	-12.5	1	1.7
1.sSMPABC160	605	17.3	0.282410	0.000057	0.001141	0.000060	0.282397	-0.2	0	1.2
1.sSMPABC150	597	16.8	0.282331	0.000057	0.000733	0.000060	0.282323	-3.0	0	1.3
1.sSMPABC192	621	17	0.282487	0.000057	0.000921	0.000060	0.282476	2.9	0	1.1
1.sSMPABC211	619	12.1	0.282454	0.000057	0.000966	0.000060	0.282443	1.7	0	1.1
1.sSMPABC232	600	11.7	0.282192	0.000057	0.001147	0.000060	0.282179	-8.1	1	1.5
1.sSMPABC235	606	12.2	0.282376	0.000057	0.001387	0.000060	0.282360	-1.5	0	1.2
1.sSMPABC234	606	12.4	0.282498	0.000057	0.000822	0.000060	0.282489	3.1	0	1.0
1.sSMPABC233	607	16.6	0.282030	0.000057	0.001259	0.000060	0.282016	-13.7	1	1.7
1.sSMPABC209	602	16.6	0.281999	0.000057	0.001326	0.000060	0.281984	-14.9	1	1.8
1.sSMPABC210	610	16.7	0.282178	0.000057	0.001330	0.000060	0.282163	-8.4	1	1.5
1.sSMPABC157	598	11.4	0.282472	0.000057	0.000625	0.000060	0.282465	2.0	0	1.1
1.sSMPABC158	675	13.1	0.282451	0.000057	0.001587	0.000060	0.282431	2.6	0	1.1
1.sSMPABC195	591	11.6	0.282117	0.000057	0.001141	0.000060	0.282104	-10.9	1	1.6
1.sSMPABC152	592	11.5	0.282244	0.000057	0.001582	0.000060	0.282226	-6.6	0	1.4
1.sSMPABC151	609	12.3	0.282512	0.000057	0.001061	0.000060	0.282500	3.5	0	1.0
1.sSMPABC148	600	11.9	0.282250	0.000057	0.001685	0.000060	0.282231	-6.2	0	1.4
1.sSMPABC198	623	12	0.281864	0.000057	0.000821	0.000060	0.281854	-19.0	2	1.9
1.sSMPABC197	612	11.8	0.282505	0.000057	0.000873	0.000060	0.282495	3.4	0	1.0
1.sSMPABC207	758	15.6	0.282468	0.000057	0.003219	0.000060	0.282422	4.1	0	1.2
1.sSMPABC149	623	12	0.282481	0.000057	0.000819	0.000060	0.282472	2.8	0	1.1
1.sSMPABC140	594	17	0.282419	0.000057	0.001921	0.000060	0.282398	-0.5	0	1.2
1.sSMPABC139	629	16.9	0.282121	0.000057	0.001501	0.000060	0.282104	-10.1	1	1.6
1.sSMPABC147	601	16.7	0.282102	0.000057	0.001096	0.000060	0.282089	-11.2	1	1.6
1.sSMPABC163	646	12.7	0.282493	0.000057	0.000751	0.000060	0.282484	3.8	0	1.1

1.sSMPABC137	605	16.8	0.282033	0.000057	0.000988	0.000060	0.282021	-13.5	1	1.7
1.sSMPABC271	631	12.6	0.282482	0.000057	0.001120	0.000060	0.282469	2.9	0	1.1
1.sSMPABC247	593	16.6	0.282076	0.000057	0.000786	0.000060	0.282067	-12.2	1	1.6
1.sSMPABC208	617	16.8	0.282113	0.000057	0.001122	0.000060	0.282100	-10.5	1	1.6
1.sSMPABC236	713	13.8	0.282494	0.000057	0.001308	0.000060	0.282477	5.0	0	1.1
1.sSMPABC230	616	16.8	0.282145	0.000057	0.001499	0.000060	0.282128	-9.5	1	1.6
1.sSMPABC237	646	12.7	0.281858	0.000057	0.000754	0.000060	0.281849	-18.7	2	1.9
1.sSMPABC252	595	11.8	0.282258	0.000057	0.001616	0.000060	0.282240	-6.0	0	1.4
1.sSMPABC255	623	12	0.282299	0.000057	0.002667	0.000060	0.282267	-4.4	0	1.4

SUPPLEMENTARY MATERIAL V

CAPÍTULO V

PRESERVATION OF PRE-COLLISIONAL ACCRETIONARY SYSTEMS AS MEGAXENOLITHS AND ROOF PENDANTS THROUGH MULTIPLE PARTIAL MELTING EPISODES: 360 MA OF OROGENIC MAGMATISM IN THE COMPOSITE CAXIXE BATHOLITH, ARAÇUAÍ-RIBEIRA OROGENIC SYSTEM OF WESTERN GONDWANA

(Artigo a ser submetido para periódico especializado)

Supplementary Material SV - 1

Lithochemical data of Caxixe batholith samples from the southern Espírito Santo state. Element ratios at the bottom of the table are normalized to the chondrite of Sun and McDonough (1989). Samples analyzed at SGS Geosol (Brazil).

Sample	503 Ma												607 Ma a 583 Ma								
	Felsic and Intermediate rock												Felsic and Intermediate rock								Enclave mafic
	26	27A	27B	28	29	33	32	35	31	30	21	47	41	49bQ	51	52	53Q	54A	54D	49aQ	54bQ
Major Elements (%)																					
Al2O3	13.61	18.3	15.43	12.14	13.78	14.16	14.72	14.48	13.19	13.55	14.54	13.9	15.24	12.94	15.42	14.53	14.09	17.93	12.2	13.93	16.37
CaO	2.79	5.84	6.04	1.12	0.65	1.32	1.7	2.56	1.9	1.47	3.53	2.11	2.96	1.5	2.62	2.2	2.66	5.14	1.31	4.53	8.4
Cr2O3	<0.01	0.01	<0.01	<0.01	<0.01	<0.01	<0.01	<0.01	<0.01	<0.01	<0.01	<0.01	<0.01	<0.01	<0.01	0.01	<0.01	<0.01	<0.01	<0.01	<0.01
Fe2O3	1.7	4.12	9.17	2.7	2.06	3.35	3.29	4.67	2.95	1.96	3.25	3.73	3.94	0.4	3.64	2.65	2.2	7.31	0.84	4.69	11.81
K2O	1.09	1.37	3.13	5.47	5.74	6.29	5.75	5.47	4.94	5.74	2.48	5.51	3.01	4.91	3.8	3.55	2.95	3.15	4.4	1.75	1.13
MgO	0.69	2.21	4.34	0.52	0.15	0.59	0.53	1.27	0.73	0.69	1.11	0.73	1.23	0.04	0.88	0.81	0.72	1.52	0.19	1.45	4.37
MnO	0.03	0.12	0.15	0.04	0.01	0.04	0.04	0.07	0.04	0.04	0.07	0.05	0.05	0.03	0.09	0.03	0.03	0.1	0.01	0.09	0.2
Na2O	4.35	4.85	2.95	2.26	2.13	2.66	2.96	2.89	2.58	2.63	3.15	2.65	3.31	2.93	2.56	2.57	2.21	3.64	2.63	3.02	3.8
P2O5	0.09	0.13	0.89	0.1	0.01	0.11	0.14	0.29	0.15	0.16	0.14	0.2	0.14	<0.01	0.08	0.09	0.1	0.24	0.03	0.14	0.3
SiO2	70.43	60.52	52.72	71.24	72.94	68.45	70.31	65.25	67.25	69.5	71.33	66.31	68.84	73.06	68.72	70.4	68.22	57.79	75.11	64.7	48.24
TiO2	0.22	0.36	1.81	0.42	0.18	0.54	0.57	0.86	0.54	0.55	0.48	0.67	0.59	0.03	0.41	0.47	0.39	0.86	0.11	0.42	1.6
LOI	0.49	0.53	0.95	0.43	1.23	0.64	0.79	0.67	0.87	0.39	0.28	1.01	0.94	0.28	0.82	1.09	1	0.81	0.51	0.5	0.67
Sum	95.49	98.36	97.58	96.44	98.88	98.15	100.8	98.48	95.14	96.68	100.36	96.87	100.25	96.12	99.04	98.4	94.57	98.49	97.34	95.22	96.89
Trace Elements (ppm)																					
Ba	156	665	2372	970	1332	1428	1489	3012	1774	2043	954	1562	930	158	1151	597	1010	3132	939	594	660
Rb	57.4	39.7	134.5	227.3	188.4	237.3	210.3	202.7	164	176.1	79.4	247.2	132.9	146.7	112.5	124.4	97.3	95.8	119.4	94.7	22
Zn	17	61	115	47	15	62	75	87	41	70	47	80	56	10	44	44	33	94	20	85	140

Zr	54	49	326	319	162	629	560	635	469	463	154	595	304	15	133	132	136	768	17	133	160
V	26	34	129	<5	<5	11	42	40	19	30	38	20	68	13	16	25	33	45	18	88	303
Sr	260	910	1163	214	395	256	278	774	442	405	315	308	256	128	264	218	269	474	360	250	447
Co	47.7	83.4	59.9	231.5	146.6	144.5	61.9	108.6	66.5	76.5	46.2	127.2	76.2	102.8	154.9	198	84.3	94.8	81.9	71.2	55.5
Cs	1.39	0.81	2.64	1.23	1.24	1.22	0.63	1.3	2.82	0.98	2.83	2.18	5.5	2.65	1.21	1.04	1.07	1.7	1.56	4.76	0.23
Cu	13	6	25	9	<5	15	7	10	19	10	<5	13	10	<5	7	6	<5	20	19	6	24
Ga	13.2	22.9	15.9	14.1	21.2	8.8	20.4	14	13.7	17	16	18.6	14.8	16	20.9	19.1	16.3	21.6	11.9	17.9	19.9
Hf	2.37	2.16	9.12	10.34	6.57	18.21	13.73	17.06	11.97	11.05	3.75	16.93	8.19	0.89	5.51	5.38	3.7	19.32	1.74	3.7	4.78
Mo	<2	3	3	5	4	3	4	3	2	5	3	4	<2	2	3	4	<2	4	3	2	2
Nb	7.23	5.92	22.83	23.3	13.78	26.21	24.56	36.95	15.14	20.94	5.87	36.95	8.84	2.36	8.48	8.66	7.92	15.66	2.43	8.04	9.5
Ni	15	28	55	8	6	8	7	13	11	11	11	10	9	<5	10	5	<5	13	8	9	16
Sn	1.3	2.5	1.5	2.2	2.7	2.4	2.9	3.4	1.6	2	0.7	3.5	1.4	<0.3	0.3	<0.3	0.5	1	1	3.2	1.2
Ta	0.74	0.97	1.61	2.46	2.62	2.77	1.83	3.02	1.58	1.77	0.41	3.66	0.99	0.52	1.25	1.36	0.5	0.87	0.55	0.62	0.73
Th	32.7	2.3	14.7	67.4	94.1	100.4	79.3	75.6	50.9	51.9	12	58.6	26.6	2	7.3	8.8	6.2	13.3	1.9	3.7	1.8
Tl	<0.5	<0.5	<0.5	<0.5	<0.5	0.6	0.5	0.5	<0.5	0.6	<0.5	<0.5	<0.5	<0.5	0.5	<0.5	<0.5	<0.5	<0.5	<0.5	<0.5
U	1.52	0.55	2.24	4.78	10.7	2.73	2.57	4.4	2.76	1.66	1.26	2.64	3.68	12.5	0.8	1.33	0.52	2.23	0.37	1.52	1.54
W	304	562.2	210.5	1514.3	1111.9	1068	433.5	710	456.6	587.3	282.2	748.6	490.9	738.9	918.7	1276.9	597.7	548.3	635.1	444.5	145.4
Y	5.56	15.98	35.96	20.14	16.88	49.72	25.49	37.12	21.42	24.67	14.08	37.79	13.64	17.35	23.16	7.82	12.79	41.21	3.24	21.82	29.29
Rare Earth Elements (ppm)																					
La	13.3	18.6	168.7	190.9	57.7	432.8	265.1	355.9	216.6	220.3	56.2	251.7	60.1	<0.1	33.6	39.9	27.7	158.5	10.7	12.5	38.4
Ce	36.4	39.7	389.9	368.9	119.4	751	489.6	653.3	414.4	417	113.2	487.6	108.6	4	87.7	79.1	56.3	308.3	15.3	30	68.1
Pr	2.5	5.45	41.83	39.84	11.48	81.96	47.46	69.23	43.54	42.4	12.05	56.46	10.78	0.46	8.88	9.91	6.81	35.61	1.56	3.64	8.19
Nd	8.1	23.2	151.7	128.7	36.9	257	157	224.9	139.4	143.9	39.6	179.6	35	1.9	32.4	35.4	27.2	122.2	5.2	14.6	34.8
Sm	1.6	4.4	23.3	16.8	6.5	34.5	18.9	30.5	17.6	19.1	5.3	24.9	5	0.5	5.7	7.4	5.7	19.5	0.9	3	7.2
Eu	0.49	2.22	5.09	1.56	0.88	4.17	2.28	5.01	2.61	2.43	1	2.95	0.67	0.52	1.37	1.25	1.1	4.11	0.48	1.07	1.86
Gd	1.39	3.77	14.23	8.6	4.77	19.94	10.42	14.75	9.31	10.41	3.66	14.9	3.49	0.93	5.16	4.65	5.13	12.16	0.66	3.44	6.86

Tb	0.2	0.53	1.77	1.03	0.77	2.36	1.19	1.86	1.08	1.26	0.46	1.87	0.46	0.23	0.7	0.6	0.65	1.5	0.08	0.6	0.99
Dy	1.13	2.98	8.71	4.48	3.86	10.72	5.62	8.16	4.89	6.15	2.54	8.98	2.55	2.11	4.41	2.52	2.81	9.18	0.59	3.92	6.02
Ho	0.2	0.55	1.45	0.77	0.65	2	0.88	1.35	0.86	0.99	0.5	1.54	0.46	0.5	1	0.35	0.43	1.61	0.1	0.8	1.11
Er	0.6	1.87	3.39	1.76	1.75	4.74	2.2	3.48	1.95	2.37	1.43	3.67	1.35	1.93	2.23	0.63	0.94	4.28	0.29	2.48	3.3
Tm	0.11	0.3	0.48	0.25	0.19	0.58	0.3	0.47	0.23	0.39	0.27	0.46	0.21	0.38	0.27	0.06	0.09	0.57	0.05	0.34	0.45
Yb	0.5	1.8	2.7	1.5	1.4	3.5	1.8	2.8	1.5	2	1.3	2.8	1.1	2.7	2	0.4	0.5	3.8	0.3	2.1	3
Lu	0.08	0.24	0.35	0.23	0.21	0.43	0.22	0.42	0.17	0.31	0.22	0.41	0.18	0.45	0.27	<0.05	0.08	0.54	<0.05	0.36	0.43
$\sum_{REE}$	66.6	105.61	813.6	765.32	246.46	1605.7	1002.97	1372.13	854.14	869.01	237.73	1037.84	229.95	16.61	185.69	182.17	135.44	681.86	36.21	78.85	180.71
Eu/Eu*	1	1.67	0.85	0.4	0.48	0.49	0.5	0.72	0.62	0.53	0.82	0.47	0.49	2.33	0.77	0.65	0.62	0.82	1.9	1.02	0.81
$(La/Yb)_N$	19.08	7.41	44.82	91.29	29.56	88.7	105.64	91.17	103.58	79.01	29.92	64.48	39.19	0.03	12.05	71.55	39.74	29.92	25.58	4.27	9.18

Supplementary Material SV - 2

U-Pb (LA-ICP-MS and SHRIMP) results for magmatic zircon crystals from the Caxixe batholith.

Sample 41A - (SHRIMP)

Spot Name	U (ppm)	Th/U	f206 (%)	$^{207}Pb/^{206}Pb$ Age	2s err	$^{206}Pb/^{238}U$ Age	2s err	4corr 207*/206*	% err	4corr 207*/235	% err	4corr 206*/238	% err	err corr	discordance (%)
41-9.1	1065,14	0,12	0,136	608	21	611	17	0,060210	0,77	0,8208	3,67	0,098875	3,59	0,98	0,57
41-2.1	440,09	0,27	0,051	594	10	608	23	0,060124	1,07	0,8003	2,05	0,096534	1,74	0,85	2,41
41-11.1	537,44	0,43	0,359	588	10	631	32	0,060757	1,47	0,7999	2,25	0,095482	1,70	0,76	7,10
41-4.1	717,65	0,08	0,000	590	9	586	17	0,059522	0,77	0,7870	1,80	0,095900	1,63	0,90	-0,73
41-6.1	1037,08	0,28	0,023	589	9	563	15	0,058898	0,68	0,7772	1,70	0,095699	1,56	0,92	-4,80
41-7.1	713,00	0,18	0,149	593	9	548	23	0,058492	1,05	0,7769	1,94	0,096328	1,63	0,84	-8,52
41-12.1	566,68	0,17	0,000	585	10	576	19	0,059255	0,86	0,7760	1,91	0,094983	1,70	0,89	-1,54
41-3.1	584,82	0,23	0,090	589	9	528	22	0,057961	0,99	0,7648	1,93	0,095694	1,65	0,86	-12,05
41-8.1	472,78	0,41	0,000	579	10	564	21	0,058923	0,98	0,7632	2,00	0,093937	1,74	0,87	-2,69
41-5.1	94,14	0,27	0,000	559	14	623	44	0,060540	2,02	0,7564	3,30	0,090620	2,62	0,79	10,68
41-10.1	453,71	0,18	0,366	568	10	581	36	0,059387	1,68	0,7549	2,43	0,092190	1,75	0,72	2,30

Sample 33 - (SHRIMP)

Spot Name	U (ppm)	Th/U	f206 (%)	$^{207}Pb/^{206}Pb$ Age	2s err	$^{206}Pb/^{238}U$ Age	2s err	4corr 207*/206*	% err	4corr 207*/235	% err	4corr 206*/238	% err	err corr	discordance (%)
33-4.1	363,00	0,09	0,000	509	9	521	25	0,057769	1,14	0,6542	2,13	0,082128	1,80	0,84	2,44
33-7.1	685,74	0,09	0,000	510	8	497	18	0,057134	0,82	0,6492	1,82	0,082411	1,62	0,89	-2,89
33-9.1	289,56	0,33	0,047	506	9	490	32	0,056949	1,47	0,6408	2,42	0,081610	1,92	0,79	-3,43

33-2.1	269,69	1,38	0,052	505	9	468	35	0,056397	1,57	0,6341	2,49	0,081541	1,94	0,78	-8,28
33-6.1	289,47	0,34	0,229	506	9	463	44	0,056276	1,99	0,6340	2,76	0,081706	1,92	0,69	-9,65
33-5.1	326,21	0,11	0,000	501	7	474	27	0,056558	1,23	0,6302	1,89	0,080809	1,44	0,76	-5,83
33-8.1	601,65	0,07	0,000	491	8	500	20	0,057224	0,91	0,6241	1,90	0,079105	1,67	0,88	1,95

Sample 49 - (SHRIMP)

Spot Name	U (ppm)	Th/U	f206 (%)	$^{207}Pb/^{206}Pb$ Age	2s err	$^{206}Pb/^{238}U$ Age	2s err	4corr 207*/206*	% err	4corr 207*/235	% err	4corr 206*/238	% err	err corr	discordance (%)
49A-3.1	291,58	0,22	0,000	574	8	597	25	0,059828	1,16	0,7676	1,85	0,093048	1,45	0,78	4,17
49A-9.1	582,47	0,25	0,037	586	9	597	19	0,059822	0,89	0,7856	1,89	0,095244	1,67	0,88	1,87
49A-1.1	531,60	0,05	0,061	581	9	577	21	0,059256	0,98	0,7711	1,91	0,094382	1,64	0,86	-0,88
49A-7.1	442,17	0,38	0,000	596	10	579	21	0,059330	0,95	0,7929	1,99	0,096923	1,74	0,88	-3,09
49A-2.1	227,54	0,38	0,048	574	11	548	32	0,058498	1,48	0,7505	2,51	0,093046	2,03	0,81	-4,78
49A-4.1	425,61	0,26	0,000	588	10	560	21	0,058796	0,98	0,7746	2,01	0,095548	1,76	0,87	-5,37
49A-5.1	364,59	0,32	0,000	595	10	553	23	0,058621	1,05	0,7817	2,09	0,096712	1,81	0,87	-7,96

Sample 18 - (LA-ICP-MS)

Spot Name	U (ppm)	Th/U	f206c	$^{207}Pb/^{206}Pb$ Age	2s err	$^{206}Pb/^{238}U$ Age	2s err	4corr 207*/206*	% err	4corr 207*/235	% err	4corr 206*/238	% err	err corr	discordance (%)
003-ZR1		0,326	0,0251	568	57	543	9	0,05901	1,31	0,715	1,63	0,0878	0,89	0,55	4,39
004-ZR2		0,536	0,0125	599	21	607	12	0,05986	0,48	0,814	1,18	0,0987	1,01	0,86	-1,31
005-ZR3		0,249	0,0047	593	14	575	10	0,05970	0,33	0,768	1,00	0,0933	0,87	0,87	3,00
006-ZR4		0,277	0,0196	593	29	549	10	0,05970	0,68	0,732	1,21	0,0889	0,92	0,77	7,37

010-ZR7	0,351	0,0064	567	24	544	7	0,05900	0,56	0,716	0,98	0,0880	0,72	0,73	4,09
011-ZR8	0,319	0,0431	571	64	549	14	0,05910	1,50	0,724	2,03	0,0888	1,32	0,65	3,90
012-ZR9	0,228	0,0015	570	22	589	7	0,05907	0,51	0,779	0,86	0,0956	0,59	0,69	-3,39
015-ZR10	0,165	0,1230	579	20	538	7	0,05932	0,46	0,712	0,93	0,0870	0,72	0,77	7,07
016-ZR11	0,502	0,0353	584	32	549	9	0,05947	0,73	0,729	1,16	0,0889	0,82	0,71	5,98
019-ZR13	0,427	0,0106	585	23	569	9	0,05948	0,54	0,757	1,06	0,0923	0,84	0,79	2,69
021-ZR15	0,207	0,0487	603	21	583	10	0,05998	0,48	0,783	1,11	0,0946	0,93	0,84	3,35
023-ZR16B	0,221	0,0227	578	28	571	11	0,05929	0,65	0,757	1,24	0,0926	0,98	0,79	1,20
024-ZR17	0,187	0,0167	556	41	594	13	0,05869	0,94	0,781	1,53	0,0965	1,15	0,75	-6,87
027-ZR18	0,216	0,0032	576	16	600	7	0,05923	0,38	0,796	0,83	0,0975	0,64	0,77	-4,23
028-ZR19	0,225	0,0192	580	14	597	9	0,05934	0,33	0,794	0,96	0,0970	0,83	0,86	-2,99
029-ZR20	0,322	0,0194	593	42	564	14	0,05972	0,97	0,752	1,63	0,0914	1,26	0,77	5,01
030-ZR21	0,231	0,0056	594	13	555	8	0,05974	0,31	0,741	0,91	0,0899	0,77	0,85	6,58
031-ZR22	0,417	0,0107	584	24	539	7	0,05947	0,57	0,715	0,99	0,0871	0,72	0,73	7,84
032-ZR23	0,466	0,0055	591	21	546	8	0,05964	0,50	0,727	0,95	0,0884	0,72	0,76	7,55
033-ZR24	0,067	0,0088	581	25	561	9	0,05939	0,58	0,745	1,08	0,0910	0,83	0,77	3,49
034-ZR25	0,287	0,0028	587	21	547	6	0,05954	0,49	0,728	0,86	0,0886	0,59	0,69	6,76
035-ZR26	0,221	0,0203	572	41	570	12	0,05914	0,94	0,754	1,50	0,0924	1,11	0,74	0,42

Sample 21A - (LA-ICP-MS)

Spot Name	U (ppm)	Th/U	f206c	$^{207}Pb/^{206}Pb$ Age	2s err	$^{206}Pb/^{238}U$ Age	2s err	4corr 207*/206*	% err	4corr 207*/235	% err	4corr 206*/238	% err	err corr	discordance (%)
005-ZR3N		0,191	0,0080	633	23	571	10	0,06083	0,54	0,777	1,11	0,0926	0,89	0,81	9,79
006-ZR3B		0,004	0,0596	602	15	602	7	0,05995	0,34	0,810	0,81	0,0980	0,63	0,78	-0,15
007-ZR4		0,388	0,0031	573	35	569	8	0,05916	0,81	0,753	1,18	0,0923	0,77	0,66	0,66
008-ZR5		0,376	0,0033	587	18	592	8	0,05954	0,41	0,789	0,89	0,0961	0,71	0,79	-0,80
009-ZR6		0,914	0,0641	605	18	574	8	0,06005	0,43	0,771	0,92	0,0932	0,73	0,79	5,15
010-ZR7		0,049	0,0085	588	22	563	7	0,05956	0,50	0,750	0,87	0,0913	0,61	0,70	4,20

011-ZR8N	0,337	0,0244	615	40	567	8	0,06032	0,94	0,765	1,26	0,0920	0,76	0,60	7,76
012-ZR8B	0,018	0,0120	595	28	566	8	0,05977	0,65	0,756	1,08	0,0917	0,78	0,72	4,95
015-ZR9N	0,324	0,0064	622	23	561	7	0,06050	0,53	0,758	0,91	0,0909	0,63	0,70	9,79
016-ZR9B	0,330	0,0105	589	34	568	8	0,05959	0,78	0,757	1,15	0,0922	0,76	0,66	3,42
017-ZR10	0,216	0,0032	615	17	555	8	0,06032	0,40	0,748	0,95	0,0899	0,78	0,82	9,73
018-ZR11N	0,604	0,0307	630	34	564	10	0,06073	0,79	0,766	1,28	0,0915	0,94	0,73	10,38
019-ZR11B	0,528	0,0029	603	18	592	8	0,05998	0,41	0,795	0,89	0,0961	0,70	0,79	1,84
021-ZR12B	0,030	0,0061	575	21	557	8	0,05921	0,49	0,737	0,98	0,0902	0,76	0,78	3,14
024-ZR14B	0,028	0,0090	582	25	598	10	0,05939	0,58	0,796	1,12	0,0972	0,89	0,79	-2,85
027-ZR15	0,428	0,0320	606	51	564	13	0,06007	1,19	0,757	1,71	0,0914	1,17	0,68	6,99
028-ZR16	0,396	0,0264	563	33	555	9	0,05890	0,75	0,731	1,18	0,0900	0,84	0,71	1,44
029-ZR17	0,235	0,0527	585	38	551	10	0,05948	0,89	0,731	1,37	0,0892	0,98	0,71	5,84
030-ZR18N	0,595	0,0351	589	48	536	10	0,05959	1,13	0,713	1,52	0,0868	0,96	0,63	8,90
031-ZR18B	0,212	0,0158	580	25	587	9	0,05935	0,58	0,780	1,05	0,0953	0,79	0,76	-1,16
033-ZR19B	0,422	0,0212	594	29	547	7	0,05974	0,67	0,730	1,02	0,0886	0,67	0,66	7,89
034-ZR20	0,425	0,0209	580	31	557	9	0,05936	0,72	0,739	1,15	0,0903	0,82	0,71	3,96
035-ZR21	0,265	0,0040	590	24	560	7	0,05962	0,57	0,745	0,93	0,0907	0,64	0,69	5,14
036-ZR22	0,838	0,0104	620	33	557	6	0,06047	0,76	0,753	1,04	0,0903	0,60	0,58	10,16
039-ZR23N	0,354	0,0073	570	23	595	8	0,05907	0,53	0,788	0,93	0,0967	0,67	0,72	-4,51
040-ZR23B	0,115	0,0100	604	25	583	8	0,06000	0,57	0,783	0,97	0,0946	0,69	0,71	3,51
041-ZR24	0,331	0,0053	584	19	568	6	0,05946	0,45	0,756	0,82	0,0922	0,57	0,70	2,66
044-ZR27	0,282	0,0471	604	48	528	11	0,06001	1,11	0,707	1,63	0,0854	1,13	0,70	12,53
045-ZR28	0,210	0,0037	593	20	583	9	0,05971	0,47	0,780	1,03	0,0947	0,84	0,81	1,67
046-ZR29N	0,359	0,0088	613	19	554	6	0,06027	0,44	0,746	0,82	0,0898	0,59	0,72	9,64
047-ZR29B	0,432	0,0162	593	36	567	8	0,05972	0,82	0,757	1,18	0,0919	0,75	0,64	4,49
048-ZR30	0,685	0,0131	615	24	582	8	0,06031	0,56	0,785	0,99	0,0944	0,73	0,74	5,35

Sample 53 - (LA-ICP-MS)

Spot Name	U	Th/U	f206c		2s		2s	4corr	%	4corr	%	4corr	%	err	discordance

	(ppm)			$^{207}Pb/^{206}Pb$ Age	err	$^{206}Pb/^{238}U$ Age	err	207*/206*	err	207*/235	err	206*/238	err	corr	(%)
003-ZR1N	0,385	0,0154		636	22	589	12	0,06092	0,51	0,804	1,24	0,0957	1,07	0,86	7,44
006-ZR3	0,187	0,0328		632	34	474	16	0,06079	0,80	0,639	1,92	0,0763	1,70	0,89	25,01
008-ZR5N	0,302	0,0979		642	33	579	9	0,06108	0,77	0,792	1,15	0,0940	0,78	0,67	9,77
015-ZR8N	0,227	0,0068		628	20	552	6	0,06067	0,47	0,747	0,82	0,0893	0,57	0,69	12,10
017-ZR9N	0,324	0,0085		634	25	565	6	0,06086	0,58	0,768	0,90	0,0915	0,57	0,64	10,98
018-ZR9B	0,102	0,0442		650	68	326	17	0,06130	1,59	0,439	3,16	0,0519	2,70	0,86	49,82
019-ZR10	0,225	0,0034		621	19	558	9	0,06049	0,45	0,754	1,05	0,0904	0,87	0,83	10,18
022-ZR13	0,269	0,0053		602	20	571	5	0,05995	0,46	0,766	0,77	0,0927	0,49	0,64	5,03
023-ZR14	0,095	0,2036		650	39	547	8	0,06132	0,90	0,749	1,25	0,0886	0,78	0,62	15,81
024-ZR16	0,362	0,0117		597	29	585	6	0,05981	0,68	0,784	0,96	0,0950	0,57	0,59	1,93
028-ZR18B	0,107	0,0900		626	30	528	9	0,06062	0,71	0,713	1,16	0,0853	0,85	0,73	15,67
030-ZR15	0,088	0,4006		683	43	384	14	0,06227	1,01	0,527	2,12	0,0614	1,83	0,86	43,80
031-ZR20N	0,202	0,0163		598	14	556	6	0,05985	0,33	0,743	0,74	0,0900	0,55	0,74	7,14
033-ZR21N	0,206	0,0044		585	17	584	8	0,05950	0,39	0,777	0,92	0,0947	0,74	0,81	0,30
034-ZR21B	0,100	0,0070		591	15	583	5	0,05965	0,35	0,778	0,70	0,0946	0,47	0,68	1,39
035-ZR22	0,130	0,0051		606	30	531	13	0,06005	0,70	0,711	1,48	0,0858	1,25	0,85	12,36
036-ZR23	0,275	0,0087		614	32	604	15	0,06028	0,75	0,816	1,53	0,0982	1,29	0,84	1,64
041-ZR25	0,497	0,0139		617	38	565	10	0,06039	0,88	0,762	1,32	0,0915	0,91	0,69	8,55
042-ZR26	0,104	0,0279		647	40	523	16	0,06121	0,93	0,714	1,90	0,0845	1,62	0,85	19,10
045-ZR28B	0,084	0,0310		629	18	528	5	0,06071	0,43	0,715	0,78	0,0854	0,54	0,69	15,98
048-ZR30B	0,119	0,0063		603	35	571	16	0,05998	0,82	0,766	1,69	0,0926	1,43	0,84	5,35
048-ZR30B	0,119	0,0062		603	35	571	16	0,05998	0,82	0,766	1,69	0,0926	1,43	0,84	5,35

Sample 54 A - (LA-ICP-MS)

Spot Name	U (ppm)	Th/U	f206c	$^{207}Pb/^{206}Pb$	2s err	$^{206}Pb/^{238}U$	2s err	4corr 207*/206*	% err	4corr 207*/235	% err	4corr 206*/238	% err	err corr	discordance (%)

			Age		Age									
003-ZR1	0,595	0,0066	614	18	622	9	0,06028	0,41	0,842	0,92	0,1013	0,74	0,80	-1,34
004-ZR2	0,643	0,0314	598	50	567	16	0,05983	1,16	0,758	1,94	0,0919	1,50	0,78	5,19
005-ZR3	0,690	0,0316	582	53	548	12	0,05942	1,24	0,726	1,75	0,0887	1,18	0,67	5,98
006-ZR4	0,456	0,0086	588	18	568	7	0,05957	0,41	0,757	0,88	0,0922	0,68	0,78	3,32
008-ZR5B	0,702	0,0084	611	18	577	7	0,06020	0,42	0,777	0,86	0,0937	0,65	0,76	5,51
010-ZR6B	0,509	0,0131	601	30	547	8	0,05992	0,69	0,731	1,11	0,0885	0,78	0,71	9,00
011-ZR7	0,455	0,0341	579	41	542	11	0,05932	0,95	0,718	1,47	0,0877	1,06	0,72	6,35
012-ZR8	0,354	0,0062	563	31	563	12	0,05888	0,71	0,741	1,34	0,0912	1,08	0,80	0,00
017-ZR9	0,413	0,0097	619	22	595	8	0,06043	0,51	0,805	0,92	0,0966	0,67	0,72	3,93
019-ZR11	0,398	0,0087	599	21	540	6	0,05987	0,48	0,721	0,87	0,0873	0,62	0,72	9,86
020-ZR12	0,135	0,0236	580	45	560	12	0,05935	1,04	0,743	1,54	0,0908	1,07	0,70	3,43
022-ZR13B	0,376	0,0108	612	22	605	8	0,06024	0,52	0,818	0,95	0,0984	0,70	0,74	1,13
023-ZR14	0,456	0,0183	570	34	606	8	0,05907	0,80	0,803	1,10	0,0986	0,67	0,60	-6,36
024-ZR15	0,647	0,0245	596	33	559	10	0,05978	0,77	0,746	1,28	0,0905	0,95	0,75	6,18
025-ZR16N	0,892	0,0374	641	45	541	13	0,06105	1,06	0,737	1,68	0,0875	1,25	0,74	15,58
029-ZR17	0,598	0,0128	596	28	599	9	0,05978	0,66	0,803	1,11	0,0974	0,81	0,73	-0,60
033-ZR21	0,518	0,0116	625	19	581	9	0,06061	0,43	0,789	1,00	0,0944	0,82	0,82	7,04
034-ZR22	0,662	0,0521	599	54	574	14	0,05987	1,26	0,769	1,80	0,0932	1,23	0,69	4,14
035-ZR23	0,888	0,0364	595	67	601	18	0,05977	1,56	0,805	2,22	0,0977	1,54	0,69	-0,95
036-ZR24N	0,344	0,0087	587	26	550	9	0,05954	0,61	0,731	1,09	0,0891	0,82	0,75	6,29
037-ZR24B	0,192	0,0140	599	39	537	10	0,05987	0,91	0,717	1,35	0,0868	0,92	0,69	10,38
041-ZR26	0,200	0,0291	575	49	568	13	0,05922	1,14	0,752	1,71	0,0920	1,22	0,72	1,35
042-ZR27	0,540	0,0472	598	59	557	17	0,05986	1,38	0,745	2,12	0,0903	1,57	0,74	6,88
043-ZR28	0,417	0,0244	611	42	545	10	0,06022	0,99	0,732	1,45	0,0882	0,99	0,69	10,90
044-ZR29	0,719	0,0453	607	58	555	14	0,06011	1,36	0,745	1,96	0,0899	1,35	0,69	8,62

Sample 54C - (LA-ICP-MS)

Spot Name	U (ppm)	Th/U	f206c	$^{207}Pb/^{206}Pb$ Age	2s err	$^{206}Pb/^{238}U$ Age	2s err	4corr 207*/206*	% err	4corr 207*/235	% err	4corr 206*/238	% err	err corr	discordance (%)
003-ZR1		1,168	0,0097	603	20	512	9	0,05999	0,48	0,684	1,11	0,0827	0,93	0,84	15,12
006-ZR4		1,408	0,0280	610	28	533	7	0,06019	0,66	0,715	1,04	0,0861	0,71	0,69	12,74
009-ZR7		0,628	0,0149	587	46	527	11	0,05955	1,06	0,699	1,54	0,0851	1,05	0,68	10,35
010-ZR8		0,176	0,0111	565	25	545	7	0,05894	0,59	0,717	0,98	0,0882	0,70	0,71	3,52
012-ZR10		0,510	0,0097	563	27	531	7	0,05888	0,62	0,697	0,99	0,0859	0,68	0,69	5,57
017-ZR11		0,760	0,0032	570	17	540	7	0,05908	0,39	0,711	0,87	0,0873	0,69	0,79	5,32
018-ZR12		1,226	0,1425	664	27	452	10	0,06172	0,63	0,618	1,37	0,0726	1,16	0,85	31,96
021-ZR15		0,533	0,0158	565	28	529	7	0,05895	0,65	0,696	1,03	0,0856	0,71	0,69	6,32
022-ZR16		0,611	0,0135	598	30	543	7	0,05985	0,70	0,726	1,07	0,0879	0,72	0,67	9,20

Supplementary Material SV - 3

Lu-Hf isotope data of Caxixe batholith from the southern Espírito Santo state, Brazil.

Sample	U-Pb age (Ma)	±	Isotope ratios				Initial ratios			
Zircon		1σ	$^{176}Hf/^{177}Hf$	±2σ	$^{176}Lu/^{177}Hf$	±2σ	$^{176}Hf/^{177}Hf_{(t)}$	$\varepsilon Hf_{(t)}$	±2σ	$T_{DM}Hf$ (Ga)
33										
7.1	510	8	0.281875	0.000018	0.000270	0.000002	0.281872	-20.9	0.48	1.88
8.1	491	8	0.281860	0.000017	0.000280	0.000002	0.281857	-21.9	0.51	1.90
9.1	506	9	0.281906	0.000016	0.000170	0.000001	0.281904	-19.9	0.48	1.83
4.1	509	9	0.281833	0.000018	0.000150	0.000001	0.281832	-22.4	0.54	1.93
41A										
6.1	589	9	0.282251	0.000025	0.001070	0.000008	0.282239	-6.2	0.14	1.40
7.1	593	9	0.282289	0.000017	0.000900	0.000005	0.282279	-4.7	0.10	1.34
8.1	579	10	0.282278	0.000012	0.001710	0.000011	0.282259	-5.7	0.13	1.39
4.1	590	9	0.282292	0.000018	0.000640	0.000004	0.282285	-4.5	0.10	1.33
12.1	585	10	0.282285	0.000017	0.000540	0.000005	0.282279	-4.9	0.12	1.33
49										
1.1	581	9	0.282141	0.000024	0.001180	0.000008	0.282128	-10.3	0.23	1.56
4.1	588	10	0.282063	0.000027	0.001220	0.000011	0.282050	-12.9	0.33	1.67
3.1	574	8	0.282088	0.000020	0.000880	0.000005	0.282079	-12.2	0.24	1.62
2.1	574	11	0.282130	0.000020	0.001040	0.000012	0.282119	-10.8	0.33	1.57
5.1	595	10	0.282132	0.000018	0.001670	0.000013	0.282113	-10.5	0.26	1.59

Supplementary Material SV - 4

Sm–Nd and Rb-Sr isotope data of Caxixe batholith samples in the southern Espírito Santo state. Initial isotope ratios are calculated for t = **Age Ma**. (m) – measured; (i) – initial (calculated). TDM model ages after DePaolo (1981).

Sample	**Sm (ppm)**	**Nd (ppm)**	**$^{147}Sm/^{144}Nd$**	**$^{143}Nd/^{143}Nd_{(m)}$ ± 2σ (abs)**	**$\varepsilon Nd_{(0)}$**	**$^{143}Nd/^{143}Nd_{(i)}$**	**$\varepsilon Nd_{(i)}$**	**T_{DM} (Ga)**	**Rb (ppm)**	**Sr (ppm)**	**$^{87}Rb/^{86}Sr_{(m)}$**	**$^{87}Sr/^{86}Sr(m)$ ± 2SE**	**$\varepsilon Sr_{(0)}$**	**$^{87}Sr/^{86}Sr_{(i)}$**	**$\varepsilon Sr_{(i)}$**	**Age (Ma)**
21 A	5.3	39.6	0.085695	0.511793	-16.5	0.511511	-9.3	1.48	79.4	315	0.729930	0.716710	173.31	0.711478	107.55	0.503
26	1.60	8.10	0.141153	0.512164	-9.2	0.511699	-5.6	1.83	57.4	260	0.638978	0.711470	98.94	0.706890	42.37	0.503
30	19.1	143.9	0.087747	0.511601	-20.2	0.511312	-13.2	1.73	176.1	405	1.259361	0.718450	198.01	0.709423	78.36	0.503
41A	5.00	35.00	0.073720	0.511867	-15.0	0.511587	-5.9	1.27	132.9	256	1.503760	0.719560	213.77	0.707124	47.00	0.580
49	3.00	14.60	0.142331	0.512030	-11.9	0.511489	-7.8	2.15	94.7	250	1.097148	0.718670	201.14	0.709597	82.13	0.580
49B	0.50	1.90	0.176799	0.512309	-6.4	0.511637	-4.9		146.7	128	3.324434	0.733690	414.34	0.706197	33.83	0.580
RF 53	5.70	27.20	0.123734	0.511862	-15.1	0.511371	-9.5	1.99	97.3	269	1.047766	0.719805	217.25	0.710765	99.16	0.605

DePaolo, D.J., 1981. Neodymium isotopes in the Colorado front range and crust-mantle evolution in the Proterozoic. Nature 291, 193-196.